

# X-RAY DIFFRACTION ANALYSIS FOR THIN FILM SAMPLES

---

## Training Textbook

Application Laboratory  
Rigaku Corporation

All rights reserved. Unauthorized reprinting or reproduction of any part of this document is prohibited by law.





# Contents

|   |    |
|---|----|
| Chapter 1 X-ray Diffractometers and Optics Used in Thin Film Analysis .....         | 1  |
| §1.1 X-ray Diffractometers for Thin Film Analysis .....                             | 1  |
| §1.2 Goniometer, Sample Stage, and Attenuator .....                                 | 3  |
| 1.2.1 Goniometer.....   | 3  |
| 1.2.2 Sample Stage .....  | 4  |
| 1.2.3 Attenuator .....  | 5  |
| §1.3 Types and Features of Optical Devices.....                                     | 6  |
| 1.3.1 Paraboloidal Synthetic Multilayer Mirror .....                                | 6  |
| 1.3.2 Channel-Cut Crystal.....  | 8  |
| 1.3.3 Optics Based on Channel-Cut Crystal.....                                      | 9  |
| 1.3.4 Width-Limiting Slit .....   | 13 |
| 1.3.5 Height Limiting Slit (Length Limiting Slit).....                              | 14 |
| 1.3.6 Soller Slit.....  | 14 |
| 1.3.7 Examples of measurement techniques using Soller slits.....                    | 16 |
| Chapter 2 Reciprocal Lattice .....  | 18 |
| §2.1 What is a Reciprocal Lattice? .....  | 18 |
| 2.1.1 A Clear Expression .....  | 18 |
| 2.1.2 Definition of the Reciprocal Lattice.....                                     | 21 |
| §2.2 Reciprocal Lattice and Diffraction Conditions .....                            | 23 |
| 2.2.1 Reciprocal Lattice and Diffraction Conditions .....                           | 23 |
| 2.2.2 Ewald Sphere .....  | 26 |
| §2.3 Reciprocal Lattice and Crystal Structure .....                                 | 27 |
| 2.3.1 Crystal Lattice and Reciprocal Lattice .....                                  | 27 |
| 2.3.2 Size of Crystallite and Spread of Reciprocal Lattice Point .....              | 30 |
| 2.3.3 Change in Lattice Constants and Position of Reciprocal Lattice Points .....   | 32 |
| 2.3.4 Change in Crystal Orientation and Position of Reciprocal Lattice Points ..... | 33 |
| §2.4 Reciprocal Lattice and Measurement Axes .....                                  | 33 |
| 2.4.1 Four-Circle Goniometer .....  | 34 |
| 2.4.2 Goniometer for In-Plane Measurement.....                                      | 36 |
| 2.4.3 Reciprocal Space Coordinates.....   | 38 |
| §2.5 Reciprocal Lattice and Resolution of Optics .....                              | 39 |
| 2.5.1 Resolution of Incident Optics.....  | 40 |

|  |    |
|--|----|
| 2.5.2 Resolution of Receiving Optics.....  | 41 |
| 2.5.3 Resolution Function .....  | 42 |
| 2.5.4 Resolution of the Goniometer .....   | 44 |
| §2.6 Single Crystal and Polycrystal.....   | 44 |
| §2.7 Summary.....  | 45 |
| Chapter 3 Diffraction Measurements .....   | 47 |
| §3.1 Relationship between Various Measurement Techniques.....  | 47 |
| §3.2 What Does Diffraction Measurement Observe? .....  | 49 |
| 3.2.1 Out-of-Plane Measurement .....   | 49 |
| 3.2.2 Thin Film Measurement .....  | 50 |
| 3.2.3 In-Plane Measurement .....   | 50 |
| 3.2.4 Pole Figure Measurement .....  | 52 |
| 3.2.5 Preferred Orientation and Crystallinity Measurement .....  | 54 |
| 3.2.6 Rocking Curve Measurement.....   | 55 |
| 3.2.7 Reciprocal Space Mapping (RSM) Measurement.....  | 56 |
| §3.3 Measurement Techniques .....  | 60 |
| 3.3.1 Out-of-Plane Measurement and Thin Film Measurement.....  | 61 |
| 3.3.2 In-Plane Measurement .....   | 63 |
| 3.3.3 Pole Figure Measurement .....  | 67 |
| 3.3.4 Rocking Curve Measurement.....   | 69 |
| 3.3.5 Reciprocal Space Mapping (RSM) Measurement.....  | 74 |
| 3.3.6 Summary .....  | 77 |
| Chapter 4 X-ray Reflectivity Method .....  | 80 |
| §4.1 Applicability of X-Ray Reflectivity Method .....  | 80 |
| §4.2 Overview of X-Ray Reflectivity Method .....   | 80 |
| §4.3 Principles of X-ray Reflectivity Method .....   | 82 |
| 4.3.1 Total Reflection and Refractive Index for X-Rays.....  | 82 |
| 4.3.2 Reflected Wave and Refracted Wave .....  | 84 |
| 4.3.3 Effects of Roughness.....  | 88 |
| §4.4 Reflectivity Analysis Method .....  | 89 |
| 4.4.1 Obtaining Film Thickness Based on the Incident Angle Dependence of the<br>Oscillation Period ..... | 89 |
| 4.4.2 Obtaining Film Thickness via Fourier Transformation .....  | 92 |
| 4.4.3 Obtaining Film Thickness, Density, and Surface or Interface Roughness<br>by Fitting .....          | 93 |

|   |     |
|---|-----|
| §4.5 Reflectivity Measurement.....                                    | 94  |
| 4.5.1 Selecting Optics .....  | 95  |
| 4.5.2 Optics Alignment .....  | 97  |
| 4.5.3 Mounting Sample .....   | 97  |
| 4.5.4 Sample Alignment.....   | 98  |
| 4.5.5 Reflectivity Measurement .....                                  | 103 |
| 4.5.6 Measurement Precautions .....                                   | 104 |
| §4.6 Example of Measurement.....                                      | 105 |
| §4.7 Examples of Analysis .....                                       | 107 |
| §4.8 Summary.....   | 110 |
| Chapter 5 High-Resolution X-ray Diffraction Method.....               | 112 |
| §5.1 Background of High-Resolution X-ray Diffraction Method .....     | 112 |
| §5.2 Multiple Crystal Method Principles .....                         | 116 |
| 5.2.1 X-ray Diffraction with a Perfect Crystal .....                  | 116 |
| 5.2.2 Application of Asymmetric Reflections .....                     | 117 |
| 5.2.3 Multiple Crystal Optics .....                                   | 118 |
| 5.2.4 Channel-Cut Crystal and Monochromator System .....              | 121 |
| 5.2.5 Practical Monochromator System .....                            | 127 |
| §5.3 Summary.....   | 130 |
| Chapter 6 Rocking Curve Measurement.....                              | 132 |
| §6.1 What is the Dynamical Theory of Diffraction? .....               | 132 |
| §6.2 Basic Equation of Dynamical Theory of Diffraction.....           | 133 |
| 6.2.1 Maxwell's Equations in Crystal .....                            | 133 |
| 6.2.2 Derivation of the Fundamental Equation .....                    | 137 |
| 6.2.3 Boundary Conditions .....                                       | 139 |
| 6.2.4 Two-Wave Approximation and Dispersion Surface .....             | 141 |
| 6.2.5 Shift from Diffraction Condition.....                           | 143 |
| 6.2.6 Rocking Curve .....   | 145 |
| 6.2.7 X-ray Standing Wave .....                                       | 150 |
| 6.2.8 Extinction Distance .....                                       | 151 |
| §6.3 Dynamical Theory of Diffraction in Multilayer Film Crystals..... | 152 |
| 6.3.1 Dynamical Theory of Diffraction for Strained Crystal .....      | 152 |
| 6.3.2 Rocking Curve of Multilayer Film.....                           | 152 |
| 6.3.3 Rocking Curve Analysis.....                                     | 155 |
| §6.4 Summary.....   | 160 |

|  |     |
|--|-----|
| Chapter 7 Kinematical Theory of Diffraction .....                              | 162 |
| §7.1 General Description of X-Ray Scattering by Materials.....                 | 162 |
| 7.1.1 Description of Scattered X-Rays.....                                     | 162 |
| 7.1.2 X-Ray Scattering from Entire Material .....                              | 163 |
| §7.2 X-Ray Scattering from Crystalline Material.....                           | 164 |
| 7.2.1 Atomic Scattering Factor and Crystal Structure Factor.....               | 164 |
| 7.2.2 Crystal Structure Factor .....   | 167 |
| 7.2.3 Laue Function.....   | 168 |
| 7.2.4 Extinction Rule.....   | 171 |
| 7.2.5 Effects on X-Ray Scattering Phenomena Other Than Crystal Structure ..... | 173 |

# Chapter 1 X-ray Diffractometers and Optics Used in Thin Film Analysis

While the crystallinity of the measured object is relatively restricted in a powder sample or a single crystal sample, a thin film sample may include a range of crystallinity types. For example, in the case of a polycrystalline film and an epitaxial film on a single crystal substrate, the former film will sometimes have low crystallinity and a low preferred orientation, while the latter film has high crystallinity comparable to a thin single crystal. A comparison of the X-ray diffraction profiles of these samples will show large differences in properties, including diffraction peak width, angle difference between two or more peaks, and peak shape. To analyze the thin film samples correctly, we must first acquire correct profiles by selecting the collimation (divergence angle) and monochromaticity of the X-rays according to the crystallinity or other properties of the sample.

Although the purpose of measurement is to observe the preferred orientation or an extremely thin layer, thin film samples can often require observations from two or more directions by thin film or in-plane measurements, in addition to ordinary  $\theta$ - $2\theta$  measurement. In such cases, we must rotate the sample or the measurement axis to an orientation different from the  $\theta$ - $2\theta$  scan and measure the angles.

This chapter gives an overview of the X-ray diffractometers used for thin film analysis and describes the optics used to set the resolution and criteria for selecting the resolution of the measurement optics.

## §1.1 X-ray Diffractometers for Thin Film Analysis

An X-ray diffractometer generally consists of three parts: an X-ray source, a mechanical section (goniometer), and a counter. Since thin film samples vary widely in crystallinity and preferred orientation, we must often measure a sample by tilting it in various directions and changing the scanning direction of the detector. Thus, an X-ray diffractometer for thin film analysis has additional functions in the mechanical section (goniometer) and sample stage section.

When we change the scanning direction of the detector or the direction to measure the diffraction angle  $2\theta$ , we must also set the angle resolution accordingly. In other cases, we may need to change the collimation and monochromaticity of the X-ray beam for measurements according to the crystallinity of the sample. In these cases, to change beam characteristics, we must add optical devices to the incident and receiving optics in the front and rear of the sample stage.

Fig. 1.1.1 shows the external appearance of the horizontal sample mount X-ray diffractometers, the SmartLab and RINT/TTR III. The figure also gives a schematic diagram of the system configuration. (The RINT/Ultima III is an X-ray diffractometer that uses an X-ray generator differing from the RINT/TTR III. This text refers to the RINT/Ultima III and RINT/TTR III simply as the RINT III series.)

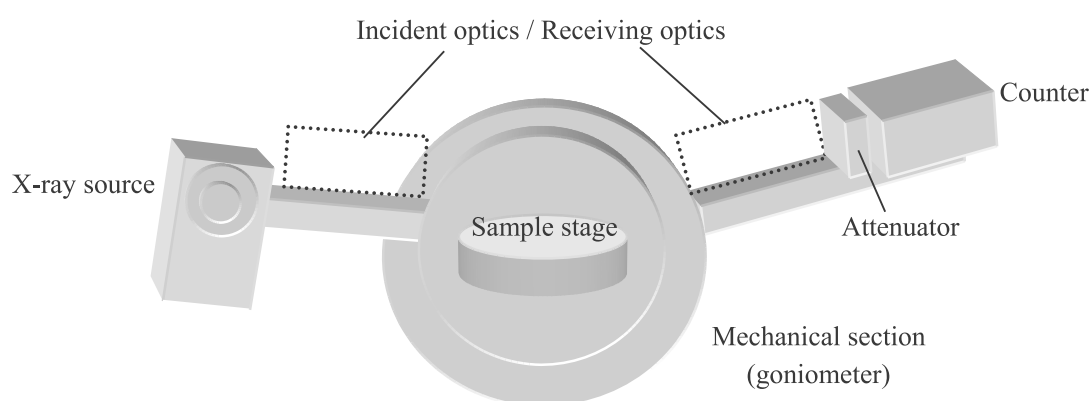
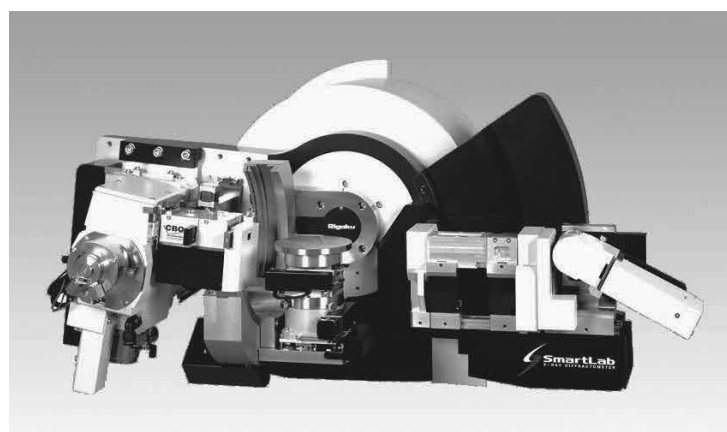
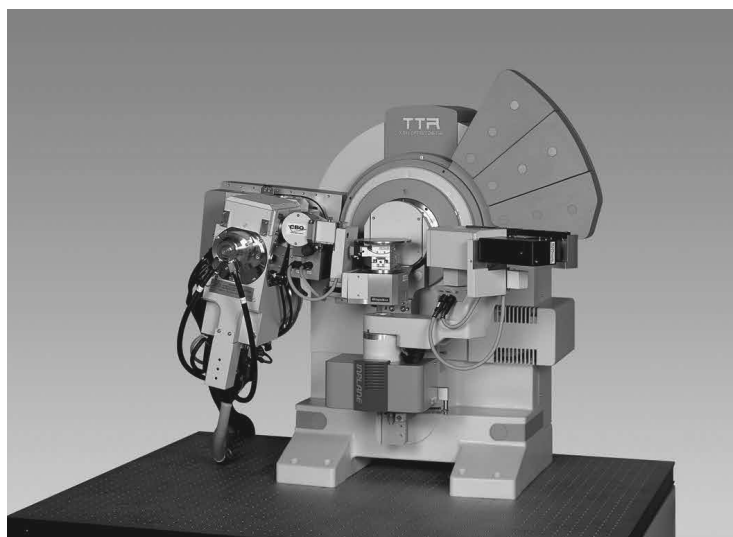


Fig. 1.1.1 Configuration of X-ray diffractometer  
 From above: external appearance of RINT/TTR III, external appearance of SmartLab (9kW),  
 and schematic diagram of the system configuration

## §1.2 Goniometer, Sample Stage, and Attenuator

### 1.2.1 Goniometer

A horizontal sample mount X-ray diffractometer has the two following goniometer axes.

- **$\theta_S$  axis:** The axis for setting the angle of the X-ray source with respect to the sample surface. (The “S” in “ $\theta_S$ ” refers to “source.”)
- **$\theta_D$  axis:** The axis for setting the angle of the detector with respect to the sample surface. (The “D” in “ $\theta_D$ ” refers to “detector.”)

The  $\theta_S$  axis and the  $\theta_D$  axis are used to set  $2\theta$ , the diffraction angle.

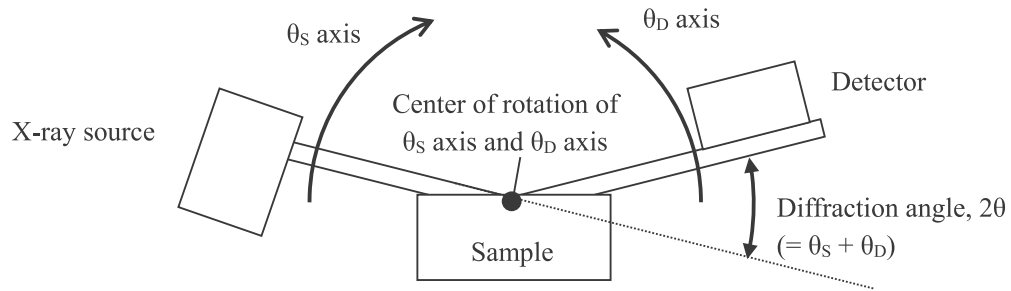
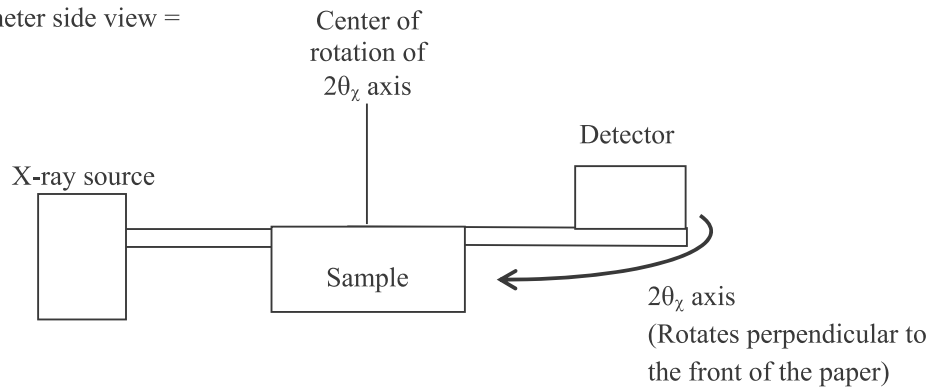


Fig. 1.2.1 Goniometer axes in horizontal sample mount X-ray diffractometer

The optional **in-plane arm** has a  $2\theta_\chi$  axis, which rotates the detector in a plane parallel to the sample surface. In in-plane measurements, which perform measurements in the range close to  $\theta_S = 0^\circ$  and  $\theta_D = 0^\circ$ , the diffraction angle  $2\theta$  can be assumed to take the same value as the  $2\theta_\chi$  axis. If the measurement range is not close to  $\theta_S = 0^\circ$  and  $\theta_D = 0^\circ$ , as in pole figure measurements or reciprocal space mapping measurements (mesh measurement), diffraction angle  $2\theta$  differs from  $2\theta_\chi$  and takes a value calculated based on angles,  $\theta_S$ ,  $\theta_D$ , and  $2\theta_\chi$ .

= Diffractometer side view =



= Top view of diffractometer =

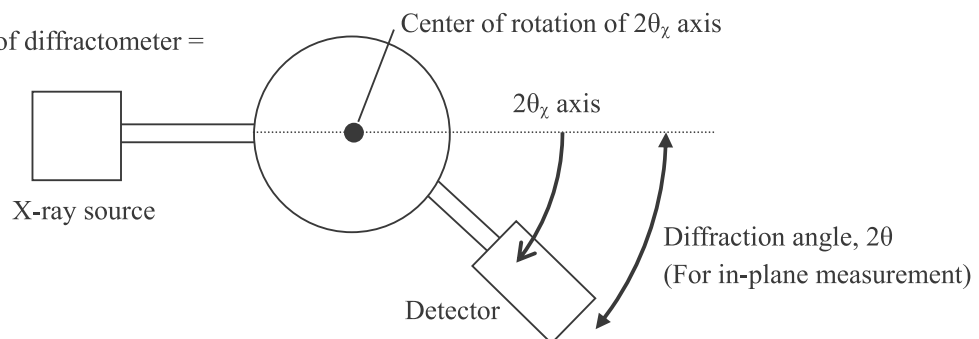


Fig. 1.2.2 In-plane axis (optional)

### 1.2.2 Sample Stage

The measurement sample is mounted on the sample stage at the center of the goniometer. The sample stage has axes for adjusting the angles and positions of the sample based on the purpose of the measurement, including sample rotation, sample swing, and sample translation. Fig. 1.2.3 shows an overview of the axes incorporated into the sample stage. Note that features such as the shape of the sample stage, the number of axes in the sample stage, and the range of motion of each axis vary depending on the model.



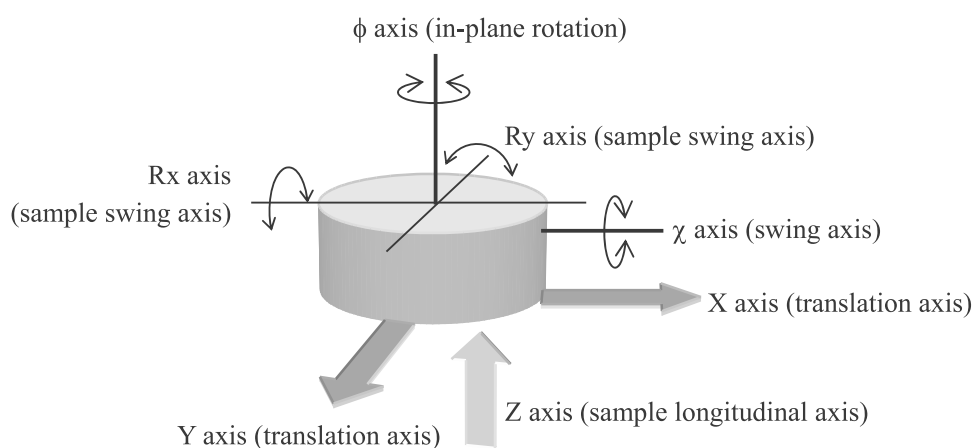


Fig. 1.2.3 Sample stage of horizontal sample mount goniometer

### 1.2.3 Attenuator

For samples with high crystallinity, the diffracted X-ray beam may have extremely high intensity, and the scintillation counter may not be able to count correctly. In general, a scintillation counter can withstand a counting rate of up to approximately 800 thousand cps. To count X-rays with intensities above this value, we must use an **attenuator**.

An attenuator is an Al plate of a specified thickness. The attenuator is placed before the scintillation counter to attenuate X-ray intensities to levels that can be counted by the scintillation counter. The intensity counted with the attenuator inserted is multiplied by the attenuation factor measured in advance for conversion to the direct X-ray intensity that would have been registered without the Al plate.

An automated attenuator incorporates two or more Al plates of differing thicknesses, switching the plates by a rotation mechanism. The plate with the suitable attenuation factor is chosen depending on the X-ray intensity to be measured.

Table 1.2.1. Types of attenuators

| Name                 | Inside the attenuator  |
|----------------------|--|
| Open                 | None   |
| Ni                   | K $\beta$ filter for Cu lines. A nickel foil whose thickness is adjusted based on the difference in absorption coefficients of Ni for Cu K $\alpha$ and K $\beta$ lines so that the intensity ratio of the Cu K $\alpha$ and K $\beta$ lines is 100:1. |
| 1/X<br>(three types) | An aluminum foil whose thickness is adjusted so that the attenuation factor for the Cu K $\alpha$ line is approximately 1/X. (The value of X varies, depending on the diffractometer.)   |

SmartLab offers an automated attenuator mode and switches attenuators automatically when it detects large intensity variations during measurement. The RINT III series provides functions for specifying the angular positions to switch attenuators and perform measurements while changing the attenuators one after another. Combined with attenuators, the scintillation counter can make correct counts of intensity variations across approximately nine orders of magnitude.

### §1.3 Types and Features of Optical Devices

Optical devices to be used for SmartLab and the RINT III series are listed below. These optical devices are combined and inserted in the incident and receiving optics and adjusted to provide the optical resolution based on the purpose. This section describes the components and features of these optical devices.

- Paraboloidal synthetic multilayer mirror
  - CBO unit
- Channel-cut crystals
  - Double-crystal monochromator
  - Four-crystal monochromator
  - Double-crystal analyzer
- Width-limiting slit
  - Incident slit
  - Receiving slit
- Height-limiting slit
- Soller slit

#### 1.3.1 Paraboloidal Synthetic Multilayer Mirror

A **paraboloidal synthetic multilayer mirror** efficiently monochromatizes and collimates the divergent beam generated from the X-ray source.

On a substrate with a flat surface, alternate layers of heavy and light elements (W film and B<sub>4</sub>C film or Si film) are stacked periodically by the sputtering technique. This structure creates regular variations in electron density and generates diffraction phenomena like a crystal. To generate the diffraction phenomena selectively in the characteristic X-rays used in the X-ray diffraction measurement and to extract the X-rays as a collimated beam, the mirror incorporates the following features.

- Each layer of the multilayer film is formed in a paraboloidal curve. When the focus of the X-ray tube is placed at the focus of the paraboloid, the diffracted X-rays form a collimated beam, like waves reflected from a parabolic antenna.
- The thickness of each layer of the multilayer film is designed so that the wavelength of the characteristic X-rays satisfies the diffraction condition. The layers do not have constant thicknesses; they are thinner in the region nearer the focus of the paraboloid and thicker in

the region farther from the focus.

As a result, the divergent X-rays generated from the X-ray source are collimated and monochromatized with wavelength components around the Cu  $K\alpha$  line. The monochromaticity in terms of the intensity ratio of the Cu  $K\alpha$  line to the  $K\beta$  line improves from the original 100:25 to 1000:1. The collimation improves with the divergence angle suppressed to approximately  $0.04^\circ$ .

The shape and thickness of the multilayer film are optimized for each of the wavelengths of the characteristic X-rays used. Thus, when we change the type of the target, we must also change the multilayer mirror.

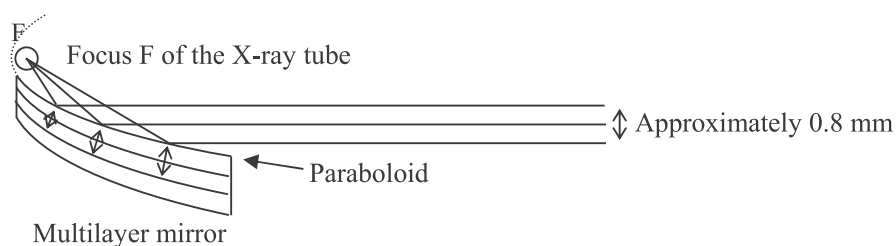


Fig. 1.3.1 Paraboloidal synthetic multilayer mirror

In the SmartLab and the RINT III series, the multilayer mirror is stored in the CBO unit.

The **CBO unit** (abbreviation for cross-beam optics) is a mechanism for conveniently switching between the parafocusing method used mainly to measure powder samples and the parallel beam method used to measure thin-film samples. Fig. 1.3.2 shows the structure of the CBO unit.

Although the divergent X-rays generated from the X-ray tube are partially reflected and collimated at the multilayer mirror, certain components do not strike the mirror, propagating instead with divergent characteristics unaltered. These two components propagate at different heights. By using a slit with an appropriate gap height (**selection slit**), we can selectively extract either of these components.

The parafocusing method uses the divergent beam generated from the X-ray tube as the incident X-ray beam as-is. The selection slit used is the “BB” (abbreviation for Bragg-Brentano parafocusing method) slit with a gap at a higher position. The parallel beam method uses the beam collimated on the multilayer mirror as the incident X-ray beam. The selection slit used is the “PB” (the abbreviation for Parallel Beam) slit with a gap at a lower position.

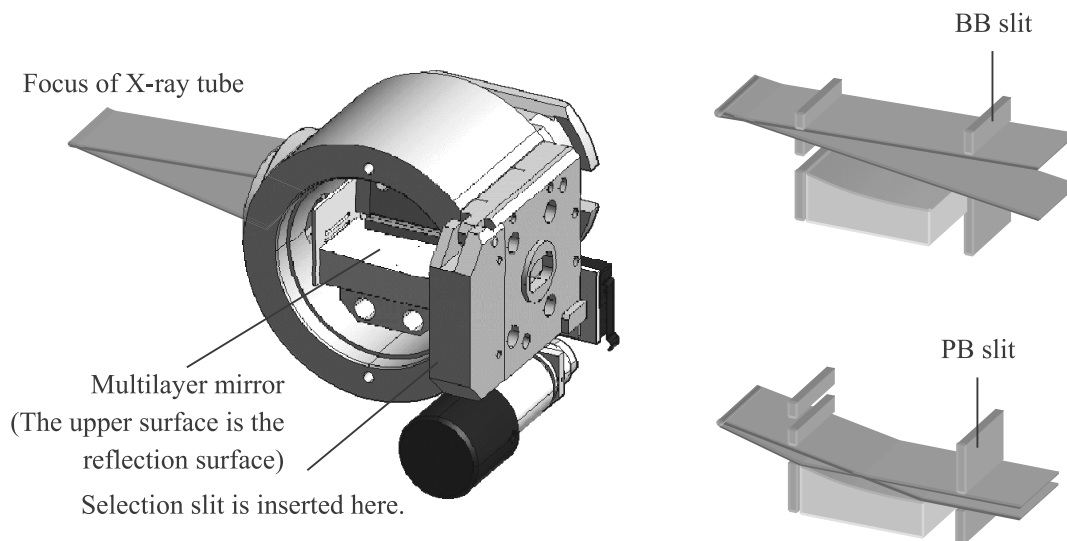


Fig. 1.3.2 CBO unit and structure of selection slit

### 1.3.2 Channel-Cut Crystal

A **channel-cut crystal** is an optical device that uses the diffraction phenomenon generated by a single crystal to monochromatize and collimate X-rays.

The channel-cut crystal used in the SmartLab and the RINT III series is a Ge single crystal block in which a channel is cut, with a structure consisting of two facing single crystals (Fig. 1.3.3). We use a Ge single crystal for its high crystallinity – Ge is sometimes referred to as a perfect crystal (only two types of single-element materials are referred to as perfect crystals: Si and Ge) – and for its atomic scattering factor, which is higher than that of Si.

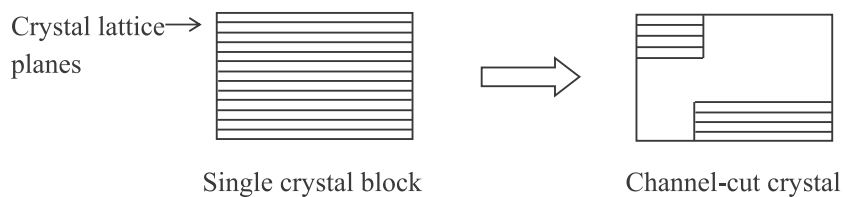


Fig. 1.3.3 Channel-cut crystal

Fig. 1.3.4 shows a schematic diagram of an X-ray beam incident on a channel-cut crystal. Among the X-rays incident on the channel-cut crystal, those incident at the diffraction angle  $\theta_B$  satisfying the Bragg formula are diffracted and output from the outlet of the channel-cut crystal. Since the crystallinity of the Ge single crystal is extremely high and significantly restricts diffraction, the X-ray beam is highly collimated and monochromatized after passing through the

channel-cut crystal.

The crystal structure reflects the X-rays twice, not once, to extract the X-ray beam parallel to the incident X-ray beam and simplify equipment design.

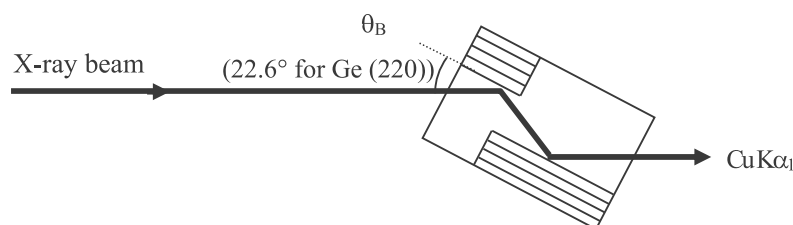


Fig. 1.3.4 Monochromatization and collimation of X-rays by Ge (220) channel-cut crystal

### 1.3.3 Optics Based on Channel-Cut Crystal

The incident and receiving optics based on a channel-cut crystal include those listed below.

- Incident optics – monochromator
  - Ge (220) double-crystal monochromator
  - Ge (220) four-crystal monochromator (SmartLab only)
  - Ge (400) double-crystal monochromator (SmartLab only)
- Receiving optics – analyzer
  - Ge (220) two-bounce analyzer (SmartLab only)
  - Ge (400) two-bounce analyzer (SmartLab only)

#### A. Monochromator

A channel-cut crystal used in the incident optics is called a **monochromator**. Inserted next to the CBO unit, a monochromator provides higher collimation and monochromaticity than a paraboloidal synthetic multilayer mirror. Channel-cut crystal monochromators are classified by the number of reflections and surface indices of the channel-cut crystal. Select a suitable model based on the crystallinity of the sample and the purpose of the measurement.

A **double-crystal monochromator** uses one channel-cut crystal (two reflections). A **four-crystal monochromator** combines two channel-cut crystals (four reflections), as shown in Fig. 1.3.5.

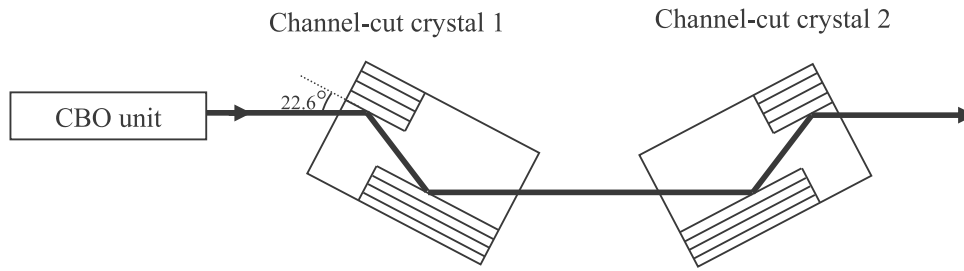


Fig. 1.3.5 Ge (220) four-crystal monochromator

The double-crystal monochromator and the four-crystal monochromator differ in the aspects listed below.

➤ Monochromaticity

The double-crystal monochromator can selectively extract only the  $\text{Cu K}\alpha_1$  line. The four-crystal monochromator can provide higher monochromaticity than the double-crystal monochromator and extracts only part of the  $\text{Cu K}\alpha_1$  line.

➤ Angular resolution

While the angular resolution (apparent X-ray divergence angle) of the X-rays output from the double-crystal monochromator depends on the diffraction angle of the measurement sample, the angular resolution of the X-rays output from the four-crystal monochromator is constant across a wide diffraction angle range. Fig. 1.3.6 shows the diffraction angle dependence of the angular resolution for each monochromator.

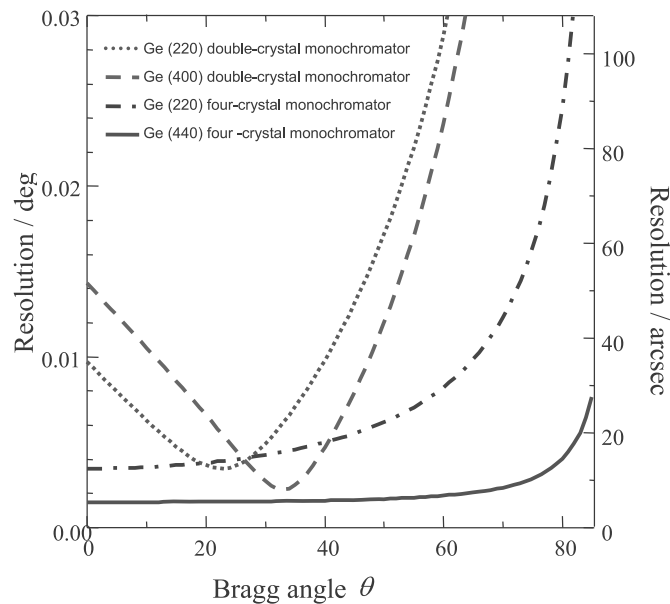


Fig. 1.3.6 Monochromators and their resolution

➤ Diffraction intensity

Since the four-crystal monochromator selects X-rays that more rigorously satisfy the diffraction condition, it results in lower X-ray intensity than the double-crystal monochromator.

Due to the preceding characteristics, select a double-crystal monochromator or four-crystal monochromator after considering both resolution and intensity. If the material and crystal lattice plane of the measured object are known, a suitable double-crystal monochromator can give both high resolution and high intensity, producing a profile rapidly. If the Bragg angle to be measured is in a low-resolution range with the double-crystal monochromator or if you need to measure various materials or two or more crystal lattice planes of the same material sequentially, select the more versatile four-crystal monochromator.

**The diffraction plane indices of the double-crystal monochromator** (Ge (220) and Ge (400)) differ in the aspects listed below.

➤ Diffraction angle dependence of angular resolution

As shown in Fig. 1.3.6, the double-crystal monochromator outputs X-rays with the angular divergence reaching the minimum (and thus the angular resolution in a diffraction measurement reaching the maximum) when the Bragg angle of the channel-cut crystal agrees with the Bragg angle of the measurement sample. The Bragg angle is  $\theta_B = 22.6^\circ$  for Ge (220) and  $\theta_B = 33.0^\circ$  for Ge (400).

➤ Diffraction intensity

The intensity of the X-rays output from a channel-cut crystal depends on the crystal structure factor of the crystal lattice planes used in the channel-cut crystal. The crystal structure factor corresponding to the Cu  $K\alpha$  line is 181.8 for Ge (220) and 155.1 for Ge (400). That is, when X-rays of the same intensity enter the crystal, X-rays diffracted on the Ge (220) crystal lattice planes have a greater intensity than those diffracted on the Ge (400) crystal lattice planes.

Given the preceding characteristics, select the Ge diffraction plane of the double-crystal monochromator based on the following criteria.

If the material and the crystal lattice plane of the measured object are known, it helps to use a monochromator with indices suitable for the diffraction angle. Since the diffraction angle of the Ge (400) monochromator ( $\theta_B =$  approximately  $33^\circ$ ) is close to the diffraction angles of GaAs (400) ( $\theta_B =$  approximately  $33.0^\circ$ ) and Si (400) ( $\theta_B =$  approximately  $34.5^\circ$ ), which are often used as substrates of thin film samples, this can be a powerful tool when evaluating epitaxial films deposited on these substrates.

Similarly, when measuring a material with a diffraction angle close to that of Ge (220) ( $\theta_B =$  approximately  $22.6^\circ$ ), the Ge (220) double-crystal monochromator can be useful. If we use a double-crystal monochromator simply to monochromatize the beam to the Cu  $K\alpha_1$  line, the Ge (220) double-crystal monochromator is more effective, since it has a higher crystal structure factor and provides higher intensity.

The diffraction plane indices of the **four-crystal monochromator** (Ge (220) and Ge (440)) differ in the aspects listed below.

➤ Angular resolution

A four-crystal monochromator provides high resolution across a wide diffraction angle range. Here, a channel-cut crystal with higher reflection indices provides higher monochromaticity and collimation.

➤ Diffraction intensity

Since the crystal structure factor of the Ge (440) plane is 121.3 and lower than the value (181.8) for the Ge (220) plane, the usable X-ray intensity is lower for the Ge (440) plane.

Given the preceding characteristics, select the Ge (440) four-crystal monochromator when measuring a single crystal substrate of a material with extremely high crystallinity (e.g., Si, GaAs, or quartz). If we use the Ge (440) four-crystal monochromator for a material with relatively low crystallinity, the measurement will be time-consuming, since the diffracted X-ray intensity from the sample is relatively low.

## B. Analyzer crystal

A channel-cut crystal used in the receiving optics is called an **analyzer**. An analyzer restricts both the  $2\theta$  take-off angle and wavelength, allowing precise observations of the diffraction angle. The  $2\theta$  angle receiving width of the Ge (220) analyzer crystal is approximately  $0.003^\circ$ .

When we use an analyzer crystal, we must also use receiving slits of the same width as the incident slit before and after the analyzer crystal to shield the scattered beam (analyzer streak) by multiple scattering (refer to Chapter 5) in the analyzer crystal.

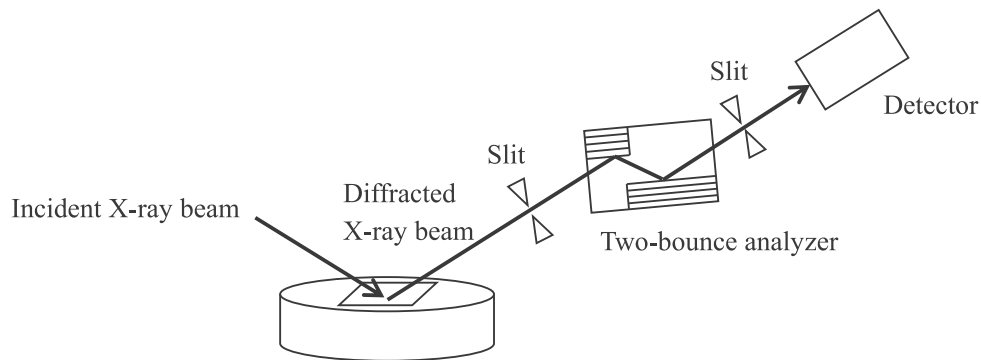


Fig. 1.3.7 Two-bounce analyzer



### 1.3.4 Width-Limiting Slit

A **width-limiting slit** restricts the size of the X-ray beam vertically. It can be controlled from the PC and is used in both incident and receiving optics.

#### A. Incident slit (IS in SmartLab and Divergence Slit (DS) in the RINT III series)

The width-limiting slit used in the incident optics restricts the width of the sample area irradiated by X-rays. In X-ray diffraction measurements, the change in area irradiated by X-rays must be suppressed during measurement, so that a sufficiently narrow slit is used to restrict the X-rays within the area of the sample, or conversely, a sufficiently wide slit is used to soak the sample in the X-rays (complete soaking). In contrast, with X-ray reflectivity measurements, a narrow slit is always used, since the area of X-ray irradiation in the sample area must be restricted. Fig. 1.3.9 shows the relationship between the width of the incident slit, the X-ray incident angle, and the width of the sample area irradiated by X-rays.

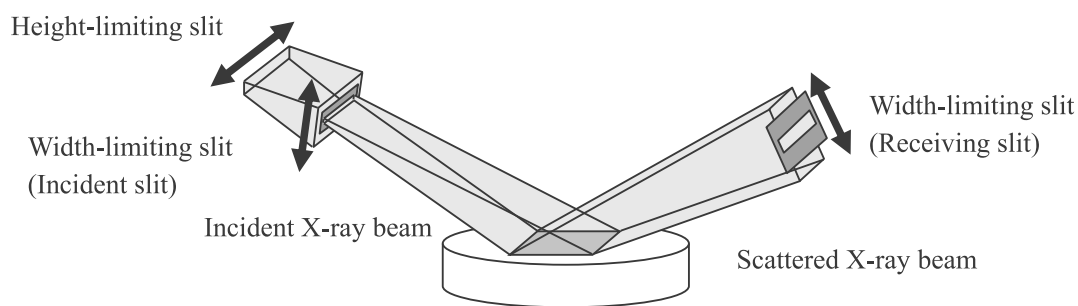


Fig. 1.3.8 Insertion direction of width-limiting slit and height-limiting slit

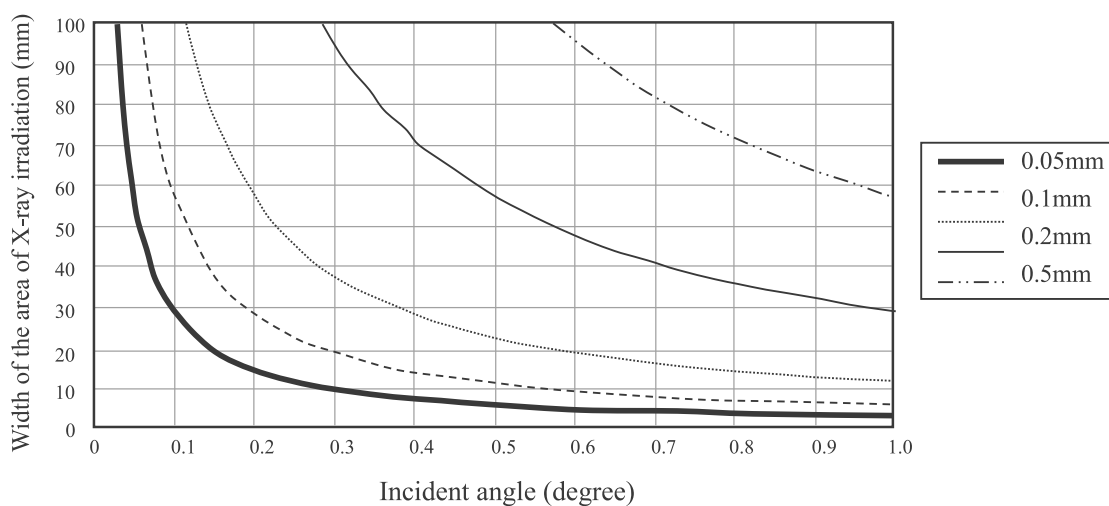


Fig. 1.3.9 Width of the area of X-ray irradiation determined by the incident slit

## B. Receiving slit (RS1 and RS2 in SmartLab and Scattering Slit (SS) and Receiving Slit (RS) in the RINT III series)

The receiving slits are used to determine the  $2\theta$  resolution or to shield the scattered X-rays.

In the symmetric  $2\theta/\omega$  measurement, in which the incident X-ray beam and the diffracted X-ray beam have the same width, the receiving slits are set to the same width as the incident slit to avoid blocking the diffracted X-rays. In thin film measurements ( $2\theta$  scan) or asymmetric  $2\theta/\omega$  measurements in which incident X-rays and diffracted X-rays have different widths or in in-plane measurements in which vertical angular resolution can be disregarded, measurements are performed with receiving slits set to widths different from the DS or with a completely open receiving slit combined with the Soller slit (described further below).

### 1.3.5 Height Limiting Slit (Length Limiting Slit)

The **height limiting slit** (the **length limiting slit** in SmartLab) restricts the width of the area of X-ray irradiation in the longitudinal direction.

The height limiting slit is used to determine the area irradiated by X-rays combined with the incident slit. Note that the paraboloidal synthetic multilayer mirror in the CBO unit collimates X-rays only vertically and that X-rays are permitted to disperse widely in the lengthwise longitudinal direction of the equipment. Thus, at the sample position, the X-ray beam spreads beyond the width set by the height limiting slit. When a thin-film sample is measured, the sample is also often rotated in-plane. For these reasons, we must select the slits after considering the width of the sample both laterally and longitudinally.



Fig. 1.3.10 Height limiting slit; left: SmartLab; right: RINT III series

### 1.3.6 Soller Slit

A **Soller slit** is a set of metal foils placed at constant intervals. It extracts only those X-rays parallel to the gaps between the metal foils, suppressing the divergence of the X-ray beam.

The divergence angle of the X-ray beam is smaller when the interval of the metal foils is smaller and the length of the Soller slit is longer. Fig. 1.3.11 shows a schematic diagram of the vertical Soller slit. The direction of collimation depends on the direction of the metal foils.

Horizontally-placed foils suppress vertical divergence of X-rays (**vertical Soller slit**), while vertically-placed foils suppress horizontal divergence of X-rays (**horizontal Soller slit**).

Angular resolution depends on the intervals at which metal foils are placed and the length of the Soller slit, ranging between several degrees to several tenth of a degree.

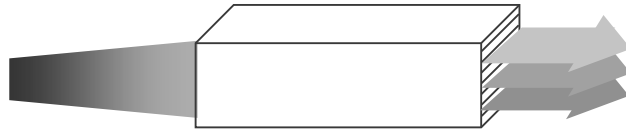


Fig. 1.3.11 Vertical Soller slit (Schematic diagram)

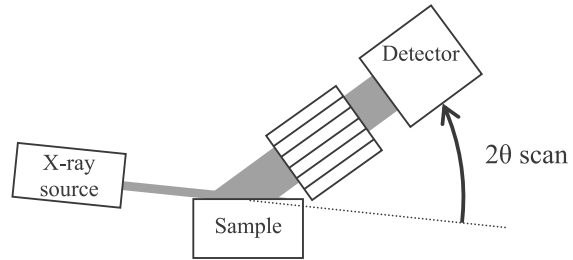
An advantage of a Soller slit is that it does not unnecessarily block wide X-ray beams while providing specific levels of angular resolution.

In measurements with a small X-ray incident angle with respect to the surface such as thin film measurements ( $2\theta$  scan), asymmetric  $2\theta/\omega$  measurements, and in-plane measurements, the irradiated area spreads widely, as does the width of the diffracted X-ray beam. If an ordinary slit is used to capture such X-ray beams, only part of the wide-diffracted beam will pass through the slit, resulting in loss of intensity. In contrast, a Soller slit has a large area through which X-rays can pass, allowing selection of only the X-rays incident in a specific range without blocking the widely spread X-ray beam.

The Soller slit for the receiving optics is designed so that a single Soller slit can be inserted vertically or horizontally. The user can set the slit by selecting the direction in which resolution is required. Two Soller slits can also be inserted side by side to set angular resolution simultaneously in the vertical and horizontal directions. This technique is used for in-plane pole figure measurements in which all possible out-of-plane and in-plane orientations take place.

Fig. 1.3.12 shows a schematic diagram of thin film and in-plane measurements in which the Soller slit is useful.

- Thin film measurement (Side view)  
A vertical Soller slit is used.



- In-plane measurement (Top view)  
A horizontal Soller slit is used.

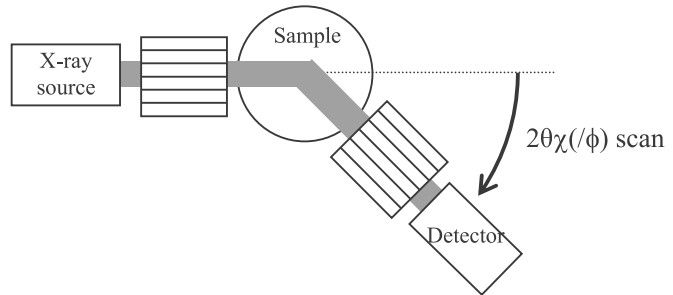


Fig. 1.3.12 Examples of measurement techniques using Soller slits

### 1.3.7 Examples of measurement techniques using Soller slits

In practical measurements, two or more optical devices are combined for measurement. Here, although higher resolution provides higher measurement precision, it reduces the intensity of the incident and diffracted X-ray beams and prolongs measurements. For efficient evaluations, we must select the optics based on the type of measurement intended and the sample condition. The selection criteria for the optics for each measurement technique are described in the measurement exercises and in the chapters on each of the measurement techniques.

## Summary

### Divergence angle of incident X-ray beam

| Name                       | Function   | Monochromaticity, $\Delta\lambda/\lambda$   | Divergence angle, $\Delta\theta$                                       |
|----------------------------|--|---|--|
| Multilayer mirror          | Suppression of divergence angle                                    | Cu K $\alpha$ /K $\beta$ intensity ratio from 100:25 to 1000:1                                  | 0.04°  |
| Channel-cut monochromator  | Suppression of divergence angle<br>Improvement in monochromaticity | $3.8 \times 10^{-4}$  | 0.008°<br>(Near $\theta = 0^\circ$ )                                   |
| Four-crystal monochromator | Suppression of divergence angle<br>Improvement in monochromaticity | Ge (220) four-crystal:<br>$1.5 \times 10^{-4}$<br>Ge(440) four-crystal:<br>$2.3 \times 10^{-5}$ | Ge (220) four-crystal:<br>0.0034°<br>Ge (440) four-crystal:<br>0.0015° |

### Receiving angle resolution

| Name             | Function   | Slit width (DS, SS, RS) | $2\theta$ resolution, $\Delta 2\theta$                   |
|------------------|--|-------------------------|--|
| Slit             | Improvement in $2\theta$ resolution  | Open                    | 0.84°  |
|                  |  | 2 mm                    | 0.34°  |
|                  |  | 1 mm                    | 0.17°  |
|                  |  | 0.5 mm                  | 0.084°   |
|                  |  | 0.2 mm                  | 0.034°   |
|                  |  | 0.1 mm                  | 0.017°   |
|                  |  | 0.05 mm                 | 0.0084°  |
| Analyzer crystal | Improvement in $2\theta$ resolution  |                         | 0.003°   |
| Soller slit      | Improvement in $2\theta$ or $2\theta\chi$ resolution (Depends on direction of insertion) |                         | (Often used for thin-film samples)<br>1°<br>0.4°<br>0.1° |

## Chapter 2 Reciprocal Lattice

The Bragg formula can be used to state the conditions under which the crystal diffracts the X-rays and to express the geometrical relationship between the positions of the crystal and the X-rays. The concept of the reciprocal lattice is introduced to more clearly illustrate the relationship between the crystal structure and the diffraction condition when describing the spread of the diffraction condition by disorders in crystallinity or when illustrating the mutual relationship between two or more lattice planes placed in three-dimensional space.

To clarify the principles of various diffraction measurement techniques using the reciprocal lattice concept, this chapter discusses how the reciprocal lattice is defined and why the concept of the reciprocal lattice is useful.

### §2.1 What is a Reciprocal Lattice?

This section discusses what a reciprocal lattice is and how it is defined.

#### 2.1.1 A Clear Expression

Before stating how a reciprocal lattice is defined, we will return to the previous discussion and consider how to express the diffraction and scattering of the X-rays by a crystal when discussing a complicated problem.

For example, Fig. 2.1.1 shows a drawing that directly expresses lattice planes three-dimensionally placed in space. Although it shows only three types of planes and their interplanar spacings  $d_{hkl}$ , the drawing is already extremely complex. Now, how are these lattice planes expressed in vector terms?

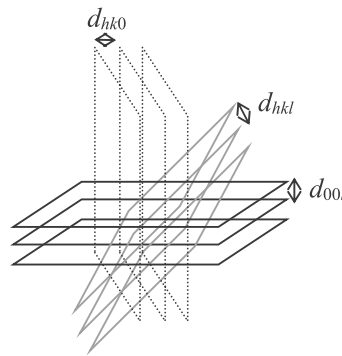


Fig. 2.1.1 Lattice planes (Planar representation)

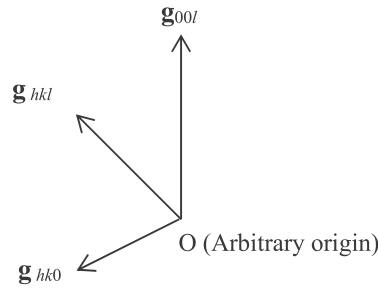


Fig. 2.1.2 Lattice planes (Vector representation)

We will represent the lattice planes with the vector  $\mathbf{g}_{hkl}$ . The direction of the vector  $\mathbf{g}_{hkl}$  is defined as identical to the normal to the corresponding lattice planes, while its length is defined to be identical to the inverse of the corresponding interplanar spacing. Fig. 2.1.2 shows a drawing of the lattice planes expressed with this vector representation. Compared to Fig. 2.1.1, replacing the planar representation of the lattice planes with the vector representation simplifies the drawing and makes it easy to understand. The vector used here is defined as follows:

The definition of the vector representing the lattice planes ( $hkl$ ):

1. Direction of lattice planes ( $hkl$ ): Identical to the normal to the lattice planes as drawn from the origin
2. Length of lattice planes ( $hkl$ ): Identical to the inverse of the interplanar spacing,  $d_{hkl}$ .

As specified above, the vector representing the lattice planes is called the **reciprocal lattice vector**, the starting point of the vector is called the **origin of the reciprocal lattice**, and the end point of the vector is called a **reciprocal lattice point**. The reciprocal lattice points corresponding to the lattice planes in a crystal form a regular lattice reflecting the crystal structure. This lattice is called the **reciprocal lattice**.

We will now consider a method for describing the diffraction condition and the spread of the diffraction condition generated by the crystal imperfections (degradation of crystallinity or disorders in the crystal lattice). First, we will illustrate the relationship between the lattice planes and the first-order X-ray beam diffracted by the planes, as in Fig. 2.1.3.

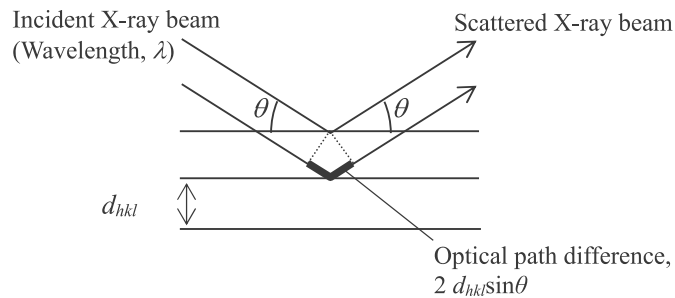


Fig. 2.1.3 Diffraction condition (planar expression)

In the representation of Fig. 2.1.3, the first-order diffraction condition is expressed by the following formula:

$$2d_{hkl} \sin \theta = \lambda \quad \text{Formula 2.1.1}$$

- $d_{hkl}$ : Interplanar spacing
- $\theta$ : Incident angle of the X-ray beam with respect to lattice planes
- $\lambda$ : Wavelength of the incident X-ray beam

However, it is difficult to express the spread of the diffraction condition generated by the imperfection of the crystal, for example, the fluctuation in the interplanar spacing  $d_{hkl}$  and the fluctuations in the orientation of the lattice planes (crystal orientation). Now, how would we express it in terms of the reciprocal lattice vector defined above? Fig. 2.1.4 illustrates the relationship between the reciprocal lattice vector corresponding to a set of lattice planes and the X-ray beam diffracted by the lattice planes.

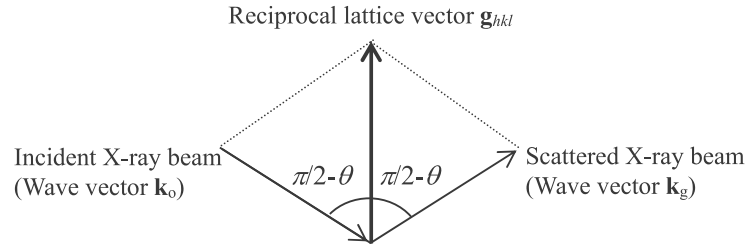


Fig. 2.1.4 Diffraction condition (Vector expression)

In this representation, the diffraction condition is expressed by the following formula:

$$\mathbf{k}_g - \mathbf{k}_o = \mathbf{g}_{hkl} \quad \text{Formula 2.1.2}$$

- $\mathbf{k}_o$ : Wave vector of incident X-ray beam
- $\mathbf{k}_g$ : Wave vector of scattered X-ray beam
- $\mathbf{g}_{hkl}$ : Reciprocal lattice vector

Here, a **wave vector** expresses an X-ray beam as a vector. It is defined as a vector whose orientation is the same as the direction of the X-ray beam and whose length equals  $1/\lambda$  (or  $2/\pi\lambda$ ), where  $\lambda$  is the wavelength. Formula (2.1.2) can be rewritten as follows, leading to the same expression as Formula (2.1.1).



$$\begin{aligned}
\mathbf{k}_g - \mathbf{k}_o &= \mathbf{g}_{hkl} \\
\rightarrow \frac{1}{\lambda} \cos(\pi/2 - \theta) + \frac{1}{\lambda} \cos(\pi/2 - \theta) &= \frac{1}{d_{hkl}} \\
\rightarrow 2d_{hkl} \sin \theta &= \lambda
\end{aligned}
\tag{Formula 2.1.3}$$

As shown in Fig. 2.1.5, in the representation in terms of the reciprocal lattice, for example, the spread in the diffraction condition due to fluctuations in interplanar spacing  $d_{hkl}$  and to fluctuations in the orientation of the lattice planes (crystal orientation) can be expressed as the spread in the length and direction, respectively, of the reciprocal lattice vector; that is, as the spread of the reciprocal lattice point. (Section 4.3 describes the details of the relationship between the crystal structure or crystallinity and the position or spread of the reciprocal lattice points.)

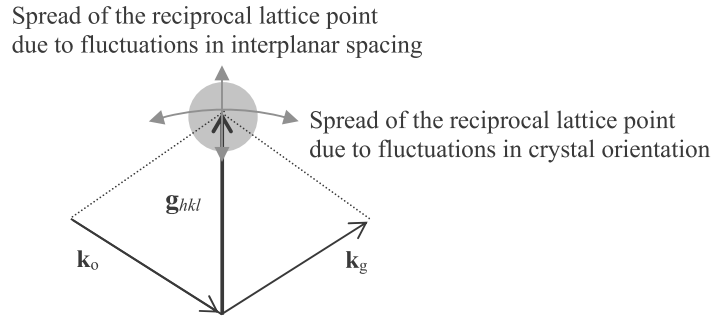


Fig. 2.1.5 Spread of diffraction condition and reciprocal lattice points

As discussed to this point, the concept of a reciprocal lattice is extremely useful when expressing the spread of the diffraction condition caused by imperfections in the crystal or when illustrating the relationship between lattice planes placed in three-dimensional space. This is because the concept can express the relationship between the crystal structure and diffraction condition in a manner that is easily understood.

## 2.1.2 Definition of the Reciprocal Lattice

Now we will consider the mathematical definition of the reciprocal lattice.

The space in which the actual lattice and the actual lattice planes exist is called the **real space**. The space in which the reciprocal lattice vectors exist is called **reciprocal space**. The actual lattice is called the **real lattice**. The crystal axes **a**, **b**, and **c**, the fundamental vectors of the real lattice, are expressed in real space. The lattice planes ( $hkl$ ) are defined as a set of planes for which the one closest to the origin intersects each of the axes at  $a/h$ ,  $b/k$ , and  $c/l$ , respectively.

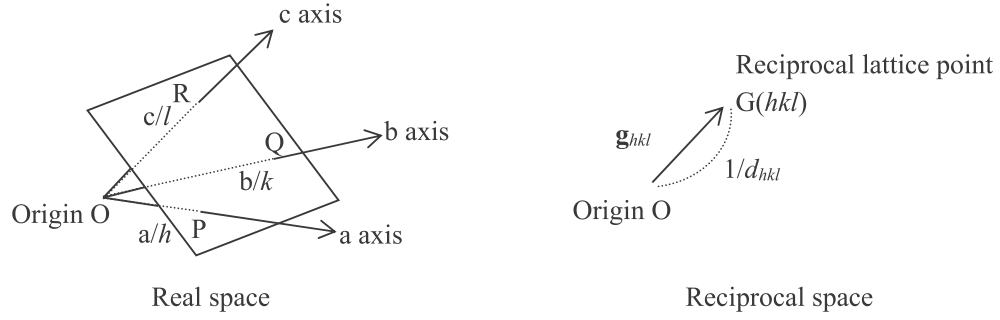


Fig. 2.1.6 Real space and reciprocal space

As discussed in the previous section, the direction of the reciprocal lattice vector  $\mathbf{g}_{hkl}$  is the same as the normal to a corresponding lattice plane, and thus parallel to the vector product  $\mathbf{p}$  of two vectors in the lattice plane. If we denote  $\mathbf{g}_{hkl}$  as  $K\mathbf{p}$  ( $K$  times  $\mathbf{p}$ ), where  $K$  is a constant, we obtain the following formula:

$$K\mathbf{g}_{hkl} = \mathbf{p} = \overrightarrow{PQ} \times \overrightarrow{QR} = \left(\frac{\mathbf{b}}{k} - \frac{\mathbf{a}}{h}\right) \times \left(\frac{\mathbf{c}}{l} - \frac{\mathbf{b}}{k}\right) = \frac{\mathbf{b} \times \mathbf{c}}{kl} + \frac{\mathbf{c} \times \mathbf{a}}{lh} + \frac{\mathbf{a} \times \mathbf{b}}{hk} \quad \text{Formula 2.1.4}$$

At the same time, the interplanar spacing  $d_{hkl}$  equals, for example, the length of  $\mathbf{a}/h$  projected onto the unit vector  $\mathbf{g}_{hkl}/g_{hkl}$ , in the direction normal to the lattice plane, leading to the following formula:

$$\frac{\mathbf{a}}{h} \cdot \frac{\mathbf{g}_{hkl}}{g_{hkl}} = d_{hkl} \quad \text{Formula 2.1.5}$$

Here, based on Formula (2.1.4) and the fact that the length  $g_{hkl}$  of the reciprocal lattice vector equals the inverse of  $d_{hkl}$ , the value of the constant  $K$  can be obtained from Formula (2.1.5).

$$\begin{aligned} \frac{\mathbf{a}}{h} \cdot K\mathbf{p} &= 1 \\ \rightarrow K &= \frac{hkl}{\mathbf{a} \cdot (\mathbf{b} \times \mathbf{c})} \end{aligned} \quad \text{Formula 2.1.6}$$

The expression  $\mathbf{a} \cdot (\mathbf{b} \times \mathbf{c})$  in Formula (2.1.6) gives the volume of the unit cell. Denoting this volume  $v_c$ , we can express constant  $K$  as  $K = hkl/v_c$ . From Formula (2.1.4),  $\mathbf{g}_{hkl}$  is expressed by the following formula:

$$\mathbf{g}_{hkl} = h \frac{\mathbf{b} \times \mathbf{c}}{v_c} + k \frac{\mathbf{c} \times \mathbf{a}}{v_c} + l \frac{\mathbf{a} \times \mathbf{b}}{v_c} \quad \text{Formula 2.1.7}$$

Here, we define the fundamental vectors  $\mathbf{a}^*$ ,  $\mathbf{b}^*$ , and  $\mathbf{c}^*$  in the reciprocal lattice corresponding to fundamental vectors,  $\mathbf{a}$ ,  $\mathbf{b}$ , and  $\mathbf{c}$  in the real lattice as follows:

$$\mathbf{a}^* = \frac{\mathbf{b} \times \mathbf{c}}{v_c}, \quad \mathbf{b}^* = \frac{\mathbf{c} \times \mathbf{a}}{v_c}, \quad \mathbf{c}^* = \frac{\mathbf{a} \times \mathbf{b}}{v_c} \quad \text{Formula 2.1.8}$$

After denoting the fundamental vectors of the reciprocal lattice in this way, we can rewrite the reciprocal lattice vector representing the reciprocal lattice point,  $G(hkl)$  corresponding to lattice planes  $(hkl)$  in the formula below obtained from Formula (2.1.7).

$$\mathbf{g}_{hkl} = h\mathbf{a}^* + k\mathbf{b}^* + l\mathbf{c}^* \quad \text{Formula 2.1.9}$$

## §2.2 Reciprocal Lattice and Diffraction Conditions

In the previous section, we discussed how to define reciprocal lattice points. This section discusses how incident and scattered X-ray beams are expressed in reciprocal space and how the corresponding diffraction condition is expressed.

### 2.2.1 Reciprocal Lattice and Diffraction Conditions

As discussed in Section 4.1.1, incident and scattered X-ray beams are represented in the reciprocal lattice by the wave vectors  $\mathbf{k}_o$  and  $\mathbf{k}_g$ , respectively, where the vector orientations are identical to the direction of propagation of the X-ray beams, and where the vector lengths are given by  $1/\lambda$ . The scattering specified by  $\mathbf{k}_o$  and  $\mathbf{k}_g$  is defined by the sum  $\mathbf{K}$  of these vectors. This vector  $\mathbf{K}$  is known as the **scattering vector**.

$$\mathbf{k}_g - \mathbf{k}_o = \mathbf{K} \quad \text{Formula 2.2.1}$$

- $\mathbf{k}_o$  : Wave vector of incident X-ray beam
- $\mathbf{k}_g$  : Wave vector of scattered X-ray beam
- $\mathbf{K}$  : Scattering vector

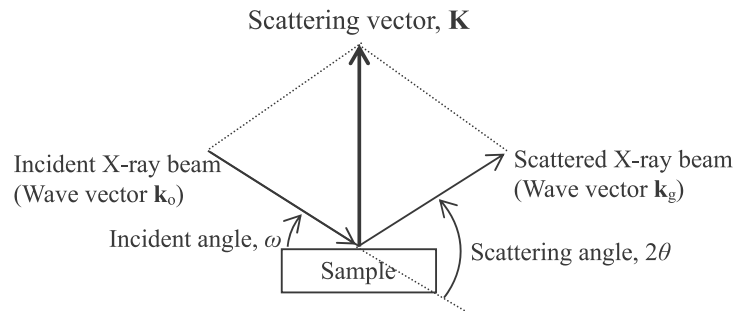


Fig. 2.2.1 Scattering vector

As we see when we compare Formulas (2.1.2) and (2.2.1), when the scattering vector  $\mathbf{K}$  agrees with the reciprocal lattice vector  $\mathbf{g}_{hkl}$  corresponding to the lattice planes ( $hkl$ ), the diffraction condition is met, and we observe a strong diffracted X-ray beam. Thus, the diffraction condition can be expressed by the following formula:

$$\mathbf{k}_g - \mathbf{k}_o = \mathbf{g}_{hkl} \quad \text{Formula 2.2.2}$$

Here, let us consider the relationship between the change in the incident angle or exit angle of the X-ray beam with respect to the sample and the change in the point indicated by the scattering vector  $\mathbf{K}$  (the point observed in the reciprocal space).

### 1. Maintaining the scattering angle and changing the incident angle

If the scattering angle is kept constant and only the incident angle is changed—that is, if only the sample is rotated—the relationship between the scattering vector and the sample changes as shown in Fig. 2.2.2. In this case, the length of the scattering vector is kept constant and only the direction with respect to the sample surface changes. That is, we can observe the diffraction by lattice planes with the same interplanar spacing (length of the reciprocal lattice vectors) but different orientations (directions of the reciprocal lattice vectors) by scanning the incident angle while maintaining the scattering angle.

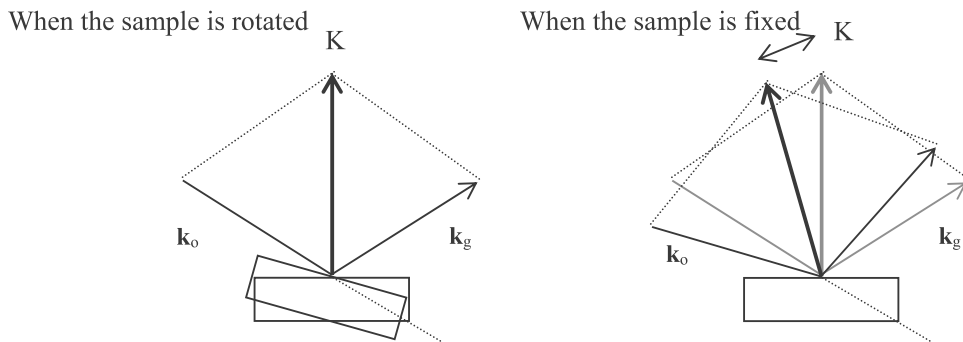


Fig. 2.2.2 Change in sample direction

### 2. Maintaining the equal incident angle and exit angle and changing the scattering angle

If the incident angle and the exit angle are kept equal and only the scattering angle is changed, the scattering vector will change as shown in Fig. 2.2.3. In this case, the direction of the scattering vector is kept constant; only its length changes. That is, we can observe diffraction by lattice planes with the same orientation (direction of reciprocal lattice vectors) but with different interplanar spacings (lengths of the reciprocal lattice vectors) by scanning the scattering angle while keeping the incident angle and exit angle equal.

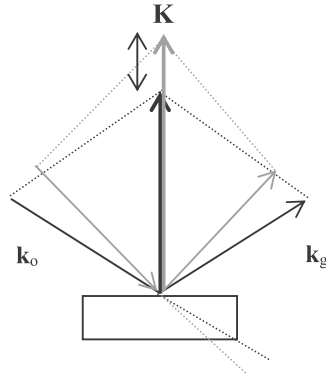


Fig. 2.2.3 Change in scattering angle

### 3. Keeping the exit angle constant and changing the incident angle

If we keep the exit angle constant and change only the incident angle, the scattering vector will change as shown in Fig. 2.2.4. In this case, both the orientation and length of the scattering vector change. We can observe the diffraction by lattice planes with different orientations (directions of the reciprocal lattice vectors) and different interplanar spacings (lengths of the reciprocal lattice vectors). The divergence angle of the incident X-ray beam can also be regarded as a change in the incident angle. If the divergence angle of the incident X-ray beam is large, the diffraction condition spreads in the direction of the arrow, indicating the change in the scattering vector in Fig. 2.2.4.

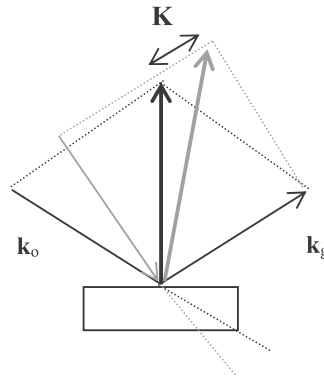


Fig. 2.2.4 Change in incident angle

### 4. Keeping the incident angle constant while changing the exit angle

If we keep the incident angle constant while changing only the exit angle, the scattering vector will change as shown in Fig. 2.2.5. As in the case in which we change only the incident angle, both the orientation and length of the scattering vector change. That is, we can observe the diffraction by lattice planes with different orientations (directions of the reciprocal lattice

vectors) and different interplanar spacings (lengths of the reciprocal lattice vectors). The receiving angle width when observing the scattered X-ray beam can also be regarded as the change in the exit angle. If the receiving angle width is large, the diffraction condition spreads in the direction of the arrow, indicating the change in the scattering vector in Fig. 2.2.5.

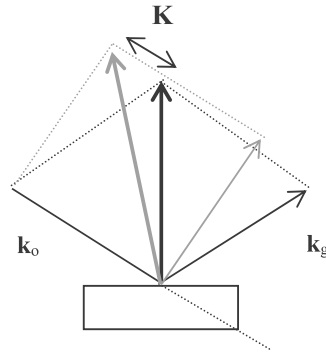


Fig. 2.2.5 Change in exit angle

### 2.2.2 Ewald Sphere

Showing vectors  $\mathbf{k}_o$  and  $\mathbf{k}_g$  in reciprocal space with their origins at the same point, Fig. 2.2.6 expresses the trajectory of the scattering vector observed with X-ray beams of a specific wavelength; that is, with a wave vector of a specified length, regardless of the incident or exit angle of the X-ray beam with respect to the sample.

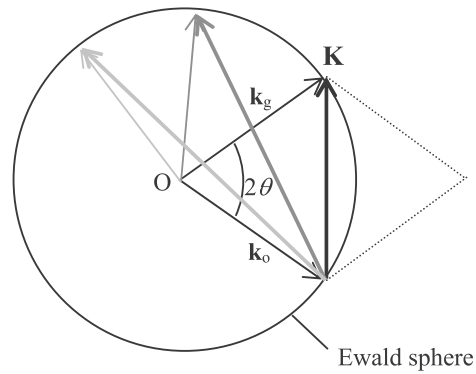


Fig. 2.2.6 Trajectory of scattering vector observed with a specific wavelength (Ewald sphere)

The radius of the circle shown in Fig. 2.2.6 is  $k = k_o = k_g = 1/\lambda$ . The center of the circle is the origin of the reciprocal lattice. It represents the trajectory of the scattering vector that can be observed by an X-ray beam of wavelength  $\lambda$ . Called the **Ewald sphere**, this sphere is defined as a sphere in three-dimensional space.

The change isolated to the exit angle discussed in the last of Section 4.2.1 corresponds to the rotation around  $\mathbf{k}_g$  alone in Fig. 2.2.6. The tip of the scattering vector, or the point at which scattering can be observed, is a moving point on the Ewald sphere.

## §2.3 Reciprocal Lattice and Crystal Structure

To grasp the relationship between the reciprocal lattice and measurement, first consider how the position, size, and spread of a reciprocal lattice point correspond to the physical states of the crystal structure and crystallinity.

As discussed in the previous section, the reciprocal space dimensional are values inversely related to those in real space. When the crystallite is small or when crystallinity is low and the region in which the atoms are regularly arranged is small, the reciprocal lattice points are large. That is, the distribution (angular dependence) of the X-ray diffraction intensity corresponds to the Fourier transform of the spatial distribution (position dependence) of the electron density in the material. To give an intuitive sense of this property, this section discusses the relationship between the crystal lattice and the reciprocal lattice and how various disorders in the crystal structure (degraded crystallinity) affect the reciprocal lattice points.

### 2.3.1 Crystal Lattice and Reciprocal Lattice

A crystal lattice contains lattice planes with various orientations and interplanar spacings. This section discusses how the reciprocal lattice points corresponding to these lattice planes are arranged in reciprocal space to form the reciprocal lattice.

Using the relationship defined in Section 4.1, we can draw the reciprocal lattice corresponding to a crystal lattice. The face-centered cubic lattice shown in Fig. 2.3.1 (a) produces the reciprocal lattice shown in Fig. 2.3.1 (b). Here, based on the extinction rule of the original crystal lattice, reciprocal lattice points not contributing to diffraction are removed.

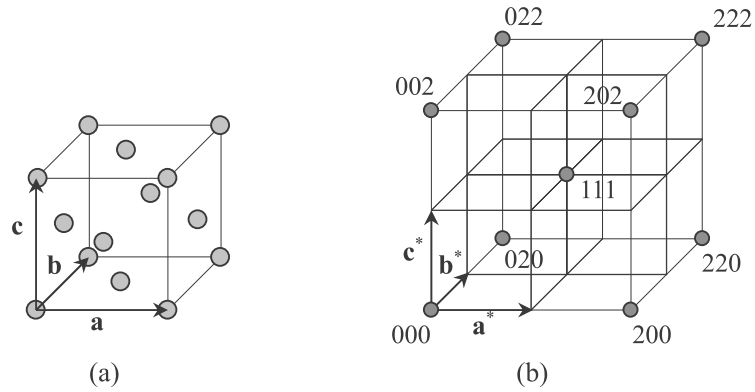


Fig. 2.3.1 Face-centered cubic lattice (a) and the corresponding reciprocal lattice (b)

As implied by the definition of the fundamental vectors of the reciprocal lattice, in the example of a tetragonal lattice with  $c$  axis longer than the  $a$  and  $b$  axes, the corresponding reciprocal lattice is shorter in the  $c^*$  direction and longer in the  $a^*$  and  $b^*$  directions.

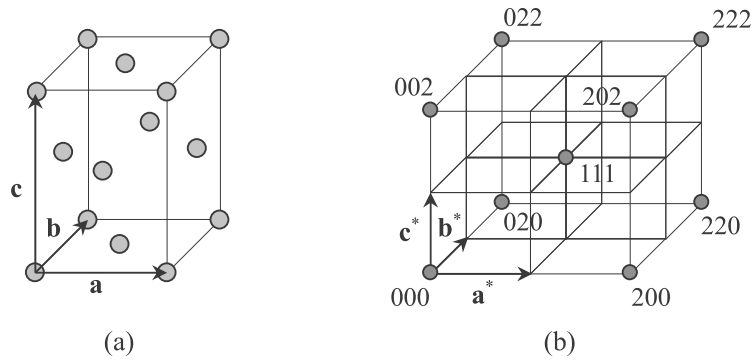


Fig. 2.3.2 Face-centered tetragonal lattice (a) and the corresponding reciprocal lattice (b)

Fig. 2.3.1 and Fig. 2.3.2 indicate only part of the reciprocal lattice. An infinite number of reciprocal lattice points corresponding to higher order reflection planes exist farther from the origin. However, the number of reciprocal lattice points that can be observed by an X-ray beam with a specific wavelength is limited. This is because it is practically impossible to observe diffractions whose diffraction angles exceed  $180^\circ$ . Consider an example in which we use the  $\text{Cu K}\alpha_1$  lines to observe various diffraction planes in a Si single crystal (diamond structure,  $a = 5.431 \text{ \AA}$ ) whose (001) plane is parallel to the surface. Among the reciprocal lattice points of Si shown in Fig. 2.3.3, only those at a distance from the origin—that is, those for which the diffraction angle does not exceed  $180^\circ$ —are observed.



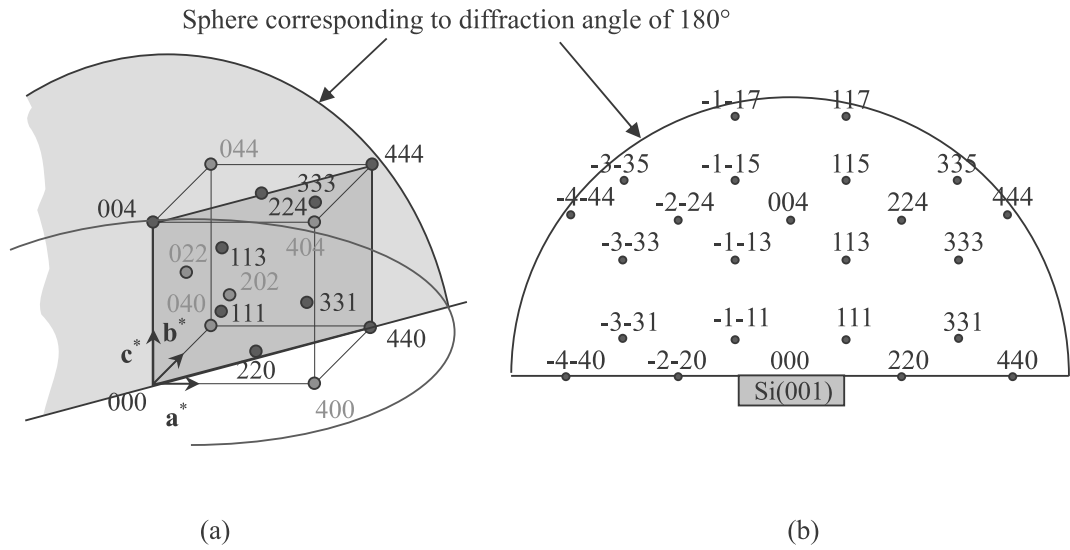


Fig. 2.3.3 Reciprocal lattice and observable range

(Part of reciprocal lattice (a) and the corresponding cross section (b))

Fig. 2.3.4 shows the incident and scattered X-ray beams added to Fig. 2.3.3(a).

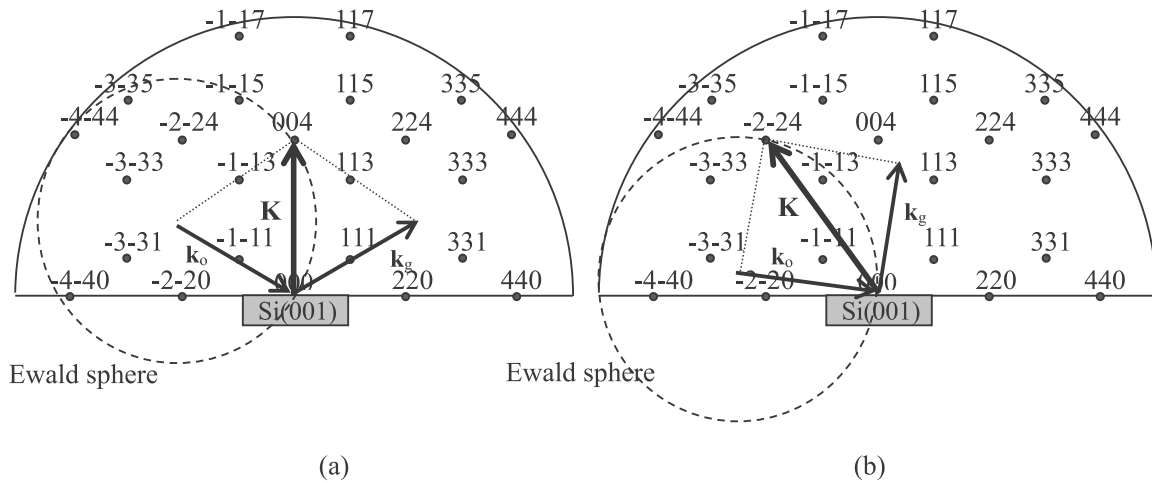


Fig. 2.3.4 Reciprocal lattice and X-ray beams

((a) Diffraction by (004) plane, (b) Diffraction by (-2-24) plane)

As implied by Fig. 2.3.3, we observe diffraction by the (004) plane, which is parallel to the surface, when the incident angle and the exit angle of the X-rays with respect to the sample surface equals the Bragg angle. We observe diffraction by the (-2-24) plane, which is tilted with respect to the surface, when the incident angle is small and the exit angle is large (or vice versa). The former is called a **symmetric reflection** while the latter is called an **asymmetric reflection**.

Fig. 2.3.4 shows the plane (scattering plane) in which the incident and scattered X-ray beams are present in the reciprocal space. This is a cross section of the reciprocal lattice. When the sample is rotated in-plane (i.e., with the surface normal as the rotation axis), other reciprocal lattice points appear on the scattering plane. We can observe the diffraction corresponding to a reciprocal lattice point on the scattering plane by selecting the appropriate incident and scattering angles of the X-ray beam with respect to the sample surface.

This section provided an overview of the reciprocal lattice in drawings and discussed how X-ray beams and diffraction conditions are expressed in drawings. The next and subsequent sections will focus on a single reciprocal lattice point and discuss how disorders in the crystal structure (degraded crystallinity) affect the reciprocal lattice point.

### 2.3.2 Size of Crystallite and Spread of Reciprocal Lattice Point

Except in very few crystals of extremely high crystallinity, the intensity of the X-rays diffracted by a crystal is proportional in many cases to the Laue function. Thus, if an orderly real lattice stretches over a large region, diffraction conditions become quite strict, dramatically restricting the range of diffraction angles over which we can observe diffraction intensity.

If an orderly real lattice occupies only a small region and has mismatches in slightly distant positions or ends there, the diffraction conditions become less rigorous, and the range of diffraction angles over which we observe diffraction intensity broadens. That is, the reciprocal lattice point spreads.

Fig. 2.3.5 assumes the  $q_x$  and  $q_y$  axes (refer to Section 4.3.3 regarding  $q_x$  and  $q_y$ ) in the reciprocal space and shows the above property as a two-dimensional distribution of diffraction intensity. As an example, the figure shows the value  $L$  of the Laue function calculated for ( $N_a = 10$ ,  $N_b = 10$ ) and ( $N_a = 4$ ,  $N_b = 4$ ), where  $N_a$  is the number of lattice repeats along the direction of the **a** axis and  $N_b$  is the number of lattice repeats along the direction of the **b** axis. Diffraction intensity in many crystals is proportional to  $L$ .

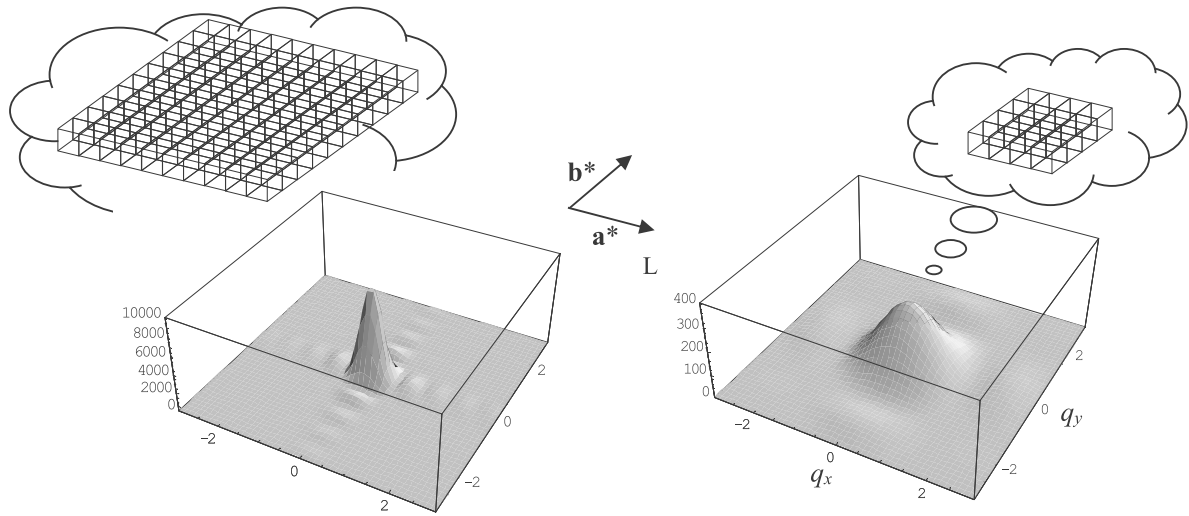


Fig. 2.3.5 Diffraction intensity distribution near reciprocal lattice point

(Left: ( $N_a = 10, N_b = 10$ ); right: ( $N_a = 4, N_b = 4$ ))

As implied by Fig. 2.3.5, diffraction intensity is lower and the distribution range wider for a smaller number of repeats of the unit cell; that is, for a smaller crystal region with a regular arrangement of atoms.

These are isotropic examples of the same crystal size along the direction of the  $\mathbf{a}$  and  $\mathbf{b}$  axes. What happens if the crystal is dimensionally anisotropic? Fig. 2.3.6 shows  $L$  for ( $N_a = 10, N_b = 4$ ).

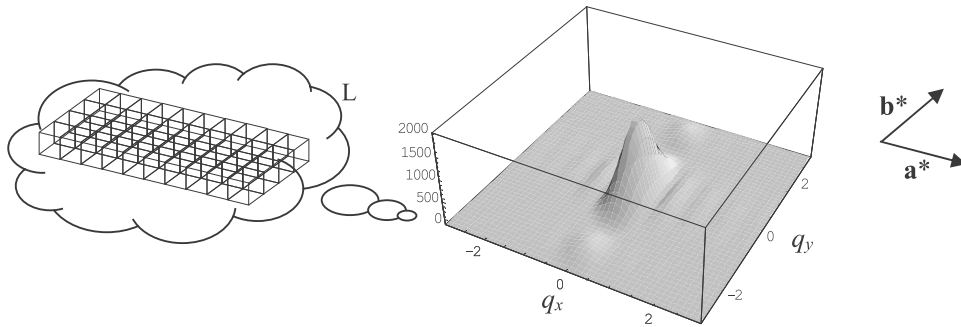


Fig. 2.3.6 Diffraction intensity distribution near reciprocal lattice point

( $N_a = 10, N_b = 4$ )

As implied by Fig. 2.3.6, if the crystal is dimensionally anisotropic, this anisotropy is reflected in the intensity distribution of the diffracted X-rays in the reciprocal space. The distribution is narrower in the direction of larger crystal size and wider in the direction of smaller crystal size.

Fig. 2.3.7 summarizes these properties on the scattering plane.

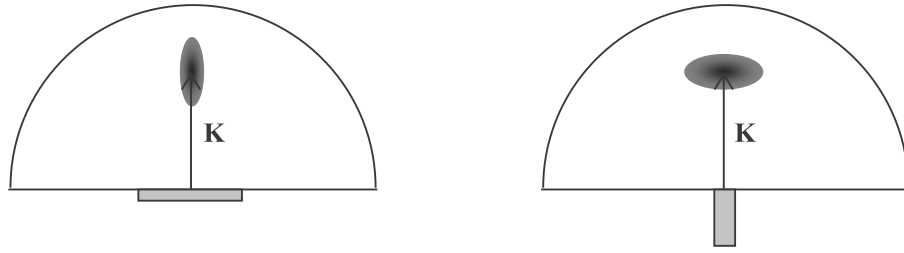


Fig. 2.3.7 Crystal size and spread of reciprocal lattice points

(When the crystal is a thin disk (left) and when the crystal is a thin column (right))

In this way, by measuring the diffracted X-ray intensity distribution, or the spread in reciprocal lattice points, we can assess the size of the crystal region in which the atoms are regularly arranged.

### 2.3.3 Change in Lattice Constants and Position of Reciprocal Lattice Points

Since the length of the reciprocal lattice vector indicating the position of the reciprocal lattice point is defined to be the inverse of interplanar spacing  $d$  of the corresponding lattice plane, the distance between the reciprocal lattice point and the origin of the reciprocal lattice is greater when  $d$  is shorter and shorter when  $d$  is longer. Fig. 2.3.8 illustrates this relationship.

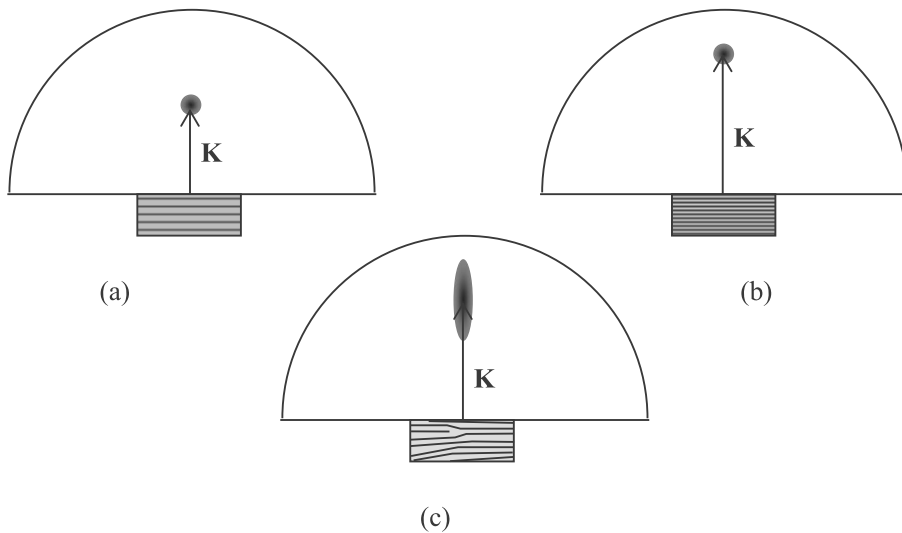


Fig. 2.3.8 Change in interplanar spacing  $d$  and the position of reciprocal lattice points

((a) when  $d$  is long, (b) when  $d$  is short, (c) when  $d$  fluctuates)

As shown in Fig. 2.3.8, we can assess interplanar spacing  $d$ , or the magnitude of the lattice constant and its fluctuations, by measuring the position and spread of the reciprocal lattice point.

#### 2.3.4 Change in Crystal Orientation and Position of Reciprocal Lattice Points

The direction of the reciprocal lattice vector indicating the position of the reciprocal lattice point is defined to be identical to the normal to the corresponding lattice plane. If the direction of the lattice plane changes (i.e., the orientation of the crystal lattice changes), the direction of the reciprocal lattice vector also changes. Fig. 2.3.9 shows this relationship.

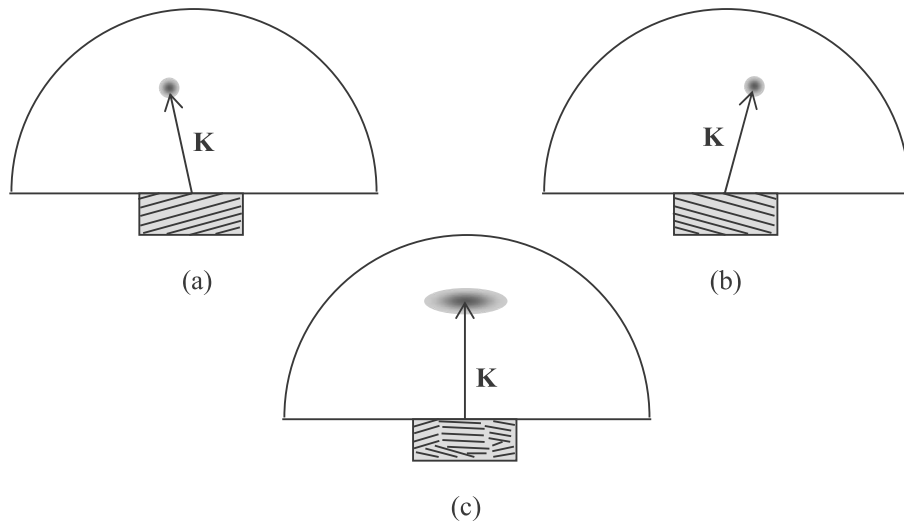


Fig. 2.3.9 Change in crystal orientation and position of reciprocal lattice points

((a) and (b) when the orientation is tilted, (c) when the orientation fluctuates)

As shown in Fig. 2.3.9, the change or fluctuation in interplanar spacing and the change or fluctuation in crystal lattice orientation affect the position and spread of the reciprocal lattice point in different ways. We can isolate these aspects of the crystal structure by measuring these changes.

#### §2.4 Reciprocal Lattice and Measurement Axes

The sections up to this point have discussed the relationship between the crystal lattice and the reciprocal lattice and the method of expressing the diffraction condition. We have also found that a change in crystal structure and crystallinity is observed as a change in the position or shape of the reciprocal lattice point. However, when measuring the position or shape of the reciprocal lattice point in practical measurements to evaluate crystal structure or the crystallinity, we need to understand the relationship between the reciprocal lattice and the measurement axes. This section discusses the relationship between the rotation axes of the sample or of the goniometer and the reciprocal lattice.

### 2.4.1 Four-Circle Goniometer

In the goniometers typically used to measure single crystals or strongly oriented polycrystals, the rotation axes of the sample and the counter, or the rotation axes of the goniometer, are defined as in Fig. 2.4.1.

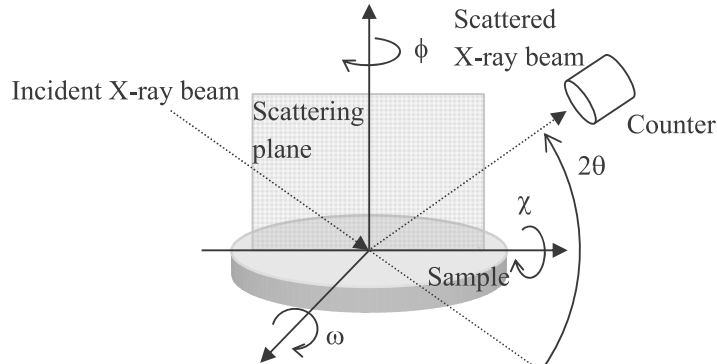


Fig. 2.4.1 Rotation axes of goniometer

In general, a goniometer with four rotation axes (three for rotating the sample and one for rotating the counter) is called a **four-circle goniometer**. The rotation axis corresponding to the incident angle of the X-ray beam in the scattering plane is called the  $\omega$  axis. The rotation axis (swing axis) perpendicular to the scattering plane is called the  $\chi$  axis. The rotation axis for the in-plane rotation of the sample is called the  $\phi$  axis. By rotating these three axes, we can orient the sample to any desired angle. The rotational angle of the counter with respect to the incident X-ray beam, or the diffraction angle, is called the  $2\theta$  axis.

Fig. 2.4.2 shows the relationship between the axes indicated in Fig. 2.4.1 in the reciprocal space.

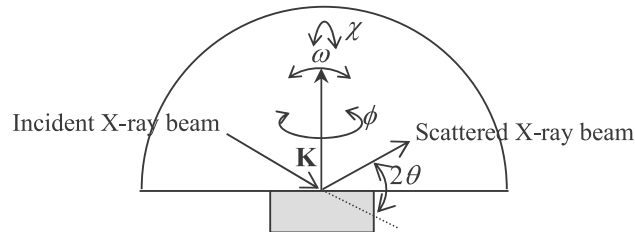


Fig. 2.4.2 Relationship between axes in reciprocal space

Fig. 2.4.2 shows the scattering plane, including incident and scattered X-ray beams. Section 4.3.1 stated that we can measure diffraction by a reciprocal lattice point on the scattering plane if the appropriate incident angle and scattering angle are selected. However, measurements by the reflection method face the limitations described below with respect to the range that can be measured.

For example, when we measure a thin-film sample on a substrate, we must select a lattice plane so that the X-ray beam enters and exits from the surface. By doing so, we obtain sufficiently strong diffracted X-ray intensity. When the incident and exit angles are restricted in this manner, an ordinary four-circle goniometer has **blind regions** on the scattering plane in the reciprocal lattice in which measurement cannot be performed.

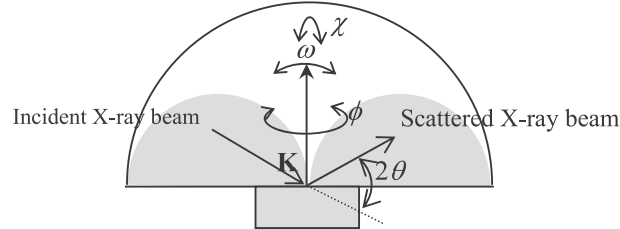
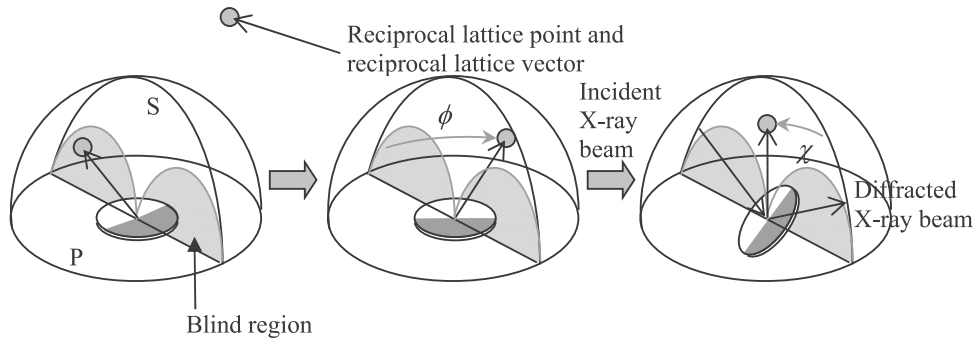


Fig. 2.4.3 Blind regions

The two semi-circular shadowed regions shown in Fig. 2.4.3 are blind regions. If we try to measure reciprocal lattice points in these regions, the geometry requires the incident X-ray beam to enter the sample from the side or rear of the sample (semi-circular region on the left) or the scattered X-ray beam to exit the sample from the side or rear of the sample (semi-circular region on the right).

To observe reciprocal lattice points in these blind regions, we need to rotate the  $\chi$  and  $\phi$  axes and move the reciprocal lattice points to the observable region (out of the blind regions).



S: Scattering plane P: Plane perpendicular to scattering plane and passing through the origin

Fig. 2.4.4 Moving reciprocal lattice points to observable region

As shown in Fig. 2.4.4, we can move a reciprocal lattice point out of the blind regions by rotating the  $\phi$  axis (sample in-plane rotation axis). We can then place the reciprocal lattice point on the scattering plane once again by rotating the  $\chi$  axis (sample swing axis). In this way, we can measure reciprocal lattice points in the observable region in the scattering plane in a geometry in which X-rays enter and exit from the surface of the sample.

However, if we measure a reciprocal lattice point as described above, we must rotate the sample swing axis through a large angle. Here, if we use a line-shaped X-ray beam, we confront the problem of incident X-ray beams irradiating out of the sample. This effect is especially marked if we measure the reciprocal lattice points in a part of the blind region near the plane perpendicular to the scattering plane and passing through the origin (P in Fig. 2.4.4). The reciprocal lattice point to be used in measurement must be selected with care.

### 2.4.2 Goniometer for In-Plane Measurement

Now we will discuss a goniometer that resolves the problem of incident X-ray beams irradiating out of the sample when we rotate the sample through the swing angle. This goniometer is used in measurements to extract precise data on the sample surface and interfaces (in-plane measurements).

Fig. 2.4.5 shows the rotation axes of the in-plane goniometer.

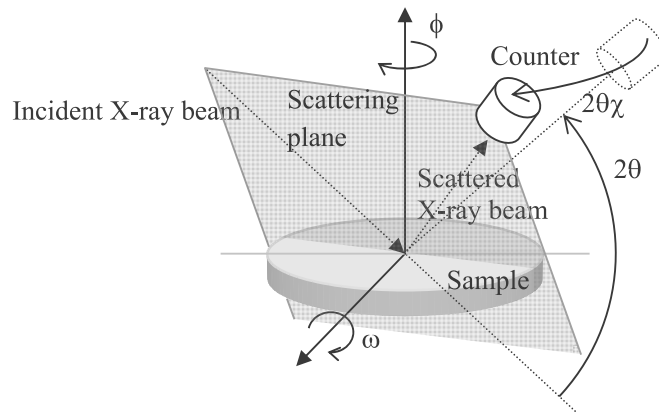


Fig. 2.4.5 Rotation axes of in-plane goniometer

The in-plane goniometer rotates the counter around the axis perpendicular to the axis of the  $2\theta$  rotation. This corresponds to pulling the counter to the front instead of repositioning the sample to face the front by tilting it  $90^\circ$ . This axis resolves the problem of incident X-ray beams irradiating out of the sample encountered in measurements with large sample swing angles (i.e., with a large  $\chi$  axis). To enable this type of measurement, the in-plane goniometer adds a  $2\theta\chi$  axis to the counter to supplement the  $2\theta$  axis.



This goniometer makes it possible to measure the reciprocal lattice points in the plane perpendicular to the scattering plane and passing through the origin (P in Fig. 2.4.4) as well as reciprocal lattice points in the blind regions. This measurement technique is called **in-plane measurement**, since it measures the diffraction that occurs in the in-plane direction of the sample surface.

Here, Fig. 2.4.6 helps clarify why the  $2\theta\chi$  axis has the same function as the  $\chi$  axis in the sense that it moves a reciprocal lattice point to an observable region (moves it out of the blind regions) and places it once again on the scattering plane. Fig. 2.4.6 shows the relationship in reciprocal space between the rotation axes indicated in Fig. 2.4.5. Compared to the four-circle goniometer in Fig. 2.4.2, the  $\chi$  axis that rotates the sample corresponds to the  $2\theta\chi$  axis that rotates the scattering plane. To observe a reciprocal lattice point, the reciprocal lattice point must be placed on the scattering plane. Here, it does not matter whether the sample (the reciprocal lattice itself) or the scattering plane is rotated as the counter is rotated. The former corresponds to the ordinary four-circle goniometer; the latter corresponds to the in-plane goniometer.

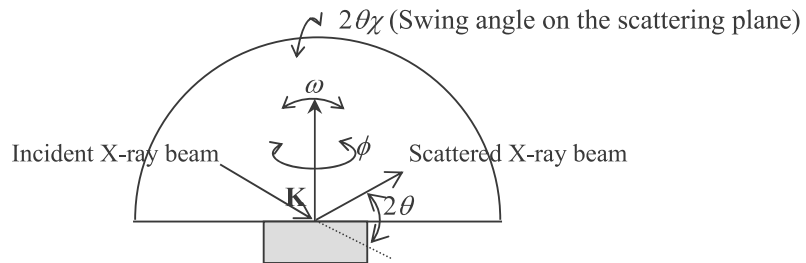
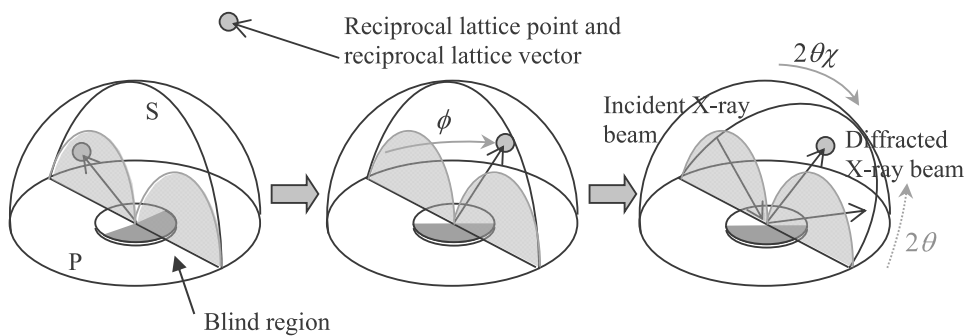


Fig. 2.4.6 Relationship between axes in reciprocal space

Now we will consider a method for measuring the reciprocal lattice points in the blind regions described in Section 4.4.1. As described previously, the in-plane goniometer does not require swinging the sample with respect to the incident X-ray beam, rotating the counter instead. Fig. 2.4.7 shows this mechanism in a manner comparable to Fig. 2.4.4.



S: Scattering plane P: Plane perpendicular to the scattering plane and passing through the origin

Fig. 2.4.7 Moving reciprocal lattice points to the observable region

As shown in Fig. 2.4.7, we can move a reciprocal lattice point out of the blind regions by rotating the  $\phi$  axis (sample in-plane rotation axis). Then, we can place the reciprocal lattice point once again on the scattering plane by rotating the  $2\theta\chi$  axis (the rotation axis perpendicular to the  $2\theta$  rotation of the counter) and thus the scattering plane, rather than by rotating the reciprocal lattice point. In this way, the reciprocal lattice points in the observable region in the scattering plane can be measured in a geometry in which the X-rays enter and exit from the surface of the sample.

When we measure the reciprocal lattice points as described above, we do not need to rotate the sample swing axis. This resolves the problem whereby the incident X-rays irradiate the sample from a tilted axis and pass out of the sample.

### 2.4.3 Reciprocal Space Coordinates

As discussed previously, we can identify the positions and shapes of the reciprocal lattice points by measuring the diffraction intensity while scanning the measurement axes in various directions. The position of the reciprocal lattice point,  $G(hkl)$ , is the end position of the reciprocal lattice vector expressed by Formula (2.1.9). To express the position and shape of  $G(hkl)$  in reciprocal space, we sometimes use Cartesian coordinates  $(q_x, q_y)$  in the reciprocal space instead of measurement axes such as  $2\theta$  and  $\omega$ . This coordinate system is called the **q coordinates** or **reciprocal space coordinates**.

We define the  $q_x$  and  $q_y$  axes as shown in Fig. 2.4.8 and consider the relationship between  $P(q_x, q_y)$  and the angular position,  $(2\theta, \omega)$ , specified by the incident X-ray beam  $\mathbf{k}_o$  and scattered X-ray beam  $\mathbf{k}_g$ . First, length  $q$  of the scattering vector is given by the following formula:

$$|q| = k_o \sin(2\theta/2) + k_g \sin(2\theta/2) = \frac{2}{\lambda} \sin \theta \quad \text{Formula 2.4.1}$$

The angle  $\delta$  between the sample surface normal and the scattering vector is  $\delta = \frac{2\theta}{2} - \omega$ . Thus,  $q_x$  and  $q_y$  are given by the following formulas:

$$\begin{aligned} q_x &= \frac{2}{\lambda} \sin \frac{2\theta}{2} \sin\left(\frac{2\theta}{2} - \omega\right) \\ q_y &= \frac{2}{\lambda} \sin \frac{2\theta}{2} \cos\left(\frac{2\theta}{2} - \omega\right) \end{aligned} \quad \text{Formula 2.4.2}$$

Formula (2.4.2) can also be expressed as follows by summing the  $x$  and  $y$  components of  $\mathbf{k}_o$  and  $\mathbf{k}_g$ .

$$\begin{aligned} q_x &= \frac{1}{\lambda} \{\cos \omega - \cos(2\theta - \omega)\} \\ q_y &= \frac{1}{\lambda} \{\sin \omega + \sin(2\theta - \omega)\} \end{aligned} \quad \text{Formula 2.4.3}$$

Formulas (2.4.4) and (2.4.5) give the same result. 2.4.4 と 2.4.5

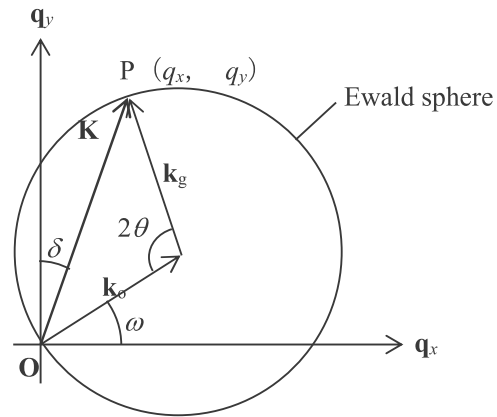


Fig. 2.4.8 Reciprocal space coordinates

## §2.5 Reciprocal Lattice and Resolution of Optics

Measurement resolution has several possible meanings. Resolution can be roughly classified as follows:

1. Resolution of incident optics: Angular divergence and wavelength dispersion of incident X-ray beam
2. Resolution of receiving optics: Resolution of the angle and wavelength on the side receiving the scattered X-ray beam
3. Resolution of goniometer: Minimum rotation angle of each axis (Minimum step)
4. Resolution of measurement position: area irradiated by X-rays and depth (irradiated volume)

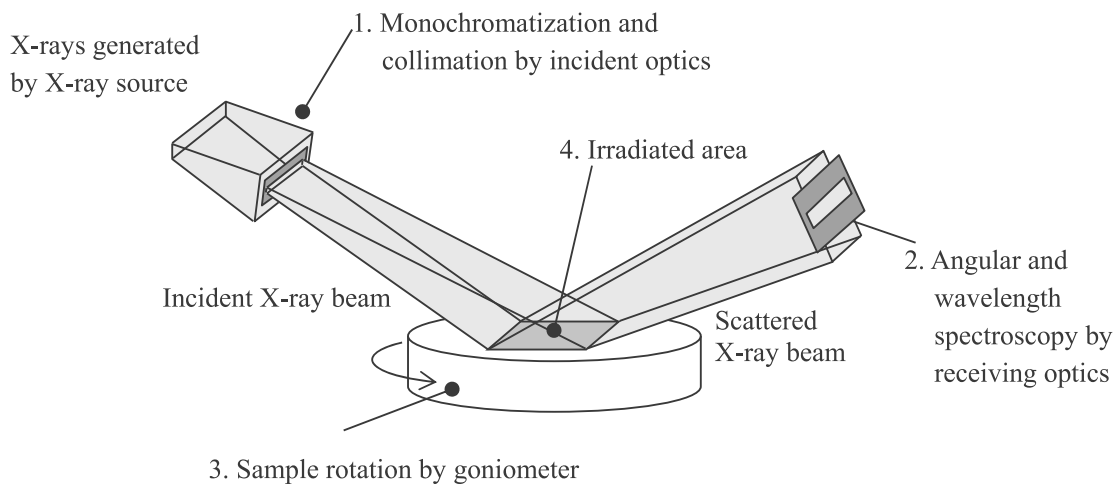


Fig. 2.5.1 Measurement resolution

Among resolutions 1 to 4, the definitions of resolutions 1 to 3 are crucial for reciprocal space. Although resolution 4 may be defined in the reciprocal space by the size of the crystal, the X-ray irradiated volume in this sense is generally extremely large and the reciprocal lattice point corresponding to this volume can be regarded as a dimensionless point.

This section discusses how resolutions 1 to 3 relate to measurements of the reciprocal lattice—that is, to diffraction measurement.

### 2.5.1 Resolution of Incident Optics

We begin by considering 1 the resolution of the incident optics.

The angular divergence of the incident X-ray beam as specified by incident optics such as the slit and the monochromator can be expressed in real space as shown in Fig. 2.5.1 and in reciprocal space as shown in Fig. 2.5.2.

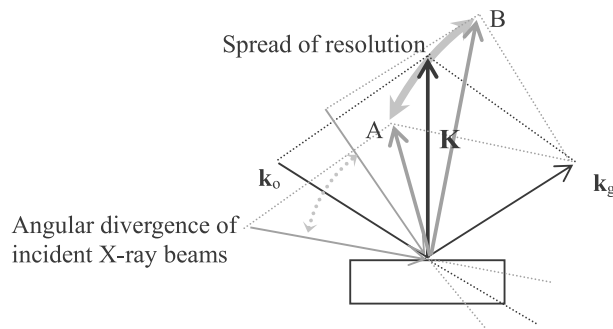


Fig. 2.5.2 Angular divergence of incident X-ray beam

If the incident X-ray beam has an angular divergence, the resolution in reciprocal space spreads in the direction indicated by the arrow in Fig. 2.5.2. That is, incident X-ray beams entering the sample at smaller and larger angles simultaneously undergo scattering corresponding to points A and B, respectively. Here, the reciprocal lattice point is observed to spread between points A and B.

Now we consider the wavelength dispersion of the incident X-ray beam as specified by incident optics such as the slit and the monochromator. This wavelength dispersion can be expressed in real space as shown in Fig. 2.5.1 and in reciprocal space as shown in Fig. 2.5.3.

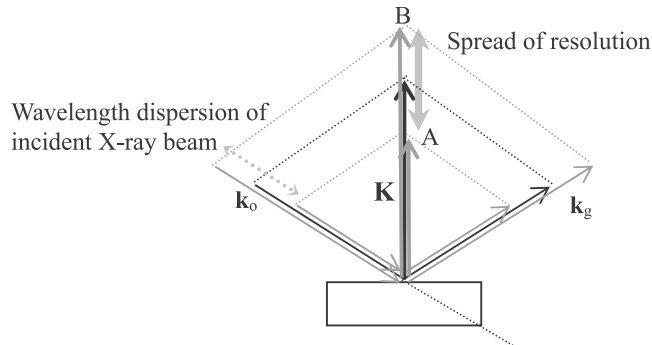


Fig. 2.5.3 Wavelength dispersion of incident X-ray beam

If the incident X-ray beam is characterized by wavelength dispersion and the receiving optics lack sufficient resolution to monochromatize the dispersion for counting, the reciprocal lattice point spreads in the direction indicated by the arrow in Fig. 2.5.3. That is, incident X-ray beams with a longer wavelength (a shorter wave vector) and a shorter wavelength (a longer wave vector) simultaneously undergo scattering corresponding to points A and B, respectively. Here, the reciprocal lattice point is observed to spread between points A and B.

## 2.5.2 Resolution of Receiving Optics

Now we consider 2., the resolution of the receiving optics.

The receiving angular width of the scattered X-ray beam as specified by receiving optics such as the slit and the analyzer can be expressed in real space as shown in Fig. 2.5.1 and in reciprocal space as shown in Fig. 2.5.4.

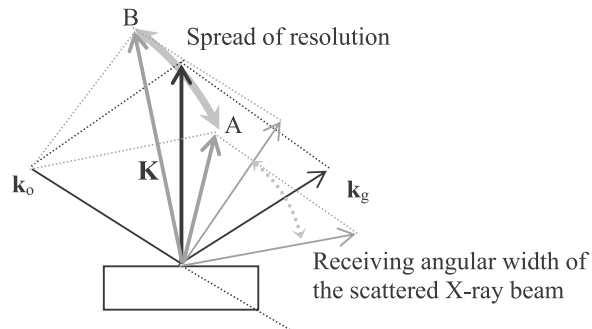


Fig. 2.5.4 Receiving angular width of the scattered X-ray beam

If the receiving optics simultaneously receive scattered X-ray beams of different scattering angles, the resolution in the reciprocal space spreads in the direction indicated by the arrow in Fig. 2.5.4. That is, the scattered X-ray beam with a smaller scattering angle corresponding to point A and the scattered X-ray beam with a larger scattering angle corresponding to point B are simultaneously received. Here, the reciprocal lattice point is observed to spread between points A and B.

Now we consider the receiving wavelength resolution of the scattered X-ray beam as specified by receiving optics such as the slit and the analyzer. This wavelength resolution can be expressed in real space as shown in Fig. 2.5.1 and in reciprocal space as shown in Fig. 2.5.5.

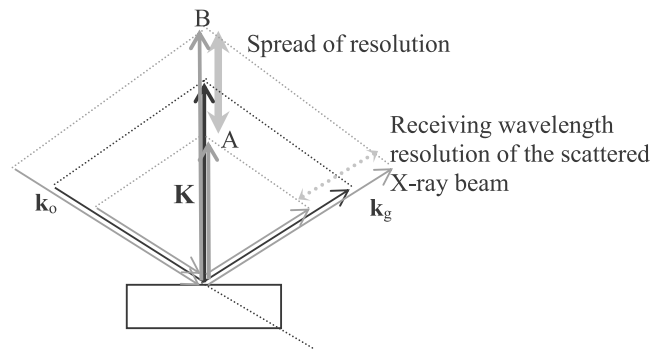


Fig. 2.5.5 Receiving wavelength resolution of the scattered X-ray beam

If the incident X-ray beam is characterized by wavelength dispersion and the receiving optics have sufficient width in resolution to monochromatize the dispersion for counting, the reciprocal lattice point spreads in the direction indicated by the arrow in Fig. 2.5.5. That is, the incident X-ray beams with longer wavelength (shorter wave vector) and shorter wavelength (longer wave vector) simultaneously undergo the scattering corresponding to points A and B, respectively, and are counted simultaneously in the width of the wavelength resolution of the receiving optics. Here, the reciprocal lattice point is observed to spread between points A and B.

### 2.5.3 Resolution Function

As determined in the previous section, if the resolution of the incident or receiving optics decreases, scattering in a region in reciprocal space is simultaneously observed. When this happens, even if the true reciprocal lattice point is an extremely small point, the reciprocal lattice point is observed with a spread corresponding to the resolution. This region in which the scattering is simultaneously observed is called the **resolution function**. The size and shape of the resolution function depends on the optics used in the measurement. The results of the investigation of the previous section show that the size and shape of the resolution function is related to the resolution of the optics shown in Fig. 2.5.6.

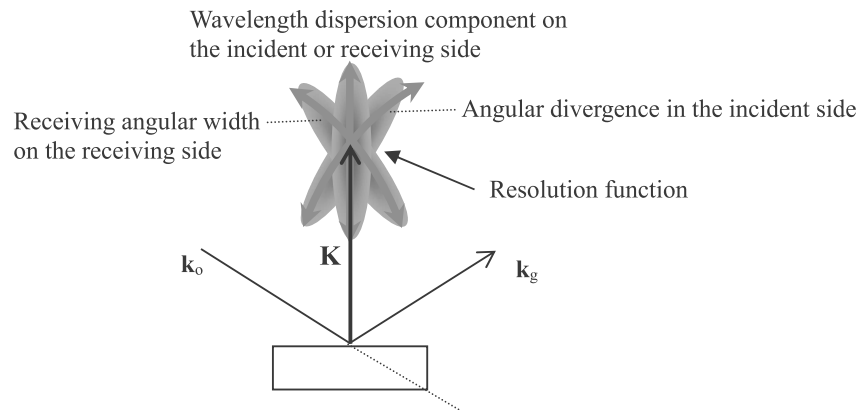


Fig. 2.5.6 Resolution function

As shown in Fig. 2.5.6, even if we measure a sample of extremely high crystallinity and sufficient size, if the resolution function spreads across a wide range, the reciprocal lattice points of that sample will not be small points but will instead be observed to spread like the resolution function.

The discussion in Section 4.3 indicates that the reciprocal lattice point spreads as shown in Fig. 2.5.7 with changes in crystal structure or degradation in crystallinity attributable to changes or fluctuations in the crystal orientation or the lattice constants.

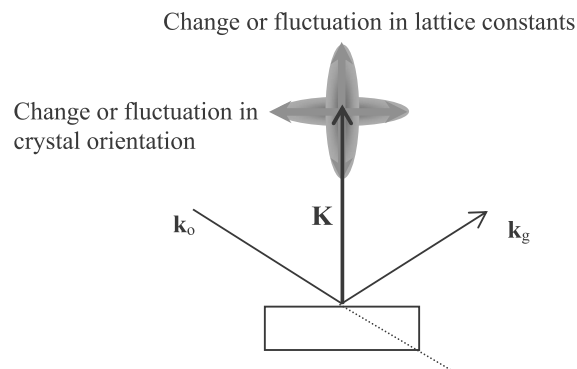


Fig. 2.5.7 Change in crystal structure and degradation in crystallinity

Here, to accurately measure the change in the position or spread of the reciprocal lattice point due to a change in crystal structure or degradation in crystallinity, we must use a resolution function that is sufficiently small relative to this change or spread. The optics for various measurements can be determined from the relationship between the size of the reciprocal lattice point to be measured and the resolution function of the measurement.

### 2.5.4 Resolution of the Goniometer

Scanning by rotating the axes of the goniometer corresponds to measuring the scattering intensity while scanning the reciprocal space using a resolution function of a specific size, as shown in Fig. 2.5.8.

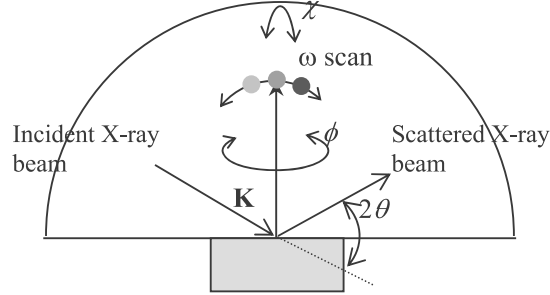


Fig. 2.5.8 Scanning of goniometer axes (for  $\omega$  axis)

Here, the minimum increments in which we can move the resolution function during measurement depends on minimum steps of the scan axis corresponding to movement. The minimum steps of the goniometer axes are thus related to resolution when measuring the reciprocal lattice.

### §2.6 Single Crystal and Polycrystal

So far, we have assumed that the sample is a single crystal in our discussion of the concept of the reciprocal lattice. However, the actual sample may be a single crystal with fluctuations in orientation, a polycrystal with a fiber orientation only, or a randomly oriented polycrystal with no orientation. How do we express the reciprocal lattice of a polycrystal with a fiber orientation or of a completely random polycrystal?

Fig. 2.6.1 schematically shows the reciprocal lattice of each of the samples above.

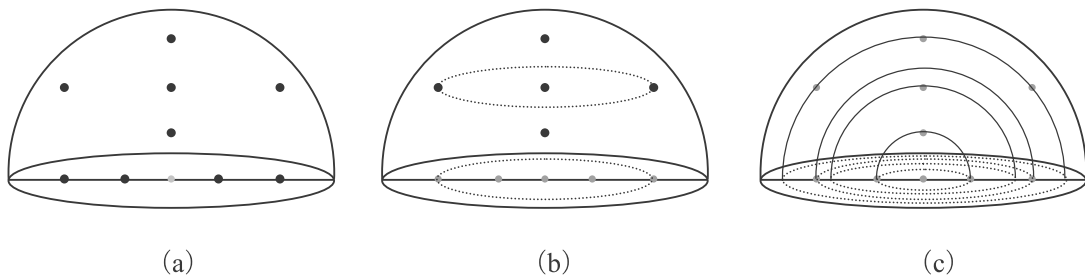


Fig. 2.6.1 Reciprocal lattice of (a) single crystal; (b); oriented polycrystal; and (c) random polycrystal



As implied by Fig. 2.6.1, the appearance of the reciprocal lattice changes depending on whether the sample crystal is a single crystal or a polycrystal and whether it has an orientation. The orientation of crystallites in a polycrystal is generally not uniform; a polycrystal contains crystallites oriented in various directions. This means the reciprocal lattice points are no longer points. For samples with a fiber orientation, a reciprocal lattice point forms a circle around the axis of the preferred orientation. If the sample is a random polycrystal with no orientation, the circle spreads to a sphere of fixed radius. The radius of the sphere equals the inverse of the interplanar spacing.

## §2.7 Summary

This chapter defined and discussed the concept of the reciprocal lattice and its physical meanings. It also discussed the relationship between the reciprocal lattice and various measurement techniques, goniometers, and optical resolution. Summarized below are the major definitions and other issues discussed in this chapter.

### 1. Definition of reciprocal lattice

Direction of lattice planes ( $hkl$ ): Identical to the normal to the lattice planes as drawn from the origin

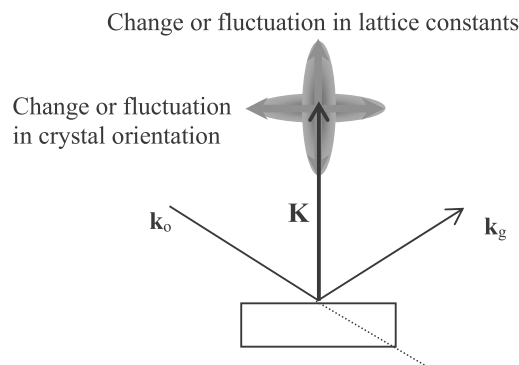
Length of lattice planes ( $hkl$ ): Equal to the inverse of the interplanar spacing  $d_{hkl}$ .

Reciprocal lattice vector:  $\mathbf{g}_{hkl} = h\mathbf{a}^* + k\mathbf{b}^* + l\mathbf{c}^*$

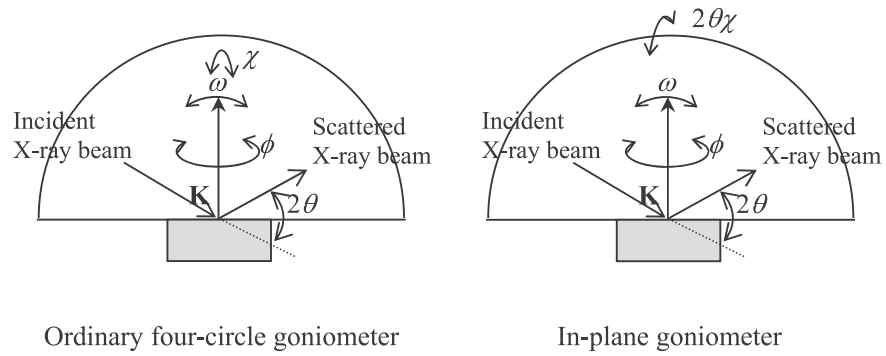
$$\mathbf{a}^* = \mathbf{b} \times \mathbf{c}, \mathbf{b}^* = \mathbf{c} \times \mathbf{a}, \mathbf{c}^* = \mathbf{a} \times \mathbf{b}$$

Diffraction condition:  $\mathbf{k}_g - \mathbf{k}_o = \mathbf{g}_{hkl}$

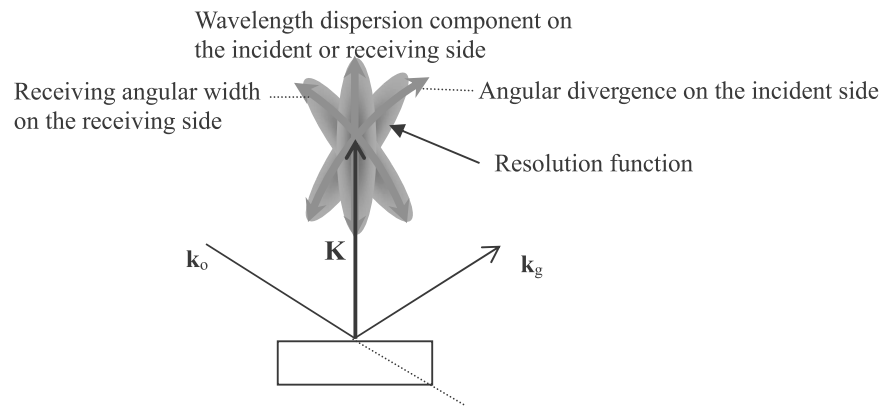
### 2. Relationship between reciprocal lattice and crystal structure



3. Relationship between reciprocal lattice and goniometer axes



4. Relationship between reciprocal lattice and resolution of measurement



## Chapter 3 Diffraction Measurements

Diffraction measurements are classified by measurement techniques. Measurement techniques vary in the relative positions of the incident X-ray beam, sample crystal, and counter; scanning directions of the axes; and optical resolution. However, all techniques are similar in measuring the change in scattering intensity while rotating the axes.

This chapter uses the concept of the reciprocal lattice introduced in Chapter 2 to discuss the relationship between measurement techniques and what information they can provide on crystal structures and crystallinity. This chapter also describes practical measurement procedures and precautions.

### §3.1 Relationship between Various Measurement Techniques

The suitable measurement technique can provide a wide range of crystallographic information, including crystal structures, crystallinity, crystal orientation, and lattice constants. As discussed in Section 4.3, changes in these parameters appear in different directions in reciprocal space. As discussed in Section 4.4, we can measure the distribution of scattering intensity in reciprocal space by rotating the axes of the goniometer. By rotating the axes in the direction corresponding to the change in the parameter to be measured, we can obtain the information needed. Diffraction measurement techniques can be classified as shown in Table 3.1.1 based on the scanning method of the axes.

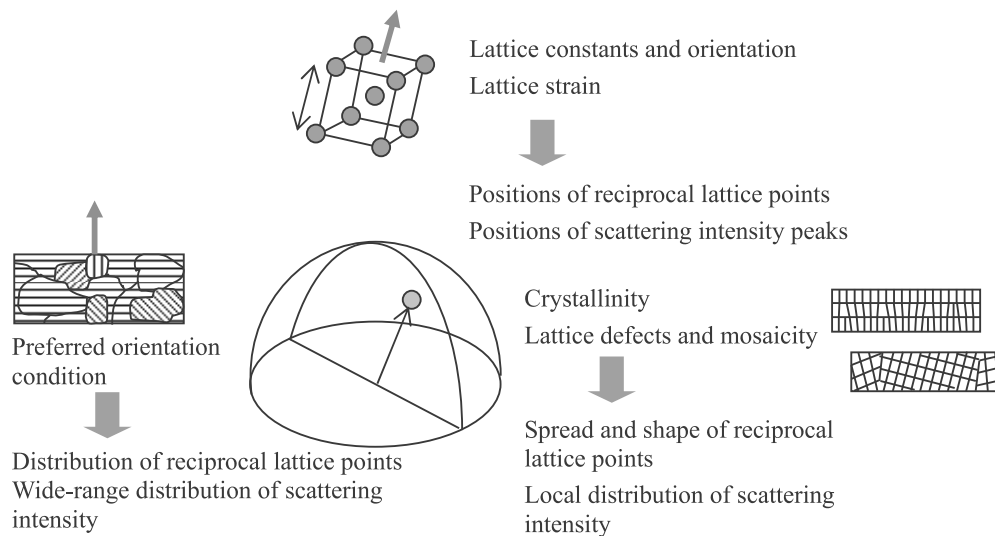


Fig. 3.1.1 Relationship between measurement parameters and techniques  
(Schematic illustration)

Table 3.1.1 Various measurement techniques

| Measurement technique  | Information obtained   | Scan axis  |
|--|--|--|
| Out-of-plane measurement<br>(One-dimensional scan)                             | Information on lattice planes parallel to sample surface<br>→ Qualitative analysis and crystal structure   | $2\theta/\omega$<br>(Always $2\theta = 2 \times \omega$ )  |
| Thin film measurement<br>(One-dimensional scan)                                | Information near sample surface (applies only to unoriented samples)<br>→ Qualitative analysis and crystal structure   | $2\theta$<br>(Incident angle, $\omega$ , is fixed near the critical angle.)  |
| In-plane measurement<br>(One-dimensional scan)                                 | Information on lattice planes near and parallel to sample surface<br>→ Qualitative analysis and crystal structure  | $2\theta\chi/\phi$<br>(Incident angle, $\omega$ , is fixed near the critical angle.)                                 |
| Pole figure measurement<br>(Two-dimensional scan)                              | Information on distribution of specific crystal orientation<br>→ Orientation analysis  | $\chi(\alpha), \phi(\beta)$<br>( $2\theta$ or sum of $2\theta$ and $2\theta\chi$ is fixed at the diffraction angle.) |
| Preferred orientation and crystallinity measurement*<br>(One-dimensional scan) | Information on degree of preferred orientation or crystallinity<br>→ Orientation and crystallinity analysis  | $\omega, \chi$ , or $\phi$   |
| Rocking curve measurement*<br>(One-dimensional scan)                           | Information on film structure and crystallinity of epitaxial or single crystal<br>→ Crystallinity, film thickness, and composition ratio   | $2\theta/\omega$   |
| RSM measurement<br>(Two-dimensional or three-dimensional scan)                 | Information on d-value of three-dimensional components of preferred orientation, crystal orientation, and degree of preferred orientation<br>→ Qualitative analysis, orientation analysis, and crystallinity analysis<br>Information on film structure and crystallinity of epitaxial or single crystal<br>→ Crystallinity analysis and epitaxial analysis | $2\theta/\omega, \omega, (\chi \text{ or } \phi)$<br>$2\theta\chi/\phi, \phi, (\chi \text{ or } \phi)$               |

\* For polycrystal measurements, the  $\omega$  scan for measuring the degree of preferred orientation is sometimes called “rocking curve measurement.” To avoid confusion, the term, “rocking curve measurement” will refer specifically to  $2\theta/\omega$  scans for an epitaxial or single crystal. The  $\omega$  scan for measuring the degree of orientation is called “orientation measurement.”

The following sections discuss measurement procedures and measurement data interpretation for the measurement techniques listed in Table 3.1.1.

## §3.2 What Does Diffraction Measurement Observe?

### 3.2.1 Out-of-Plane Measurement

**Out-of-plane measurement** measures diffraction by lattice planes parallel to the sample surface. As Fig. 3.2.1 shows, the incident angle and the exit angle of the X-rays with respect to the sample surface are always equal when you measure diffraction by lattice planes parallel to the sample surface. Such measurements essentially scan the  $2\theta/\omega$  axis while maintaining a relationship in which the diffraction angle  $2\theta$  is twice the incident angle  $\omega$ .

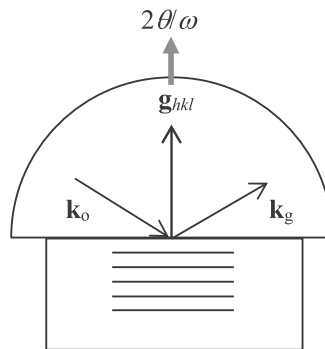


Fig. 3.2.1 Schematic illustration of out-of-plane measurement

For example, in the case of a single crystal sample with a surface parallel to the (001) plane, out-of-plane measurement observes the lattice planes parallel to the (001) plane but with different interplanar spacings, such as the (002) and (003) planes. For an oriented polycrystal sample having a fiber orientation such that the (001) plane is parallel to the surface, this technique similarly observes planes parallel to the (001) plane but with different interplanar spacings, such as the (002) and (003) planes. For random polycrystal samples, this technique observes all lattice planes, although the diffraction spots observed here are diffracted from crystallites with lattice planes parallel to the surface.

Thus, out-of-plane measurements can be used for qualitative analysis and for determining the presence or absence of a preferred orientation, interplanar spacings of the lattice planes parallel to the surface, lattice constants corresponding to these interplanar spacings, and the crystallinity of a crystal lattice parallel to the surface. However, out-of-plane measurements cannot observe lattice planes perpendicular to the surface and cannot provide information on the presence or absence of the in-plane orientation. It cannot distinguish between a fiber-oriented and a single crystal sample. To evaluate in-plane orientation, we use asymmetric reflection or in-plane measurement.

### 3.2.2 Thin Film Measurement

**Thin film measurement** is an efficient technique for measuring scattering from the region near the surface while avoiding scattering from the substrate. It uses X-ray incidence at a grazing angle relative to the sample surface, changing only the scattering angle during measurement. Here, the incident angle is set near the critical angle at which the X-ray depth of penetration into the sample is extremely low. We can also investigate the depth dependence of sample states using several types of thin film measurement performed while changing the incident angle.

This measurement technique is equivalent to scanning just the scattering angle  $2\theta$  while maintaining the incident angle  $\omega$  at a small angle. Here, as Fig. 3.2.2 shows, as scattering angle  $2\theta$  changes, the orientation of the crystal observed changes. Thin film measurement observes lattice planes oriented in all directions with respect to the sample surface. With a single crystal or an oriented sample, this technique observes just the lattice planes corresponding to the reciprocal lattice points that incidentally enter the trajectory of the  $2\theta$  scan, as indicated in Fig. 3.2.2.

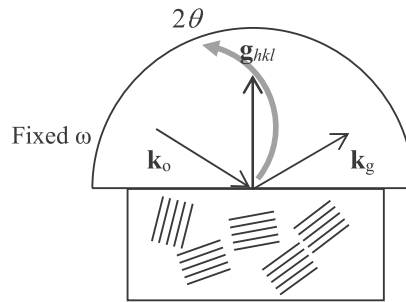


Fig. 3.2.2 Schematic illustration of thin film measurement

Thin film measurement can be used for qualitative analysis of an unoriented (or weakly oriented) polycrystal sample and to investigate lattice constants and the crystallinity of such a sample. We can also investigate the depth dependence of these physical quantities. However, this method generally cannot be used to analyze a strongly oriented polycrystal sample or a single crystal sample, since these samples with this technique generate no or virtually no diffraction peaks.

### 3.2.3 In-Plane Measurement

**In-plane measurement** measures lattice planes perpendicular to the sample surface. Like thin film measurement, in-plane measurement relies on X-ray incidence at a grazing angle relative to the sample surface. It can acquire information on crystal states in the direction of depth by performing two or more sets of measurements with different incident angles.

If the X-ray beam is incident on the sample at a grazing angle, the total reflection phenomenon will occur if the incident angle is less than the critical angle, in which case X-rays incident on the sample propagate parallel to the sample surface.

When X-rays propagating parallel to the sample surface are diffracted by lattice planes perpendicular to the sample surface, the diffracted X-rays also exit the surface at a grazing angle. Measuring this diffraction is equivalent to scanning the  $2\theta/\phi$  axis while maintaining a relationship in which the diffraction angle  $2\theta$  perpendicular to the sample surface is twice the sample in-plane rotation angle  $\phi$ . Fig. 3.2.3 shows the direction of the scan in reciprocal space.

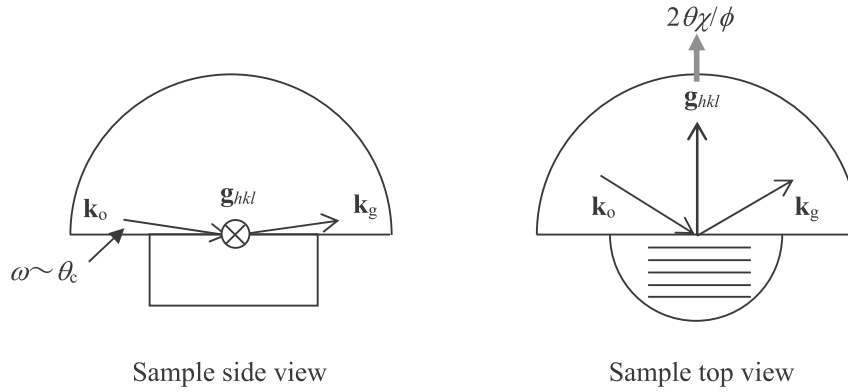


Fig. 3.2.3 Schematic illustration of in-plane measurement

Consider a cubic crystal sample. Assume a single crystal sample with surface parallel to the (001) plane and perpendicular to the (110) plane and a (110) plane in the direction indicated as  $2\theta/\phi$  in the top view of Fig. 3.2.3. In this case, the  $2\theta/\phi$  scan observes planes parallel to the (110) plane but with different interplanar spacings, such as the (220) and (330) planes. For an oriented polycrystal sample having a fiber orientation such that the (001) plane is parallel to the surface, this technique observes all planes perpendicular to the (001) plane, such as the (100) and (120) planes, in addition to planes parallel to the (110) plane but with different interplanar spacings, such as the (220) and (330) planes. For a random polycrystal sample, this technique observes all lattice planes, although the diffraction spots observed here are diffracted from crystallites having lattice planes perpendicular to the surface.

Thus, in-plane measurement can be used for qualitative analysis and for investigating the presence or absence of the preferred orientation, the interplanar spacings of the lattice planes perpendicular to the surface, lattice constants corresponding to these interplanar spacings, and the crystallinity of the crystal lattice perpendicular to the surface. In addition, since in-plane measurement can observe lattice planes perpendicular to the surface, it can provide information on the presence or absence of in-plane orientation. For example, it can distinguish between a fiber-oriented sample and a single crystal sample or confirm the presence or absence of twinning.

As described above, in-plane measurement can change the depth of analysis by varying the incident angle. The figure below shows the relationship between the incident angle and depth of penetration (the depth at which the incident X-ray intensity drops to  $1/e$ ).

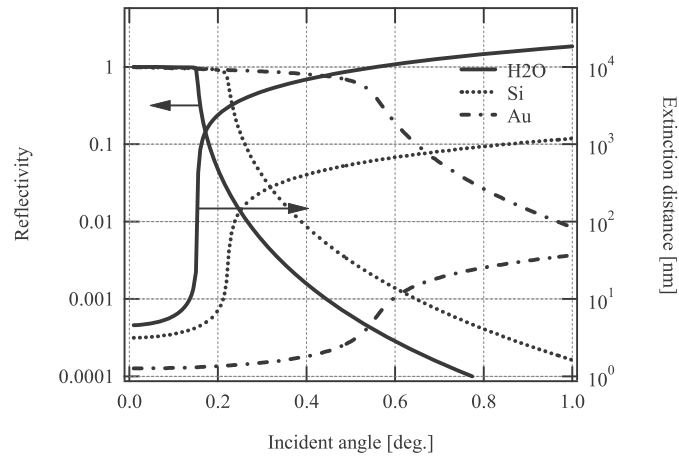


Fig. 3.2.4 Incident angle and depth of penetration

As implied by Fig. 3.2.4, the depth of penetration changes abruptly near the critical angle. We can investigate changes in crystal structure or crystallinity in the direction of depth by performing in-plane diffraction measurements while varying the incident angle across the critical angle. We can also identify deposits at the surface or interfaces by qualitatively analyzing two or more measurement results with different incident angles.

### 3.2.4 Pole Figure Measurement

**Pole figure measurement** measures diffraction intensity distributions by rotating the sample in all directions while keeping the diffraction angle constant. The direction at which high diffraction intensity is observed corresponds to the preferred direction of the pole figure axes (indicating that crystallites with the measurement planes oriented in that direction are dominant). The pole figure measurement expresses the preferred orientation of the sample with pole figure axes  $\alpha$  and  $\beta$ . As shown in Fig. 3.2.5,  $\alpha$  and  $\beta$  correspond to the  $\chi$  and  $\phi$  axes of the four-circle goniometer, respectively.

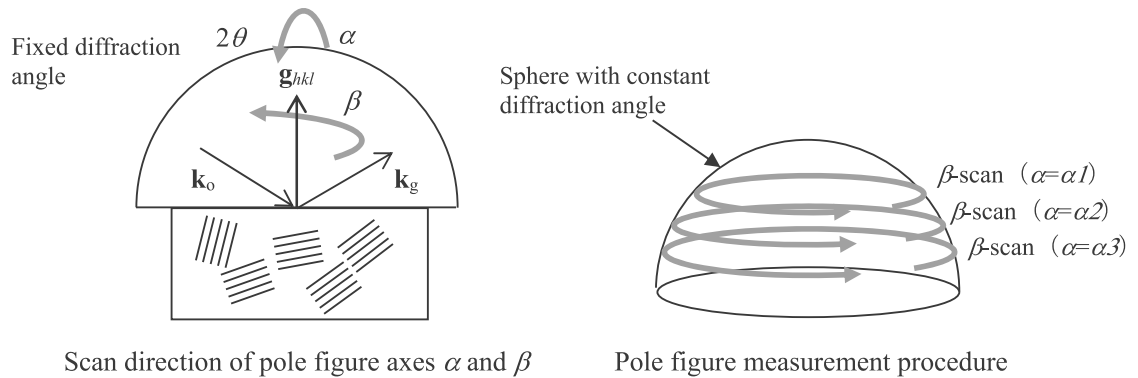


Fig. 3.2.5 Schematic illustration of pole figure measurement



The results of pole figure measurement are expressed as a **pole figure** (Fig. 3.2.6).

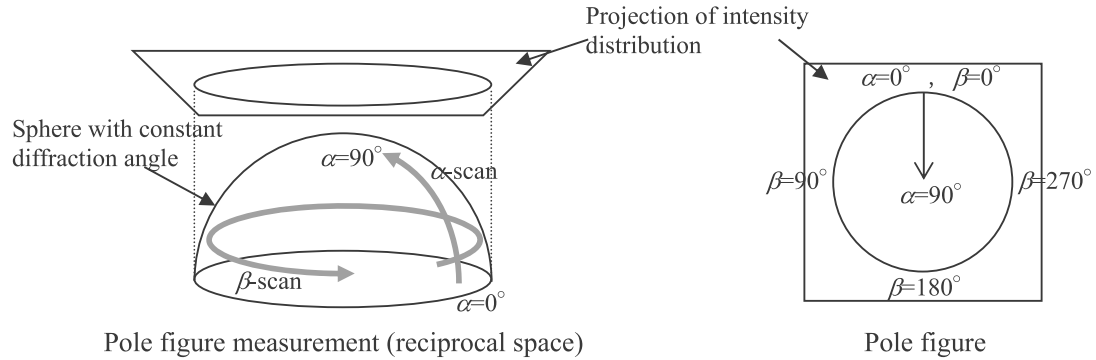


Fig. 3.2.6 Pole figure

Consider the example of a cubic crystal sample. Fig. 3.2.7 shows the results of a pole figure measurement of the (111) plane and of the (220) plane perpendicular for three cases: 1. a randomly oriented sample; 2. a sample with the (111) plane fiber-oriented parallel to the surface; and 3. a single crystal sample with the (111) plane parallel to the surface.

For a randomly oriented sample with no preferred orientation as indicated in 1, the pole figures show only a small change in the diffraction intensity in different orientations, producing a flat intensity distribution. The slight orientation dependence of the diffraction intensity is not caused by preferred orientation, but by the change in the area of X-ray irradiation and in absorption accompanied by changes in X-ray incidence and exit angles relative to the surface.

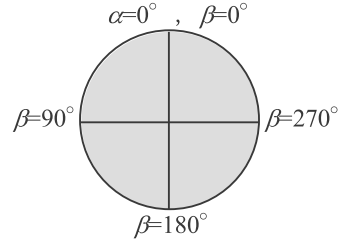
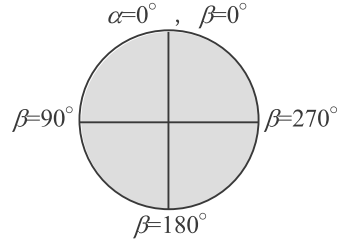
For a sample having the {111} fiber orientation shown in 2, the pole figure of the (111) surface shows strong diffraction intensity at the center (at the point corresponding to the component parallel to the sample surface). This high intensity indicates the dominance of the components satisfying the diffraction condition in this direction—that is, the dominance of crystallites with (111) plane parallel to the surface. For a cubic crystal sample, the {111} planes ((-111), (11-1), and (1-11) planes) are found oriented  $70.5^\circ$  to the (111) plane. All these planes have the same diffraction angle. The pole figure also shows strong diffraction intensity in the direction at  $\alpha = 70.5^\circ$ . However, since it lacks an in-plane ( $\beta$  direction) orientation, the pole figure does not have a distribution and shows a ring-shaped intensity distribution. The pole figure of the (220) plane shows the diffraction intensity distribution produced by the {220} planes at  $35.3^\circ$  and  $90.0^\circ$  to the (111) plane.

For a single crystal sample with the (111) plane parallel to the surface of 3, the pole figure of the (111) surface shows strong diffraction intensity at the center and at  $70.5^\circ$  from the (-111); (11-1); and (1-11) planes. Here, the intensity distribution in the  $\beta$  direction does not form a ring-shaped distribution. We observe strong intensity only in the directions in which the {111} planes exist in the single crystal, resulting in the pole figure shown in 3. of Fig. 3.2.7. The pole figure for the (220) plane shows the diffraction intensity distribution produced by the {220} planes found oriented at  $35.3^\circ$  and  $90.0^\circ$  to the (111) plane, as shown in 3. of Fig. 3.2.7.

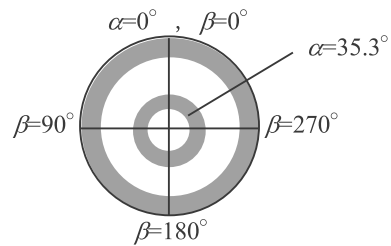
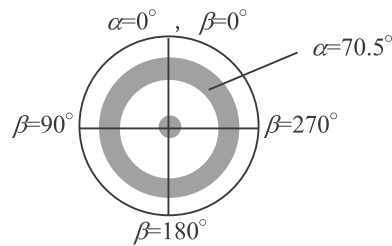
Pole figure of (111) plane

Pole figure of (220) plane

1. Randomly oriented sample



2. (111) fiber-orientated sample



3. (111) single crystal sample

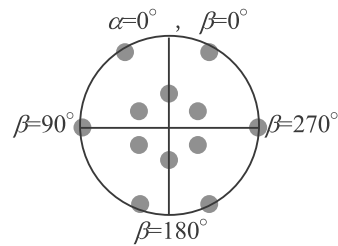
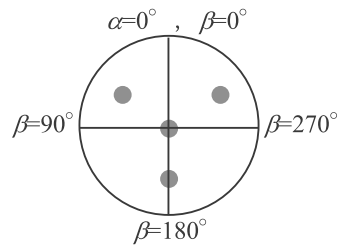


Fig. 3.2.7 Examples of pole figures

### 3.2.5 Preferred Orientation and Crystallinity Measurement

Preferred orientation measurement measures a cross-section of a pole figure measurement. That is, it scans the  $\alpha$  axis or the  $\beta$  axis and measures the spread (width) of the diffraction intensity distribution. The underlying principles are the same as for pole figure measurement. Here, the spread of the diffraction intensity is related to quantities such as the **degree of preferred orientation** or **mosaicity**.

The degree of preferred orientation is a term for expressing the amount of preferred orientation present in the sample compared to a randomly oriented sample. For example, in a randomly oriented sample, the diffraction intensity is uniformly distributed in the range  $\beta = 0^\circ$  to  $360^\circ$ . In an oriented sample in which the diffraction intensity is observed in the range  $\beta = 81^\circ$  to  $109^\circ$  and  $\beta = 261^\circ$  to  $279^\circ$ , the degree of preferred orientation is calculated as follows: (spread of diffraction intensity)/ $360 = 36/360 = 10\%$ .

Mosaicity is a term for the amount of fluctuation in orientation compared to a perfect single crystal. While mosaicity lacks a specific quantitative definition, if a perfect crystal does not show a spread in the diffraction intensity with width of  $0^\circ$  and a sample shows a spread in diffraction intensity from the center of  $\pm 0.5^\circ$ , the crystal orientation of that sample can be regarded to fluctuate across a range of  $1^\circ$ . In this case, mosaicity can be expressed as  $1^\circ$ .

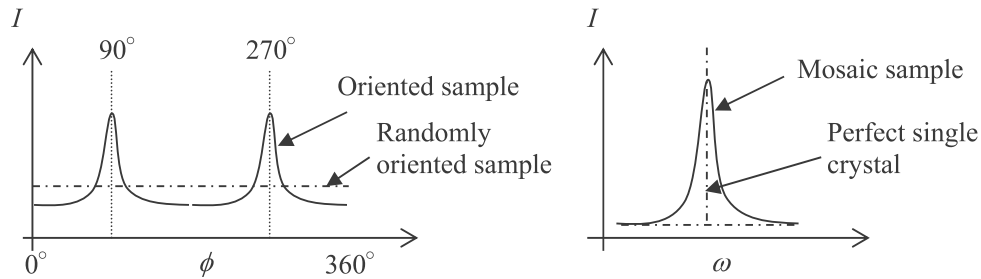


Fig. 3.2.8 Degree of preferred orientation (left) and mosaicity (right)

### 3.2.6 Rocking Curve Measurement

**Rocking curve measurement** measures diffraction intensity distributions along a reciprocal lattice vector. As Fig. 3.2.9 shows, this measurement does not require the incident angle and exit angle of X-rays relative to the surface to be equal. It scans the  $2\theta/\omega$  axis while maintaining a relationship in which a change in diffraction angle  $2\theta$  is always twice the change in incident angle  $\omega$ . Since rocking curve measurement measures the diffraction intensity distribution along a reciprocal lattice vector, it can measure changes in interplanar spacing.

Rocking curve measurement is generally used to evaluate the thickness or mixed crystal ratio of an epitaxial film on a sample called a perfect crystal—i.e., one with extremely high crystallinity. Chapter 7 gives a detailed discussion of the principles underlying rocking curve measurement.

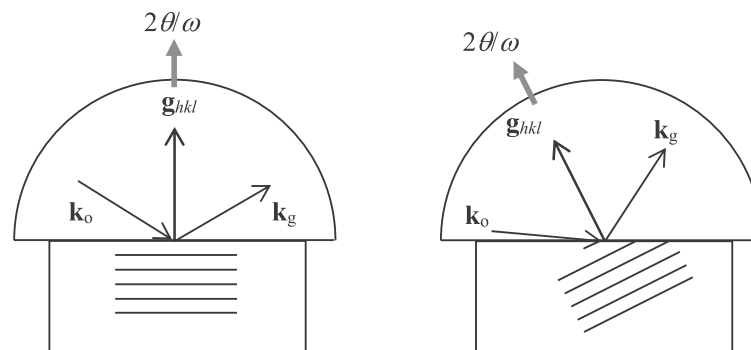


Fig. 3.2.9 Schematic illustration of rocking curve measurement:  
(left) symmetric plane; (right) asymmetric plane

### 3.2.7 Reciprocal Space Mapping (RSM) Measurement

**Reciprocal space Mapping (RSM)** measurement measures diffraction intensity distributions by scanning both the diffraction angle and sample rotation axes and plots the result in reciprocal space. As described in Chapter 2, the reciprocal lattice includes information on the crystal structure, crystal orientation relationships, crystallinity, and the preferred orientation of the sample investigated. The central coordinates, shapes, and positional relationships of the reciprocal lattice points appearing in the two-dimensional (or three-dimensional) data plotted in reciprocal space provide a wide range of information on crystal structure.

As Fig. 3.2.10 shows, RSM measurement measures the positions and shapes of reciprocal lattice points by scanning the  $2\theta$  and  $\omega$  axes in the scattering plane as specified by the specific values for  $\chi$  and  $\phi$ . Three types of scanning methods are used: “ $\omega$  step  $2\theta/\omega$  scan,” which repeats the  $2\theta/\omega$  scan while gradually changing  $\omega$ ; “ $2\theta/\omega$  step  $\omega$  scan,” which repeats the  $\omega$  scan while gradually changing  $2\theta/\omega$ ; and “mesh measurement,” which scans the axes while maintaining constant step intervals in  $q$  coordinates.

A diffractometer capable of performing in-plane measurements can also perform in-plane reciprocal space mapping measurements. Two types of scanning methods are used: “ $\phi$  step  $2\theta\chi/\phi$  scan,” which repeats the  $2\theta\chi/\phi$  scan while gradually changing  $\phi$ ; and “ $2\theta\chi/\phi$  step  $\phi$  scan,” which repeats the  $\phi$  scan while gradually changing  $2\theta\chi/\phi$ .

When measurement is performed by a scanning method other than “mesh measurement,” the angular position on each axis is converted into  $q$  coordinates using Formula 3.2.1 or Formula 3.2.2. A reciprocal space map plots the diffraction intensity in  $q$  coordinates in different colors.

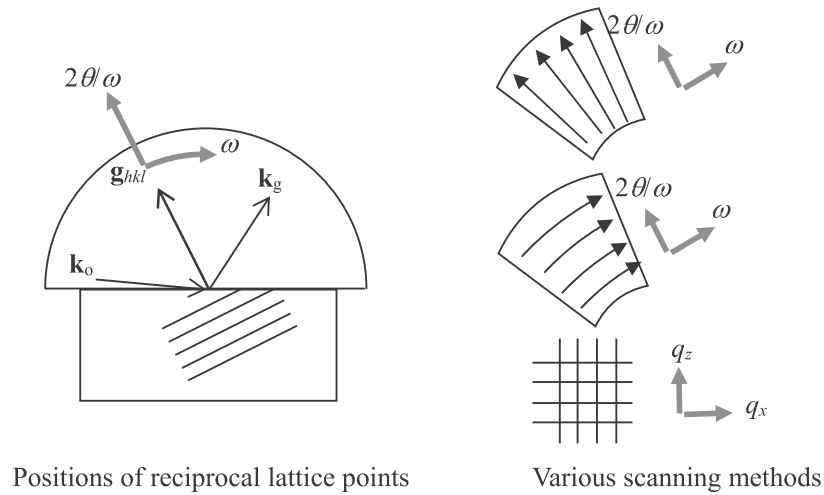


Fig. 3.2.10 Schematic illustration of RSM measurement

Consider the example of a heteroepitaxial sample in which a cubic crystal film is epitaxially grown on a cubic crystal substrate. The film has lattice constants slightly greater than the substrate. If a beam diffracted from the film produces a distribution in the reciprocal lattice point centered at  $(q_x, q_y)$ , it provides the following information:

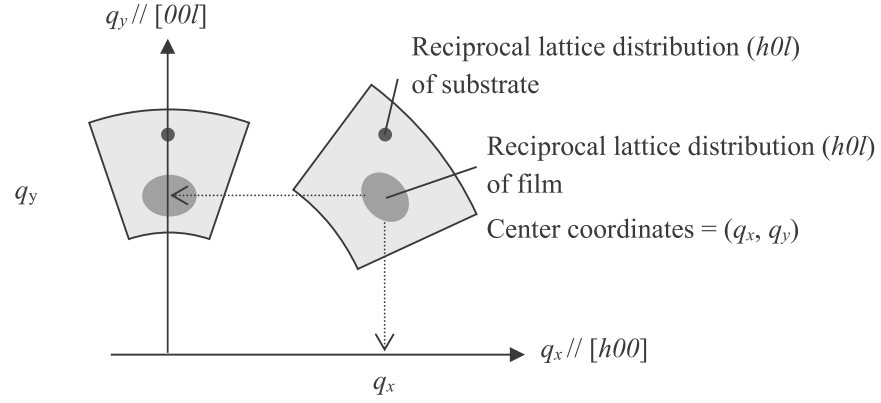


Fig. 3.2.11 RSM map of  $(h0l)$  plane

- Information provided by the center coordinates of the reciprocal lattice distribution

From the center coordinates of the reciprocal lattice, we can calculate interplanar spacing  $d$ . Since the length  $|q|$  of the reciprocal lattice vector is the inverse of  $d$ , the following formula holds:

$$d = \frac{1}{|q|} = \frac{1}{\sqrt{q_x^2 + q_y^2}} \quad \text{Formula 3.2.1}$$

When  $q_x$  and  $q_y$ , the axes of the  $q$  coordinates, are parallel to crystallographic axes  $[h00]$  and  $[00l]$  of the sample, respectively, we can calculate  $d_{h00}$  and  $d_{00l}$  separately based on the values of the center coordinates  $(q_x, q_y)$  of the  $(h0l)$  reciprocal lattice distribution. The operation used to match the axes of the  $q$  coordinates with the crystallographic axes of the sample is performed as part of sample alignment in the measurement.

$$d_{h00} = \frac{1}{|q_x|}, \quad d_{00l} = \frac{1}{|q_y|} \quad \text{Formula 3.2.2}$$

Multiplying the values of  $d_{h00}$  and  $d_{00l}$  by the Miller indices produces lattice constants  $a$  and  $c$ . In addition, if the reciprocal space map is similarly measured for the Miller indices in which  $k$  is not zero, we can also calculate lattice constant  $b$ . In this manner, we can determine the lattice constants and crystal system based on the results of RSM

measurements for two or more Miller indices.

- Information provided by spread of reciprocal lattice distribution

If the crystallinity of the epitaxial film is less than that of the substrate, the reciprocal lattice point distribution will broaden. The direction in which the distribution broadens depends on the type of change in crystallinity. Fig. 3.2.12 illustrates this property.

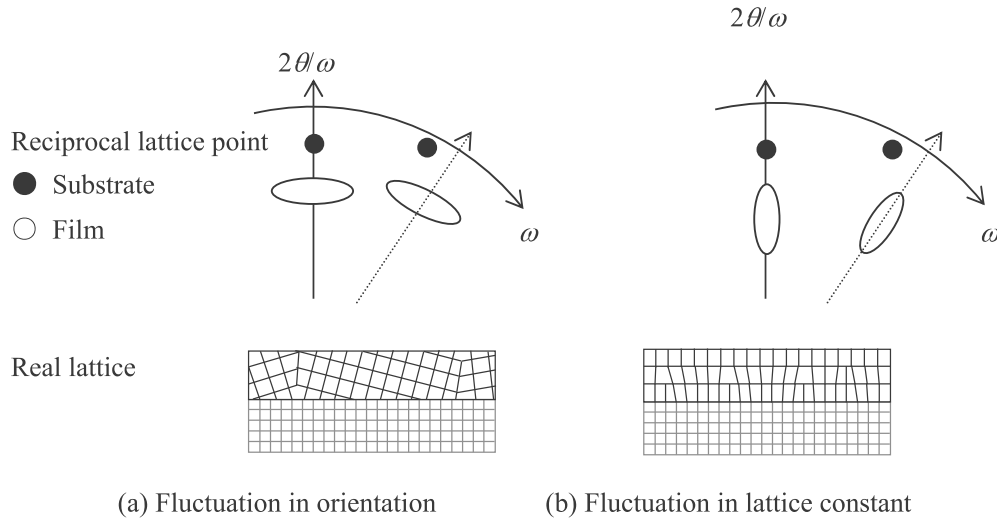


Fig. 3.2.12 Reciprocal space map of heteroepitaxial layer (crystallinity)

If the epitaxial film is a mosaic crystal or if the lattice is bent by stress, the crystal orientation fluctuates, and the reciprocal lattice points of the film spread in the  $\omega$  direction (the direction of the arc of the RSM measurement range) with respect to that of the substrate as shown in Fig. 3.2.12 (a).

If the epitaxial film has a dislocation, parts with a mixture of relaxed and unrelaxed lattices, or variations in composition ratios, the lattice constants will fluctuate, and the reciprocal lattice points of the film will spread along the  $2\theta/\omega$  direction (the radial axis of the RSM measurement range) with respect to that of the substrate, as shown in Fig. 3.2.12 (b).

- Information provided by relative positions with respect to reciprocal lattice points of substrate

The relative positions of the reciprocal lattice points of the epitaxial film and the substrate change, depending on lattice matching and the presence or absence of lattice relaxation. Fig. 3.2.13 schematically illustrates the entire reciprocal space map.

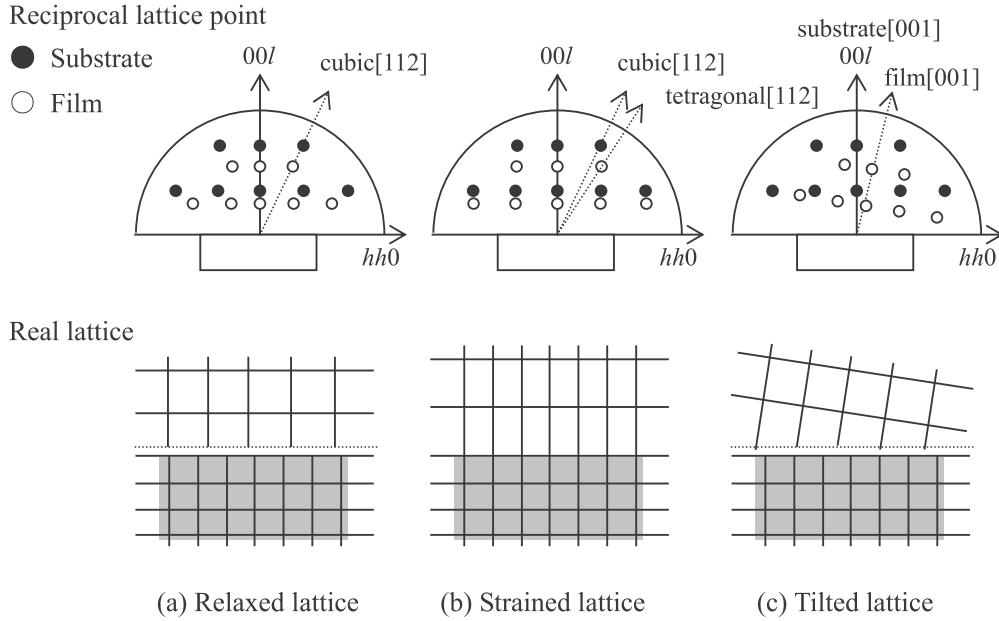
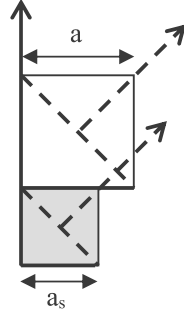


Fig. 3.2.13 Reciprocal space map of heteroepitaxial layer (lattice relaxation)

The term **lattice relaxation** refers to the state of an epitaxial film having the same cubic crystal structure as the bulk of the material composing the film, as shown in Fig. 3.2.13 (a). In this case, the reciprocal lattice point of the film with the indices  $(hkl)$  is positioned on the line connecting the reciprocal lattice point  $(hkl)$  of the substrate and the origin of the reciprocal lattice—along the line of the  $2\theta/\omega$  scan for both symmetric and asymmetric reflections.

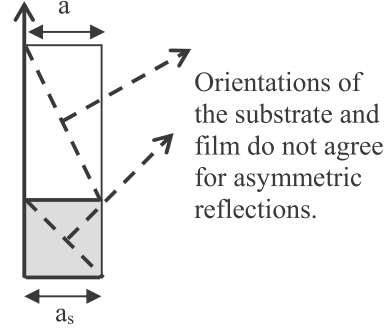
If the lattice of the film is strained at the interface between the epitaxial film and the substrate in a manner such that the in-plane lattice constants ( $a$  and  $b$  in Fig. 3.2.13) of the epitaxial film and substrate match, the reciprocal lattice point of the film with the indices  $(hkl)$  is positioned directly below the reciprocal lattice point  $(hkl)$  of the substrate for both symmetric and asymmetric reflections, as shown in Fig. 3.2.13 (b). Here, for asymmetric reflections, the reciprocal lattice points of the substrate and the film are not positioned on the same line of the  $2\theta/\omega$  scan. As Fig. 3.2.14 shows, the lattice of the film is strained to form a tetragonal crystal structure ( $a = b \neq c$ ), so that the  $(hkl)$  direction differs from that for the cubic crystal structure of the substrate.

Orientations of the substrate and film agree for both symmetric and asymmetric reflections.



Relaxed lattice

Orientations of the substrate and film agree for symmetric reflections.



Strained lattice

Fig. 3.2.14 Asymmetric reflection of strained lattice

Depending on the layer structure and heat treatment conditions of the epitaxial film, the interface may assume a state intermediate between the “relaxed lattice” and “strained lattice” indicated in Fig. 3.2.14. The degree of relaxation is expressed by the relaxation rate. The relaxation rate is calculated from the in-plane lattice constants of the substrate and epitaxial film. If we denote the lattice constant of the substrate as  $a_s$ , the lattice constant of the completely relaxed epitaxial film as  $a_0$ , and the lattice constant of the measurement sample as  $a$ , the relaxation rate is given by the following formula:

$$\text{Relaxation rate} = \frac{a - a_s}{a_0 - a_s} \times 100(\%) \quad \text{Formula 3.2.3}$$

For the “relaxed lattice,”  $a = a_0$ , and the relaxation rate is 100%. For the “strained lattice,”  $a = a_s$ , and the relaxation rate is 0%.

Regardless of the presence or absence of lattice relaxation, if the crystal orientation of the film (the direction of the  $c$  axis in Fig. 3.2.13) is tilted with respect to that of the substrate, the reciprocal lattice points of the film will shift relative to the reciprocal lattice points of the substrate based on the tilt. The amount of shift corresponds to the shift in crystal orientation between the substrate and the film and equals the shift in reciprocal lattice points for the symmetric reflection.

### §3.3 Measurement Techniques

As discussed in the previous section, the diffraction measurements can provide a wide range of information on crystal structure and crystallinity. Extracting accurate information requires care with respect to several aspects of measurement. This section discusses the measurement procedures and precautions for each measurement technique.



### 3.3.1 Out-of-Plane Measurement and Thin Film Measurement

Fig. 3.3.1 shows the procedures for out-of-plane measurement and thin film measurement.

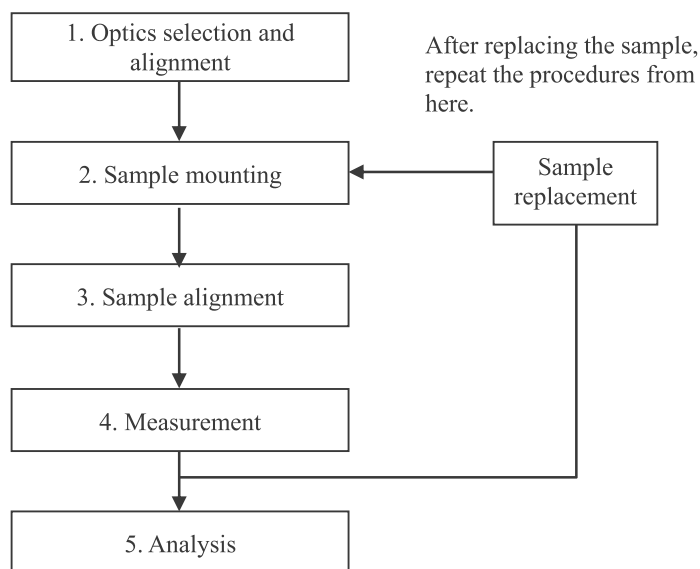


Fig. 3.3.1 Flow of measurement

Select the optics, using Table 3.3.1 as a guide.

Table 3.3.1 Guide for selecting optics

| Sample crystallinity   | Appropriate optics                           | Remarks   |
|--|--|---|
| Randomly oriented to strongly oriented polycrystals (metals, dielectric materials, etc.) | Medium resolution PB<br>Thin film (standard) | Select $K\alpha$ line with multilayer mirror.                   |
| Single crystals (GGG, SiC, etc.)   | Double-crystal monochromator                 | Select only $K\alpha_1$ line with double-crystal monochromator. |

Set the slits so that the size of the incident X-ray beam in the lengthwise direction is approximately equal to the size of the sample, while the size of the X-ray beam in the vertical direction is 1 mm for out-of-plane measurements and 0.2 mm or less for thin-film scans. In thin-film scans, set the slit width so that the incident X-ray beam does not irradiate out of the sample at the incident angle (usually near the critical angle) during measurement.

Refer to Table 3.3.2 for the critical angle of various materials and to Fig. 3.3.2 for the relationship between the slit width and irradiated area (the spread of X-ray beam on the sample surface).

Table 3.3.2 Critical angle of various materials

| Material (density [g/cm <sup>3</sup> ]) | Critical angle [degree] |
|---|-------------------------|
| Si (2.33)                               | 0.22                    |
| Al (2.70)                               | 0.23                    |
| Ge (5.32)                               | 0.28                    |
| Au (19.32)                              | 0.56                    |

The critical angle is calculated for the Cu K $\alpha_1$  line (Wavelength of 1.54056 Å) as the incident X-ray beam.

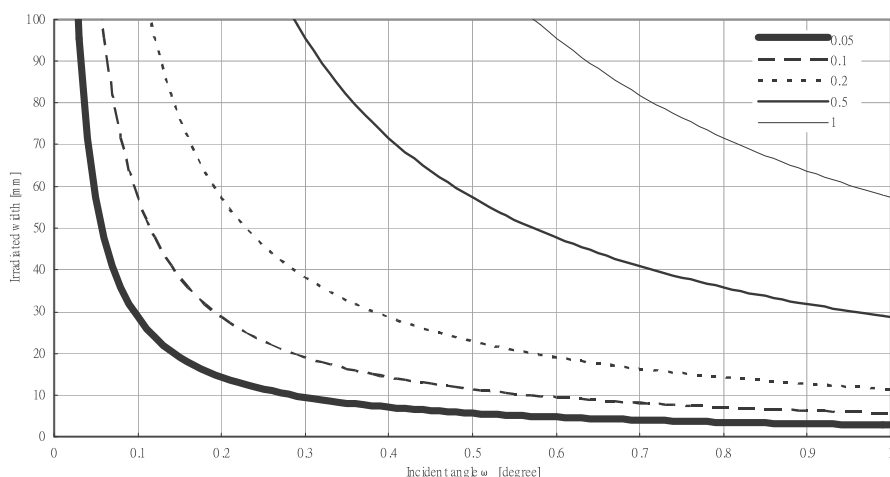


Fig. 3.3.2 Relationship between incident angle and the irradiated area

The figure indicates the irradiated width in the horizontal direction. The irradiated width in the vertical direction will be approximately twice the width of the height-limiting slit used.

After setting the sample on the sample stage, perform sample alignment—i.e., adjust vertical position and tilting. Here, when performing thin-film scan measurements or when measuring a slight tilt (offset angle) between the sample surface and a lattice plane almost parallel to it in out-of-plane measurement, perform halving adjustments by using the direct beam, then performing fine halving adjustment using the total reflection. Refer to Section 4.5.4 for a detailed account of adjustment procedures.

If you are performing out-of-plane measurements, measure the diffraction patterns with a  $2\theta/\omega$  scan following sample alignment.

If you are performing thin film measurement, set the incident angle  $\omega$  close to the critical angle

to obtain information corresponding to the desired depth of the sample. Measure the diffraction patterns using a  $2\theta$  scan.

Fig. 3.3.3 shows an example of an out-of-plane measurement of a poly-Si sample with the (111) plane oriented parallel to the sample surface.

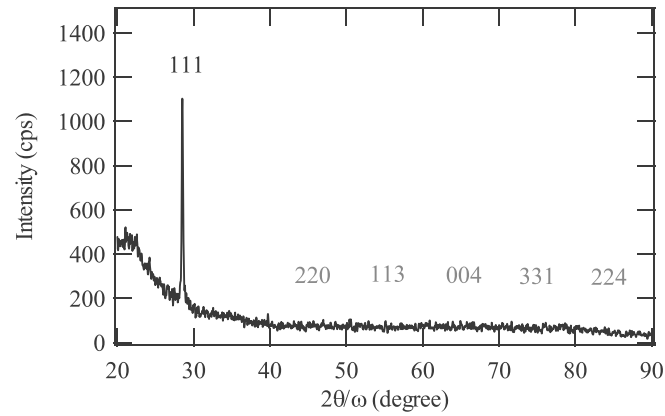


Fig. 3.3.3 Out-of-plane measurement of {111} oriented poly-Si

### 3.3.2 In-Plane Measurement

Fig. 3.3.4 illustrates the procedures for in-plane measurement.

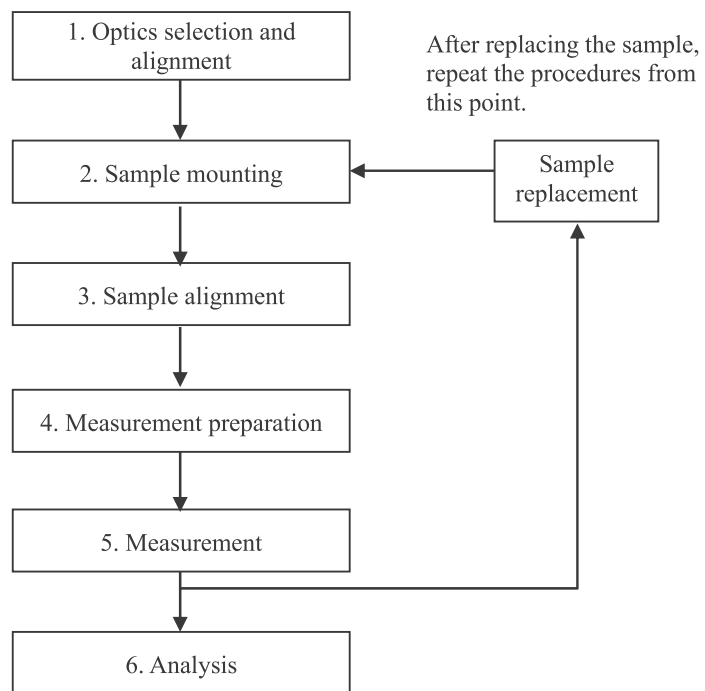


Fig. 3.3.4 Flow of measurement

Referring to Table 3.3.3, select the optics in the direction of the incident angle (the direction of  $\omega$  rotation). In the direction of the diffraction angle (the direction of the  $\phi$  or  $2\theta\chi$  rotation) perpendicular to the direction of the incident angle, insert Soller slits with apertures of approximately  $0.1^\circ$  to  $0.5^\circ$  on both the incident and receiving sides.

Table 3.3.3 Guide for selecting optics

| Sample crystallinity                              | Appropriate optics                                | Remarks   |
|---|---|---|
| Polycrystal                                       | Medium resolution PB<br>•<br>Thin film (standard) | Select $K\alpha$ line with multilayer mirror.                   |
| Strongly oriented polycrystals to single crystals | Double-crystal monochromator                      | Select only $K\alpha_1$ line with double-crystal monochromator. |

Set the slits so that the size of the incident X-ray beam in the lengthwise direction is approximately the same as the size of the sample and the size of the X-ray beam in the vertical direction is 0.2 mm or less. Set the slit width so that the incident X-ray beam does not irradiate out of the sample at the incident angle (usually near the critical angle) during measurement.

Refer to Table 3.3.2 for critical angles for various materials and to Fig. 3.3.2 for an illustration of the relationship between the slit width and irradiated area (the spread of X-ray beams on the sample surface).

After setting the sample on the sample stage, perform sample alignment (i.e., adjust the vertical position and tilting). The incident angle of the X-ray beam relative to the sample surface must not change when the sample is rotated in-plane ( $\phi$  rotation). Align the positions using total reflection so that the  $\phi$  rotation axis is in the same direction as the sample surface normal.

Here, consider why the in-plane rotation axis must be in the same direction as the sample surface normal and how they match.

As shown in Fig. 3.3.5, if the direction of the  $\phi$  rotation axis differs from the direction of the sample surface normal, the incident angle changes when the sample is rotated in-plane. The sample surface normal and the in-plane rotation axis must match to keep the incident angle of the X-ray beam unchanged with respect to the sample surface when the sample is rotated in-plane during measurement. Discussed next is an example illustrating this alignment procedure.

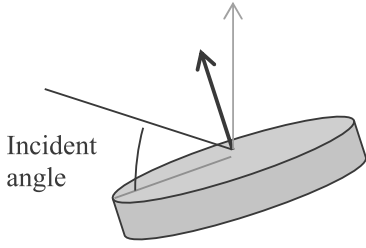
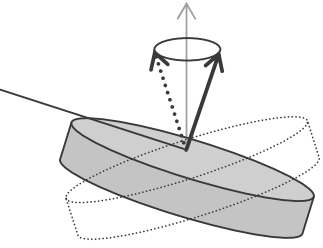
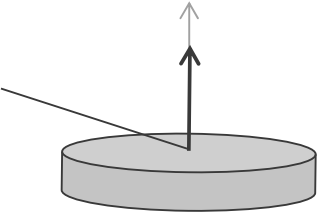
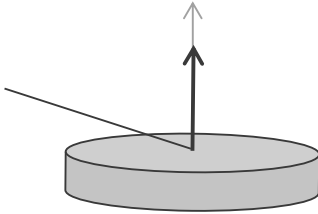
|   | $\phi = 0^\circ$  | $\phi = 180^\circ$   |
|---|---|--|
| When the sample surface normal (thick arrow) and the rotation axis of the sample stage (thin arrow) are not in the same direction,<br><br>the incident angle of the X-ray beam (medium line) changes. |  |  |
| When the sample surface normal (thick arrow) and the rotation axis of the sample stage (thin arrow) are aligned,<br><br>the incident angle of the X-ray beam (medium line) remains constant.          |  |  |

Fig. 3.3.5 Relationship between  $\phi$  rotation axis and sample surface normal

To adjust the sample surface normal and the sample in-plane rotation axes to the same direction, as shown in Fig. 3.3.6, fix the counter and measure the total reflection angles of  $\omega_\phi = -90^\circ$ ,  $\omega_\phi = 0^\circ$ ,  $\omega_\phi = 90^\circ$ , and  $\omega_\phi = 180^\circ$  at each position of  $\phi$ . Here, based on these angles, we calculate the shift  $\Delta R_x$  and  $\Delta R_y$  between the  $\phi$  rotation axis and the sample surface normal using Formula 5.3.1.

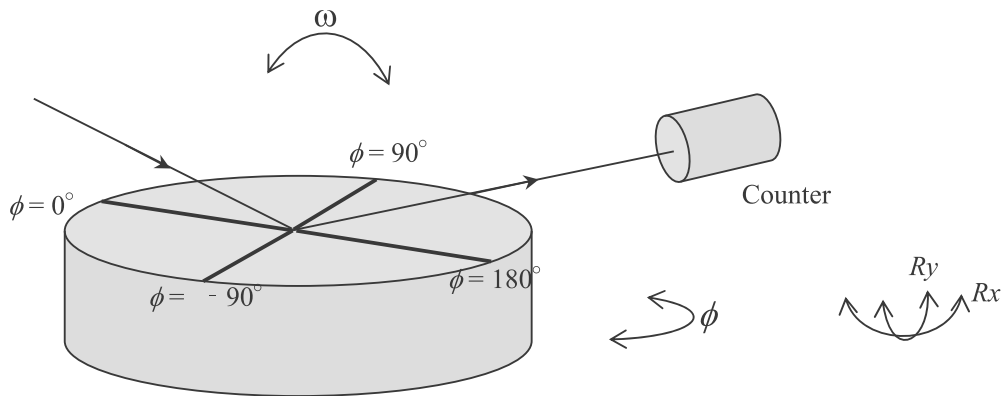


Fig. 3.3.6 Relationship between total reflection angles ( $\omega_\phi = -90^\circ$ ,  $\omega_\phi = 0^\circ$ ,  $\omega_\phi = 90^\circ$ , and  $\omega_\phi = 180^\circ$ ) and rotation axes ( $R_x$  and  $R_y$ )

$$\Delta Rx = \omega_{\phi=0} - \frac{(\omega_{\phi=0} + \omega_{\phi=180})}{2}$$

$$\Delta Ry = \omega_{\phi=-90} - \frac{(\omega_{\phi=-90} + \omega_{\phi=90})}{2}$$

Formula 3.3.1

Using the rotation axes  $Rx$  and  $Ry$  for the sample shown in Fig. 3.3.6, we can calculate  $\Delta Rx$  and  $\Delta Ry$  from Formula 3.3.1 to match the  $\phi$  rotation axis and the sample surface normal.

Following sample alignment, set the incident angle  $\omega$  near the critical angle to obtain information corresponding to the desired depth of the sample and measure the diffraction patterns with a  $2\theta/\phi$  scan. Insufficient alignment of the sample surface normal will lead to inaccurate information along the direction of depth: Take special care with alignment when performing an analysis in the direction of depth.

Fig. 3.3.7 shows an example of the in-plane measurement of a poly-Si sample with the (111) plane parallel to the sample surface.

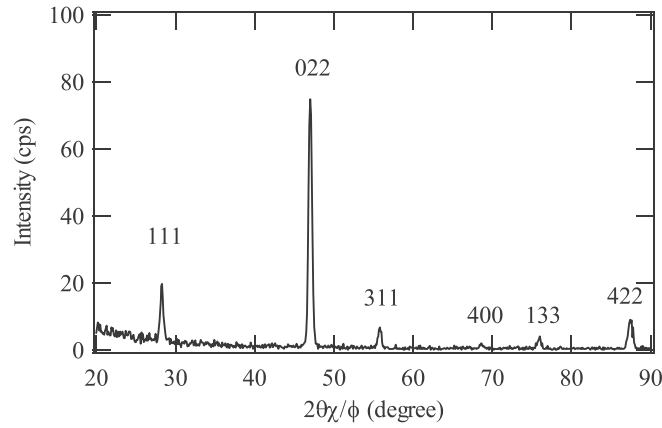


Fig. 3.3.7 In-plane measurement of {111} oriented poly-Si

In this example of measurement, the diffraction intensity of the (022) plane is relatively high. This is because the diffraction intensity of the lattice planes oriented perpendicular to the sample surface (in other words, the diffraction intensity of the (022) plane perpendicular to the (111) plane) is relatively prominent in in-plane measurement, as indicated in Fig. 3.3.8.

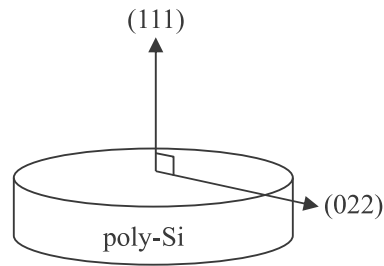


Fig. 3.3.8 Relationship between (111) plane and (022) plane of poly-Si (cubic crystal)

### 3.3.3 Pole Figure Measurement

Fig. 3.3.9 illustrates the pole figure measurement procedure.

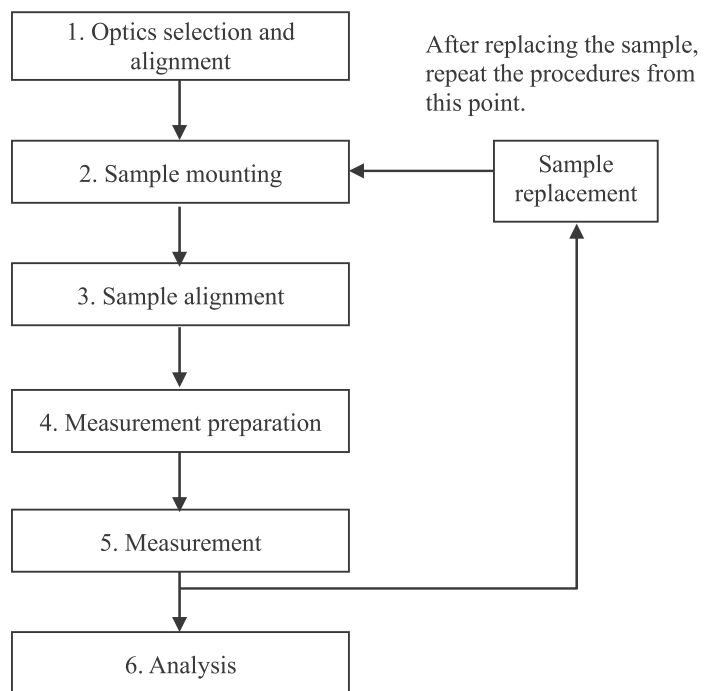


Fig. 3.3.9 Measurement flow

Use Table 3.3.4 as a guide to select the optics.

Table 3.3.4 Guide to selecting optics

| Sample crystallinity                              | Appropriate optics                           | Remarks   |
|---|--|---|
| Polycrystal                                       | Medium resolution PB<br>Thin film (standard) | Select $K\alpha$ line with multilayer mirror.                   |
| Strongly oriented polycrystals to single crystals | Double-crystal monochromator                 | Select only $K\alpha_1$ line with double-crystal monochromator. |

Set the slits so that the X-ray beam does not irradiate out of the sample during measurement.

After setting the sample on the sample stage, perform sample alignment (i.e., adjust the vertical position and tilting). Here, when measuring a slight tilt (offset angle) between the sample surface and a lattice plane nearly parallel to the sample surface, perform halving adjustment with the direct beam, then perform fine halving adjustment using the total reflection. Refer to Section 4.5.4 for a detailed account of the adjustment procedure.

Following sample alignment, specify the diffraction angle of the diffraction peak to be measured and the measurement range for  $\alpha$  and  $\beta$  and measure the pole figure.

Fig. 3.3.10 shows an example of pole figure measurement for the (111) and (220) planes of a (111) fiber-oriented Cu film.

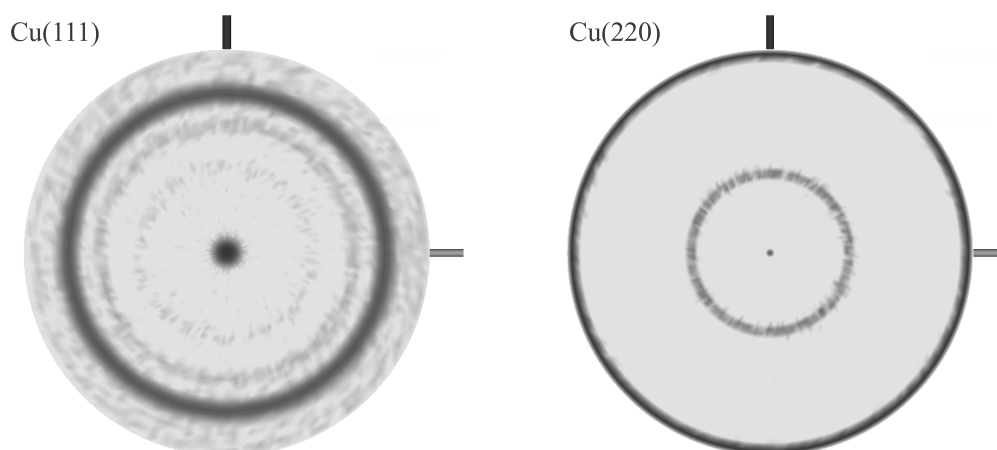


Fig. 3.3.10 Pole figure measurement for (100) plane of Cu film



### 3.3.4 Rocking Curve Measurement

Fig. 3.3.11 illustrates the steps for performing rocking curve measurement.

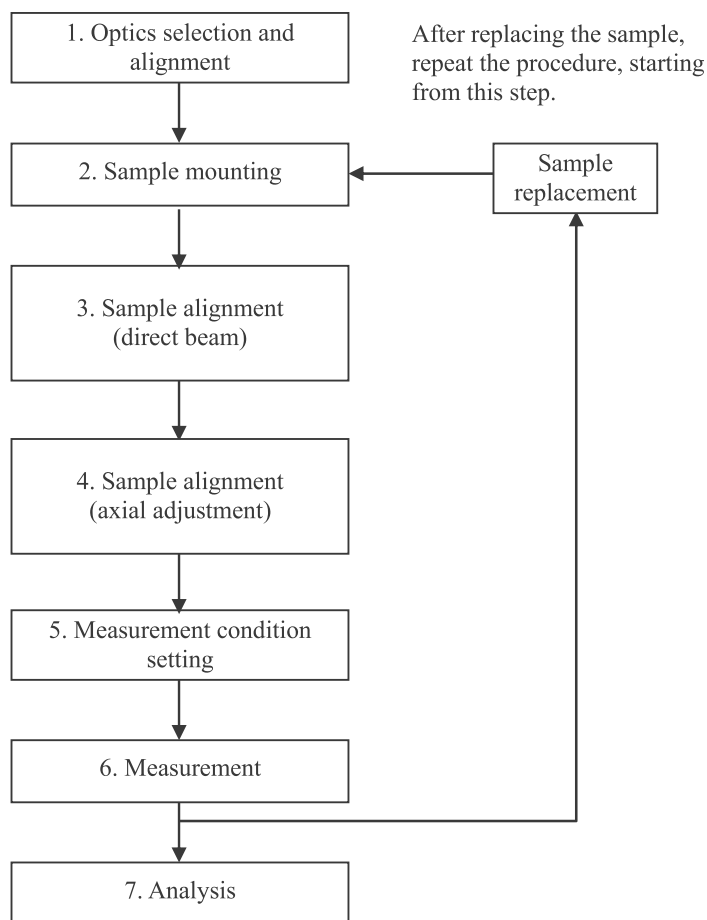


Fig. 3.3.11 Measurement flow

Use Table 3.3.5 as a guide when selecting optics.

Table 3.3.5 Guide for selecting optics

| Sample crystallinity   | Appropriate optics                                | Remarks   |
|--|---|---|
| Randomly oriented to strongly oriented polycrystals (metals, dielectric materials, etc.) | Medium resolution PB<br>•<br>Thin film (standard) | Select $K\alpha$ line with multilayer mirror.                             |
| Single crystals (GGG, SiC, etc.)   | Double-crystal monochromator                      | Select only $K\alpha_1$ line with double-crystal monochromator.           |
| Perfect crystals (Si, Ge, GaAs, etc.)  | Four-crystal monochromator                        | Double-crystal optics are acceptable when using pseudo-parallel geometry. |

In rocking curve measurement, set the incident optics so that the sizes of the reciprocal lattice points of the crystal of interest (substrate or epitaxial film) and the intervals between two or more reciprocal lattice points of the film or substrate can be measured with adequate resolution. For example, as indicated in Fig. 3.3.12 (a), if the resolution of the incident optics is low, the reciprocal lattice points (diffraction peaks) of the substrate and the film are observed simultaneously and not separated. As indicated in Fig. 3.3.12 (b), when the resolution is adequate, the reciprocal lattice points of the substrate and the film are observed separately.

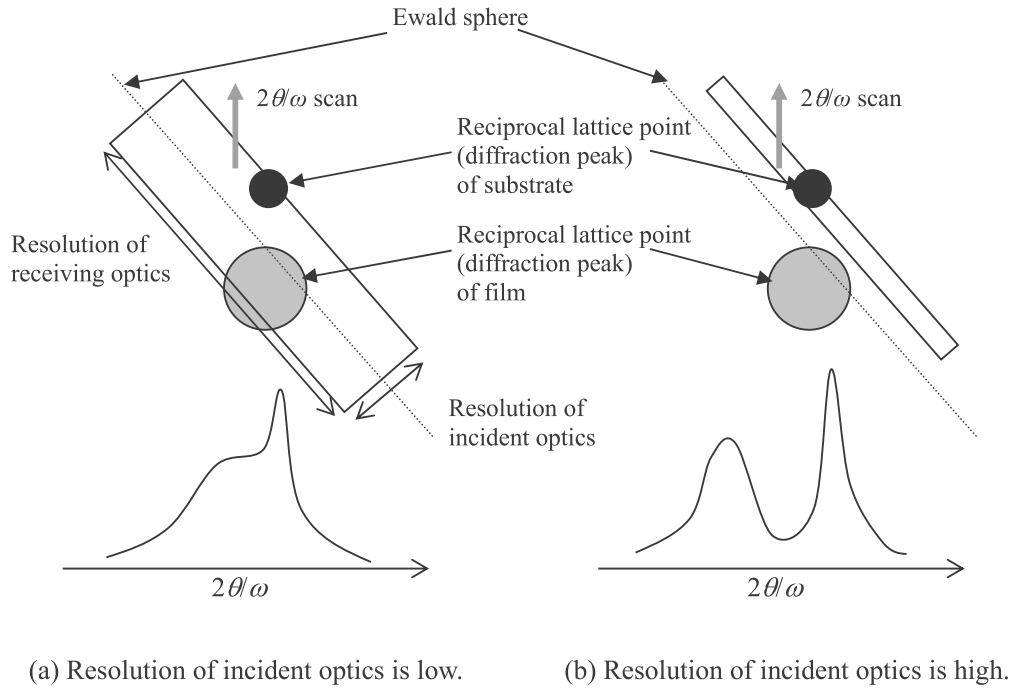


Fig. 3.3.12 Resolution and rocking curve

If you perform measurements after selecting optics based on Table 3.3.4 and the diffraction peaks are insufficiently resolved as shown in Fig. 3.3.12 (a), you must replace the current optics with higher resolution optics.

In general, use only receiving slits in the receiving optics. Increasing the resolution of the receiving optics beyond the point necessary by using additional optical devices such as an analyzer reduces the resolution function too far with respect to the reciprocal lattice points (diffraction peaks) and makes it difficult to identify diffraction peaks. Receiving slits can prevent the generation of a background (e.g., by diffuse scattering) without reducing the resolution function more than necessary.

Nevertheless, when measuring a sample that exhibits spreads of the reciprocal lattice points due to thin film mosaicity (e.g., a GaN-based compound semiconductor), using an analyzer crystal can sometimes reduce the effects of the mosaicity and produce a clear profile.

Set the slits so that the X-ray beam does not irradiate out of the sample during measurement. After setting the sample on the sample stage, perform the sample alignment (e.g., adjust the vertical position and tilting). Here, perform only the halving adjustment with the direct beam. Refer to Section 4.5.4 for a detailed account of the adjustment procedure.

Next, move the measurement axes to the angles at which you observe diffraction with the indices to be measured. For example, when a Si single crystal with its sample surface normal in the  $[001]$  direction is measured with the X-ray incidence angle in the  $[110]$  direction, the  $(004)$  plane and the  $(224)$  plane are observed at positions indicated in Fig. 3.3.13.

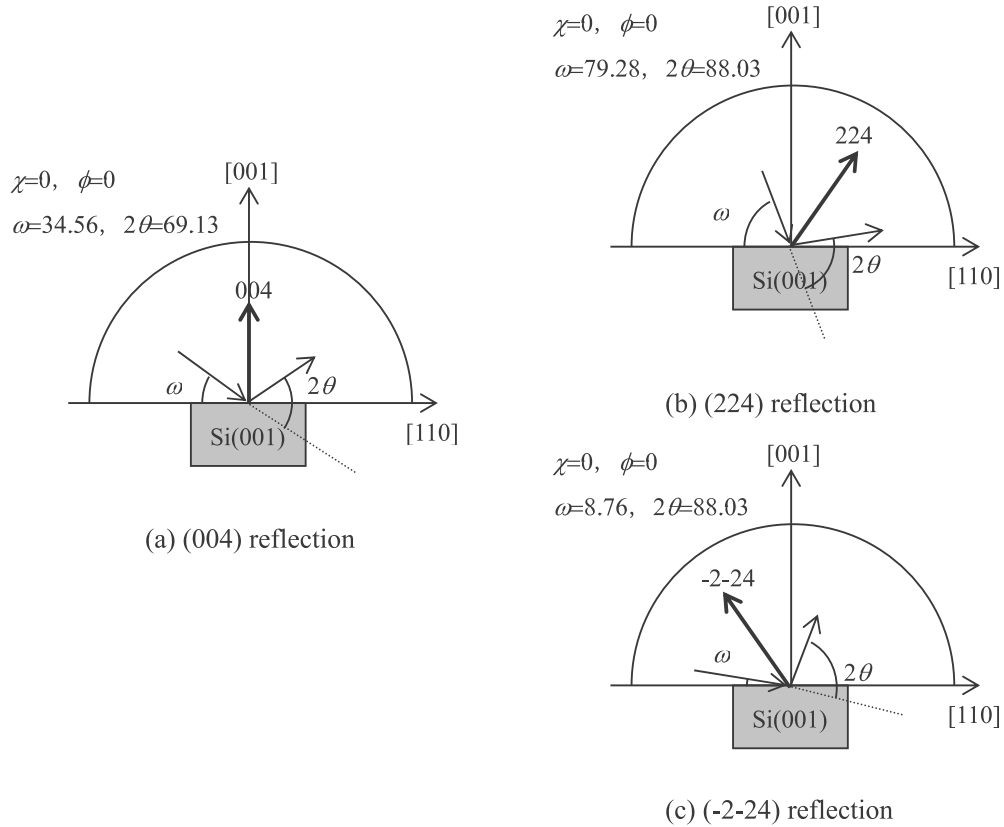


Fig. 3.3.13 Various reflection angles

The positions of the measurement axes at which the diffraction peaks are observed shift slightly depending on the offset angle or the manner in which the sample is mounted. After moving the axes to the calculated positions, scan the  $\omega$  axis and find a diffraction peak. Here, the  $\omega$  axis is scanned first because the rocking curve measurement normally uses a monochromator in the incident optics to reduce divergence in the incident angle and only slits in the receiving optics, narrowing the resolution function in the direction of the  $\omega$  axis while leaving it wide in the directions of other axes (Fig. 3.3.12). When the  $\omega$  axis is scanned, a nearby reciprocal lattice point enters the range of the resolution function, and a diffraction peak is observed.

Adjust the shifts in the measurement axes after finding a diffraction peak. To measure the rocking curve accurately, the diffraction (reciprocal lattice point) must be present in the scattering plane formed by the incident and diffracted X-ray beams, as shown in Fig. 3.3.14 (a). To place the reciprocal lattice point in the scattering plane, adjust the  $\chi$  axis for a symmetric reflection and the  $\phi$  axis for an asymmetric reflection of high asymmetry. These axes are called the **swing** or **tilt axes**.

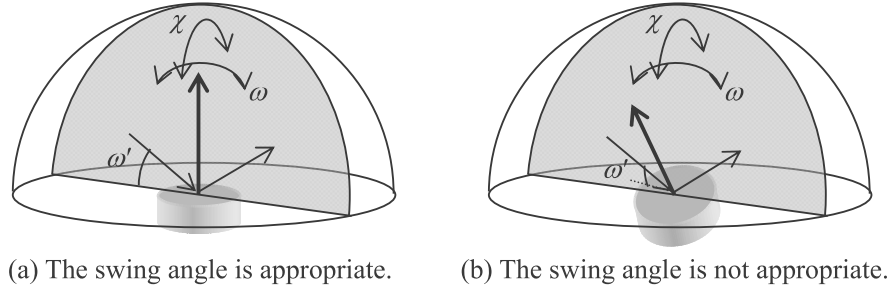


Fig. 3.3.14 Change in incident angle following shift in swing angle

As shown in Fig. 3.3.14 (a), if the swing angle is appropriate, the incident angle  $\omega'$  of the X-ray beam with respect to the sample surface equals  $\omega$ , and as shown in Fig. 3.3.14 (b), if the swing angle is not appropriate, the incident angle  $\omega'$  will be smaller than  $\omega$ . If the swing angle is not suitable, the position of the diffraction peak will shift to the higher angle side of the true position, the peak width will spread, and the intensity of the diffraction peak will drop. Fig. 3.3.15 shows an example of a  $\omega$  scan performed while gradually changing the swing angle.

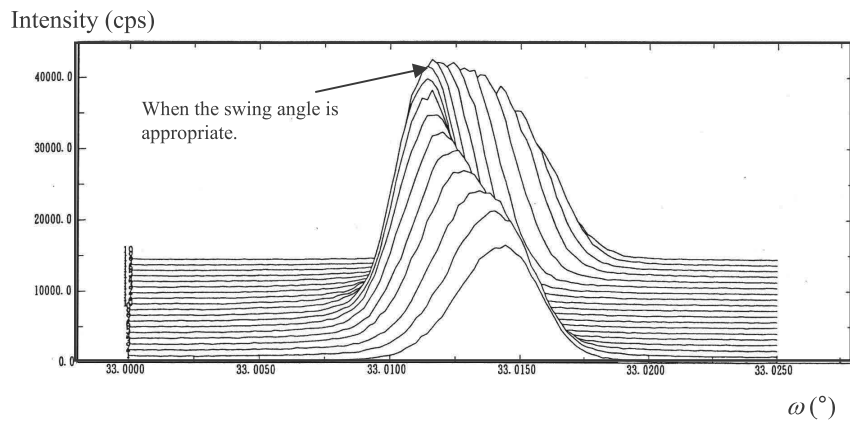


Fig. 3.3.15 Swing angle dependence of  $\omega$  scan

The adjustment of the swing angle is called axial adjustment. Two methods of axial adjustment are used. One involves scanning the  $\omega$  axis while changing the swing angle gradually, as shown in Fig. 3.3.15, and determining the position of the swing axis so that the peak position is at the smallest angle, full width at half maximum (FWHM) of the peak is narrowest, or peak intensity is greatest. (These three conditions are met at approximately the same swing angle.) The other

method is to scan the swing axis directly and determine the position at which the peak intensity is greatest. With the latter method, the following procedures are repeated: scan the  $\omega$  axis, set the  $\omega$  axis at the peak position, scan the swing axis ( $\chi$  scan or  $\phi$  scan), and set the swing axis to the peak position. Normally, after these procedures are repeated approximately three times, the peak position will not change in either the  $\omega$  scan or the swing angle scan, indicating that the shift in swing angle is properly adjusted. Here, if the swing angle shifts significantly at the beginning, the peak may split in the swing scan. If so, move the swing axis to the position corresponding to the average of the two peak positions.

Following axial adjustment, set the measurement conditions and measure the rocking curve. Here, set the measurement conditions so that the characteristics of the diffraction peaks of the substrate and film are measured accurately.

Fig. 3.3.16 shows an example of measurement for the (004) plane of the AlGaAs/InGaAs/GaAs (001) surface together with rocking curve simulation.

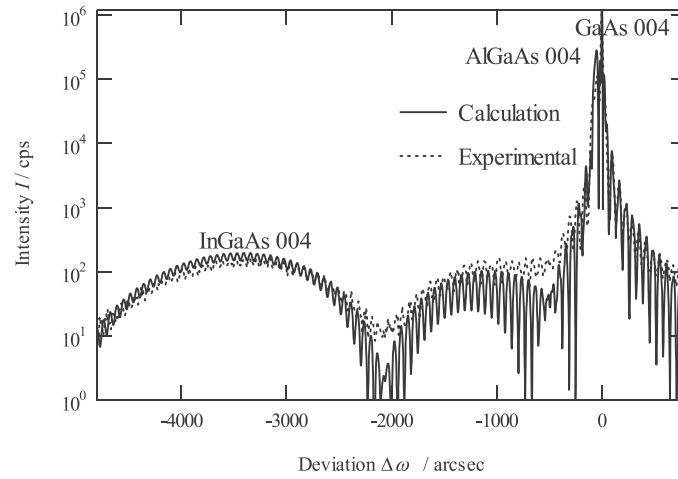


Fig. 3.3.16 Example of rocking curve measurement

### 3.3.5 Reciprocal Space Mapping (RSM) Measurement

Fig. 3.3.17 shows the flow of reciprocal space mapping (RSM) measurement.

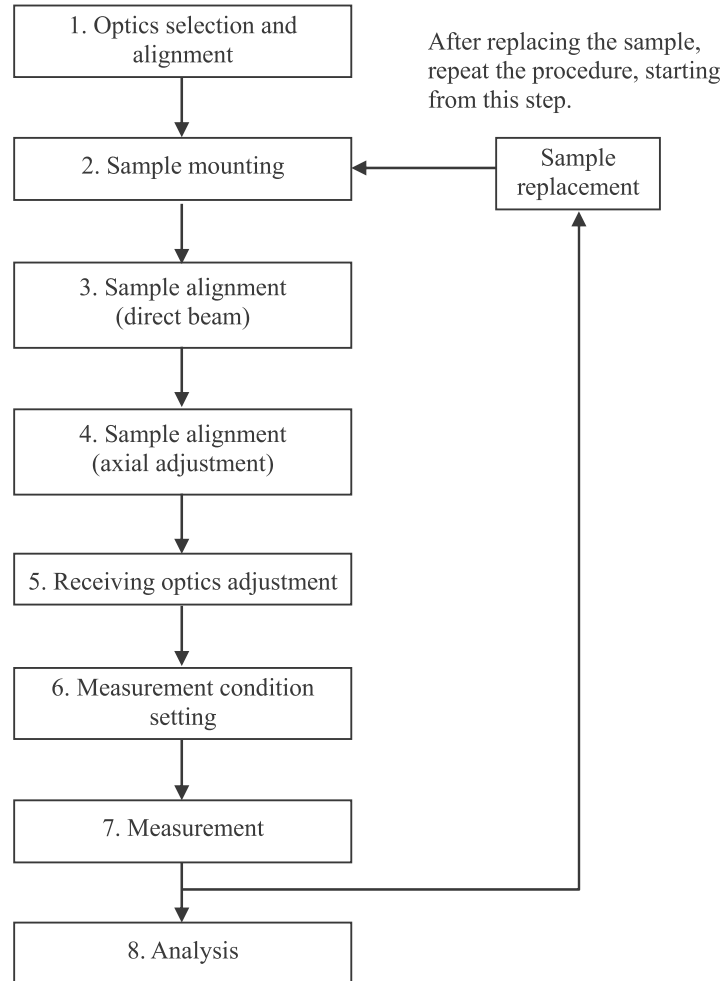


Fig. 3.3.17 Measurement flow

The procedure, down to the selection of incident optics and sample alignment (halving adjustment by direct beam and axial adjustment), are identical to the procedure for rocking curve measurement.

In ordinary rocking curve measurements, the reciprocal lattice points of the substrate and film are observed in a one-dimensional scan ( $2\theta/\omega$  scan) using a resolution function narrow in the one-dimensional direction (i.e., only the incident optics has high resolution; the receiving optics uses slit collimation). However, RSM measurement scans in two-dimensional directions ( $2\theta/\omega$  scan +  $\omega$  scan). This means the resolution function must be small enough in the

two-dimensional directions. To make the resolution function sufficiently small in the two-dimensional directions, the receiving optics uses narrow slits or an analyzer. Here, the resolution function has the shape shown in Fig. 3.3.18 to enable measurement of the two-dimensional distribution of the diffraction intensity in reciprocal space.

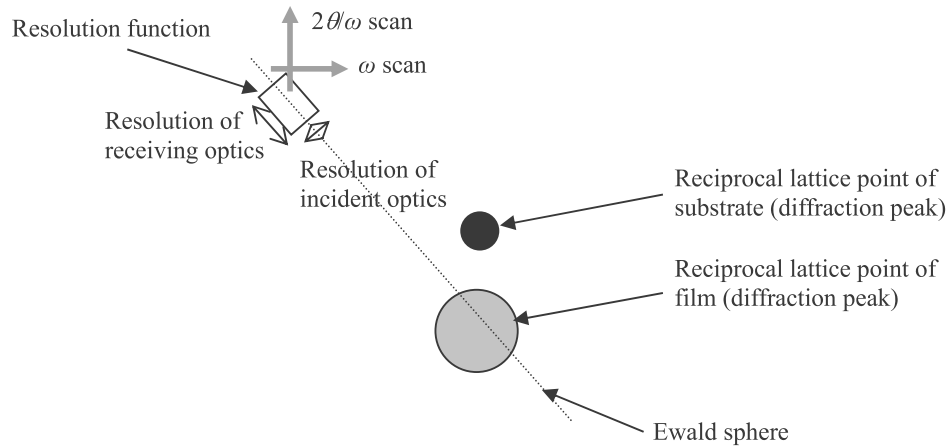


Fig. 3.3.18 Resolution function of reciprocal space mapping measurement

Use Table 3.3.6 as a guide to select the optics. Table 3.3.6

Table 3.3.6 Guide for selecting optics

| Sample crystallinity   | Appropriate optics      | Remarks   |
|--|-------------------------|---|
| Randomly oriented to strongly oriented polycrystals (metals, dielectric materials, etc.) | Receiving slit          | Insert a slit of width ranging from 0.05 mm to 1 mm.  |
| Single crystals (GGG, SiC, etc.)   | Double-crystal analyzer | Suppress the resolution of the receiving optics to the diffraction angle width of the analyzer crystal. (When using a pseudo-parallel geometry, use the same crystal plane as the incident optics.) |
| Perfect crystals (Si, Ge, GaAs, etc.)  | Double-crystal analyzer | Suppress the resolution of the receiving optics to the diffraction angle width of the analyzer crystal. (When using a pseudo-parallel geometry, use the same crystal plane as the incident optics.) |

When using a double-crystal analyzer in the measurement, perform the steps of the procedure leading up to axial adjustment with a receiving slit, then, attach the analyzer before beginning measurement. This is done because high receiving optics resolution from the outset will make it extremely difficult to identify diffraction peaks in the  $\omega$  scan and perform axial adjustments. Until you have confirmed the diffraction peaks of both the substrate and the film and performed axial adjustment using either diffraction peak, use just the receiving slit.

Fig. 3.3.19 shows an example of RSM measurement for the (004) plane and the (224) plane of the Si epitaxial film sample (SiGe film (Ge content 3.8%, film thickness 380 nm)/Si (100) substrate). Spots of high intensity correspond to the reciprocal lattice points of Si and SiGe. The vertical line represents CTR scattering and appears when the sample surface is highly flat.

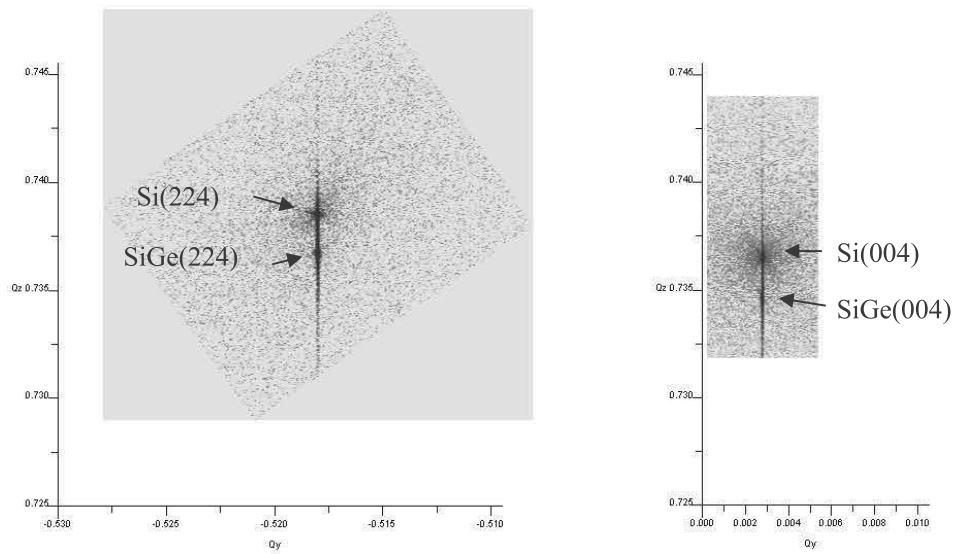


Fig. 3.3.19 Example of RSM measurement

Left: Si, SiGe (224) plane; right: Si, SiGe (004) plane



### 3.3.6 Summary

This chapter discussed the various crystal structures and crystallinity characteristics we can evaluate using various diffraction measurements and the corresponding measurement procedures and precautions. Summarized below are the key concepts presented in this Chapter.

#### 1. Information provided by various diffraction measurements

| Various measurement techniques  |  |  |
|---|--|--|
| Measurement technique   | Information obtained   | Scan axis  |
| Out-of-plane measurement<br>(One-dimensional scan)                            | Information on lattice planes parallel to sample surface<br>→ Qualitative analysis and crystal structure   | $2\theta/\omega$<br>(Always $2\theta = 2 \times \omega$ )  |
| Thin film measurement<br>(One-dimensional scan)                               | Information near sample surface (applies only to sample with no orientation)<br>→ Qualitative analysis and crystal structure   | $2\theta$<br>(Incident angle, $\omega$ , is fixed near the critical angle.)  |
| In-plane measurement<br>(One-dimensional scan)                                | Information on lattice planes near and parallel to sample surface<br>→ Qualitative analysis and crystal structure  | $2\theta\chi/\phi$<br>(Incident angle, $\omega$ , is fixed near the critical angle.)                                 |
| Pole figure measurement<br>(Two-dimensional scan)                             | Information on distribution of specific crystal orientation<br>→ Orientation analysis  | $\chi(\alpha), \phi(\beta)$<br>( $2\theta$ or sum of $2\theta$ and $2\theta\chi$ is fixed at the diffraction angle.) |
| Preferred orientation and crystallinity measurement<br>(One-dimensional scan) | Information on degree of preferred orientation or crystallinity<br>→ Orientation and crystallinity analysis  | $\omega, \chi$ , or $\phi$   |
| Rocking curve measurement*<br>(One-dimensional scan)                          | Information on film structure and crystallinity of epitaxial or single crystal<br>→ Crystallinity, film thickness, and composition ratio   | $2\theta/\omega$   |
| RSM measurement<br>(Two-dimensional or three-dimensional scan)                | Information on d-value of three-dimensional components of preferred orientation, crystal orientation, and degree of preferred orientation<br>→ Qualitative analysis, orientation analysis, and crystallinity analysis<br>Information on film structure and crystallinity of epitaxial or single crystal<br>→ Crystallinity analysis and epitaxial analysis | $2\theta/\omega, \omega (\chi \text{ or } \phi)$<br>$2\chi/\phi, \phi (\chi \text{ or } \phi)$                       |

## 2. Precautions for measurement

The optical resolution required will vary, depending on the measurement technique and the sample measured. Use the following table below to select appropriate optics.

Out-of-plane measurement and thin film measurement

| Sample crystallinity   | Appropriate optics                                | Remarks   |
|--|---|---|
| Randomly oriented to strongly oriented polycrystals (metals, dielectric materials, etc.) | Medium resolution PB<br>•<br>Thin film (standard) | Select $K\alpha$ line with multilayer mirror.                   |
| Single crystals (GGG, SiC, etc.)   | Double-crystal monochromator                      | Select only $K\alpha_1$ line with double-crystal monochromator. |

In-plane measurement

| Sample crystallinity   | Appropriate optics                                | Remarks   |
|--|---|---|
| Randomly oriented to strongly oriented polycrystals (metals, dielectric materials, etc.) | Medium resolution PB<br>•<br>Thin film (standard) | Select $K\alpha$ line with multilayer mirror.                   |
| Single crystals (GGG, SiC, etc.)   | Double-crystal monochromator                      | Select only $K\alpha_1$ line with double-crystal monochromator. |

Insert Soller slits with apertures of approximately  $0.1^\circ$  to  $0.5^\circ$  in the direction of the diffraction angle ( $\phi$  or  $2\theta$  direction).

Caution: To control the incident angle precisely, adjust the sample surface normal and sample in-plane rotation axis so that they are aligned.

Pole figure measurement

| Sample crystallinity                             | Appropriate optics                                | Remarks   |
|--|---|---|
| Polycrystal                                      | Medium resolution PB<br>•<br>Thin film (standard) | Select $K\alpha$ line with multilayer mirror.                   |
| Strongly oriented polycrystals to single crystal | Double-crystal monochromator                      | Select only $K\alpha_1$ line with double-crystal monochromator. |

Caution: To measure the diffraction intensity precisely, to the extent possible, set the slit so that the incident X-ray beam does not irradiate out of the sample.

Rocking curve measurement and RSM measurement (Incident optics)

| Sample crystallinity   | Appropriate optics                           | Remarks  |
|--|--|--|
| Randomly oriented to strongly oriented polycrystals (metals, dielectric materials, etc.) | Medium resolution PB<br>Thin film (standard) | Select $K\alpha$ line with multilayer mirror.                      |
| Single crystals (GGG, SiC, etc.)   | Double-crystal monochromator                 | Select only $K\alpha_1$ line with double-crystal monochromator.    |
| Perfect crystals (Si, Ge, GaAs, etc.)  | Four-crystal monochromator                   | Double-crystal optics are acceptable for pseudo-parallel geometry. |

Caution: Perform axial adjustments for precise rocking curve measurements.

RSM measurement (Receiving optics)

| Sample crystallinity   | Appropriate optics       | Remarks   |
|--|--------------------------|---|
| Randomly oriented to strongly oriented polycrystals (metals, dielectric materials, etc.) | Receiving slit           | Insert a slit of width ranging from 0.05 mm to 1 mm.  |
| Single crystals (GGG, SiC, etc.)   | Double-crystal analyzer  | Suppress the resolution of the receiving optics to the diffraction angle width of the analyzer crystal. (When using a pseudo-parallel geometry, use the same crystal plane as the incident optics.) |
| Perfect crystals (Si, Ge, GaAs, etc.)  | Double -crystal analyzer | Suppress the resolution of the receiving optics to the diffraction angle width of the analyzer crystal. (When using a pseudo-parallel geometry, use the same crystal plane as the incident optics.) |

Caution: Confirm the positions of the diffraction peaks of both the substrate and the film and perform axial adjustments using either diffraction peak before switching to high-resolution receiving optics to make further adjustments.

## Chapter 4 X-ray Reflectivity Method

If the surface and the interfaces are flat, the X-ray reflectivity method can be used whether the sample is crystalline or amorphous. X-ray reflectivity has drawn particular attention as a measurement technique capable of evaluating the film thickness, density, and surface or interface roughness of the thin-film materials used in semiconductor devices.

This chapter provides an overview of the principles of X-ray reflectivity, measurement procedures, and analysis methods. It also discusses the procedural flow from measurement to analysis, as well as precautions.

### §4.1 Applicability of X-Ray Reflectivity Method

Thin-film materials have found use in a wide range of devices in recent years, gaining the status of an essential category of advanced materials. The diverse characteristics of the devices depend significantly on the thickness, density, and surface or interface roughness of thin-film materials. These parameters must be correctly evaluated and film growth conditions properly controlled.

Used to evaluate these parameters, X-ray reflectivity involves X-ray incidence at grazing angles with respect to sample surfaces. The method is used to analyze X-ray reflection intensity profiles versus incident angles and to determine structural parameters (thickness, density, and surface or interface roughness) of the thin film in question. Areas of application are given below. X-ray reflectivity can be used to do the following:

1. Measure thickness from several to several thousand nanometers.
2. Evaluate the surface roughness and interface width (arising from roughness and interdiffusion).
3. Evaluate the density of the film of known composition.
4. Evaluate the structure of a multilayer or single layer film.
5. Perform these tasks with a wide range of materials, whether crystalline or amorphous, including semiconductors and superconducting, magnetic, metal, and polymer films.
6. Measure samples nondestructively.

### §4.2 Overview of X-Ray Reflectivity Method

When X-rays are incident at a grazing angle to a flat surface of a material, **total reflection** occurs below incident angle  $\theta_c$ . This angle is called the **total reflection critical angle** (critical angle hereafter). The critical angle for the Cu K $\alpha$  line is small, with values such as  $0.22^\circ$  for Si,  $0.42^\circ$  for Ni, and  $0.57^\circ$  for Au and changes with the electron density (refractive index) of the material. As the X-ray incident angle increases to values beyond this angle, the X-rays gradually penetrate deeper into the material. In a material with ideal planes, reflectivity rapidly decreases proportionally to  $\theta^4$  at angles equal to or larger than  $\theta_c$ , decreasing faster with substances having rough surfaces.

If a substrate composed of such a material is overlaid with a material having a differing electron density, the X-rays reflected on the interface between the substrate and the film and the X-rays reflected from the surface of the film will interfere constructively or destructively. This interference is visible as an oscillation in the reflectivity profile. First observed by Kiessig in 1931, this oscillation is known as the **Kiessig fringe**.

Fig. 4.3.1 shows the reflectivity profile of a Au film deposited on a Si substrate by sputtering. The graph shows the results of measurement for three types of films with thicknesses differing by approximately 10 nm.

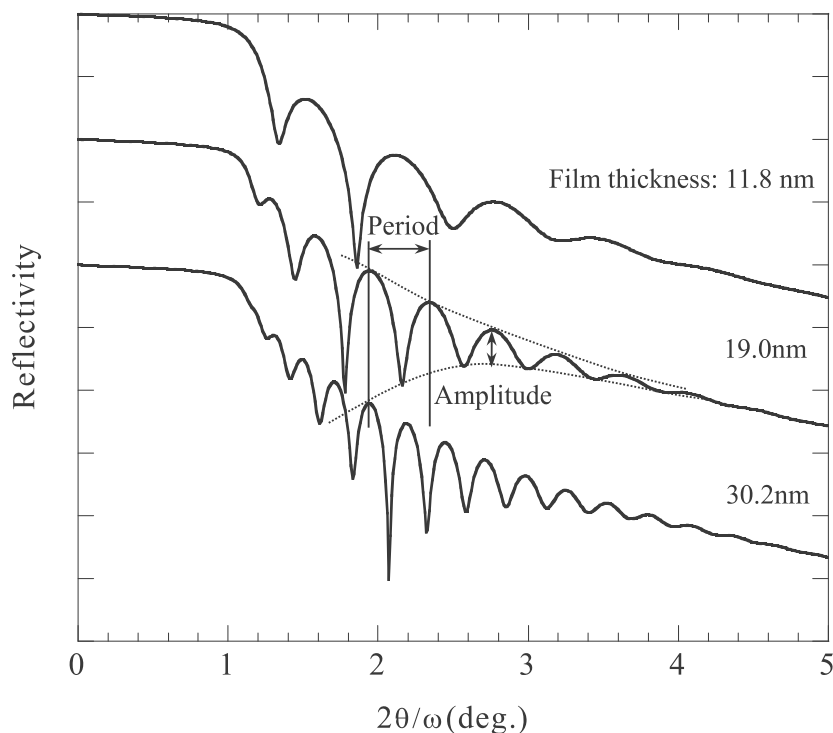


Fig. 4.2.1 Reflectivity of Au film/Si substrate

The results indicate that the period of the oscillation provides information on the film thickness. The amplitude of the oscillation is angle-dependent and contains information on film density and surface or interface roughness. The X-ray reflectivity method analyzes this profile to obtain film thickness, density, and surface or interface roughness.

Listed below are examples of methods other than the X-ray reflectivity method for measuring film thickness.

1. Optical methods (such as an ellipsometer)
2. Cross-sectional TEM or SEM method
3. X-ray fluorescence method

The X-ray reflectivity method differs from these methods in the following ways:

Optical methods have the disadvantage that they cannot be applied to opaque films. X-ray reflectivity can be used with opaque films, including those made of metal.

The cross-sectional TEM method is a destructive method that involves complex sample preparations. X-ray reflectivity is nondestructive and allows measurements to be performed in air.

The X-ray fluorescence method obtains the mass of the analyzed element per unit volume through quantitative analysis and cannot provide film thickness directly. It also requires a reference sample, and precision declines with film thickness. The method makes it difficult to analyze samples with interdiffusion and cannot be used with systems containing layers of similar materials. The reflectivity method, in contrast, can be used in these cases—a major advantage.

The X-ray reflectivity method has the following characteristics:

1. The sample must be sufficiently flat and smooth. (Surface or interface roughness must be on the order of several nanometers or less.)
2. It can be applied to polycrystalline and amorphous materials.
3. It is extremely sensitive to surface states.
4. It is independent of crystal orientation or strain.
5. It is insensitive to changes in composition.
6. It can be used to evaluate film thicknesses of up to approximately 1,000 nm. It is not ideal for thicker films.

## §4.3 Principles of X-ray Reflectivity Method

### 4.3.1 Total Reflection and Refractive Index for X-Rays

Since the **refractive index** of a material for X-rays is slightly less than 1, the X-rays undergo total reflection when incident on a flat surface of a material at a grazing angle.

The refractive index  $n$  of a material for X-rays is given by Formula 4.3.1.

$$n = 1 - \delta - i\beta \quad \text{Formula 4.3.1}$$

$$\delta = \left( \frac{r_e \lambda^2}{2\pi} \right) N_0 \rho \sum_i x_i (z_i + f_i') / \sum_i x_i M_i \quad \text{Formula 4.3.2}$$

$$\beta = \left( \frac{r_e \lambda^2}{2\pi} \right) N_0 \rho \sum_i x_i f_i'' / \sum_i x_i M_i \quad \text{Formula 4.3.3}$$

$r_e$ : Classical radius of an electron ( $2.818 \times 10^{-9}$  m)

$N_0$ : Avogadro number

$\lambda$ : X-ray wavelength

$\rho$ : Density ( $\text{g/cm}^3$ )

$z_i$ : Atomic number of the  $i$ -th atom

$M_i$ : Atomic weight of the  $i$ -th atom

$x_i$ : Atomic ratio (molar ratio) of the  $i$ -th atom

$f_i', f_i''$ : Atomic scattering factors of the  $i$ -th atom (anomalous dispersion term)

As suggested by Formula 4.3.1, the refractive index is expressed as a complex number. The parameter  $\delta$  in the formula is of the order of magnitude of  $10^{-5}$  to  $10^{-6}$  for X-rays at wavelengths of approximately 1 Å and depends on X-ray wavelength and the density and composition of the material. An additional 1 to 2 orders of magnitude smaller, the parameter  $\beta$  is a quantity related to X-ray absorption, expressed by linear absorption coefficient  $\mu$  in the following formula.

$$\beta = \lambda \mu / 4\pi \quad \text{Formula 4.3.4}$$

If we disregard absorption, the critical angle  $\theta_c$  for total reflection is given by the following formula:

$$\theta_c = \sqrt{2\delta} \quad \text{Formula 4.3.5}$$

Thus, we can obtain the density of the surface film from the total reflection critical angle. When the incident angle is less than the critical angle, the incident X-ray beam undergoes total reflection. If absorption is ignored, the reflected X-ray beam has approximately the same intensity as the incident X-ray beam (reflectivity is 1.0). If the incident angle is greater than the critical angle, the X-ray beam is refracted, and reflectivity rapidly decreases roughly in proportion to the value of the incident angle to a power of -4. The critical angle is usually  $0.2^\circ$  to  $0.5^\circ$ . It is generally greater with longer X-ray wavelengths and when the material is composed of heavier elements of greater density—in short, when the material has greater average electron density.

### 4.3.2 Reflected Wave and Refracted Wave

When the total reflection phenomenon occurs, the incident wave generates a specularly reflected wave and a refracted wave, as shown in Fig. 4.3.1.

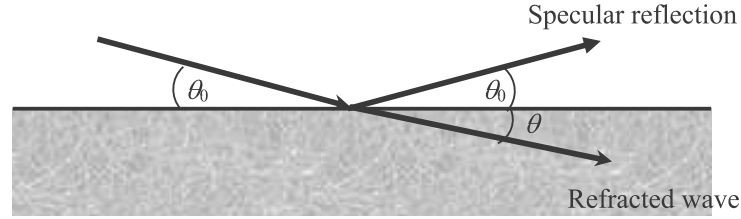


Fig. 4.3.1 Reflection and refraction of X-rays at material surface

If the density of the material is uniform, the specular reflectivity of the X-ray beam of wavelength  $\lambda$  at an ideally flat surface depends on the incident angle  $\theta$  and can be expressed by the following formulas:

**Boundary conditions:**

$$R(\theta) = \frac{(\theta - A)^2 + B^2}{(\theta + A)^2 + B^2} \quad \text{Formula 4.3.6}$$

$$A = \sqrt{\frac{\sqrt{(\theta^2 - 2\delta)^2 + 4\beta^2} + (\theta^2 - 2\delta)}{2}} \quad \text{Formula 4.3.7}$$

$$B = \frac{\beta}{A} \quad \text{Formula 4.3.8}$$

Fig. 4.3.2 shows the reflectivity of Si as given by Formula 4.3.6. It shows a rapid change at critical angle  $\theta_c$  (near  $0.2^\circ$  here).



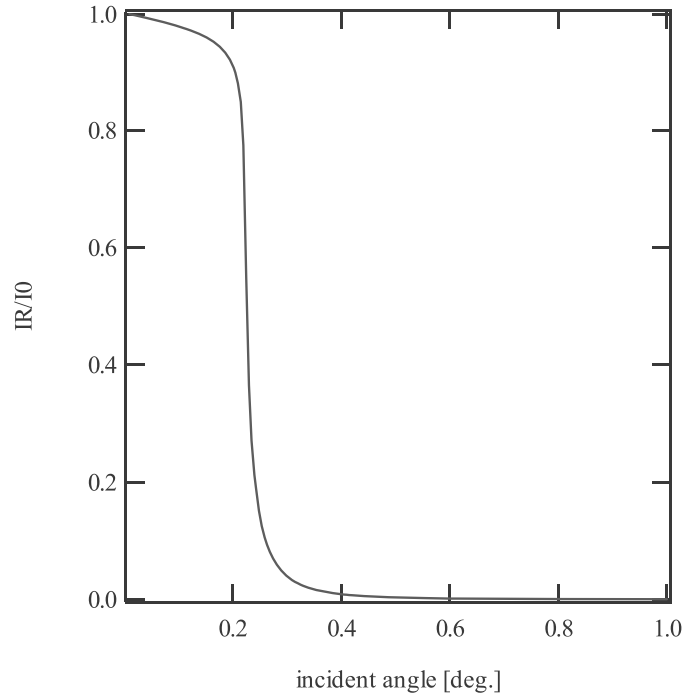


Fig. 4.3.2 Reflectivity curve of Si

The intensity of the refracted wave decays exponentially in the depth direction (**evanescent wave**). For the incident angle  $\theta$ , the intensity at depth  $z$  is expressed by the following formulas:

$$I(\theta, z) = S(\theta) \exp\left(-\frac{z}{D(\theta)}\right) \quad \text{Formula 4.3.9}$$

$$S(\theta) = \frac{4\theta^2}{(\theta + A)^2 + B^2} \quad \text{Formula 4.3.10}$$

$$D(\theta) = \frac{\lambda}{4\pi B^2} \quad \text{Formula 4.3.11}$$

Here,  $S(\theta)$  is the X-ray intensity at the surface and  $D(\theta)$  the penetration depth. Formula 4.3.9 applies to the case in which  $z$  is positive or zero. The intensity distribution for a negative value of  $z$  (the intensity distribution on the vacuum or gas side of the surface), is expressed by the following formula and indicates the interference caused by superposition with the reflected waves.

$$I(\theta, z) = \frac{S(\theta)}{2\theta^2} \left[ \theta^2 + A^2 + B^2 + (\theta^2 - A^2 - B^2) \cos\{\tau(\theta)\} + B\theta \sin\{\tau(\theta)\} \right] \quad \text{Formula 4.3.12}$$

$$\tau(\theta) = \frac{4\pi\theta}{\lambda} |z| \quad \text{Formula 4.3.13}$$

Similarly to Formula 4.3.9,  $I(\theta, z) = S(\theta)$  when  $z = 0$ . Formula 4.3.12 indicates a standing wave forms with period  $\lambda/2\theta$  at incident angle  $\theta$ .

If the material has an interface at which the refractive index is discontinuous in the depth direction (as with a thin film on a substrate), we must consider the interference arising from multiple reflections at the interface. Rather than declining monotonically on reaching the critical angle, specular reflectivity oscillates, based on the interference. The intensity of the refracted wave has a complex distribution in the depth direction and cannot be expressed as an exponential function. To understand this behavior, consider the boundary conditions of the electric field vector at each interface in a generic multilayer model (Figure 4.3.3). As with uniform materials, we can calculate reflectivity by considering the boundary conditions of the electric field vector for the X-rays at each interface. Fig. 4.3.3

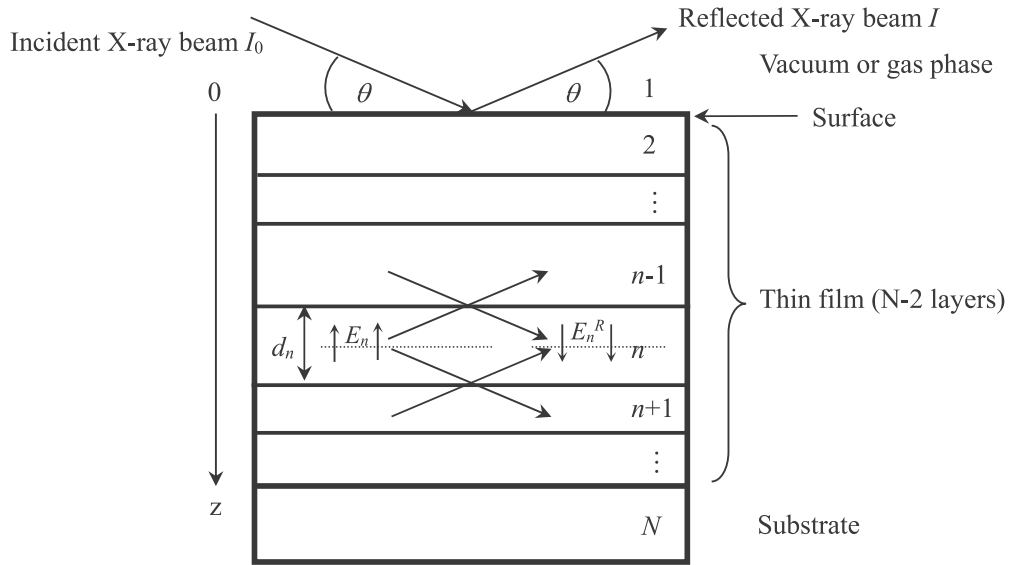


Fig. 4.3.3 Multilayer film model

That is, when the amplitudes of the electric field vectors of the incident wave (wave propagating deeper) is denoted  $\mathbf{E}_n$  and the reflected wave (wave propagating towards the surface) at the center of the  $n$ -th layer is denoted  $\mathbf{E}_n^R$ , the continuity at the interface between the  $(n-1)$ -th and  $n$ -th layers imposes the boundary conditions give by the formulas below:

$$a_{n-1}\mathbf{E}_{n-1} + a_{n-1}^{-1}\mathbf{E}_{n-1}^R = a_{n-1}\mathbf{E}_n + a_n\mathbf{E}_n^R \quad \text{Formula 4.3.14}$$

$$(a_{n-1}\mathbf{E}_{n-1} + a_{n-1}^{-1}\mathbf{E}_{n-1}^R)f_{n-1}k = (a_{n-1}\mathbf{E}_n + a_n\mathbf{E}_n^R)f_nk \quad \text{Formula 4.3.15}$$

Here, the parameters are expressed as follows:

$$k = \frac{2\pi}{\lambda} \quad \text{Formula 4.3.16}$$

$$f_n = \sqrt{\left\{(\theta^2 - 2\delta) - i2\beta\right\}} = A_n - iB_n \quad \text{Formula 4.3.17}$$

$$a_n = \exp\left(-i\frac{kf_nd_n}{2}\right) \quad \text{Formula 4.3.18}$$

The parameter  $d_n$  represents the thickness of the  $n$ -th layer. The parameter  $f_n$  is related to the Fresnel coefficient,  $F_{n-1,n}$ , by the following formula:

$$F_{n,n-1} = \frac{f_{n-1} - f_n}{f_{n-1} + f_n} \quad \text{Formula 4.3.19}$$

$A_n$  and  $B_n$  are quantities given by Formula 4.3.6 for the material in the  $n$ -th layer. The parameter  $a_n$  gives the phase difference generated when the X-ray beam propagates half the thickness of the layer and the phase difference when waves reflected from the interfaces interfere with each other.

We can calculate reflection coefficient  $R_{n-1,n} (= a_{n-1}^2 E_n / E_n^R)$  at the interface between the  $(n-1)$ '-th and  $n$ -th layers by applying Formulas 4.3.14, 4.3.15, and 4.3.19, and express the relationships in a recurrence formula:

$$R_{n-1,n} = a_{n-1}^4 \frac{R_{n,n+1} + F_{n-1,n}}{R_{n,n+1}F_{n-1,n} + 1} \quad \text{Formula 4.3.20}$$

If we assume that the substrate is sufficiently thick and that we can disregard the possibility of reflections from the rear side—that is, that  $R_{n,n+1} = 0$ —we can calculate the reflection coefficients of the interfaces one by one from the lowest interface towards the surface using Formula 4.3.20. Finally, the formula below gives specular reflectivity:

$$R(\theta) = \frac{I}{I_0} = |R_{1.2}|^2 \quad \text{Formula 4.3.21}$$

Reference: L. G. Parratt; Phys. Rev., **95**, 359 (1954)

### 4.3.3 Effects of Roughness

Most measurement samples do not have an ideally flat surface. Roughness at the surface or at interfaces affect reflectivity measurements. Assume that the position of the interface between the  $(n-1)$ '-th and  $n$ -th layers is expressed by a Gaussian distribution and that **root mean square (rms) roughness** is  $\sigma_{n-1}$ . Then, the Fresnel coefficient can be corrected as shown in the formula below using scattering vectors  $q_{n-1}$  and  $q_n$  at the interface.

$$F'_{n-1,n} = F_{n-1,n} \exp\left(-\frac{\sigma_{n-1}^2 q_{n-1} q_n}{2}\right) \quad \text{Formula 4.3.22}$$

Here, for scattering with equal angles such as specular scattering, the scattering vectors are expressed as follows:

$$q_{n-1} = 2kf_{n-1} = \frac{4\pi}{\lambda} f_{n-1} \quad \text{Formula 4.3.23}$$

We can calculate specular reflectivity with Formula 4.3.20 by substituting the correction of Formula 4.3.22 for the Fresnel coefficient. The specular reflectivity of a uniform system without a layered structure is calculated using the following formula, instead of Formula 4.3.6:

$$R(\theta) = \frac{(\theta - A)^2 + B^2}{(\theta + A)^2 + B^2} \exp\left(-\frac{16\pi^2}{\lambda^2} \sigma^2 \theta A\right) \quad \text{Formula 4.3.24}$$

Reference: L. Nevot and P. Croce;, **15**, 761 (1980)

## §4.4 Reflectivity Analysis Method

Reflectivity can be analyzed by the three following methods:

1. Method giving film thickness based on the incident angle dependence of the oscillation period.
2. Method giving film thickness via the **Fourier transformation**.
3. Method giving film thickness, density, and surface or interface roughness by fitting.

Methods 2 and 3 are practical under most conditions. Reflectivity analysis generally involves one of these two methods.

### 4.4.1 Obtaining Film Thickness Based on the Incident Angle Dependence of the Oscillation Period

This method can only be applied to a single layer film on a substrate. While the reflectivity profile from a single layer film shows a simple oscillation, the peak positions of the oscillation are more contracted at lower incident angles. This is because the effects of refraction are more pronounced at lower angles of X-ray incidence.

The relationship between film thickness  $d$  and angular position  $\theta_m$  of the  $m$ -th order peak is given by the following formulas:

1. When the  $\delta$  value ( $\delta_l$ ) of the film is greater than the  $\delta$  value ( $\delta_s$ ) of the substrate

$$\theta_m^2 \approx \sin^2 \theta_m = \left( \frac{\lambda}{2d} \right)^2 \left( m + \frac{1}{2} \right)^2 + 2\delta_l \quad \text{Formula 4.4.1}$$

$$m = 0, 1, 2, 3, \dots$$

2. When the  $\delta$  value ( $\delta_l$ ) of the film is less than the  $\delta$  value ( $\delta_s$ ) of the substrate

$$\theta_m^2 \approx \sin^2 \theta_m = \left( \frac{\lambda}{2d} \right)^2 m^2 + 2\delta_l \quad \text{Formula 4.4.2}$$

$$m = 0, 1, 2, 3, \dots$$

These formulas are solvable if we can obtain the two peaks  $\theta_{m1}$  and  $\theta_{m2}$  corresponding to the orders  $m_1$  and  $m_2$  of two oscillations. Thus,  $d$  and  $\delta_l$  are given by the following formulas:

$$d = \frac{\lambda}{2} \sqrt{\frac{m_2^2 - m_1^2}{\theta_{m2}^2 - \theta_{m1}^2}} \quad \text{Formula 4.4.3}$$

$$\delta_l = \frac{1}{2} \frac{\theta_{m_1}^2 m_2^2 - \theta_{m_2}^2 m_1^2}{m_2^2 - m_1^2} \quad \text{Formula 4.4.4}$$

If we plot the square of the incident angle versus the square of order  $m$ , as shown in Fig. 4.4.1, the peak value can be approximated by a line. The extrapolated value gives  $2d$  ( $= \theta_c^2$ ), and the gradient of the line gives film thickness.

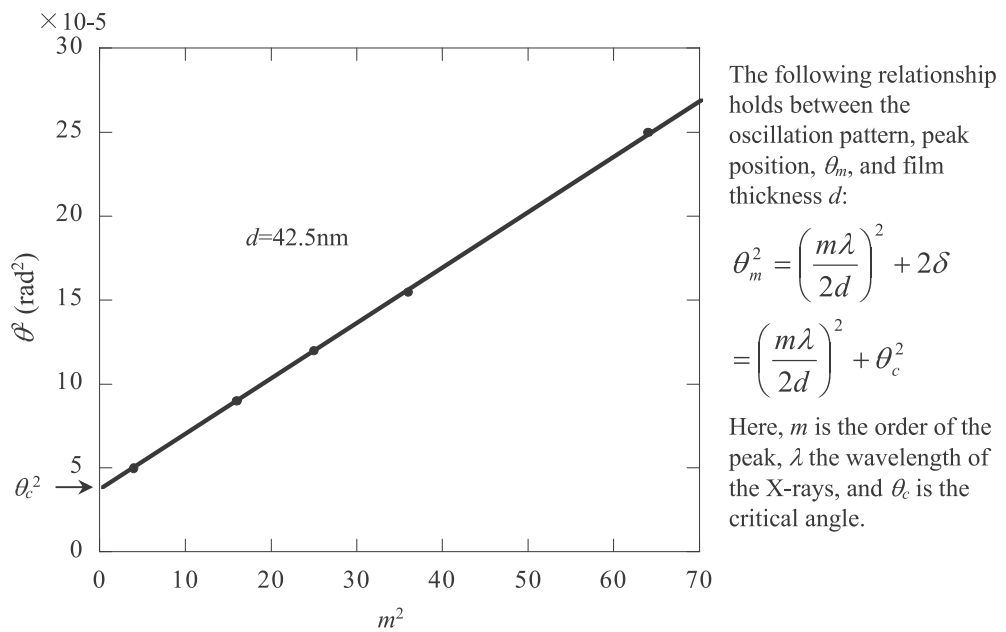
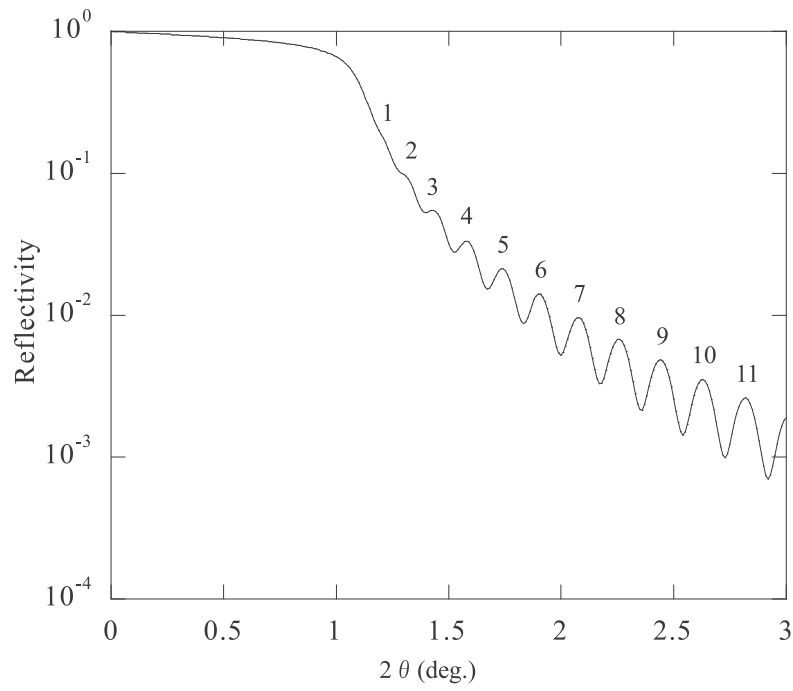


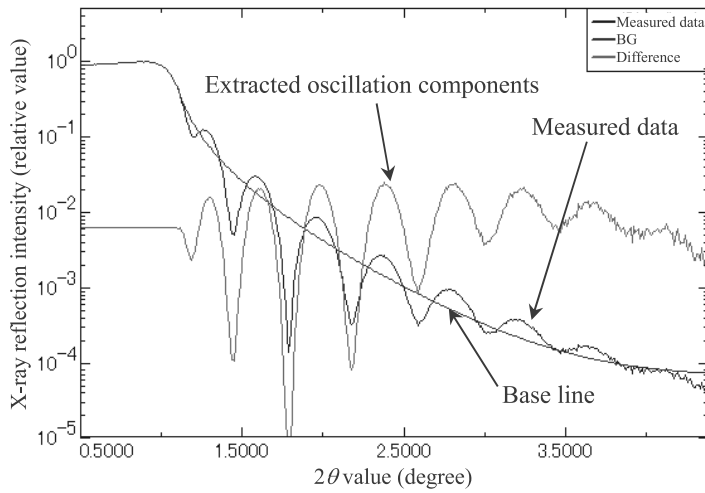
Fig. 4.4.1 Determining the thickness of a single-layer film

#### 4.4.2 Obtaining Film Thickness via Fourier Transformation

The Fourier transformation of the oscillating components extracted from the reflectivity profile makes it possible to estimate film thickness. The procedure is given below.

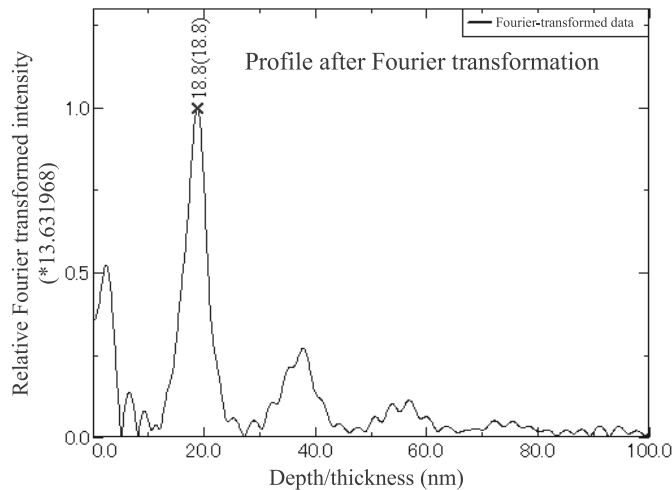
1. From the measured reflectivity profile, determine a polynomial-based curve as the baseline, as shown in Figure 3.4.2. Subtract the baseline from the data and normalize the result to extract the oscillation.
2. Perform data angle correction with refractive index ( $\delta$  value) of the film and obtain the oscillating components without contraction.
3. Then, apply a Fourier transform to the data and estimate thickness from the oscillating components.

Apply the results to the method based on the theoretical calculation given in the next section for efficient analysis.



The oscillating components are extracted by subtracting the average reflectivity (baseline) from the measured reflectivity and normalizing the result.

The oscillating components are further processed by angle correction with the refractive index and by Fourier transformation.



The oscillation period gives film thickness. The results obtained are used in simulation calculations for efficient analysis.

Fig. 4.4.2 Fourier transformation method



#### 4.4.3 Obtaining Film Thickness, Density, and Surface or Interface Roughness by Fitting

A reflectivity profile including oscillation sensitively reflects the film structure. A non-linear least mean square fitting of a profile with a profile given by theoretical calculations based on a film model makes it possible to evaluate film thickness and density, as well as surface or interface roughness.

The simulation is based on the recurrence formula formulated by Parratt, as shown by Formula 4.3.20 in Section 3.3.2, combined with the surface or interface roughness described in Formula 4.3.22 in Section 3.3.3. Thus, reflectivity  $I/I_0$  is given by  $|R_{1,2}|^2$  (Formula 4.3.21).

The roughness is handled by approximating the change in average electron density at the interface between the  $(n-1)$ '-th and  $n$ -th layers as a Gaussian function and by correcting the Fresnel coefficient as in Formula 4.3.22. Roughness is expressed as root mean square (rms) roughness,  $\sigma_{n-1}$ .

## §4.5 Reflectivity Measurement

Reflectivity measurements must accurately measure a wide range of intensity changes in the extremely low angle range of grazing X-ray incidence. With grazing X-ray incidence, even extremely narrow X-ray beams produce a widespread radiation field on the sample surface. This makes correct optics alignment, sample mounting, and sample alignment before measurement particularly important.

The figure below shows the procedural flow of reflectivity measurement.

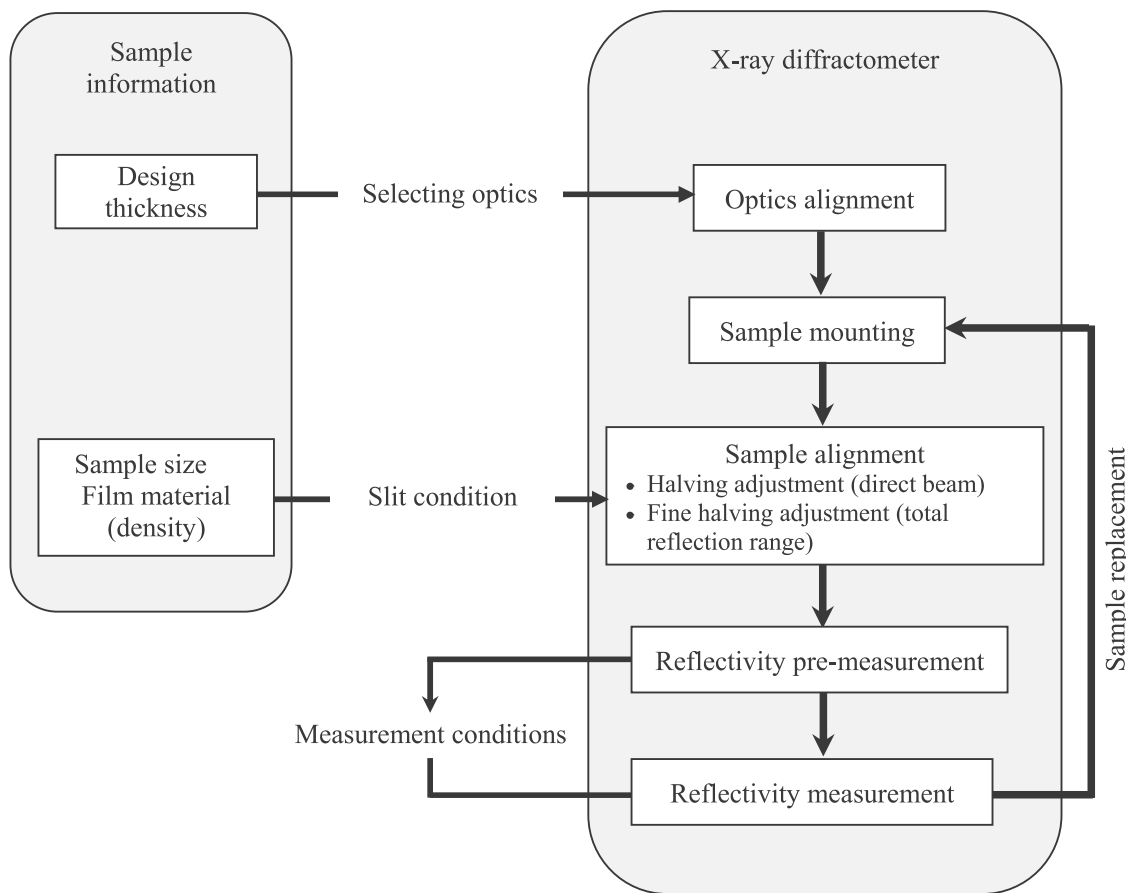


Fig. 4.5.1 Procedural flow of reflectivity measurement

### 4.5.1 Selecting Optics

Fig. 4.6.2 is a schematic diagram of the optics used to measure reflectivity.

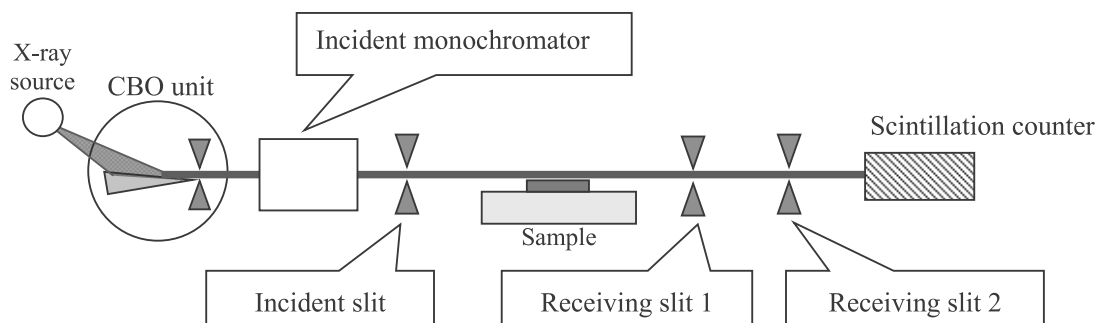


Fig. 4.5.2 Optics for reflectivity measurement

The names of the monochromator and slits will vary, depending on the diffractometer model.

When performing reflectivity measurements, we must select the optics based on anticipated film thickness. This is because the period of the oscillation changes depending on film thickness. With larger film thicknesses, the period of the oscillation is smaller, and the resolution of the optics must be increased.

Table 4.5.1 Overview of optics used in reflectivity measurements and guide to applicable film thickness provides an overview of the optics used in reflectivity measurement and guidelines for applicable film thickness.

Table 4.5.1 Overview of optics used in reflectivity measurements and guide to applicable film thickness

| Monochromator                                | None                              | Ge (220) double-crystal | Ge (400) double-crystal | Ge (220) four-crystal |
|--|-----------------------------------|-------------------------|-------------------------|-----------------------|
| Relative intensity<br>(Reference estimation) | 200                               | 10                      |                         | 1                     |
| Resolution<br>(Angular divergence)           | up to 0.04°                       | up to 0.02°             |                         | up to 0.003°          |
| Wavelength<br>monochromaticity               | $K\alpha_1 + K\alpha_2 (+K\beta)$ | $K\alpha_1$             | $K\alpha_1$             | Part of $K\alpha_1$   |
| Applicable film<br>thickness                 | 0.5 to 100nm                      | 50 to 200nm             | 50 to 200nm             | 200nm or greater      |
| RINT III series                              | ○                                 | ○                       |                         |                       |
| SmartLab                                     | ○                                 | ○                       | ○                       | ○                     |

As the reflectivity measurement measures the low angle range near  $2\theta = 0^\circ$ , the X-ray beam is diffused across a wide area of the sample surface, even with a narrow incident slit. If the spread of the X-ray beam is large near the critical angle and the X-ray beam irradiates out of the sample, the critical angle cannot be determined accurately, and analysis may not be possible. We must select a sufficiently narrow slit and keep the X-ray beam from irradiating from the sample near the critical angle.

The critical angle changes depending on film material density. Table 4.5.2 shows the standard slit width for each diffractometer. Fig. 4.5.3 shows the relationship between the density of the material and the critical angle. Fig. 4.5.4 shows the relationship between the slit width and the irradiated width on the sample. Use these as guides in selecting slit width.

Table 4.5.2 Standard width and height of slits used in reflectivity measurement

| Slit name             | Incident side                | Receiving side               |                              |
|-----------------------|------------------------------|------------------------------|------------------------------|
|                       |                              | RS1                          | RS2                          |
| SmartLab              | IS                           | RS1                          | RS2                          |
| RINT III series       | DS                           | SS                           | RS                           |
| Slit width and height | Width 0.1 mm<br>Height 10 mm | Width 0.2 mm<br>Height 10 mm | Width 0.2 mm<br>Height 10 mm |

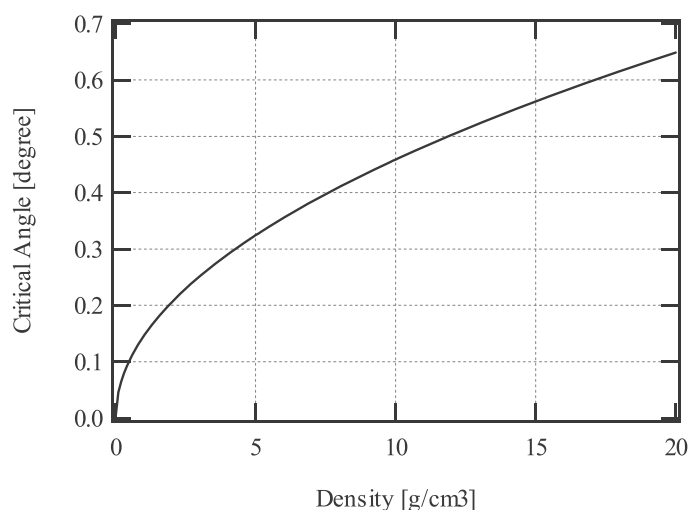


Fig. 4.5.3 Density and critical angle

The critical angle is estimated when the incident X-ray is the Cu  $K\alpha_1$  line (Wavelength of 1.54056Å). Values will differ slightly, depending on sample composition.

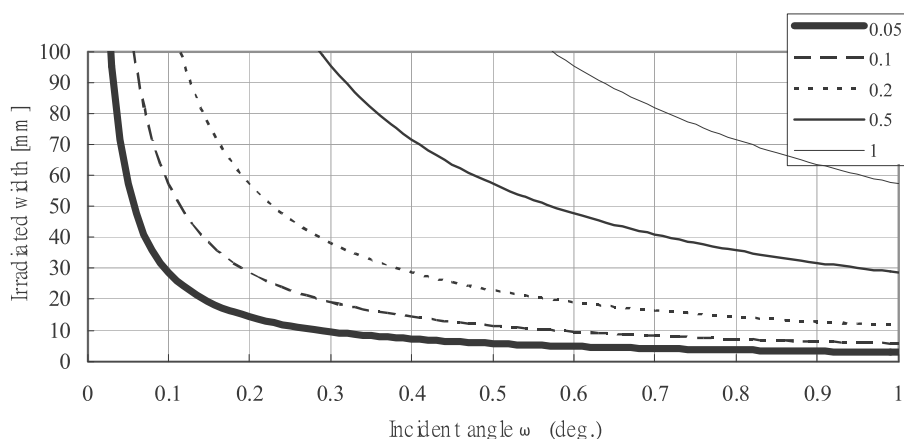


Fig. 4.5.4 Relationship between incident angle and irradiated width

The figure shows the irradiated width in the horizontal direction. The irradiated width in the vertical direction differs depending on the height-limiting slit used. However, it will be approximately twice the height of the S2 (DS) slit.

#### 4.5.2 Optics Alignment

We recommend performing optics alignment when replacing optics. Since X-ray reflectivity measurement uses a narrow slit, the large dynamical range requires precise alignment of optics.

#### 4.5.3 Mounting Sample

Carefully set the sample on the wafer sample plate and attach magnets along the perimeter of the sample to keep it from falling.

Fig. 4.5.5 shows an example of a 4-inch wafer mounted. In reflectivity measurements, the incident X-ray beam produces a widespread radiation field on the sample surface. Place the sample with its long side directed sideways at  $\phi = 0^\circ$ .

When placing the round fixing magnets around the sample, confirm that the magnets do not shield the X-ray beam. To avoid applying excessive strain, avoid applying excessive force when pressing the sample. If the sample is small and the fixing magnets shield the X-ray beam, you may use grease or the surface tension of alcohol instead.

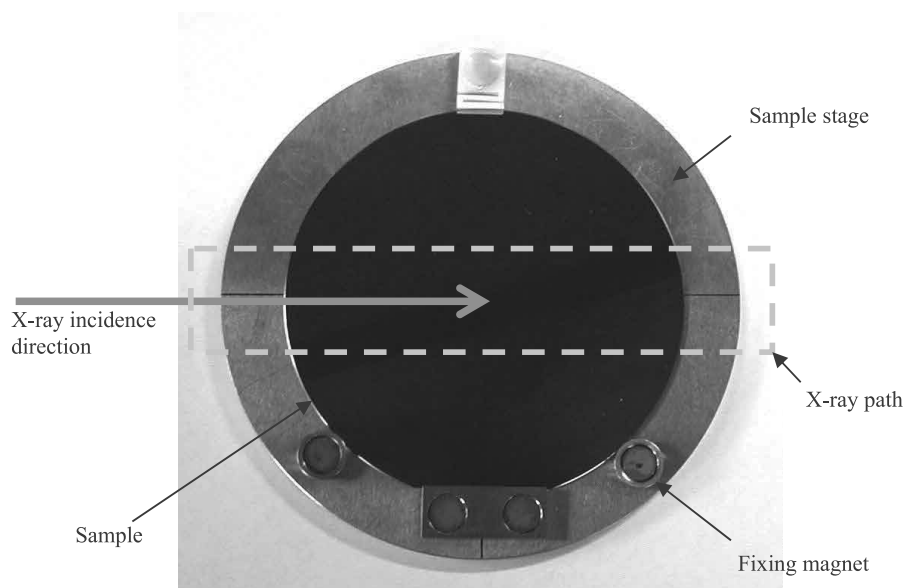


Fig. 4.5.5 Mounting sample

#### 4.5.4 Sample Alignment

To ensure detection of X-ray beams specularly reflected from the sample, perform sample alignments each time you replace the sample. Sample alignment includes the following two types of adjustments.

##### A. Halving Adjustment (Direct Beam)

Halving adjustment adjusts the sample rotation axis ( $\omega$  axis) so that the incident X-ray beam (direct beam) is parallel to the sample surface and adjusts the sample lengthwise axis ( $Z$  axis) so that beam widths are divided into halves. Perform the halving adjustment as follows:

1. Set the  $2\theta$  axis to  $0^\circ$ . Set the sample and retract the  $Z$  axis to the rear to avoid blocking the incident X-ray beam. Check intensity in this geometry.
2. Scan the  $Z$  axis. Set the  $Z$  axis at the position at which intensity is half the intensity measured in 1.

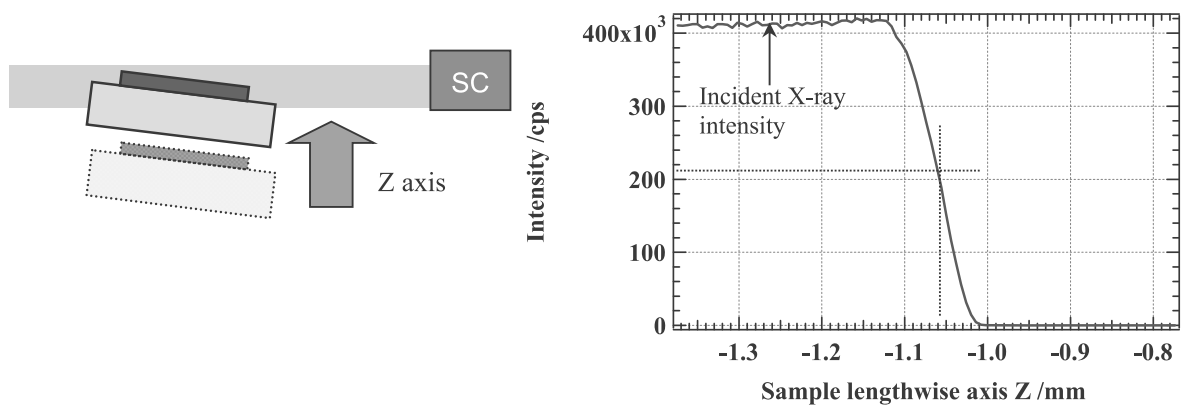


Fig. 4.5.6 Halving adjustment (Z scan)

3. Scan the  $\omega$  axis and adjust the alignment until the sample surface and incident X-ray beam are parallel.

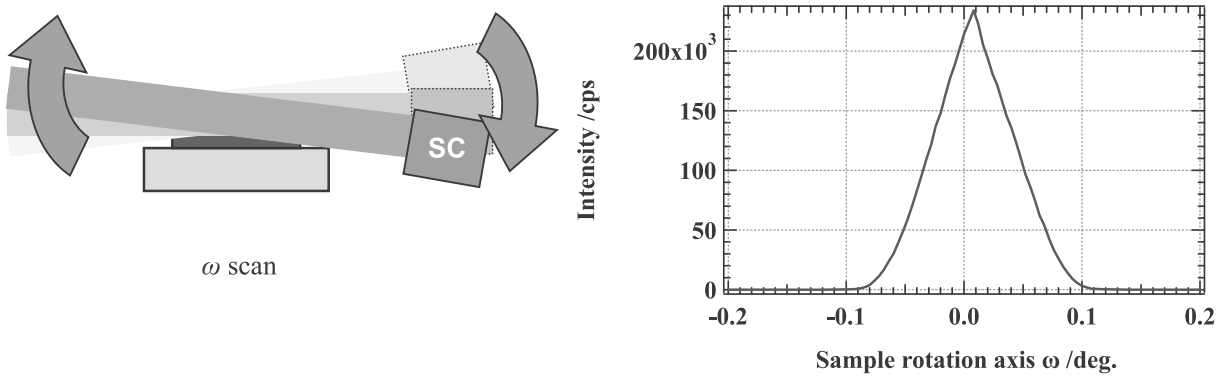


Fig. 4.5.7 Halving adjustment ( $\omega$  scan)

4. Repeat the scan of the Z axis and adjust the alignment to make the X-ray intensity half the incident X-ray intensity.

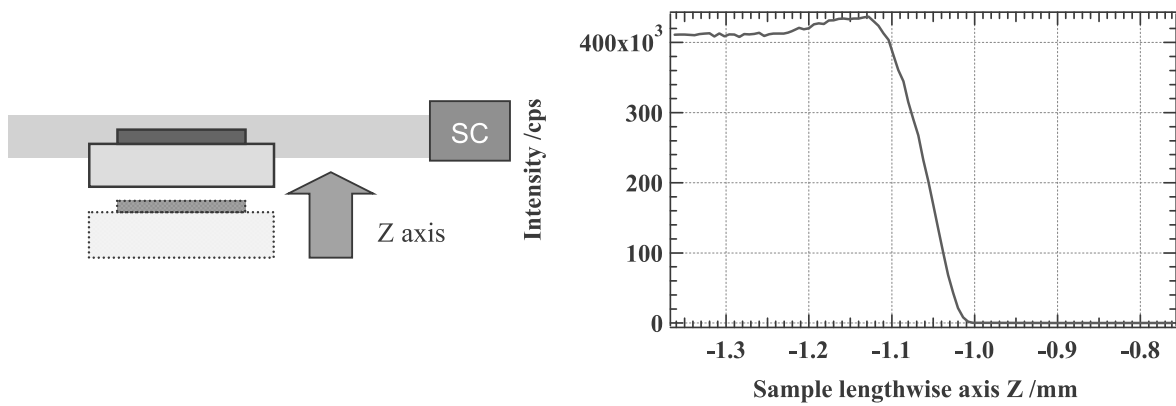


Fig. 4.5.8 Halving adjustment (Z scan)

In Step 3, the shape of the  $\omega$  scan profile will sometimes be trapezoidal rather than a peak. If so, the sample surface is behind the X-ray beam when the sample and the X-ray beam are parallel. If this happens, perform a peak search by the Full Width at Half Maximum (FWHM) middle point method, drive the  $\omega$  axis to approximately the center, and repeat the adjustment steps 4 and 3, in that order. This ends halving adjustment.

For ordinary X-ray diffraction measurements, this halving adjustment will be adequate. However, X-ray reflectivity measurements require finer halving adjustments.

Rather than a perfectly collimated beam, the incident X-ray beam has divergence. At halving adjustment, part of the incident X-ray beam is reflected from the sample surface, passes through the receiving slit, and is detected. For this reason, even after halving adjustment, the sample surface may not be at the center of the incident X-ray beam. Thus, reflectivity measurements require finer halving adjustments involving total reflection, in addition to halving adjustments using the direct beam.

### B. Fine Halving Adjustment (Total Reflection Range)

Reflectivity measurements use an extremely narrow incident X-ray beam with widths ranging from 0.05 mm to 0.2 mm. Since the X-ray beam is incident on the sample at a grazing angle, a strict halving adjustment is necessary. In addition to the halving adjustment performed with the direct beam as described in Section 3.5.3 A, we perform halving adjustment in the total reflection range. With adjustments in this range, the angular position of the  $2\theta$  axis is set in the total reflection range (approximately  $0.3^\circ$  to  $0.4^\circ$  for Si), and the  $Z$ ,  $\omega$ , and  $\chi$  axes are scanned and set to the positions at which we obtain maximum intensity.

Perform halving adjustments in the total reflection range as follows:

1. Match the zero position of the  $2\theta$  axis and the zero position of the  $\omega$  axis obtained in the previous halving adjustment and perform the reflectivity measurement by the  $2\theta/\omega$  scan.

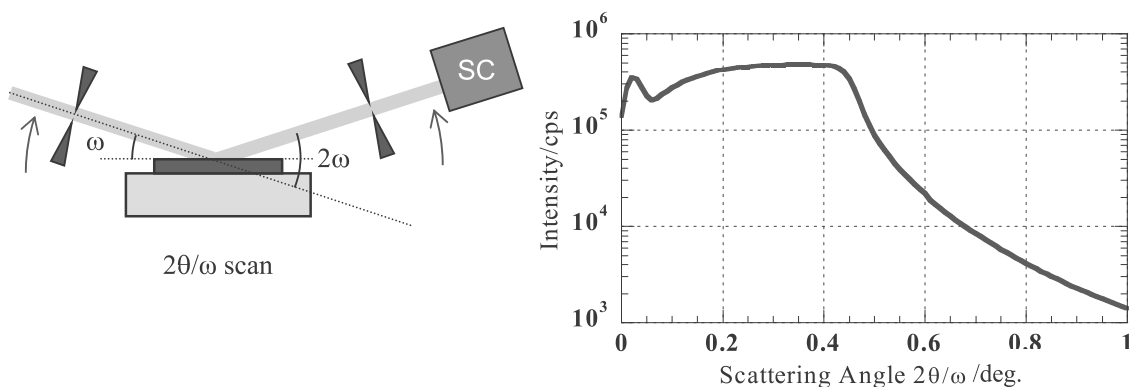


Fig. 4.5.9 X-ray reflectivity measurement after halving adjustment



In this case, the total reflection occurs in the range near  $0.24^\circ$  to  $0.4^\circ$  on the  $2\theta/\omega$  axis. Here, we perform halving adjustment with total reflection at  $2\theta = 0.3^\circ$ .

2. Set  $2\theta/\omega$  to  $0.3^\circ$  and scan the  $\omega$  axis

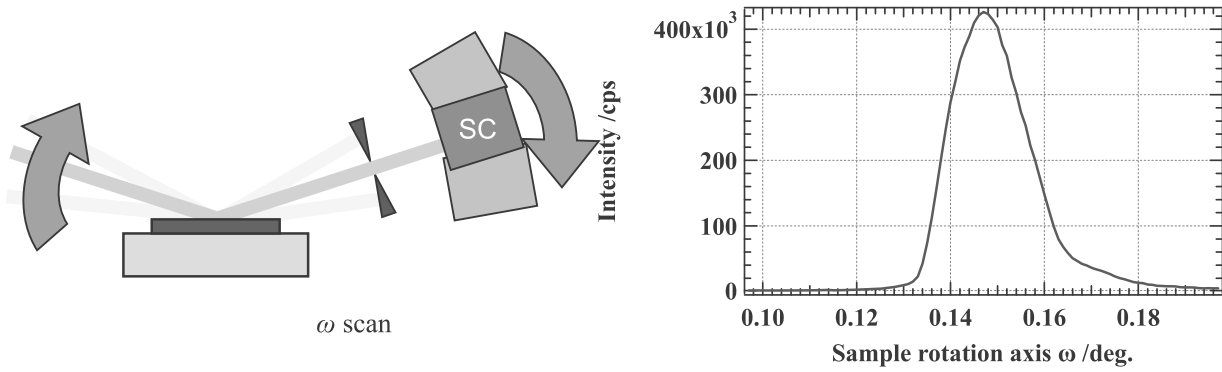


Fig. 4.5.10 Halving adjustment in total reflection range ( $\omega$  scan)

We observe total reflection when the incident X-ray beam and the scattered X-ray beam have the same angle with respect to the sample surface. The peak position in Fig. 4.5.10 is approximately half of the position on the  $2\theta$  axis.

3. Set the  $\omega$  axis at the peak position in Fig. 4.5.10 and scan the  $Z$  axis.

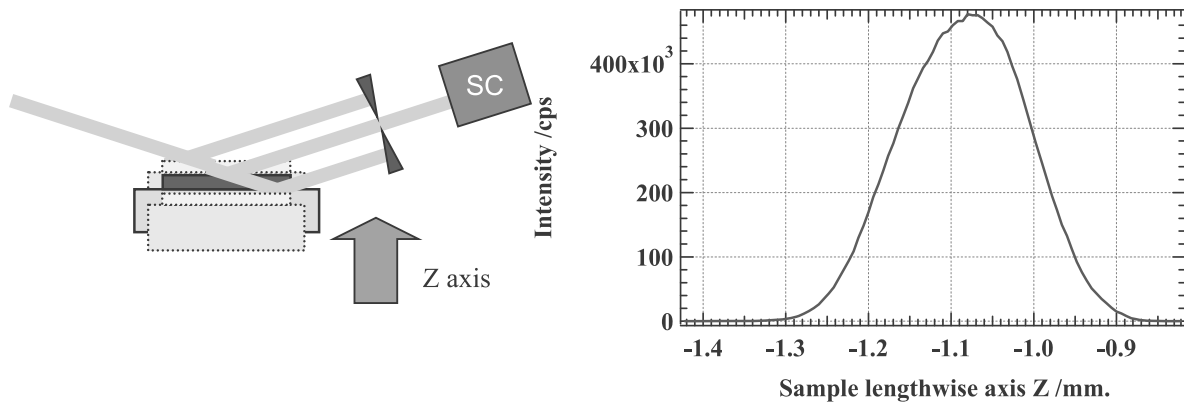


Fig. 4.5.11 Halving adjustment in total reflection range ( $Z$  scan)

- Set the Z axis at the peak position in Fig. 4.5.11 and scan the sample swing axis.

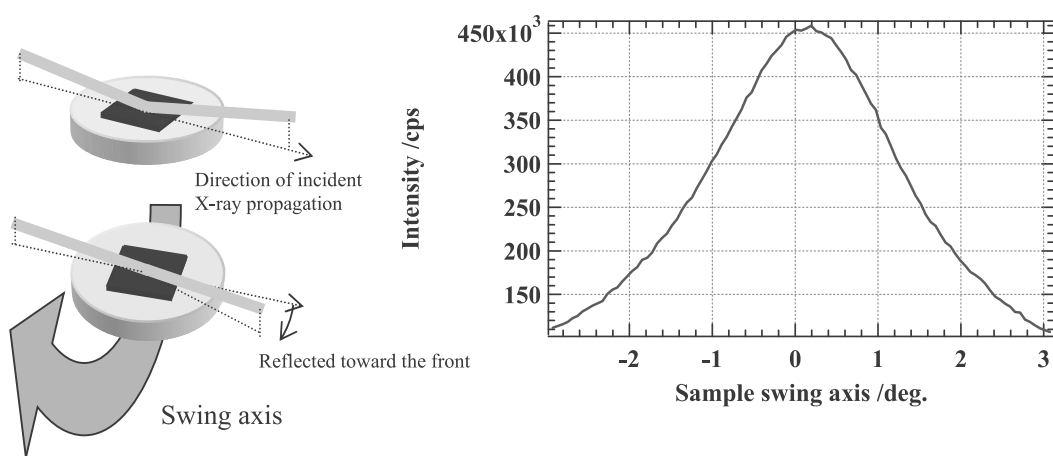


Fig. 4.5.12 Halving adjustment in total reflection range (swing axis scan)

- Set the swing axis at the peak position in Fig. 4.5.12 and scan the  $\omega$  axis to complete the adjustment.

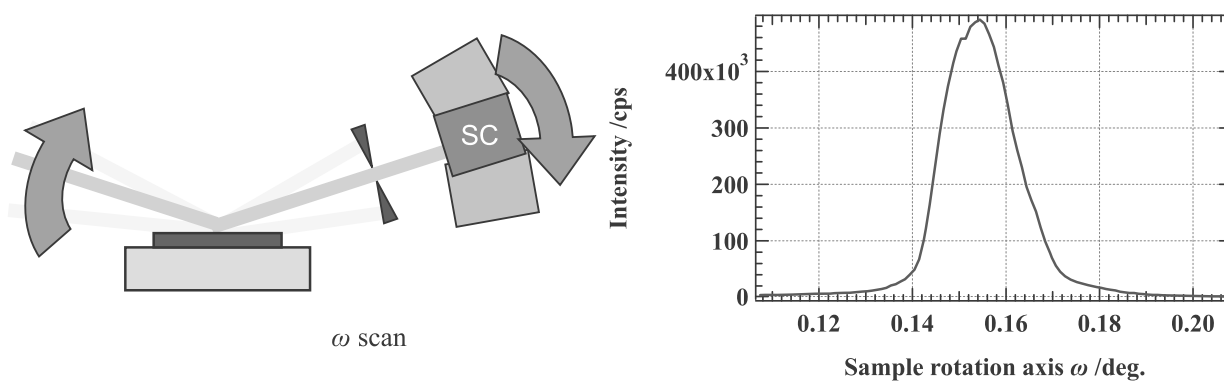


Fig. 4.5.13 Halving adjustment in total reflection range ( $\omega$  scan)

- Repeat Steps 3 to 5 until the peak positions on the Z and  $\omega$  axes agree with those in the previous scan.

### 4.5.5 Reflectivity Measurement

Following sample alignment, perform pre-measurement to determine reflectivity measurement conditions. Measurement conditions vary depending on the optics used and the sample. A guide to pre-measurement is given below.

#### ☞ Guide to pre-measurement conditions

|                |   |   |
|----------------|---|---|
| Scan axis      | : | $2\theta/\omega$                              |
| Scanning range | : | 0° to 10°                                     |
| Sampling width | : | 0.005°  |
| Scanning speed | : | Several degrees/min                           |
| Attenuator     | : | Automatic (Fixed at 1/800 in RINT III series) |

Following pre-measurement, use the results as a guide to set measurement conditions so that the oscillation in the reflectivity profile is clearly observed.

#### ☞ Guide for measurement conditions

|                 |   |
|-----------------|---|
| Scanning range: | 0° to the angle at which the reflection intensity decreases to the level of the background (where the intensity observed is flat, up to approximately 4° to 12°)  |
| Sampling width: | Width in which the profile shape near the critical angle or the oscillation in the reflection intensity is clearly observed without being squashed (0.001° to 0.01°)<br>← Approximately 1/5 to 1/7 of the minimum period of the oscillation observed in the pre-measurement profile         |
| Scanning speed: | Speed at which statistical fluctuations are suppressed to levels that permit clear observation of the oscillation in the reflection intensity, clear of noise (0.1°/min to 1°/min)  |
| Attenuator:     | Since reflection intensity generally changes across a wide range (six to eight orders of magnitude), the attenuator must be switched during measurement. In SmartLab, set the attenuator to “Automatic”; in the RINT III series, specify switching angles based on pre-measurement results. |

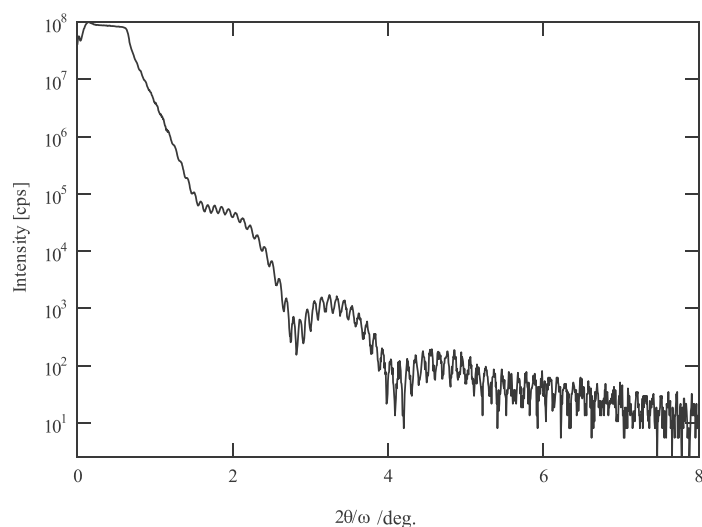


Fig. 4.5.14 Example of reflectivity measurement

Scanning range:  $0^\circ$  to  $8^\circ$ ; sampling width:  $0.006^\circ$ ; scanning speed:  $0.5^\circ/\text{min}$

#### 4.5.6 Measurement Precautions

If the sample is bent or corrugated, total reflection intensity may be stronger or weaker than that of the incident X-ray beam.

If the sample is bent convexly, X-ray beams reflected from the sample will diverge. The divergent components are shielded by the receiving slit, and intensity decreases.

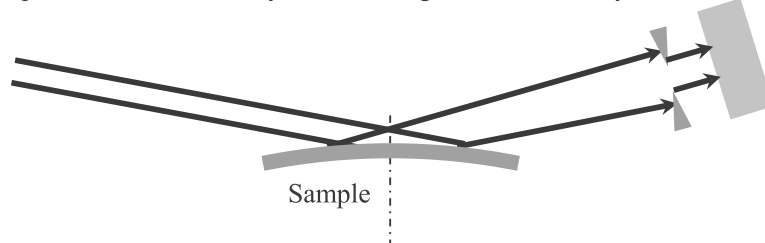


Fig. 4.5.15 Effects when sample is bent convexly

When the sample is concavely bent, the X-ray beam reflected from the sample converges, including the original divergent component in the incident X-ray beam, potentially resulting in higher intensity.

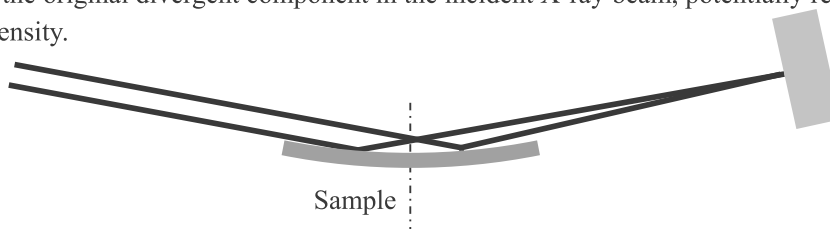


Fig. 4.5.16 Effects when sample is bent concavely

If the sample is not bent uniformly but is corrugated, both of the effects above occur simultaneously.

If the sample is bent as above, we recommend replacing the receiving slit with one slightly larger (e.g., replace the 0.2-mm wide slit with a 0.5-mm wide slit) to detect all total reflection components.

Replace the slit with a wider slit and perform sample alignment. If the sample is bent, the Z axis value obtained by ordinary halving adjustment and that obtained by fine total reflection halving adjustment may differ significantly (by approximately several dozens of a micrometer). In this case, use the Z axis position determined in fine halving adjustment. Repeat the adjustment of the Z axis and the  $\omega$  axis until the fluctuations in the Z axis converge to several micrometers or less.

Rough sample surfaces may keep reflectivity profiles from exhibiting oscillations clearly. In this case, depending on the extent of the roughness, using an analyzer crystal in the receiving optics may help observe clear oscillations.

#### §4.6 Example of Measurement

Fig. 4.6.1 shows an example of reflectivity measurement for various samples.

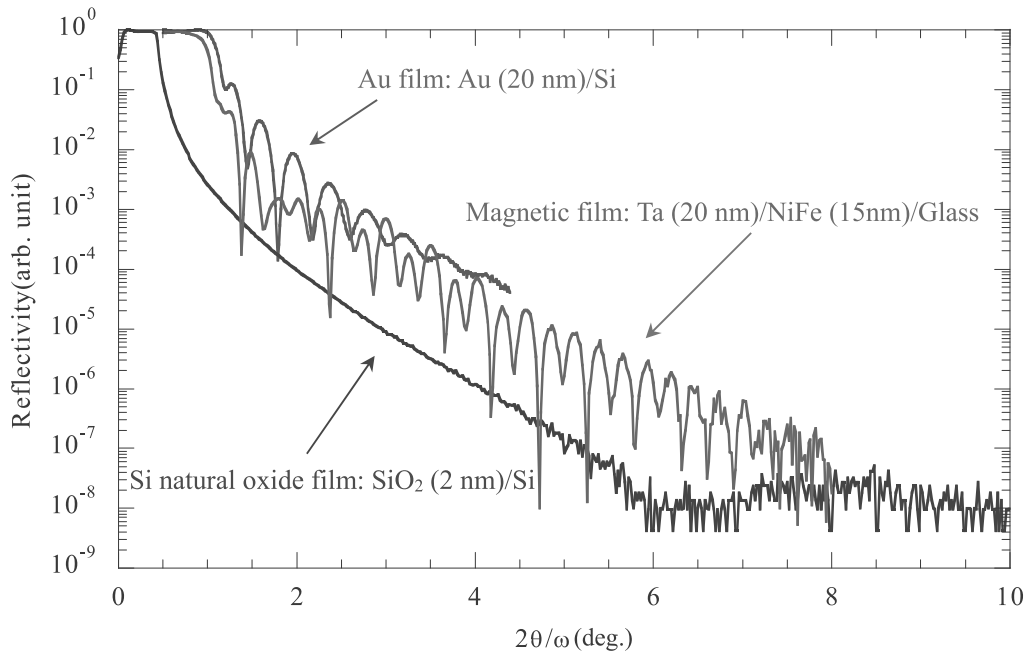


Fig. 4.6.1 Examples of reflectivity profiles for various films

Fig. 4.6.2 shows an example of a measurement for a superlattice multilayer film. This profile corresponds to the superlattice multilayer film shown in Fig. 4.6.2. The profile shows the superlattice peaks corresponding to the thickness of the period of the layers.

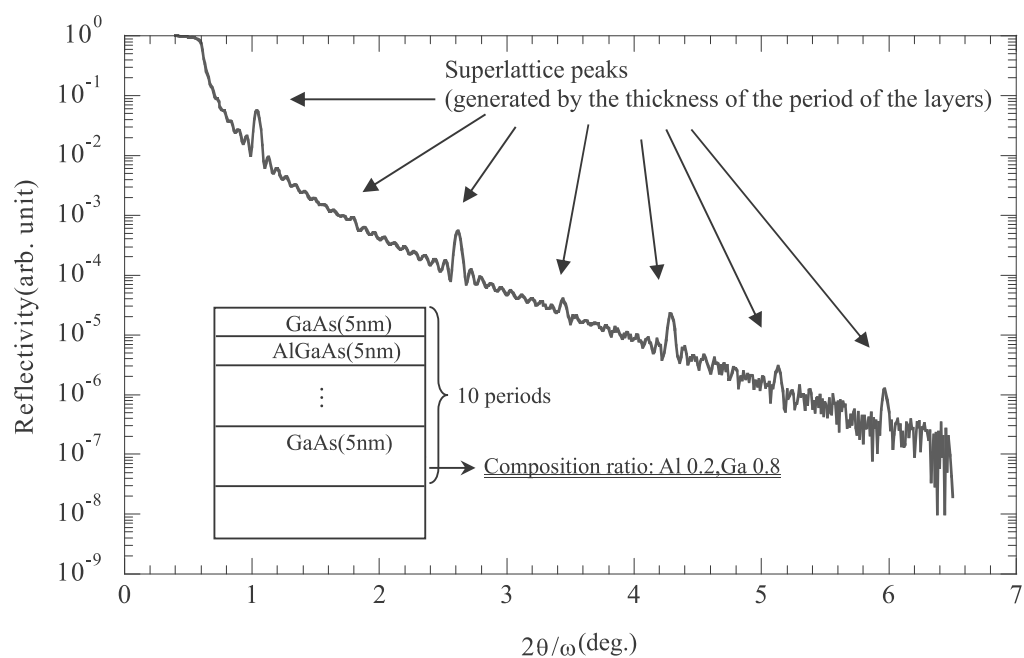


Fig. 4.6.2 Example of reflectivity profile for superlattice multilayer film

### §4.7 Examples of Analysis

Here we take the example of the magnetic film shown in Fig. 4.6.1 to demonstrate a general analysis of reflectivity.

The analysis is performed as indicated in the flowchart shown in Fig. 4.7.1.

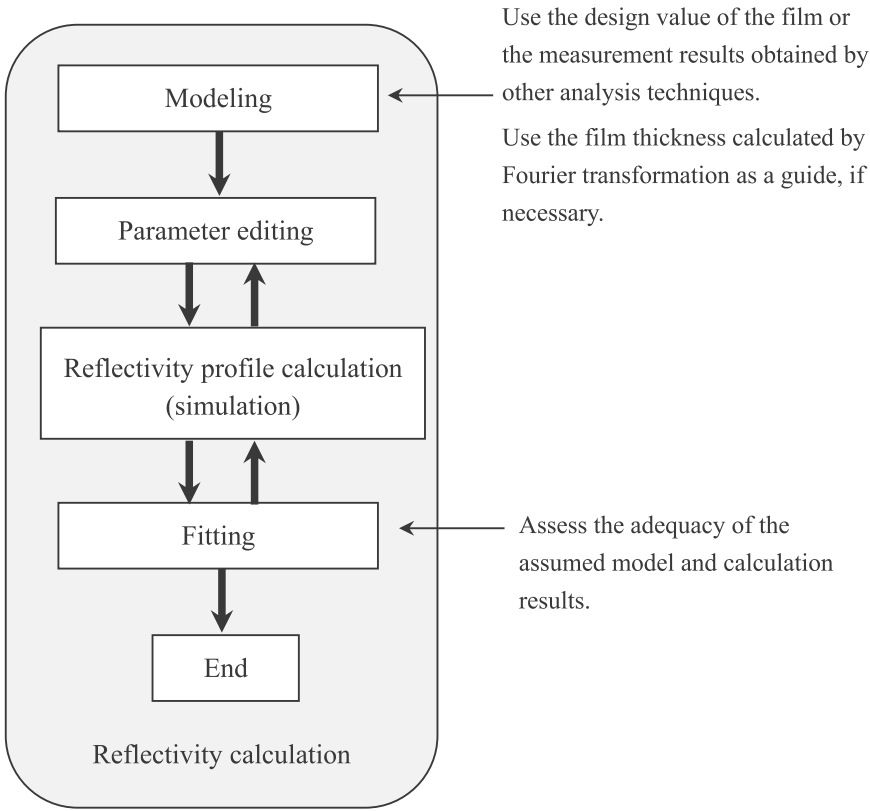


Fig. 4.7.1 Procedural flow of reflectivity analysis

Fig. 4.7.2 shows the multilayer film model for the sample analyzed.

|                 |  |
|-----------------|--|
| Ta 20nm         | → Several nanometers of Ta oxides are expected on the surface. |
| NiFe 15nm       | → Permalloy (Ni <sub>4</sub> Fe) is assumed.                   |
| Glass substrate | → SiO <sub>2</sub> is assumed.                                 |

Fig. 4.7.2 Multilayer model of magnetic film

Load the measurement data.

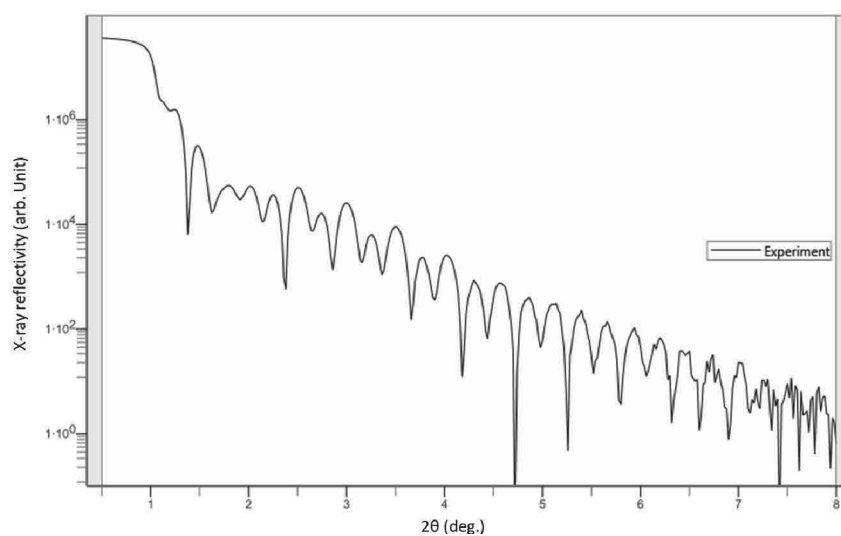


Fig. 4.7.3 Measurement data

Set the model and input the thickness of each layer. The results of simulations with these parameters are as follows:

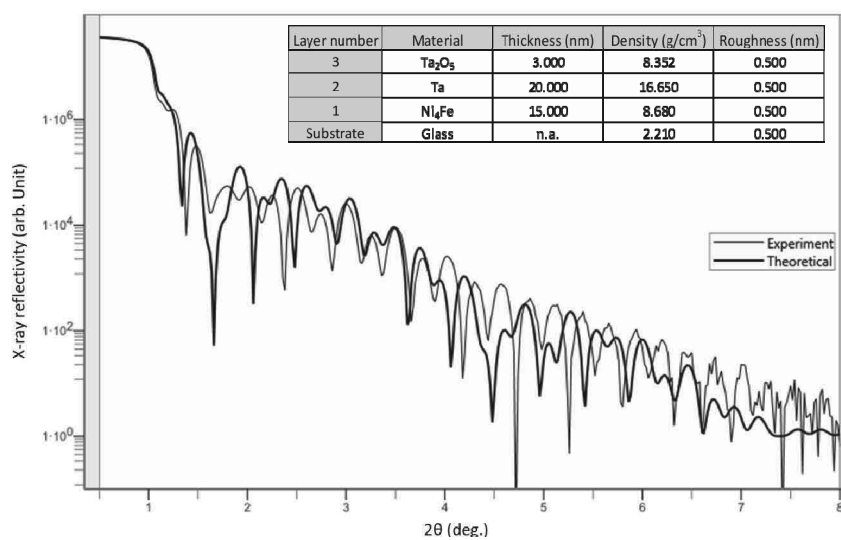


Fig. 4.7.4 Results of simulation



Change the values of the parameters to bring the simulation results closer to the measured profile. Here, we reduce the thickness of the Ta.

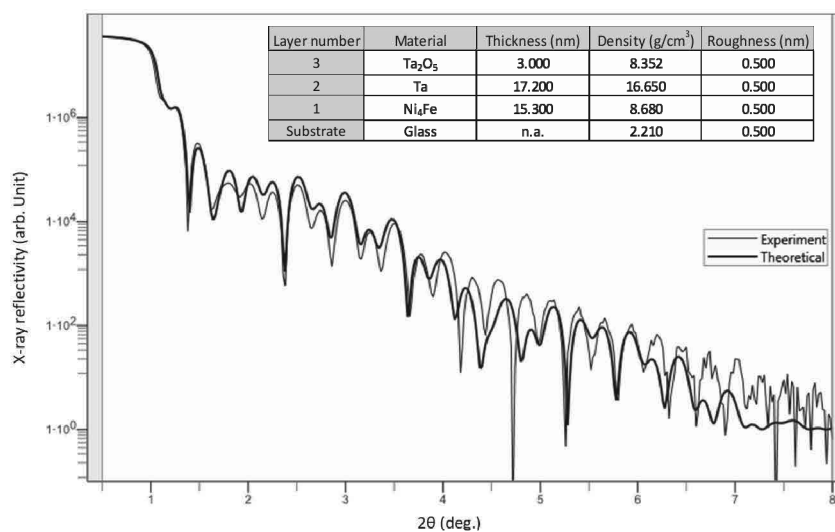


Fig. 4.7.5 Results of simulation (Second trial)

The measured profile and the simulation results are now in rough agreement. Now, perform fitting.

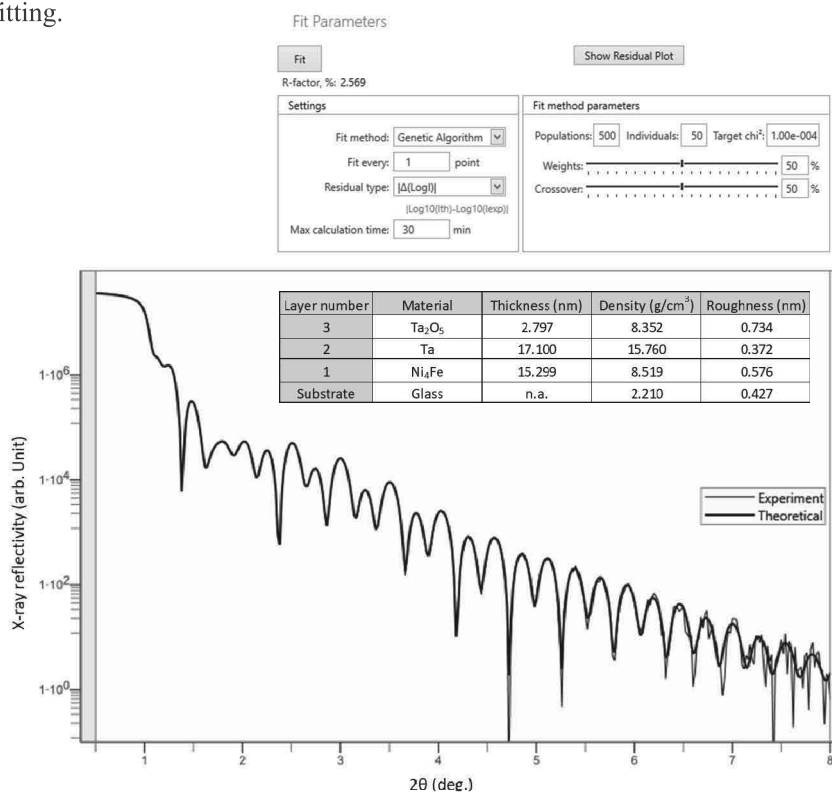


Fig. 4.7.6 Results of fitting

In this analysis, the fitting is successful, and the measured profile and calculation result are in near-perfect agreement. The R value displayed below the parameter box in Fig. 4.7.6 indicates the degree of agreement in the method of least squares. As this value approaches zero, the measured profile and the calculation result are in closer agreement. (Use this only as a guide; use the profile to judge whether the measurement and calculations agree.)

In this example, the fitting is successful in the first trial. For fitting to succeed in this way, the simulation result must be as close as possible to the measured profile.

Even when the fitting is successful, there is no guarantee that the calculated value is correct in absolute terms. We need to investigate to confirm whether the calculated solution is adequate.

If the measured profile and the simulation result do not agree, the model assumed may be wrong. In such cases, the model needs to be reconsidered.

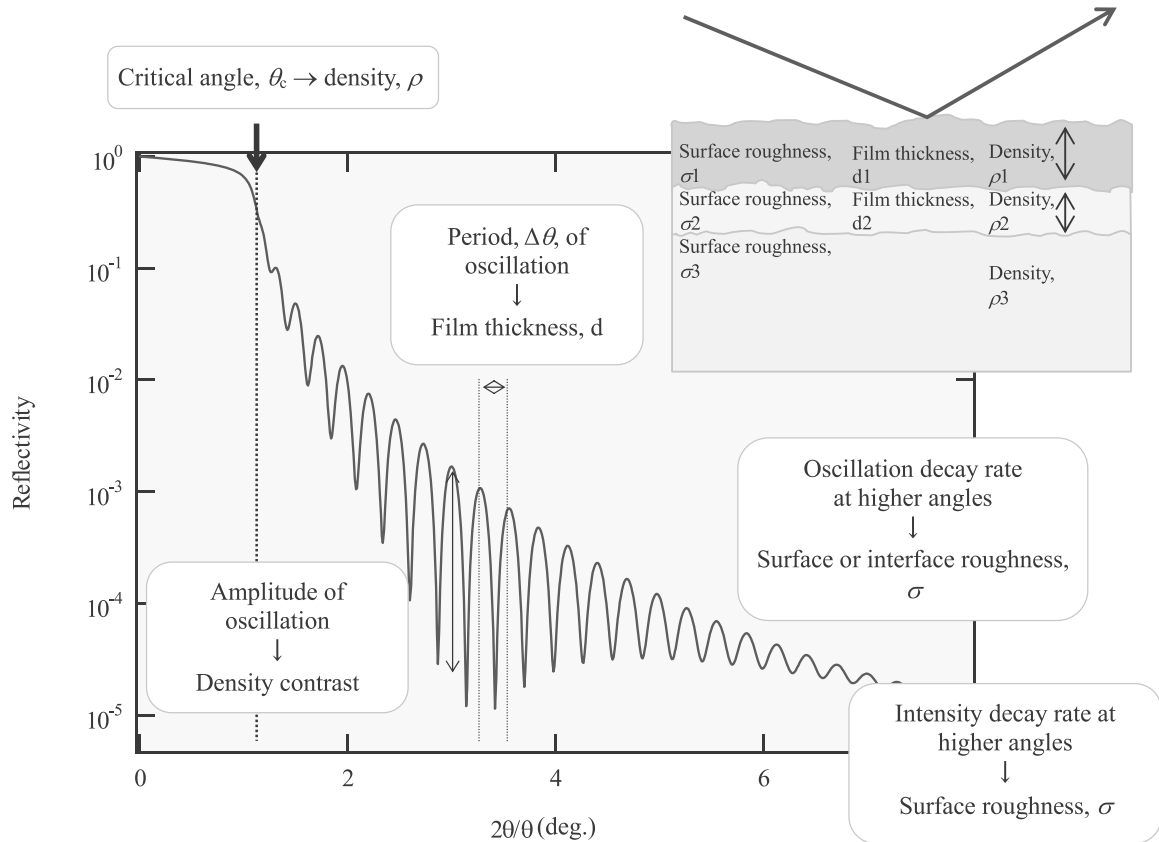
## **§4.8 Summary**

This chapter discusses the principles of the X-ray reflectivity method, measurement procedures, and analysis method. Summarized below are the topics described in this chapter.

### **(1) Features of X-ray reflectivity method**

1. The sample must be sufficiently flat and smooth. (Surface or interface roughness must be on the order of several nanometers or less.)
2. The method can be applied to polycrystalline and amorphous materials.
3. The method is extremely sensitive to surface states.
4. The method is independent of crystal orientation or strain.
5. The method is insensitive to changes in composition.
6. The method can be used to evaluate film thickness of up to approximately 1,000 nm. It is not suited to use with thicker films.

(2) Information provided by X-ray reflectivity profile



(3) Analysis method

1. Method giving film thickness from the incident angle dependence of the oscillation period.
2. Method giving film thickness via Fourier transformation.
3. Method giving film thickness, density, and surface or interface roughness by fitting.

Methods 2 and 3 are now practical under most conditions.

## Chapter 5 High-Resolution X-ray Diffraction Method

### §5.1 Background of High-Resolution X-ray Diffraction Method

Powder crystals and imperfect crystals often contain many lattice defects, such as dislocations, and their three-dimensional periodicity tends to be disordered. A mosaic crystal models this disorder as an assembly of a large number of minute regions, without disorders in periodicity, but with slight differences in orientation. In a mosaic crystal, a region in which X-rays can interfere with each other is small, and incident X-ray beams in most cases may be scattered only once in the crystal. The kinematical theory of diffraction applies to these cases involving many inorganic and organic crystals and even amorphous materials and liquids.

**Multiple scattering** will occur in near-perfect crystals. The **dynamical theory of diffraction** accounts for this multiple scattering. Materials such as Si, Ge, and GaAs have high perfection, and this dynamical theory can be applied in these cases to relatively large samples. As Fig. 5.1.1 shows, if the wave in the incident direction (transmission direction) is scattered by a lattice plane in a perfect crystal, waves are generated in the diffraction direction and transmission direction. These waves reflect repeatedly from many lattice planes. When such reflections are repeated, various diffraction phenomena arise due to interference between these waves within the crystal.

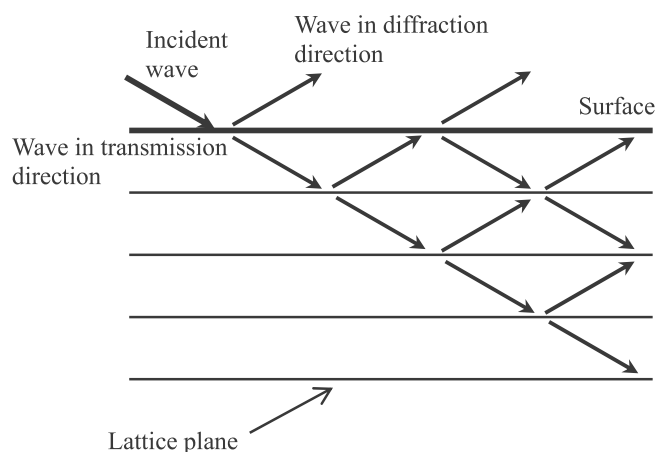


Fig. 5.1.1 Diffraction phenomena in perfect crystal

The optics used for measuring ordinary powder samples (such as the Bragg-Brentano focusing or the parallel beam method) are inadequate for measuring near-perfect crystals to which the dynamical theory of diffraction applies. We must improve resolution by increasing the collimation and monochromaticity of the X-ray beam and the precision of the goniometer. The measurement techniques deployed with such optics are collectively referred to as the **high-resolution X-ray diffraction method**.

The high-resolution X-ray diffraction method is an X-ray diffraction method based on the **multiple crystal method**. It is known as a precise experimental method for evaluating the perfection of a single crystal or measuring the lattice constants of a single crystal.

The multiple crystal method uses one or more crystals other than the sample to provide the functions of a monochromator, restricting the wavelength range of the X-rays, and of a collimator, increasing the collimation of the X-ray beam. It can be used to adjust the characteristics of X-rays incident on the sample crystal based on the perfection of the crystal to be measured or the purpose of the measurement. Fig. 5.1.2 shows the arrangement of a high-resolution X-ray diffractometer using a multiple crystal geometry.

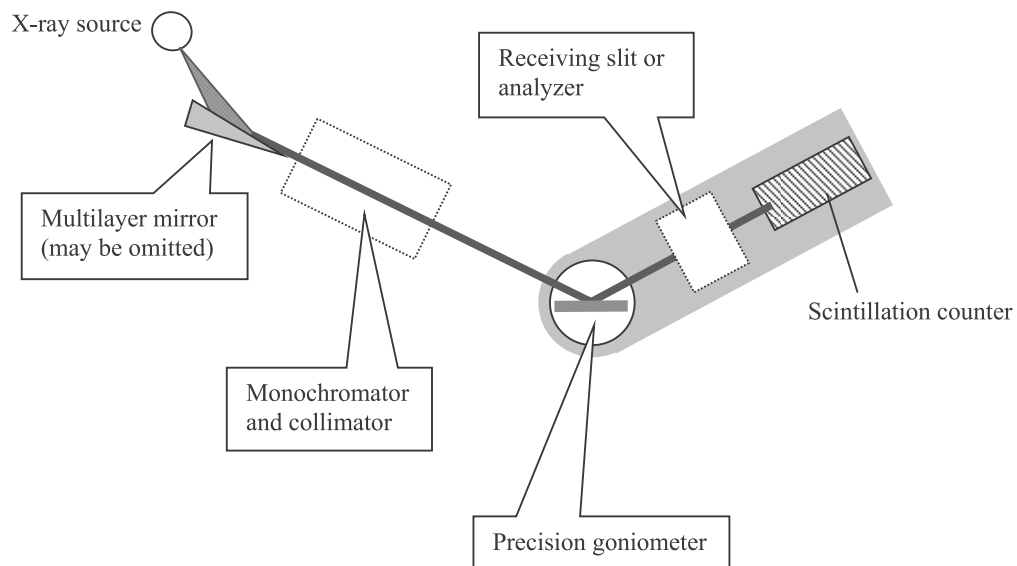


Fig. 5.1.2 Arrangement of high-resolution X-ray diffractometer

Between the X-ray source and the sample, we can insert a multilayer mirror to collimate and monochromatize the divergent beam efficiently from the X-ray source. This optical device can produce a collimated beam with higher luminance than conventional optical devices. After the mirror, depending on the sample to be measured, we can insert a **monochromator and collimator** to further collimate and monochromatize the X-ray beam. The sample is mounted on the precision goniometer, and the X-ray beam diffracted from the sample is detected by an X-ray detector (e.g., scintillation counter). Depending on the specific purpose of the measurement, we can leave the receiving slit fully open or set it to a specified height or width. If high resolution is required on the receiving side, we can use an analyzer crystal instead of the receiving slit.

The crystal materials to be evaluated or measured include Si and III-V group compound semiconductors. Current applications include measurements of a wide range of materials, including thin-film single crystals epitaxially grown on such crystal substrates and superlattice structures.

The high-resolution X-ray diffraction method has seen dramatic progress in these areas. Here, we discuss the relationship between compound semiconductors and the high-resolution X-ray diffraction method.

One feature of compound semiconductors is that mixed crystals are formed by mixing two or more compounds of arbitrary composition. Material parameters such as band gap and lattice constants change continuously with mixed crystal ratios. Fig. 5.1.3 shows the relationship between the lattice constant and band gap of representative compound semiconductors.

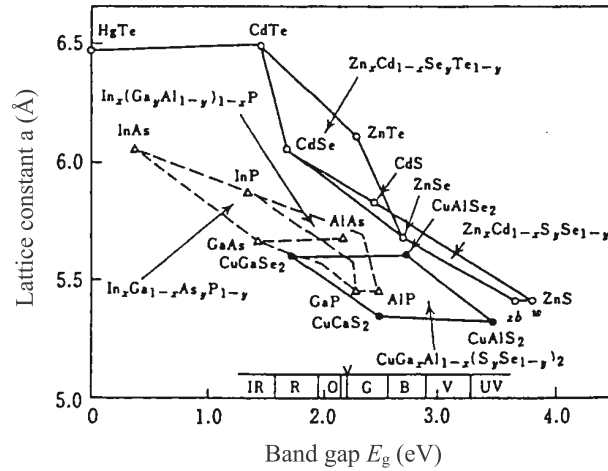


Fig. 5.1.3 Relationship between lattice constant and band gap

For example, a binary compound semiconductor (e.g., AlAs or GaAs) in the figure has a band gap and a lattice constant characteristic of the material. However, a ternary semiconductor,  $\text{Al}_x\text{Ga}_{1-x}\text{As}$ , a mixed crystal of these materials, will have a value in between, based on composition parameter  $x$ . In particular, the lattice constant adheres to **Vegard's law**, changing almost linearly with respect to composition (Fig. 5.1.4). All this means that a material having the required characteristics can be synthesized by controlling the composition. This technique is already applied to semiconductor lasers and light emitting diodes and has applications in daily life. Although the X-ray diffraction method can measure lattice constants precisely, what degree of precision is needed?

The lattice constants of GaAs and AlAs are given below:

$$a_{\text{GaAs}} = 5.6537 \text{ Å}$$

$$a_{\text{AlAs}} = 5.6616 \text{ Å}$$

The difference is only  $0.0079 \text{ Å}$ ; in terms of relative value,  $\Delta a/a = 1.4 \times 10^{-3}$ . To determine the composition to a precision of 1%, the lattice constant must be determined to 1/100 of this precision. This corresponds to measuring the Bragg angle at a precision on the order of several ten-thousandths of a degree. This precision is more than an order of magnitude greater than the precision required for ordinary powder X-ray diffraction. Thus, it requires a high-resolution

X-ray diffractometer and multiple crystal geometry.

Incidentally, these mixed crystals are single crystal films grown by epitaxial techniques such as the molecular beam epitaxy (MBE) and metal organic chemical vapor deposition (MOCVD) onto single crystal substrates of known lattice constants. The X-ray diffraction peaks are generated by both the epitaxial layer and substrate crystal. The lattice constant of the epitaxial layer can be obtained as a value relative to that of the substrate crystal; measurements of absolute value are not always necessary. Fig. 5.1.5, which shows the X-ray diffraction intensity profile versus the incident angle obtained from such a crystal, is known as a **rocking curve**. With the high-resolution X-ray diffraction method, the full width at half maximum (FWHM) of the peak is approximately 10 seconds, which enables high-precision measurements.

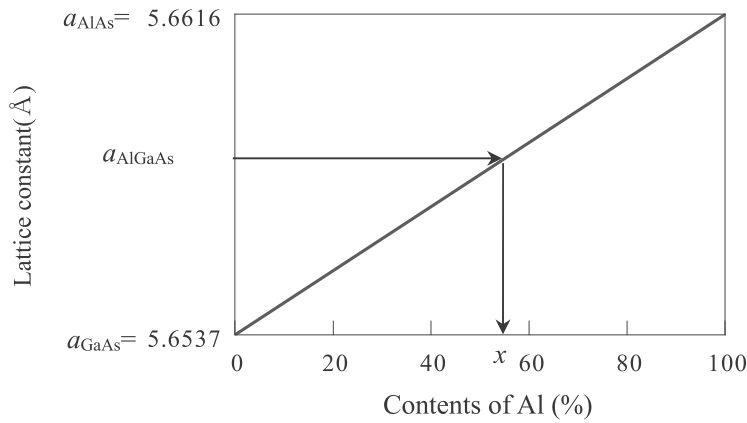


Fig. 5.1.4 Vegard's law and determining composition

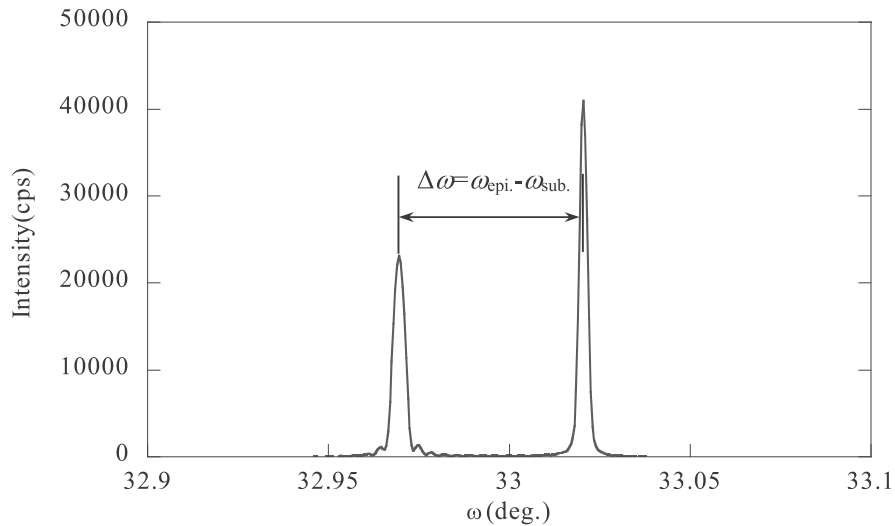


Fig. 5.1.5 Rocking curve

## §5.2 Multiple Crystal Method Principles

### 5.2.1 X-ray Diffraction with a Perfect Crystal

The crystal used as the monochromator and collimator in the multiple crystal method is a near-perfect single crystal. As discussed in the previous chapter, the X-ray diffraction that occurs in a crystal with high perfection is called dynamical diffraction, and the associated theory differs from the theory for kinematical diffraction encountered in powder and imperfect crystals. Fig. 5.2.1 shows the reflectivity curve for monochromatic, divergent X-rays incident on a perfect crystal, indicating reflectivity near 100% when the diffraction condition is met.  $W$  in this figure is the normalized angle parameter indicating the shift in the incident angle from the Bragg condition. When no absorption occurs, the angle range with 100% reflectivity corresponds to the angle range  $-1 \leq W \leq 1$ .

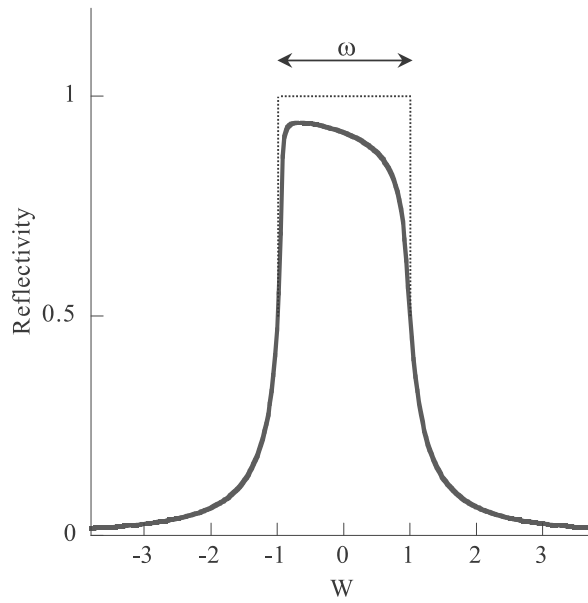


Fig. 5.2.1 Reflectivity curve

The diffraction line width  $\omega_s$  of the symmetric diffraction from a perfect crystal is given by the following formula:

$$\omega_s = 2 \cdot r_e \cdot \frac{\lambda^2}{\pi V} \cdot \frac{|F_{hkl}|}{\sin 2\theta} \quad \text{Formula 5.2.1}$$

This formula is known as the Darwin-Prins formula.

Here,  $r_e$  is the classical radius of an electron,  $\lambda$  the X-ray wavelength,  $V$  the volume of the unit cell,  $2\theta$  the diffraction angle, and  $F_{hkl}$  the structure factor.



Table 5.2.1 shows the theoretical values of this angle range  $\omega_s$  for the following perfect crystals: Si, Ge, and  $\alpha$ -quartz. The values for  $\omega_s$  are extremely small, ranging from several seconds to less than 20 seconds, and proportional to the absolute values of the crystal structure factor  $F_h$ . The parameter  $I$  in Table 5.2.1 is the integrated reflection intensity corresponding to the area below the curve shown in Fig. 5.2.1. It is also proportional to  $|F_h|$ , differing here from results for kinematical diffraction, in which it is proportional to  $|F_h|^2$ .

Table 5.2.1 Diffraction width of perfect crystals (wavelength:  $\lambda = 1.54\text{\AA}$ )

| Crystal          | $hkl$        | $\omega_s$   | I                 |
|------------------|--------------|--------------|-------------------|
|                  |              | (arc second) | ( $\times 10^6$ ) |
| Silicon          | 111          | 7.395        | 39.9              |
|                  | 220          | 5.459        | 29.7              |
|                  | 311          | 3.192        | 16.5              |
|                  | 400          | 3.603        | 19.3              |
|                  | 331          | 2.336        | 11.8              |
|                  | 422          | 2.925        | 15.5              |
|                  | 333          | 1.989        | 9.9               |
|                  | (511)        |              |                   |
|                  | 440          | 2.675        | 14.0              |
|                  | 531          | 1.907        | 9.3               |
| Germanium        | 111          | 16.338       | 85.9              |
|                  | 220          | 12.449       | 67.4              |
|                  | 311          | 7.230        | 37.1              |
|                  | 400          | 7.951        | 42.3              |
|                  | 331          | 5.076        | 25.4              |
|                  | 422          | 6.178        | 32.4              |
|                  | 333          | 4.127        | 20.2              |
|                  | (511)        |              |                   |
|                  | 440          | 5.339        | 27.5              |
|                  | 531          | 3.719        | 17.7              |
| $\alpha$ -Quartz | 100          | 3.798        | 18.8              |
|                  | 101          | 7.453        | 40.9              |
|                  | 110          | 2.512        | 12.2              |
|                  | 10 $\bar{2}$ | 2.488        | 12.9              |
|                  | 200          | 2.252        | 11.5              |
|                  | 112          | 2.927        | 15.5              |
|                  | 202          | 2.072        | 10.6              |
|                  | 212          | 2.042        | 10.7              |
|                  | 20 $\bar{3}$ | 2.430        | 12.9              |
|                  | 301          | 2.368        | 12.6              |

## 5.2.2 Application of Asymmetric Reflections

Reflections occurring when the surface of the crystal and diffraction plane are parallel are called **symmetric reflections**. When these planes are not parallel, reflections are referred to as **asymmetric reflections**. The angle range  $\omega_s$  in Table 5.2.1 represents the diffraction width of symmetric reflections. It can be decreased or increased by approximately an order of magnitude using asymmetric reflection. If the lattice plane is at angle  $\alpha$  with respect to the crystal surface, **asymmetry factor**  $b$  is given by the following formula ( $\theta_B$  is the Bragg angle):

$$b = \frac{\sin(\theta_B - \alpha)}{\sin(\theta_B + \alpha)} \quad \text{Formula 5.2.2}$$

For symmetric reflections,  $b = 1$  holds. When  $\omega_o$  denotes the angle divergence of the incident X-ray beam causing the diffraction and  $\omega_h$  denotes the angle divergence of the diffracted X-ray beam, the following relationship holds:

$$\omega_h = b\omega_o = \sqrt{b}\omega_s \quad \text{Formula 5.2.3}$$

The relationship given by the formula below holds between the width of the incident X-ray beam  $l_o$  and the width of the diffracted X-ray beam  $l_h$ .

$$l_h = l_o / b \quad \text{Formula 5.2.4}$$

Selecting the appropriate value for  $b$  makes it possible to increase or decrease the divergence angle and spatial width of X-ray beams.

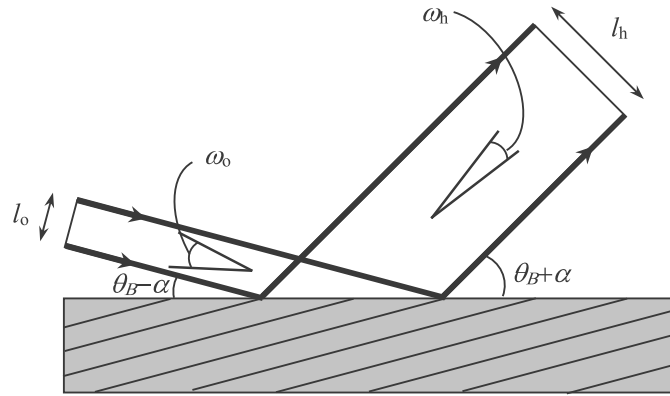


Fig. 5.2.2 Asymmetric reflection

### 5.2.3 Multiple Crystal Optics

This section discusses the specific case of double crystal optics among the general category of multiple crystal optics. Discussions up to the previous section assumed that incident X-ray beams are monochromatic. However, X-rays emitted from an X-ray source have a wavelength distribution, and the effects of this wavelength dispersion must be taken into account with double crystal optics. The manner in which this effect emerges depends on the double crystal arrangement. The **DuMond diagram** schematically illustrates the relationship between X-ray wavelength and incident angle and is used to describe the mechanism. Fig. 5.2.3 shows the DuMond diagram for a single crystal.

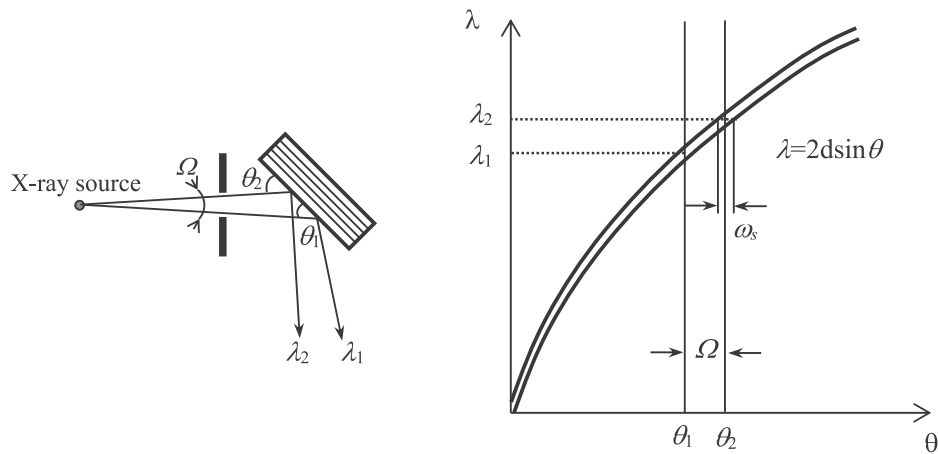
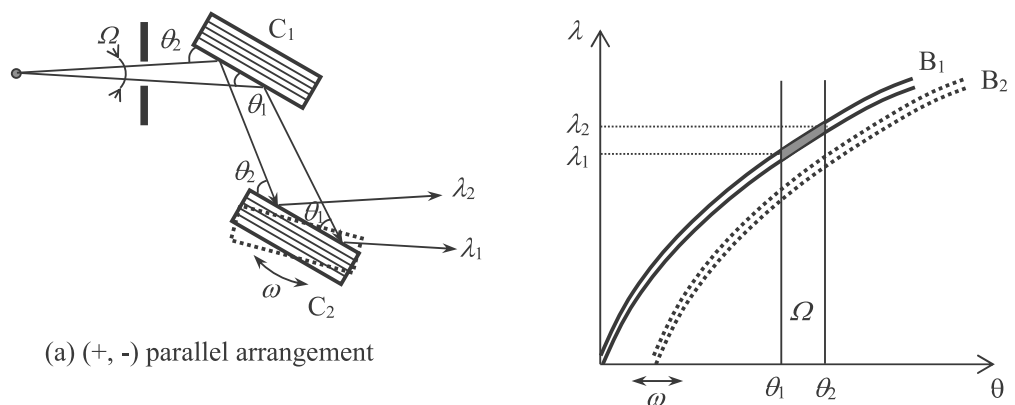


Fig. 5.2.3 DuMond diagram

The vertical axis corresponds to wavelength  $\lambda$ , while the horizontal axis corresponds to angle,  $\theta$ . The diffraction condition of the crystal is expressed by the curve  $\lambda = 2d \sin \theta$ . This sine curve is assigned a width corresponding to the dynamical diffraction width  $\omega_s$ , which is characteristic of the crystal.

Now, assume that an X-ray beam with divergence angle  $\Omega$  is incident on the crystal through a slit. In the DuMond diagram, the effects of the slit appear as a vertical band of width  $\Omega$ . The region in which the curve and band overlap corresponds to the angle-wavelength distributions of the diffracted beam. In Fig. 5.2.3, the angle distribution is from  $\theta_1$  to  $\theta_2$  and the wavelength distribution from  $\lambda_1$  to  $\lambda_2$ .

Fig. 5.2.4 shows the double crystal arrangements and their DuMond diagrams. There are two types of double crystal arrangements: the (+, -) arrangement and the (+, +) arrangement. The (+, -) arrangement is further divided into two subtypes: the (+, -) **parallel arrangement**, in which the interplanar spacing ( $d$  value) of the two crystals are identical, and the (+, -) **non-parallel arrangement**, in which the interplanar spacing ( $d$  value) of the two crystals differ.



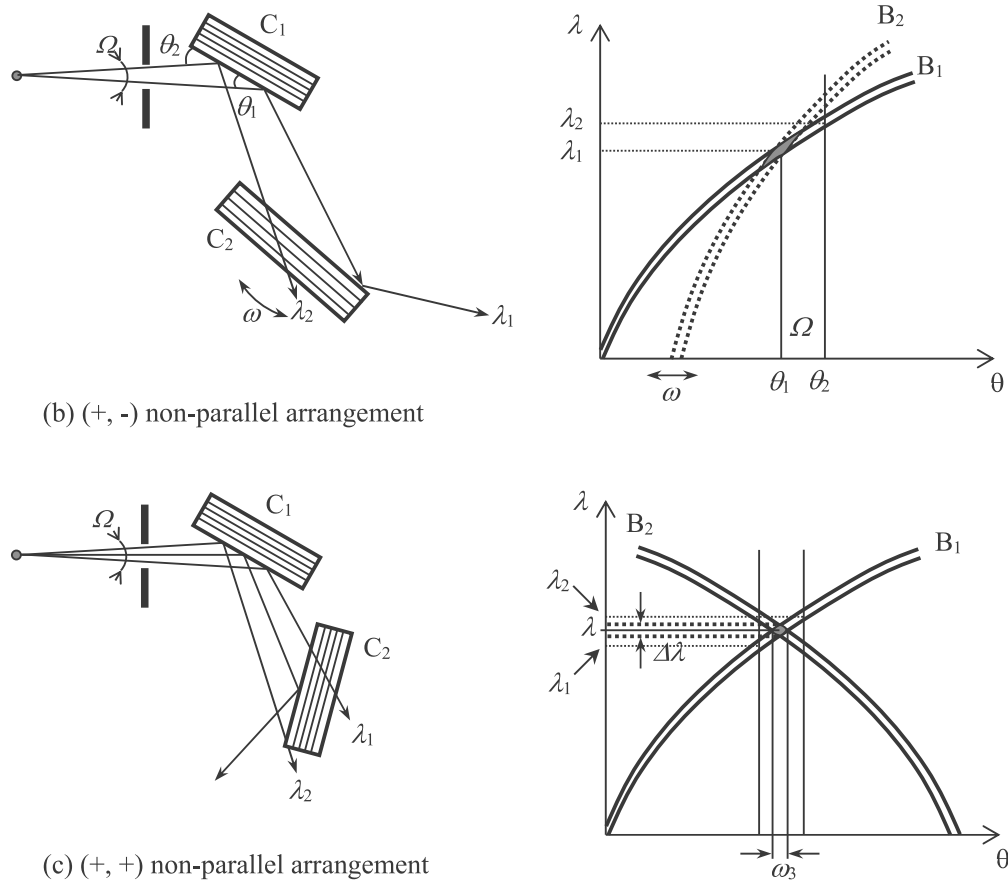


Fig. 5.2.4 Double crystal arrangements and corresponding DuMond diagrams

Fig. 5.2.4 (a) shows the (+, -) parallel arrangement. The X-ray beam with wavelength distributions from  $\lambda_1$  to  $\lambda_2$  is diffracted by the first crystal,  $C_1$ , and is incident on the second crystal,  $C_2$ . With the first crystal positioned at an angle, the second crystal is rotated ( $\omega$  rotation) to render the lattice planes of the two crystals parallel. The wavelength components distributed from  $\lambda_1$  to  $\lambda_2$  now satisfy the diffraction condition simultaneously. In the DuMond diagram, the band  $B_1$  indicating the diffraction condition of the first crystal and band  $B_2$  indicating the diffraction condition of the second crystal, overlap with the same shape, and a broad range of X-ray wavelengths X-rays contribute to the diffraction. The X-rays in this broad range of wavelengths are restricted by divergence angle  $\Omega$ , depending on the size of the X-ray source, slit width, and other factors. Diffraction intensity is high, since a broad range of wavelengths can be used.

Fig. 5.2.4 (b) shows the (+, -) non-parallel arrangement. Since the  $d$  values of the first and second crystals differ, the  $\omega$  angle that satisfies the diffraction condition for the X-ray beam

with wavelength  $\lambda_1$  cannot simultaneously satisfy the diffraction condition for an X-ray beam with wavelength  $\lambda_2$ . As the  $\omega$  angle rotates, different wavelength components satisfy the diffraction condition from  $\lambda_1$  to  $\lambda_2$  at different positions on the crystal. In the DuMond diagram, the region in which the bands  $B_1$  and  $B_2$  overlap undergoes diffraction, and this region moves as the  $\omega$  angle rotates. In this case, the rocking curve shows an angle spread caused by the wavelength spread of the X-rays incident on the first crystal.

Fig. 5.2.4 (c) shows the (+, +) arrangement. Here, the direction of the horizontal axis is reversed for band  $B_2$ . The arrangement produces an X-ray beam having angle spread and wavelength distribution corresponding to the region in which the bands  $B_1$  and  $B_2$  overlap. The widths of  $B_1$  and  $B_2$  along the  $\theta$  axis are extremely narrow, approximately  $10^{-5}$  rad. The corresponding wavelength spread is also narrow, with  $\Delta\lambda/\lambda$  to  $10^{-5}$ . In this manner, this arrangement can produce an X-ray beam with extremely high monochromaticity. (For reference, the natural width of the Cu  $K\alpha_1$  line is  $\Delta\lambda/\lambda = 3.8 \times 10^{-4}$ , part of which is selected.)

#### 5.2.4 Channel-Cut Crystal and Monochromator System

The monochromator system uses combinations of channel-cut crystals.

A **channel-cut crystal** is an optical device proposed by Bonse and Hart. A channel is cut in a Si or Ge perfect crystal block to cause multiple instances of Bragg diffraction (Fig. 5.2.5).

A channel is cut in a perfect crystal block.

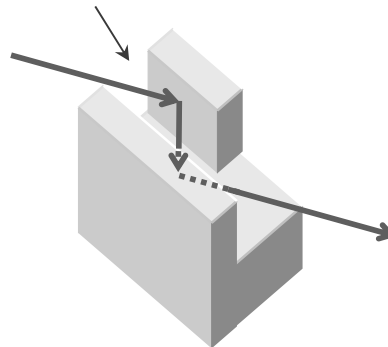


Fig. 5.2.5 Schematic diagram of channel-cut crystal

When the beam is reflected an even number of times, the X-ray beam output from the optical device has the same direction as the X-ray beam incident on the optical device. Since all reflections overlap in the bands with the same shape in the DuMond diagram, the wavelength spread persists up to the last reflection. However, the reflectivity curve is basically similar to that of the single reflection shown in Fig. 5.2.1.

Fig. 5.2.6 compares the reflectivity curves of a single reflection and reflections from channel-cut crystals. The advantages of repeating reflections are given below.

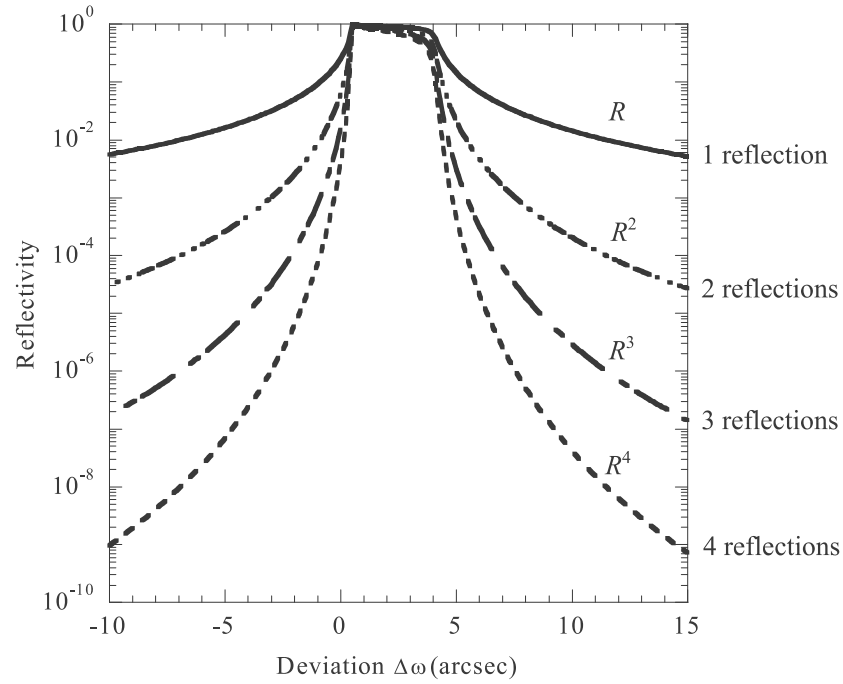


Fig. 5.2.6 Reflectivity curves of channel-cut crystal

In the case of a single reflection, reflectivity curve  $R$  has a long tail on both sides of the peak. The reflectivity curve after  $n$  reflections is given by its power,  $R^n$ . The center region ( $|W| < 1$ ) of the reflectivity curve shows a reflectivity near 100% and does not significantly attenuate after repeated reflections. However, reflectivity decreases significantly in the tails ( $|W| > 1$ ). Thus, repeated reflections remove the intensity in the tails and produce an X-ray beam with an angular distribution without a tail.

Thus,  $n$  reflections in a channel-cut crystal have the effect of making the angular distribution rectangular. Nevertheless, it does not reduce the diffraction width or wavelength width.

#### A. Double-Crystal Monochromator

A double-crystal monochromator is basically equivalent to a single-reflection flat crystal monochromator. In the DuMond diagram, it is expressed as a single band with a width of  $\omega_s$ . The rocking curve produced using this monochromator takes the non-parallel arrangement if the lattice constants of the monochromator and sample differ. Thus, the width of the rocking curve has an angle spread attributable to wavelength dispersion.

The DuMond diagram (Fig. 5.2.4 (b)) explains the angle spread caused by wavelength dispersion. Fig. 5.2.7 magnifies the region in which the two bands cross. This figure ignores the diffraction width of the crystal itself and indicates the bands as lines.

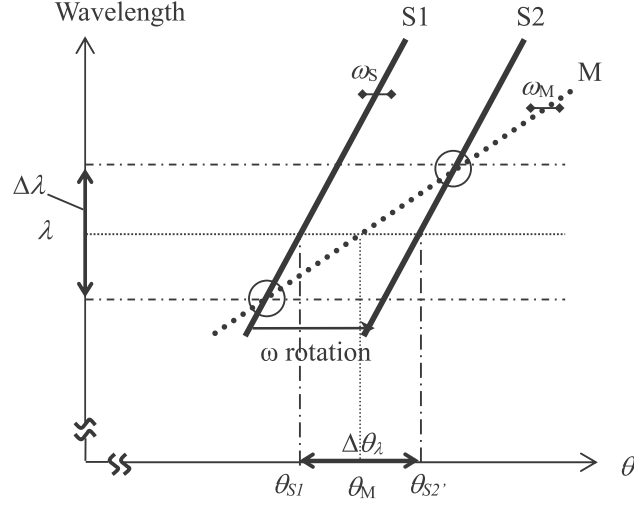


Fig. 5.2.7 Angle spread caused by wavelength dispersion

In this figure, M indicates the band of the double-crystal monochromator. We assume that the diffraction condition is met in the wavelength range  $\Delta\lambda$ , around  $\lambda$ . The range  $\Delta\lambda$  is restricted by the divergence angle of the X-ray beam incident on the monochromator. S in the figure indicates the band of the sample crystal. The  $\omega$  rotation of the sample corresponds to the parallel translation of this band about the  $\theta$  axis.

The sample diffracts the X-ray beam when band S intersects with band M in the range  $\Delta\lambda$ ; in short, when the band of the sample is found between the lines S1 and S2 in the figure. (Intersections are circled.) The difference between the sample angles  $\theta_{S1}$  and  $\theta_{S2}$  corresponding to the cases in which the band S is at the positions S1 and S2, respectively, is the angle spread  $\Delta\theta_\lambda$  caused by wavelength dispersion.

Angle spread  $\Delta\theta_\lambda$  is calculated as shown below. When the gradient of a band is denoted as G, it is given by differentiating Bragg's equation as follows:

$$G = d\lambda/d\theta = 2d \cos \theta = \lambda / \tan \theta \quad \text{Formula 5.2.5}$$

Thus, when  $G_M$  and  $G_S$ , respectively, denote the gradients of the bands of the monochromator and the sample,  $\Delta\theta_\lambda$  is expressed by the following formula:

$$\Delta\theta_\lambda = \Delta\lambda \left( \frac{1}{G_M} - \frac{1}{G_S} \right) = \left( \frac{\Delta\lambda}{\lambda} \right) (\tan \theta_M - \tan \theta_S) \quad \text{Formula 5.2.6}$$

The approximate full width at half maximum (FWHM) of the rocking curve in the non-parallel arrangement is given by the following formula by adding the diffraction width of the crystal itself to the angle spread attributable to wavelength dispersion.

$$FWHM = \sqrt{\omega_M^2 + \Delta\theta_\lambda^2 + \omega_s^2} \quad \text{Formula 5.2.7}$$

Here,  $\omega_M$  is the diffraction width of the monochromator and  $\omega_s$  the diffraction width of the sample crystal.

As an example, calculate FWHM when the monochromator is a Ge (220) channel-cut crystal and the sample is GaAs (400).

#### Calculations

With parameters  $\omega_M$  (Ge (220)) = 0.0034°,  $\omega_s$  (GaAs (400)) = 0.0022°,  $\theta_M = 22.65^\circ$ , and  $\theta_s = 33.02^\circ$ , when extracting only the Cu K $\alpha$  line:  $\Delta\lambda/\lambda = 3.8 \times 10^{-4}$  and  $\Delta\theta_\lambda = 8.8 \times 10^{-5}$  rad. = 0.005°

Calculations give FWHM = 0.0065°.

The value of  $\Delta\theta$  is extremely small when the Bragg angles of the monochromator and the sample are close. For example, when the monochromator is Ge (400) and the sample is GaAs (400), the Bragg angles are virtually identical, so that width  $\Delta\theta_\lambda$  is almost zero. When the sample is InP (400),  $\Delta\theta_\lambda$  is approximately two seconds, which is not extremely large. Known as the pseudo-parallel arrangement, this arrangement can produce high resolution rocking curves.

### **B. Four-Crystal Monochromator**

The four-crystal monochromator is a monochromator first put to practical use by Barters, based on an idea proposed by DuMond. Two channel-cut crystals are placed in a mirror symmetric arrangement to reflect the beam four times, including a (+, +) arrangement. In this manner, the four-crystal monochromator forms a monochromator and collimator system with high wavelength selectivity. The four-crystal monochromator makes it possible to maintain high resolution regardless of the Bragg angle. It is free of the inconvenience associated with replacing and adjusting the monochromator each time the sample or the reflection indices are changed in the double-crystal method.

Fig. 5.2.8 shows the example of rocking curve measurement using a Ge (440) four-crystal monochromator. Figures (a), (b), and (c) show examples of measurements for a ZnSeS film on a GaAs substrate with different reflection indices. Figure (d) shows the rocking curve of an InGaAsP film on an InP substrate. The rocking curves are obtained regardless of the reflection indices or materials.



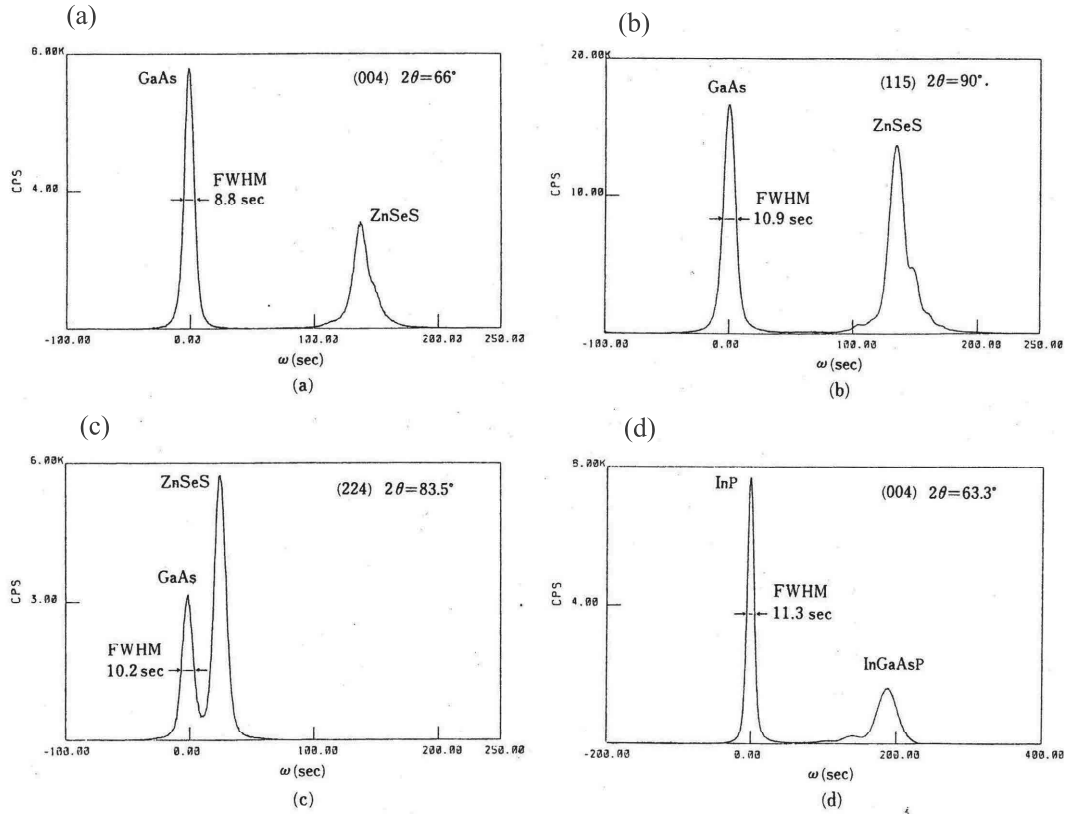


Fig. 5.2.8 Examples of rocking curves measurement using a four-crystal monochromator

Fig. 5.2.9 shows the DuMond diagram of the X-ray beam produced by a four-crystal monochromator. It shows a rhombic region of restricted wavelength range and angle range. The full width at half maximum (FWHM) of a rocking curve with a four-crystal monochromator can be expressed as the range in which this range and the band of the sample overlap. The FWHM is given by Formula 5.2.6. Here, we can obtain  $\Delta\theta_\lambda$  by calculating  $\Delta\theta_\lambda = (\Delta\lambda/\lambda)\tan\theta_s$ . Here,  $\Delta\lambda/\lambda$  is the wavelength width (Table 5.2.2 in Section 5.2.5) restricted by the four-crystal monochromator, while  $\theta_s$  is the Bragg angle of the sample. Since  $\Delta\theta_\lambda$  includes the tangent of the Bragg angle, it is quite large for reflections of large  $\theta_s$  angles near  $90^\circ$ .

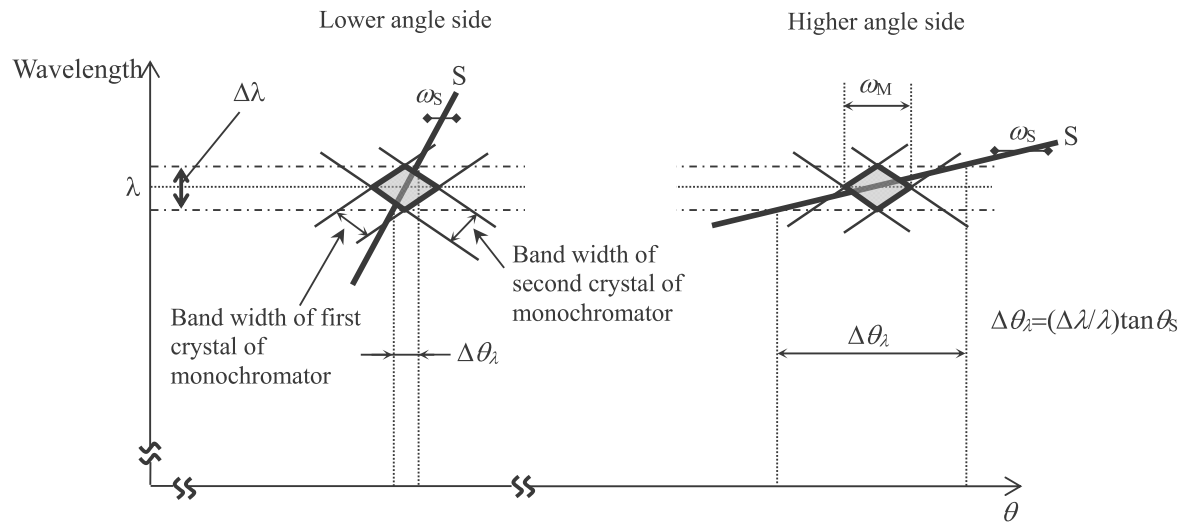


Fig. 5.2.9 Angle spread in high-angle reflections

For example, for Si (444), which diffracts the beam at a high-angle reflection at  $2\theta = 158.624^\circ$ , the width of the rocking curve with a Ge (220) four-crystal monochromator is  $0.022^\circ$ , a relatively large value.

### 5.2.5 Practical Monochromator System

Rigaku's X-ray diffractometers (SmartLab and the RINT III series) support monochromator systems, which are boxed channel-cut crystals as shown in Fig. 5.2.10. The channel-cut crystal used is a block of Ge single crystal, a perfect crystal, cut with a channel, with the crystal surface (channel surface) parallel to the (110) plane or the (100) plane (only SmartLab). The box is characterized by mounting reproducibility and can be adjusted by computer. For this reason, measurements can be started immediately after the monochromator is set to its position, and the operator can adjust it to the optimal conditions if more reliable data is needed.

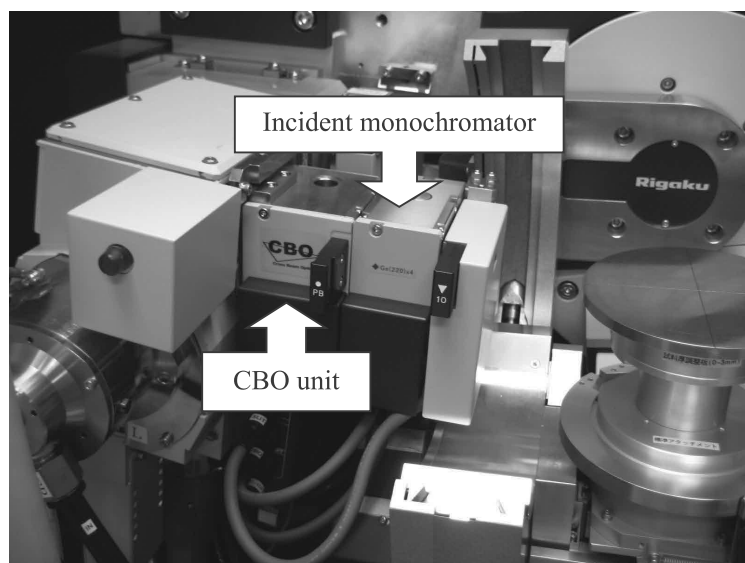
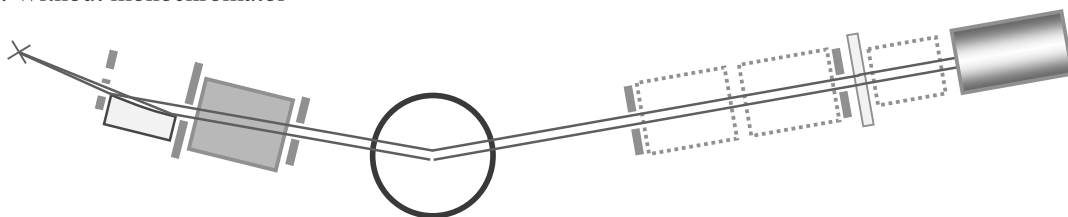


Fig. 5.2.10 Monochromator box (SmartLab)

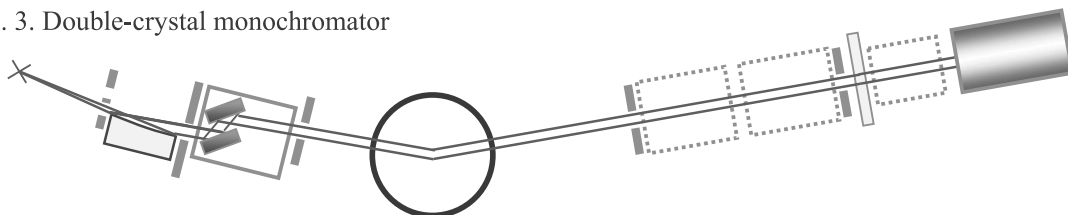
SmartLab and the RINT III series support the four optics below.

1. Without monochromator (**Medium resolution PB** in SmartLab and **Thin film (General)** in the RINT III series)
2. Double-crystal monochromator optics (**High resolution PB-Ge (220)x2** and **High resolution PB-Ge (400)x2** in SmartLab and **Thin film (High resolution)** in RINT III series)
3. Four-crystal monochromator optics (Only in SmartLab, **Ultra high resolution PB-Ge (220)x4** and **Ultra high resolution PB-Ge(440)x4** )

1. Without monochromator



2. 3. Double-crystal monochromator



4. Four-crystal monochromator

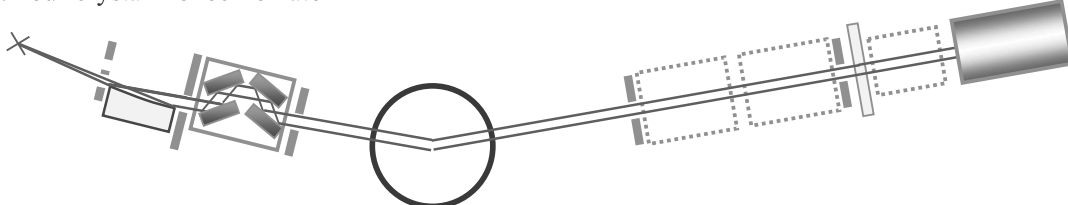


Fig. 5.2.11 Switching optics

(1) Without monochromator

The optics use an incident slit to extract part of the direct beam collimated by the reflection on a multilayer mirror. It does not use a channel-cut crystal. The divergence angle of the X-ray beam depends on the multilayer mirror and is approximately  $0.04^\circ$ .

(2) Double-crystal monochromator optics

The optics use a double-crystal monochromator system containing a set of channel-cut crystals. When the rotational angle of the channel-cut crystal is set to the  $\omega$  angle of the (220) reflection ((400) reflection for the high resolution PB-Ge (400)x2), the Ge single crystal diffracts the incident X-ray beam, and the diffracted X-ray beam is extracted. The X-ray beam is then shaped to the required size by the incident slit.

The double-crystal monochromator outputs the diffracted X-ray beam parallel to the incident X-ray beam, but the position is shifted. When  $D$  denotes the distance between the two crystals in the channel cut crystal and  $\theta$  denotes the Bragg angle, the shift  $H$  is given by the following formula below:

$$H=2D\cos\theta$$

Here,  $D$  is approximately 5 mm, and  $\theta$  is  $22.5^\circ$  for the Ge (220) reflection, so  $H$  is approximately 9.5 mm. The incident slit and the goniometer must be horizontally shifted by this amount. This shift is corrected using the goniometer T axis.

Since the channel-cut crystal uses the double crystal (+, -) parallel arrangement, the wavelength range selected in the first reflection is conserved in the second reflection. Thus, the X-ray beam extracted has a spread in wavelength dispersion. The divergence angle is approximately 32 seconds for Ge (220) and approximately 40 seconds for Ge (400).

### (3) Four-crystal monochromator optics

The optics use a four-crystal monochromator system incorporating two sets of channel-cut crystals. When the two channel-cut crystals are placed in a mirror symmetric geometry and the rotational angle is set to the  $\omega$  angle of the (220) reflection, the Ge single crystal diffracts the incident X-ray beams, and the diffracted X-ray beam is extracted. The X-ray beam is then shaped to the required spread by the incident slit.

The four-crystal monochromator outputs the X-ray beam diffracted by the Ge crystal parallel to the incident X-ray beam at approximately the same position.

An important feature of the four-crystal monochromator is that it contains the (+, +) arrangement in the four crystal arrangement. This results in a wavelength window that significantly restricts the divergence angle and wavelength range of the extracted X-ray beam. Measurements with a four-crystal monochromator can always be performed at high resolution regardless of the sample crystal type or the indices of the lattice plane used for diffraction. With the Ge (220) settings, the divergence angle is approximately 12 seconds, and the wavelength range is 39% of the natural width of the Cu  $K\alpha_1$  line. With the Ge (440) four-crystal monochromator, the divergence angle is reduced to approximately 5 seconds, and the wavelength range is reduced to approximately 6%. Table 5.2.2 below summarizes the monochromator optics and the monochromaticity and collimation of the X-ray beams obtained.

Table 5.2.2 Wavelength width and collimation by common monochromator system

| Optics  | Wavelength width $\Delta\lambda/\lambda$ | Collimation $\Delta\theta$ (seconds) | Relative intensity |
|---|--|--------------------------------------|--------------------|
| Medium resolution PB (Thin film (general))                  |  | 150                                  | 200                |
| High resolution PB-Ge (220)x2 (Thin film (high-resolution)) | $3.8 \times 10^{-4}$                     | 32                                   | 10                 |
| High resolution PB-Ge (400)x2                               |  | 40                                   | 5                  |
| Ultra high resolution PB-Ge (220)x4                         | $1.5 \times 10^{-4}$                     | 12.4                                 | 1                  |
| Ultra high resolution PB-Ge (440)x4                         | $2.3 \times 10^{-5}$                     | 5.4                                  | 0.05               |

### §5.3 Summary

This chapter discussed high-resolution optics for measuring crystals with high perfection, such as Si, Ge, and GaAs. Summarized below are the topics covered.

#### 1. Diffraction by perfect crystal

An ordinary powder crystal or imperfect crystal sample has a disordered three-dimensional periodicity. X-rays are scattered only once in a crystal.

→ Kinematical theory of diffraction

In a near-perfect crystal, X-rays undergo multiple scattering.

→ Dynamical theory of diffraction

The optics used to measure ordinary powder samples are inadequate for measuring samples to which the dynamical theory of diffraction applies. We must improve X-ray beam collimation and monochromaticity.

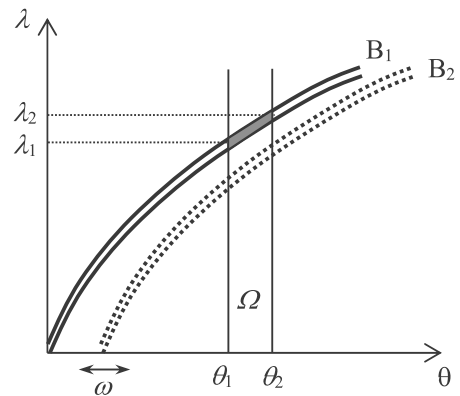
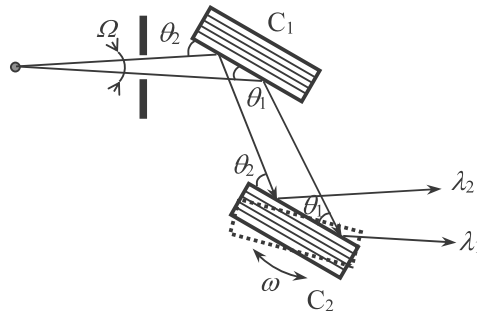
→ High-resolution X-ray diffraction method

#### 2. Multiple crystal optics

Double crystal arrangement

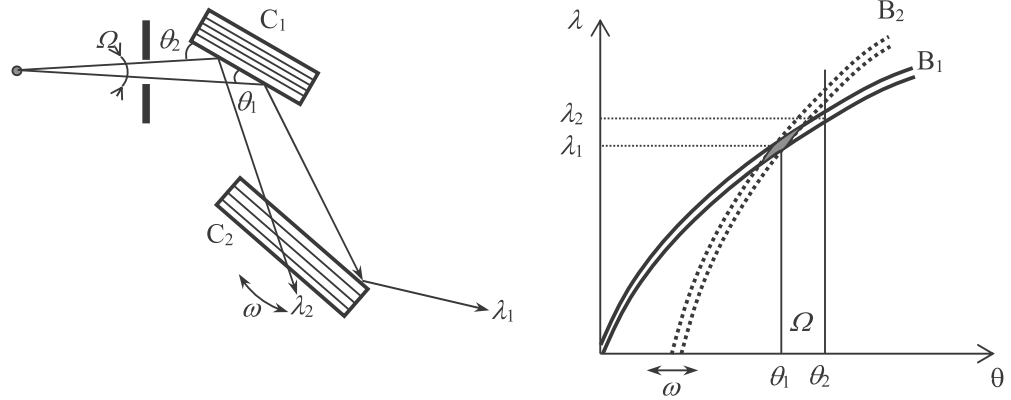
(1) (+, -) parallel arrangement

The interplanar spacings of the two crystals are identical. A broad range of wavelengths (depending on divergence angle  $\Omega$ ) can be used.



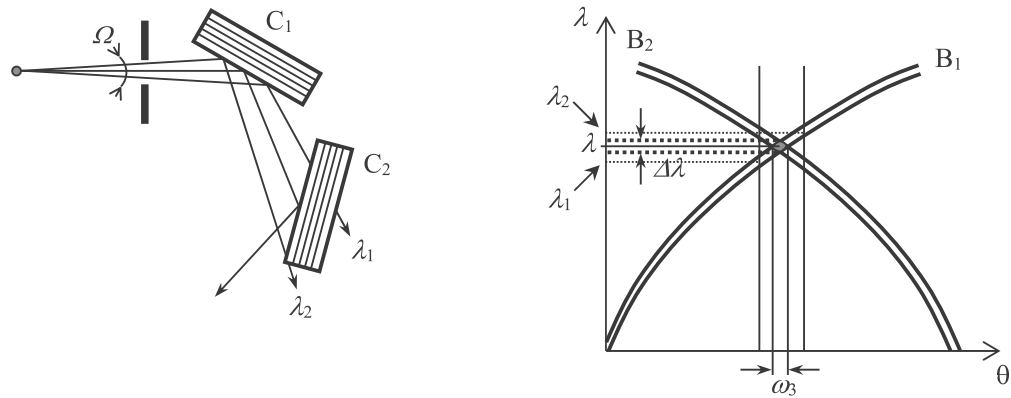
(2) (+, -) non-parallel arrangement

The interplanar spacings of the two crystals differ. An angle spread is caused by the wavelength spread of the incident X-ray beam.



(3) (+, +) non-parallel arrangement

The interplanar spacings of the two crystals are identical, resulting in an extremely narrow angle spread and wavelength distribution.



### 3. Monochromator

Wavelength width and collimation by common monochromator systems

| Optics  | Wavelength width $\Delta\lambda/\lambda$ | Collimation $\Delta\theta$ (seconds) | Relative intensity |
|---|--|--------------------------------------|--------------------|
| Medium resolution PB (Thin film (general))                  |  | 150                                  | 200                |
| High resolution PB-Ge (220)x2 (Thin film (high resolution)) | $3.8 \times 10^{-4}$                     | 32                                   | 10                 |
| High resolution PB-Ge (400)x2                               |  | 40                                   | 5                  |
| Ultra high resolution PB-Ge (220)x4                         | $1.5 \times 10^{-4}$                     | 12.4                                 | 1                  |
| Ultra high resolution PB-Ge (440)x4                         | $2.3 \times 10^{-5}$                     | 5.4                                  | 0.05               |

## Chapter 6 Rocking Curve Measurement

As in Chapter 5, there are two theories on diffraction phenomena by crystallization: the kinematical theory of diffraction and the dynamical theory of diffraction. Since semiconductor crystals such as Si, Ge, GaAs, and GaN feature high perfection (near-perfect uniformity of lattice constants and crystal orientation), the latter dynamical theory of diffraction is applied to substrates made of these crystals. When rocking curve measurements are performed to evaluate the composition and film thickness of epitaxial films grown on such semiconductor substrate crystals, the measurement results are generally analyzed using the dynamical theory of diffraction.

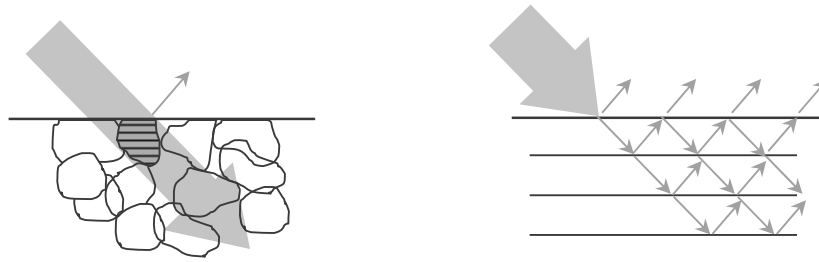
This chapter discusses the basics of the dynamical theory of diffraction and its use in evaluating epitaxial films

### §6.1 What is the Dynamical Theory of Diffraction?

Most crystalline materials are assemblies of extremely small crystals, each of which can be regarded as a **perfect crystal** completely free of lattice disorders. Of those small crystals, the majority of samples called single crystals are **mosaic crystals**, assemblies of even smaller crystals with slightly differing orientations. In such crystals, each perfect crystal free of lattice disorders is extremely small (on the submicron order or smaller), and X-rays incident on such crystals are scattered just once. However, if X-rays are incident on a sample formed entirely of a single perfect crystal, the X-rays transmitted through part of the sample without being scattered are scattered in a deeper region of the sample. In such samples, the propagating X-rays are scattered numerous times. This is called **multiple scattering**.

The kinematical theory of diffraction assumes that the incident X-rays are scattered just once in the material. This makes it unsuitable for near-perfect crystals of relatively large volumes in which multiple scattering can occur. When multiple scattering occurs, the transmitted X-rays and scattered X-rays interfere within the crystal, and propagation of these waves in the crystal must be accounted for. To assess such diffraction phenomena, we must calculate the X-rays incident on the surface of the sample, the wave fields in crystals connected to the incident X-rays, and the waves transmitted and diffracted out of the sample connected to this wave field. The word “connected” here refers to satisfying the boundary conditions. The **dynamical theory of diffraction** is a diffraction theory that considers the phenomena occurring in such near-perfect crystals.





(a) Single scattering by mosaic crystal      (b) Multiple scattering by perfect crystal

Fig. 6.1.1 Single scattering and multiple scattering

The dynamical theory of diffraction was almost solely established by Darwin (1914) and Ewald (1917). Ewald used Thomson scattering as the fundamental process and explored three-dimensional multiple scattering. Darwin considered reflections from a single atomic plane as the fundamental process and formulated multiple scattering on this basis. Darwin's method bore resemblances to the method for calculating the reflectivity of multilayer films. Later, Laue (1931) regarded the entire crystal as a polarizable medium and established a method for solving Maxwell's wave equations. Here, we describe the diffraction phenomena characteristic of the dynamical theory of diffraction according to Laue, the version most commonly applied.

## §6.2 Basic Equation of Dynamical Theory of Diffraction

Assume two or more incident waves and scattered waves within a crystal, interfering with each other constructively or destructively. We calculate the waves emerging from (or existing in) this environment by solving Maxwell's equations while regarding the crystal as a region of periodic permittivity into which X-rays—electromagnetic waves forming an oscillating electric field—enter. The formula thus obtained that expresses the waves that can exist within the crystal is called the **fundamental equation**. In this section, we derive the fundamental equation, calculate the waves that can exist within the crystal, and calculate the observed transmitted and diffracted waves by considering the boundary conditions at the interface between the vacuum (or air) and the crystal. In doing so, we will also examine diffraction conditions under the dynamical theory of diffraction.

### 6.2.1 Maxwell's Equations in Crystal

We can calculate the X-rays allowed to exist in a crystal by solving Maxwell's equations while regarding the crystal as a region of periodic permittivity. Permittivity can be regarded as a constant in the more commonly encountered optical systems that handle light of longer wavelengths, but permittivity corresponding to X-rays changes locally in a material.

This section begins by discussing Maxwell's equations in a crystal.

Maxwell's equations in a material are generally given as follows:

$$\text{rot } \mathbf{B} = \mu_0 (\mathbf{j} + \mathbf{j}_p + \mathbf{j}_m) + \varepsilon_0 \mu_0 \frac{\partial \mathbf{E}}{\partial t} \quad \text{Formula 6.2.1}$$

$$\text{rot } \mathbf{E} = -\frac{\partial \mathbf{B}}{\partial t} \quad \text{Formula 6.2.2}$$

$$\text{div } \mathbf{E} = \frac{1}{\varepsilon_0} (\rho + \rho_p) \quad \text{Formula 6.2.3}$$

$$\text{div } \mathbf{B} = 0 \quad \text{Formula 6.2.4}$$

**E**: Electric field

**j**: Actual current

**B**: Magnetic flux density

**j<sub>p</sub>**: Polarization current

$\varepsilon_0$ : Permittivity of vacuum

**j<sub>m</sub>**: Magnetizing current

$\mu_0$ : Magnetic permeability of vacuum

$\rho$ : Actual charge density

$\rho_p$ : Polarization charge density

Since we are considering a periodically changing electromagnetic field, we remove the electromagnetic field attributable to the actual current **j** and actual charge density  $\rho$  by assuming **j** = 0 and  $\rho$  = 0.

Consider the electric field. The polarization charge density  $\rho_p$  is the charge density generated by electric polarization **P**, and polarization current **j<sub>p</sub>** is the current generated by the time variation of electric polarization **P**. These quantities are given by the following formulas:

$$\mathbf{j}_p = \frac{\partial \mathbf{P}}{\partial t} \quad \text{Formula 6.2.5}$$

$$\rho_p = -\text{div } \mathbf{P} \quad \text{Formula 6.2.6}$$

Electric field **E** is related to electric flux density **D**, as follows:

$$\begin{aligned} \mathbf{D} &= \varepsilon_0 \mathbf{E} + \mathbf{P} \\ &= \varepsilon \mathbf{E} \end{aligned} \quad \text{Formula 6.2.7}$$

Here,  $\varepsilon$  is the permittivity of the material. Polarization  $\mathbf{P}$  is given by the following formula:

$$\mathbf{P} = \varepsilon_0 \chi \mathbf{E} \quad \text{Formula 6.2.8}$$

Here,  $\chi$  is electric susceptibility, which indicates the degree of polarization generated in the material when an electric field  $\mathbf{E}$  is applied. It also indicates how easily the material scatters X-rays. Electric susceptibility and the permittivity of the material have the relationship indicated by the following Formula, as derived from Formulas 6.2.7 and 6.2.8:

$$\varepsilon = \varepsilon_0 (1 + \chi) \quad \text{Formula 6.2.9}$$

Here, at the microscopic scale, the electric polarization expressed in Formula 6.2.8 can be regarded as the vector sum of the electric dipole moment per unit volume in the material. If we ignore radiation damping, in which electrons lose energy by emitting electromagnetic waves, and the constraining force to which electrons are subject by the electron cloud, we can express electric polarization in terms of frequency  $\omega$  of the electric field and electron density distribution  $\rho(\mathbf{r})$  in the material, as in the following formula:

$$\mathbf{P} = -\frac{e^2}{m\omega^2} \rho(\mathbf{r}) \mathbf{E} \quad \text{Formula 6.2.10}$$

Based on Formulas 6.2.8 and 6.2.10, the following formula gives the relationship between electric susceptibility and electron density at position  $\mathbf{r}$  in the material when electromagnetic waves of frequency  $\omega$  and wavelength  $\lambda$  are incident on the material:

$$\begin{aligned} \chi(\mathbf{r}) &= -\frac{e^2}{m\omega^2 \varepsilon_0} \rho(\mathbf{r}) \\ &= -\frac{e^2 \lambda^2}{4\pi^2 \varepsilon_0 m c^2} \rho(\mathbf{r}) \\ &= -r_e \frac{\lambda^2}{\pi} \rho(\mathbf{r}) \end{aligned} \quad \text{Formula 6.2.11}$$

Here,  $c$  is the speed of light and  $r_e$  the classical electron radius. Since electric susceptibility  $\chi(\mathbf{r})$  has the same periodicity as the crystal lattice, it can be expanded into a Fourier series, as in the following formula:

$$\chi(\mathbf{r}) = \sum_g \chi_g \exp(i\mathbf{g} \cdot \mathbf{r}) \quad \text{Formula 6.2.12}$$

Here,  $\mathbf{g}$  is the reciprocal lattice vector and  $\mathbf{r}$  the position vector in the crystal lattice.

We can also express  $\rho(\mathbf{r})$  in terms of the crystal structure factor  $F_g$  and unit cell volume  $v_c$ , similarly to a Fourier series.

$$\rho(\mathbf{r}) = \frac{1}{v_c} \sum_g F_g \exp(i\mathbf{g} \cdot \mathbf{r}) \quad \text{Formula 6.2.13}$$

From Formulas 6.2.12 and 6.2.13, we obtain the following relational expression between electric susceptibility and the crystal structure factor:

$$\chi_g = -\frac{r_e \lambda^2}{\pi v_c} F_g \quad \text{Formula 6.2.14}$$

Formula 6.2.14 shows that  $\chi_g$  is a negative value of lesser magnitude than  $F_g$  by an order of  $10^{-5}$  to  $10^{-6}$ .

Next, we consider the magnetic field. In general, magnetic field  $\mathbf{H}$  is related to magnetic flux density  $\mathbf{B}$  as follows:

$$\mathbf{B} = \mu \mathbf{H} \quad \text{Formula 6.2.15}$$

Here,  $\mu$  is the magnetic permeability of the material. Since we are considering the interaction between the material and the X-rays, we assume the material to be magnetically identical to a vacuum. Thus, magnetizing current is  $\mathbf{j}_m = 0$ . In this case,  $\mu = \mu_0$  holds true, and we can rewrite Formula 6.2.15 as follows:

$$\mathbf{B} = \mu_0 \mathbf{H} \quad \text{Formula 6.2.16}$$

Based on the discussion above, we can rewrite Maxwell's equations as follows:

$$\text{rot } \mathbf{H} = \frac{\partial \mathbf{D}}{\partial t} \quad \text{Formula 6.2.17}$$

$$\text{rot } \mathbf{E} = -\mu_0 \frac{\partial \mathbf{H}}{\partial t} \quad \text{Formula 6.2.18}$$

$$\text{div } \mathbf{D} = 0 \quad \text{Formula 6.2.19}$$

$$\text{div } \mathbf{H} = 0 \quad \text{Formula 6.2.20}$$

### 6.2.2 Derivation of the Fundamental Equation

Consider the X-rays in a crystal and derive the fundamental equation expressing the waves allowed to exist in the crystal.

According to Bloch's theorem, the electron density distribution in a material having periodicity due to the crystal lattice modulates the plane wave,  $E = \exp\{i(\mathbf{k}_o \cdot \mathbf{r} - \omega t)\}$ , incident on the material; thus, the following formula describes the X-rays observed in the material:

$$\mathbf{E} = \exp\{i(\mathbf{k}_o \cdot \mathbf{r} - \omega t)\}u(\mathbf{r}) \quad \text{Formula 6.2.21}$$

Here,  $\mathbf{k}_o$  is the wave vector of the incident X-ray wave and  $u(\mathbf{r})$  a function having the periodicity of the crystal lattice. If this function is expanded into a Fourier series, electric field  $\mathbf{E}$  is given by the following formula:

$$\begin{aligned} \mathbf{E} &= \exp\{i(\mathbf{k}_o \cdot \mathbf{r} - \omega t)\} \sum_{\mathbf{g}} \mathbf{E}_{\mathbf{g}} \exp(i\mathbf{g} \cdot \mathbf{r}) \\ &= \exp(-i\omega t) \sum_{\mathbf{g}} \mathbf{E}_{\mathbf{g}} \exp(i\mathbf{k}_{\mathbf{g}} \cdot \mathbf{r}) \end{aligned} \quad \text{Formula 6.2.22}$$

Here,  $\mathbf{k}_{\mathbf{g}}$  is the wave vector of the diffracted wave, related to the reciprocal lattice vector  $\mathbf{g}$  as follows:

$$\mathbf{k}_{\mathbf{g}} = \mathbf{k}_o + \mathbf{g} \quad \text{Formula 6.2.23}$$

The time-dependent oscillating component  $\exp(-i\omega t)$  in Formula 6.2.22 is averaged out in discussions of the diffraction condition and diffraction intensity and is therefore omitted hereafter.

As implied by Formula 6.2.22, the X-ray wave in the crystal is consequently expressed as a superposition of the plane waves of wave vectors  $\mathbf{k}_{\mathbf{g}}$ . This wave is called the **Bloch wave**.

In Formulas 6.2.17 and 6.2.18, the time-dependent oscillating components of electric flux density  $\mathbf{D}$  and magnetic field  $\mathbf{H}$  are the same as that of electric field  $\mathbf{E}$ . Thus, these formulas can be rewritten as follows:

$$\frac{\partial \mathbf{D}}{\partial t} = -i\omega \mathbf{D} \quad \text{Formula 6.2.24}$$

$$\frac{\partial \mathbf{H}}{\partial t} = -i\omega \mathbf{H} \quad \text{Formula 6.2.25}$$

When we take the rotation of both sides of Formula 6.2.18, substitute Formula 6.2.17 into  $\text{rot}\mathbf{H}$ , and apply Formula 6.2.7 and 6.2.9, we obtain the following formula:

$$\text{rot rot}\mathbf{E} = K^2(1 + \chi)\mathbf{E} \quad \text{Formula 6.2.26}$$

Here,  $K$  is the wave number of the X-ray wave in a vacuum. To transform Formula 6.2.26, we apply the following calculation:

$$\text{rot}\{\mathbf{E}_g \exp(i\mathbf{k}_g \cdot \mathbf{r})\} = i\mathbf{k}_g \times \mathbf{E}_g \exp(i\mathbf{k}_g \cdot \mathbf{r}) \quad \text{Formula 6.2.27}$$

$$\begin{aligned} \text{rot rot}\{\mathbf{E}_g \exp(i\mathbf{k}_g \cdot \mathbf{r})\} &= -\mathbf{k}_g \times (\mathbf{k}_g \times \mathbf{E}_g) \exp(i\mathbf{k}_g \cdot \mathbf{r}) \\ &= k_g^2 \mathbf{E}_{g[\perp \mathbf{k}_g]} \exp(i\mathbf{k}_g \cdot \mathbf{r}) \end{aligned} \quad \text{Formula 6.2.28}$$

Here,  $\mathbf{E}_{g[\perp \mathbf{k}_g]}$  is the component of  $\mathbf{E}_g$  perpendicular to  $\mathbf{k}_g$ . The following formula gives the product of  $\chi$  and  $\mathbf{E}$ :

$$\begin{aligned} \chi(\mathbf{r})\mathbf{E}(\mathbf{r}) &= \sum_{h'} \sum_h \chi_{h'} \exp(i\mathbf{h}' \cdot \mathbf{r}) \mathbf{E}_h \exp(i\mathbf{k}_h \cdot \mathbf{r}) \\ &= \sum_g \sum_h \chi_{g-h} \mathbf{E}_h \exp(i\mathbf{k}_g \cdot \mathbf{r}) \end{aligned} \quad \text{Formula 6.2.29}$$

$$\mathbf{h}' + \mathbf{k}_h = \mathbf{k}_g, \quad \mathbf{h}' + \mathbf{h} = \mathbf{g} \quad \text{Formula 6.2.30}$$

Substituting Formulas 6.2.28 and 6.2.29 into Formula 6.2.26 and denoting the wave vector in vacuum as  $\mathbf{K}$  produces the following formula:

$$\sum_g \left\{ k_g^2 \mathbf{E}_{g[\perp \mathbf{k}_g]} - K^2 \mathbf{E}_g - K^2 \sum_h \chi_{g-h} \mathbf{E}_h \right\} \exp(i\mathbf{k}_g \cdot \mathbf{r}) = 0 \quad \text{Formula 6.2.31}$$

For this formula to hold everywhere in the crystal, this formula must hold for an arbitrary value of  $\mathbf{r}$ . To meet this condition, the coefficients of the terms with the factor  $\exp(i\mathbf{k}_g \cdot \mathbf{r})$  must be zero, and ["in which case"] we obtain the following formula:

$$\frac{k_g^2 \mathbf{E}_{g[\perp \mathbf{k}_g]} - K^2 \mathbf{E}_g}{K^2} = \sum_h \chi_{g-h} \mathbf{E}_h \quad \text{Formula 6.2.32}$$

This formula is the fundamental equation of the dynamical theory of diffraction. The electric field  $\mathbf{E}$  of the X-ray wave allowed to exist in and out of the crystal when the X-ray wave with wave vector  $\mathbf{K}$  is incident on a crystal with electric susceptibility  $\chi$  is a solution of this formula. When  $n$  waves exist within the crystal, this formula is a set of  $n$  simultaneous equations.

As  $\chi_g$  takes an extremely small value, we can assume  $\mathbf{E}_{g[\perp \mathbf{k}_g]} = \mathbf{E}_g$ , then rewrite the fundamental equation of Formula 6.2.32 as follows:

$$\frac{k_g^2 - K^2}{K^2} \mathbf{E}_g = \sum_h \chi_{g-h} \mathbf{E}_h \quad \text{Formula 6.2.33}$$

### 6.2.3 Boundary Conditions

In the previous section, we derived the fundamental equation that must be satisfied by an X-ray wave in a crystal. This section discusses the boundary conditions that must be satisfied when the incident X-ray wave enters the crystal from a vacuum (or air) and when the diffracted X-ray wave and transmitted X-ray wave exit the crystal.

Take the  $z$  axis perpendicular to a flat surface of the crystal and assume that the surface is at  $z = Z_s$ . Fields  $(\mathbf{E}, \mathbf{D})$  in the crystal and fields,  $(\mathbf{E}^a, \mathbf{D}^a)$  out of the crystal satisfy the boundary conditions only if the electric field components parallel to the interface in and out of the crystal are the same at  $z = Z_s$  and the electric flux density components perpendicular to the interface in and out of the crystal are the same at  $z = Z_s$ . That is, the following relationships must hold:

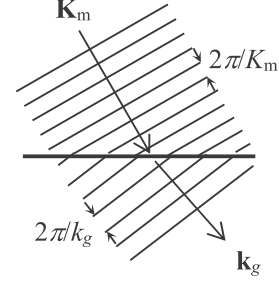
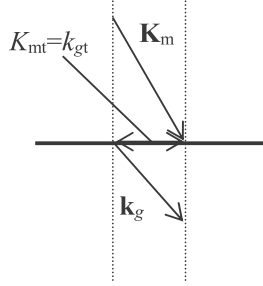
$$E_t = E_t^a, \quad D_z = D_z^a \quad \text{Formula 6.2.34}$$

Here, indices  $t$  and  $z$ , respectively, indicate the parallel and perpendicular components of the fields with respect to the interface. The magnetic field  $\mathbf{H}$  components parallel to the interface in and out of the crystal must be the same at  $z = Z_s$ , and the magnetic flux density  $\mathbf{B}$  components perpendicular to the interface in and out of the crystal must be the same at  $z = Z_s$ , which are also boundary conditions. However, for electromagnetic waves in the X-ray range, the continuity of the electric field and the continuity of the magnetic field are considered equivalent. When two of four are satisfied, the boundary conditions are regarded as met.

As discussed in the previous section, a wave field can be expressed as a superposition of plane waves (Formula 6.2.22). Each plane wave component is a product of the amplitude ( $E_g$ ) and the phase factor ( $\exp(i\mathbf{k}_g \cdot \mathbf{r})$ ). For a wave field thus expressed to be continuous at any position on the interface, the components of the wave vectors ( $\mathbf{k}_g$  and  $\mathbf{K}_m$ ) in the plane of the interface must be the same in and out of the crystal. If this condition is not satisfied, even if Formula 6.2.34 holds at a position on the interface (at position  $\mathbf{r}$ ), it will not hold at other positions. This condition is equivalent to Snell's Law. Thus, the relationship below is a precondition:

$$k_{gt} = K_{mt}$$

Formula 6.2.35



(a) Agreement of the components of the wave vectors in the plane of the interface (b) Agreement of the wave front on the interface

Fig. 6.2.1 Continuity of the wave phases on interface

Assume the wave fields in and out of the crystal are expressed by the following formulas and calculate the wave fields that specifically satisfy the boundary conditions.

$$\begin{aligned} \mathbf{E} &= \sum_g \mathbf{E}_g \exp(i\mathbf{k}_g \cdot \mathbf{r}), \quad \mathbf{D} = \sum_g \mathbf{D}_g \exp(i\mathbf{k}_g \cdot \mathbf{r}) \quad (\text{in crystal}) \\ \mathbf{E}^a &= \sum_m \mathbf{E}_m^a \exp(i\mathbf{K}_m \cdot \mathbf{r}), \quad \mathbf{D}^a = \sum_m \mathbf{D}_m^a \exp(i\mathbf{K}_m \cdot \mathbf{r}) \quad (\text{out of crystal}) \end{aligned}$$

Formula 6.2.36

When  $\mathbf{z}$  and  $\mathbf{t}$  denote the unit vectors in the directions perpendicular and parallel to the interface, respectively, the wave vectors in the crystal can be expressed as follows:

$$\begin{aligned} \mathbf{k}_g &= k_{gz} \mathbf{z} + k_{gt} \mathbf{t} \\ \mathbf{K}_m &= K_{mz} \mathbf{z} + K_{mt} \mathbf{t} \end{aligned}$$

Formula 6.2.37



From Formulas 6.2.36 and 6.2.37, the boundary conditions of Formula 6.2.34 can be expressed at  $z = Z_s$  as follows:

$$\sum_{k_{gt}=K_{mt}} E_{gt} \exp(ik_{gz} Z_s) = \sum_{k_{gt}=K_{mt}} E_{mt}^a \exp(iK_{mz} Z_s) \quad \text{Formula 6.2.38}$$

$$\sum_{k_{gt}=K_{mt}} D_{gt} \exp(ik_{gz} Z_s) = \sum_{k_{gt}=K_{mt}} D_{mt}^a \exp(iK_{mz} Z_s) \quad \text{Formula 6.2.39}$$

The summation  $\sum_{k_{gt}=K_{mt}}$  indicates that the sum is taken over components satisfying the

boundary condition for phase factor as indicated in Formula 6.2.35. Since  $\chi_g$  takes extremely small values,  $D_{gz}$  in Formula 6.2.39 can be replaced by  $E_{gz}$ . Consequently, the following single formula summarizes Formulas 6.2.38 and 6.2.39 to a good approximation:

$$\sum_{k_{gt}=K_{mt}} E_g \exp(ik_{gz} Z_s) = \sum_{k_{gt}=K_{mt}} E_m^a \exp(iK_{mz} Z_s) \quad \text{Formula 6.2.40}$$

This is the boundary condition that must be satisfied by the wave fields in and out of the crystal.

#### 6.2.4 Two-Wave Approximation and Dispersion Surface

So far, we have considered all wave fields allowed to exist in and out of the crystal. However, under typical experimental conditions, only a single type of lattice plane is considered to diffract the X-ray beam. A situation in which only two waves, a wave (O wave) propagating in the incident direction and a wave (G wave) propagating in the diffraction direction, can be approximated. The amplitudes of other waves may be regarded to be zero. This approximation is called the **two-wave approximation**.

Denote the wave vector of the wave propagating in the incident direction as  $\mathbf{k}_o$  and the wave vector of the wave propagating in the diffraction direction as  $\mathbf{k}_g$ . Here, the indices  $o$  and  $g$  correspond to the origin of the reciprocal lattice O and the reciprocal lattice point G, respectively. Under the conditions of the two-wave approximation, the electric field of Formula 6.2.22 can be expressed as follows, omitting the time-dependent component:

$$\mathbf{E} = \mathbf{E}_o \exp(i\mathbf{k}_o \cdot \mathbf{r}) + \mathbf{E}_g \exp(i\mathbf{k}_g \cdot \mathbf{r}) \quad \text{Formula 6.2.41}$$

If we substitute Formula 6.2.41 into the fundamental equation 6.2.34, the corresponding coefficients of the position-dependent factors  $\exp(i\mathbf{k}_o \cdot \mathbf{r})$  and  $\exp(i\mathbf{k}_g \cdot \mathbf{r})$  must be the same on both sides of the formula. Thus, the fundamental equation can be expressed in terms of polarization factor  $P$  as in the following formulas:

$$\begin{aligned} (k_o^2 - k^2)E_o - K^2 P \chi_g E_g &= 0 \\ K^2 P \chi_g E_o - (k_g^2 - k^2)E_g &= 0 \end{aligned} \quad \text{Formula 6.2.42}$$

$E_o$  and  $E_g$  are the components of  $\mathbf{E}_o$  and  $\mathbf{E}_g$  perpendicular or parallel to the plane including  $\mathbf{k}_o$  and  $\mathbf{k}_g$  (scattering plane), respectively. The perpendicular components correspond to the  $\sigma$  polarization, while the polarization factor in this case is  $P = 1$ . The parallel components correspond to the  $\pi$  polarization. The polarization factor in this case is  $P = \cos 2\theta_B$ , where  $2\theta_B$  is the diffraction angle.

For the simultaneous equations of Formula 6.2.42 to hold, the so-called secular equation below must be satisfied:

$$\begin{vmatrix} k_o^2 - k^2 & K^2 P \chi_g^- \\ K^2 P \chi_g & k_g^2 - k^2 \end{vmatrix} = 0 \quad \text{Formula 6.2.43}$$

Here,  $\mathbf{k}_o$  and  $\mathbf{k}_g$  are vectors whose tips are at the origin of the reciprocal lattice and at the reciprocal lattice point G corresponding to the diffraction, respectively. The trajectories of the starting points of these vectors satisfy Formula 6.2.43. The trajectories of the starting points of these vectors form two spheres if no diffraction occurs; thus,  $\chi_g = \chi_g^- = 0$  is satisfied. These spheres are called **dispersion spheres**. If diffraction occurs,  $\chi_g \neq 0, \chi_g^- \neq 0$  is satisfied, and the trajectories of the starting points of the wave vectors form two curved surfaces that approach the dispersion spheres asymptotically. These surfaces are called **dispersion surfaces**.

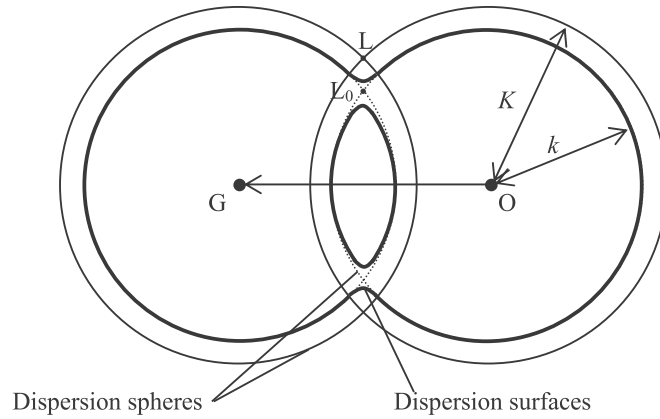


Fig. 6.2.2 Relationship between dispersion surfaces of two-wave approximation and reciprocal lattice points

The condition under which the starting points of the vectors  $\mathbf{k}_o$  and  $\mathbf{k}_g$  are on  $L_0$  in Fig. 6.2.2 corresponds to the condition under which the diffraction condition is satisfied under the kinematical theory of diffraction. Here, the starting point of the wave vector,  $\mathbf{K}$ , observed out of the crystal is on L in Fig. 6.2.2. This point L is called the **Laue point**. In the dynamical theory of diffraction, the starting points of the vectors  $\mathbf{k}_o$  and  $\mathbf{k}_g$  are on the dispersion surfaces, so that  $\mathbf{k}_o$  and  $\mathbf{k}_g$  satisfying the diffraction condition have two types of starting points corresponding to

the two dispersion surfaces above and below  $L_0$ . The dispersion surface closer to the Laue point  $L$  is called the  **$\alpha$  branch**, while the surface further from the Laue point is called the  **$\beta$  branch**.

The waves in the crystal expressed by the wave vectors whose starting points are on the  $\alpha$  and  $\beta$  branches are called the **Bloch wave  $\alpha$**  and **Bloch wave  $\beta$** , respectively. The wave vector of the Bloch wave allowed to exist within the crystal has its starting point at the point specified by the boundary condition on the dispersion surface, a point called the **dispersion point**. As discussed later, the two waves, Bloch wave  $\alpha$  and Bloch wave  $\beta$ , interfere with each other in the crystal and cause phenomena characteristic to the dynamical theory of diffraction.

As discussed up to this point, in the two-wave approximation that holds under typical experimental conditions, the wave vectors of the waves propagating in the incident and diffraction directions, respectively, have their starting points on the dispersion surfaces specified by the fundamental equation and their end points on the origin of the reciprocal lattice and on the reciprocal lattice point at which diffraction is excited. Rotating the crystal with respect to the incident X-ray beam moves the starting points of these wave vectors on the dispersion surfaces. Here, the electric field,  $\mathbf{E}$ , in and out of the crystal at each point can be calculated from the boundary conditions and the fundamental equation, and the diffraction intensity can be calculated as the square of this electric field.

The measured diffraction intensity and the amount of the shift from the diffraction condition need to be calculated separately for each arrangement of the crystal with respect to the incident and diffracted waves. These arrangements include the Laue case, in which the diffracted wave exits the crystal from a surface other than the incident surface, and the Bragg case, in which the diffracted wave exits the crystal from the same surface as the incident surface. Here, we consider the Bragg case, which is used for the thin film measurement.

Also regarding the polarization condition, we consider the  $\sigma$  polarization for the sake of simplicity.

### 6.2.5 Shift from Diffraction Condition

As discussed in the previous section, the diffraction intensity can be calculated as a function of the incident X-ray angle with respect to the lattice plane by using the boundary conditions and the fundamental equation in the two-wave approximation. This angle dependence of the diffraction intensity is called the **rocking curve**. In preparations for calculating the rocking curve, this section discusses the relationship between the amount of the shift of the incident angle from the diffraction condition and the electric fields of the incident and diffracted waves for the Bragg case.

When  $\mathbf{z}$  denotes the vector perpendicular to the sample surface pointing to the depth direction, the point at which the dispersion surface and the  $\mathbf{z}$  intersect is the dispersion point. Fig. 6.2.3 illustrates this for the symmetric reflection in the Bragg case. Fig. 6.2.3 exaggerates the proximity of the Laue point.

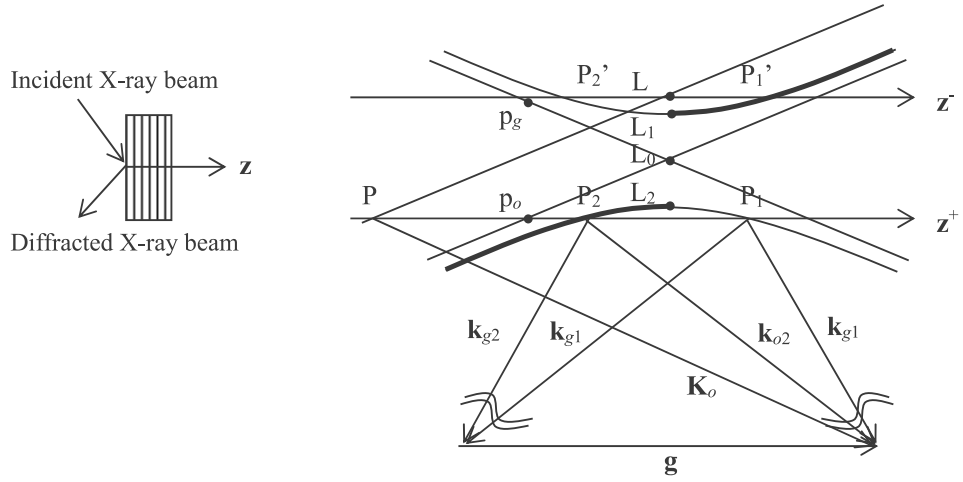


Fig. 6.2.3 Dispersion point for symmetric Bragg case

When the incident angle is scanned from the lower angle to the higher angle,  $z$  moves from  $z^-$  through  $L_0$  to  $z^+$ . When  $z$  is above  $L_0$  (lower angle side of the diffraction peak) or when  $z$  is below  $L_0$  (higher angle side of the diffraction peak),  $z$  has two intersecting points on the same branch. When  $z$  is between the  $\alpha$  and  $\beta$  branches,  $z$  does not intersect with the dispersion surfaces. In this region, the diffraction condition is always satisfied and a total reflection occurs. A dispersion point corresponding to a position of  $z$  moves on the dispersion surface in the sequence  $P_1' \rightarrow L_1 \rightarrow L_0 \rightarrow L_2 \rightarrow P_2$ .

Consider the relationship between diffraction intensity and the amount of the shift of the incident angle  $\theta$  with respect to the sample from the Bragg angle,  $\theta_B$ . We can express this shift in terms of  $W$ , the distance between the points  $p_o$  and  $p_g$ , as defined in Fig. 6.2.3, normalized by the distance between the points  $L_1$  and  $L_2$ . We define  $W$  so that  $W$  increases when  $\theta$  increases. Then, the following formula holds:

$$W = \frac{\overline{p_o p_g}}{\overline{L_1 L_2}} = \frac{2\Lambda \sin \theta_B}{\lambda} (\theta - \theta_B - \Delta\theta_o) \quad \text{Formula 6.2.44}$$

Here,

$$\Lambda = \frac{2\pi \cos \theta_B}{K|P|\chi_g} = \frac{\lambda \cos \theta_B}{|P|\chi_g} \quad \text{Formula 6.2.45}$$

$$\Delta\theta_o = \frac{-\chi_o}{\sin 2\theta_B} = \frac{2(1-n)}{\sin 2\theta_B} \quad \text{Formula 6.2.46}$$

where  $\Delta\theta_o$  is the shift in the Bragg angle due to refraction.

Of the two intersecting points of  $\mathbf{z}$  on the same branch of the dispersion surfaces, consider the  $j$ -th dispersion point. We calculate the ratio  $r_j$  of the amplitudes of the electric fields  $\mathbf{E}_{oj}$  and  $\mathbf{E}_{gj}$  of the waves in the incident and diffraction directions using  $W$ , as in the following formula:

$$r_j = \frac{E_{gj}}{E_{oj}} = \frac{|P|}{P} \exp(i\alpha_g) (-W \mp \sqrt{W^2 - 1}) \quad \text{Formula 6.2.47}$$

Here, the higher of the double signs corresponds to  $j = 1$  and the lower to  $j = 2$ , while  $\exp(i\alpha_g)$  expresses the phase component of electric susceptibility  $\chi_g$ .

### 6.2.6 Rocking Curve

In the previous section, we obtained the amplitude ratio between the electric fields  $\mathbf{E}_{oj}$  and  $\mathbf{E}_{gj}$  of the waves in the incident and diffraction directions, respectively. Next, consider the rocking curve observed in the experiment. For the sake of simplicity, we ignore the absorption in the discussion. Then, we include the absorption in the discussion.

Earlier we noted that two Bloch waves exist within the crystal in the range  $W \geq 1$ . These two waves correspond to the component from the crystal surface toward the interior of the crystal and the component from the inside toward the surface. Here, the component from the interior toward the exterior of the crystal must be reflected from the rear surface of the crystal. If the crystal is thin, the Bloch wave reflected from the rear surface exists. If the crystal is infinitely thick, this Bloch wave is absorbed, and only the Bloch wave moving from the surface toward the interior remains. Here, we call a crystal of sufficient thickness compared to the extinction distance discussed later as an “infinitely thick crystal” and one that having thickness approximately equal to the extinction distance as a “thin crystal”.

#### 1. Infinitely thick crystal

First, consider an infinitely thick crystal in which a reflection from the rear surface does not exist and only a single Bloch wave is present in the crystal. In this case, given the boundary conditions, the following formulas hold at the surface at  $z = 0$ .

$$E_o^a = \begin{cases} E_{o1} : W \leq -1 \\ E_{o2} : W \geq 1 \end{cases} \quad E_g^a = \begin{cases} E_{g1} : W \leq -1 \\ E_{g2} : W \geq 1 \end{cases} \quad \text{Formula 6.2.48}$$

Here, the amplitude of the diffracted wave can be expressed by the following formula using Formula 6.2.47.

$$E_g^a = \begin{cases} \frac{|P|}{P} \exp(i\alpha_g) (-W \mp \sqrt{W^2 - 1}) E_o^a & : |W| \geq 1 \\ \frac{|P|}{P} \exp(i\alpha_g) (-W + i\sqrt{1 - W^2}) E_o^a & : |W| < 1 \end{cases} \quad \text{Formula 6.2.49}$$

Here, the higher of the double signs in Formula 6.2.49 corresponds to  $j = 1$ , while the lower corresponds to  $j = 2$ .  $E_{oj}$  is given by  $E_o^a$  regardless of the value of  $W$ . The rocking curve as a ratio of the incident intensity  $I_o$  and diffraction intensity  $I_g^W$  is given by the following formula:

$$\frac{I_g^W}{I_o} = \left| \frac{E_g^a}{E_o^a} \right|^2 = \begin{cases} \left( |W| - \sqrt{W^2 - 1} \right)^2 & : |W| \geq 1 \\ 1 & : |W| < 1 \end{cases} \quad \text{Formula 6.2.50}$$

Formula 6.2.50 gives a profile shaped like a top hat (Fig. 6.2.4). This profile is called the Darwin curve. In the range  $|W| < 1$ , all incident X-rays are diffracted, a phenomenon called total reflection. Called the total reflection width, the width of the range across which total reflection occurs is 2 in the scale of  $W$  and  $2|P| \|\chi_g\| / \sin 2\theta_B$  converted to an angle.

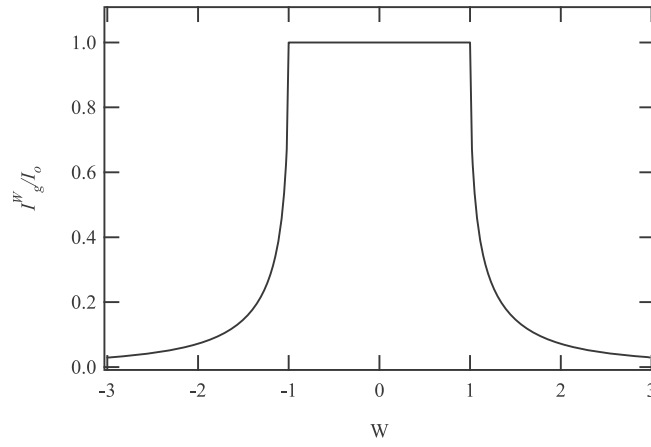


Fig. 6.2.4 Rocking curve for Bragg case

(Infinitely thick crystal, disregarding absorption)

## 2. Thin crystal

Now consider the case in which the reflection from the rear surface exists in the range  $|W| \geq 1$ . Here, based on the boundary condition, the following formulas hold at the surface at  $z = 0$ .

$$\begin{aligned} E_o^a &= E_{o1} + E_{o2} \\ E_g^a &= E_{g1} + E_{g2} \end{aligned} \quad \text{Formula 6.2.51}$$

On the rear surface at  $z = T$ , the following formulas hold:

$$E_{o1} \exp(ik_{o1z}T) + E_{o2} \exp(ik_{o2z}T) = E_d^a \exp(ik_{oz}T) \quad \text{Formula 6.2.52}$$

$$E_{g1} \exp(ik_{g1z}T) + E_{g2} \exp(ik_{g2z}T) = 0 \quad \text{Formula 6.2.53}$$

The right hand side of Formula 6.2.52 corresponds to the transmitted wave moving from the rear side.

Here, from Formula 6.2.47, the amplitudes of the waves are expressed as follows:

$$\begin{aligned} E_{o1} &= \frac{r_2 \exp(ik_{g2z}T)}{r_2 \exp(ik_{g2z}T) - r_1 \exp(ik_{g1z}T)} E_o^a, & E_{g1} &= r_1 E_{o1} \\ E_{o2} &= \frac{r_1 \exp(ik_{g1z}T)}{r_1 \exp(ik_{g1z}T) - r_2 \exp(ik_{g2z}T)} E_o^a, & E_{g2} &= r_2 E_{o2} \end{aligned} \quad \text{Formula 6.2.54}$$

As with the thick crystal above,  $E_{oj}$  is given by  $E_o^a$  regardless of the value of  $W$ , and the rocking curve as a ratio of incident intensity  $I_o$  and diffraction intensity  $I_g^W$  is given by the following formula:

$$\frac{I_g^W}{I_o} = \left| \frac{E_g^a}{E_o^a} \right|^2 = \begin{cases} \frac{\sin^2(\pi T \sqrt{W^2 - 1} / \Lambda)}{W^2 - 1 + \sin^2(\pi T \sqrt{W^2 - 1} / \Lambda)} & : |W| \geq 1 \\ \frac{\sinh^2(\pi T \sqrt{1 - W^2} / \Lambda)}{1 - W^2 + \sinh^2(\pi T \sqrt{1 - W^2} / \Lambda)} & : |W| < 1 \end{cases} \quad \text{Formula 6.2.55}$$

Formula 6.2.55 gives the profile shown in Fig. 6.2.5. This oscillates according to the rotational angle and thickness of the crystal. The oscillations in the range  $|W| \geq 1$  are generated by two mutually interfering waves on the same branch and are called **Pendellosung fringes**. In this case, the total reflection in the range  $|W| < 1$  is not observed.

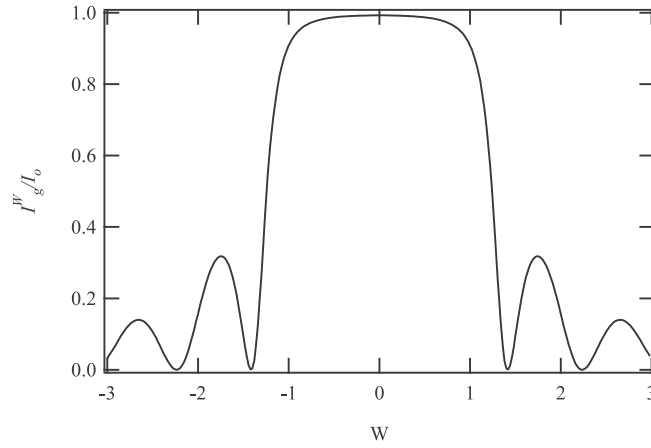


Fig. 6.2.5 Rocking curve for Bragg case

(Thin crystal,  $T/\Lambda = 1$ , disregarding absorption)

So far, the discussion has disregarded the effects of absorption. At the end of this section, we will now discuss the rocking curve while taking absorption into account.

With respect to absorption, the atomic scattering factor also includes a real component  $f'$  and an imaginary component  $f''$  of the anomalous scattering factors. Accordingly, electric susceptibility  $\chi_g$ , also includes  $\chi_g'$  and  $\chi_g''$ . Here, we expand Formula 6.2.14 as follows:

$$\chi_g = \chi_g' + i\chi_g'' \quad \text{Formula 6.2.56}$$

$$\chi_g' = -\frac{r_e \lambda^2}{\pi v_c} F_g' = -\frac{r_e \lambda^2}{\pi v_c} \sum_j (f_j' + f_j'') \exp(-i\mathbf{g} \cdot \mathbf{r}_j) \quad \text{Formula 6.2.57}$$

$$\chi_g'' = -\frac{r_e \lambda^2}{\pi v_c} F_g'' = -\frac{r_e \lambda^2}{\pi v_c} \sum_j f_j'' \exp(-i\mathbf{g} \cdot \mathbf{r}_j) \quad \text{Formula 6.2.58}$$

$\chi_g'$  and  $\chi_g''$  are generally complex numbers and have the following relationships:

$$\chi_g'^- = \chi_g'^*, \quad \chi_g''^- = \chi_g''^* \quad \text{Formula 6.2.59}$$

In particular, when the crystal has a symmetry center and the origin is placed at the symmetry center,  $\chi_g'$  and  $\chi_g''$  are real numbers and the relationships  $\chi_g'^- = \chi_g'$  and  $\chi_g''^- = \chi_g''$  hold.

Here, the following relationship holds:

$$\chi_g^- = \chi_g \quad \text{Formula 6.2.60}$$



Since the relationship,  $\chi_g'' \ll \chi_g'$ , generally holds, the following formula also holds:

$$\chi_g \chi_g^- = \chi_g'^2 + 2i\chi_g' \chi_g'' \quad \text{Formula 6.2.61}$$

We use this condition here.

If we use the relationship above, the rocking curve of an infinitely thick crystal having a symmetry center is given by the following formulas:

$$\frac{I_g}{I_o} = L - \sqrt{L^2 - 1} \quad \text{Formula 6.2.62}$$

$$L = \frac{W^2 + g^2 + \sqrt{(W^2 - g^2 - 1 + \kappa^2)^2 + 4(gW - \kappa)^2}}{1 + \kappa^2} \quad \text{Formula 6.2.63}$$

$$g = \frac{\chi_o''}{|P| |\chi_g'|} \quad \text{Formula 6.2.64}$$

$$\kappa = \frac{\chi_g''}{\chi_g'} \quad \text{Formula 6.2.65}$$

Normally,  $g \leq 0$ ,  $\kappa > 0$ , and  $|g| \geq |\kappa|$  hold. Formula 6.2.63 gives the rocking curve as indicated in Fig. 6.2.6. Here, the figure shows the cases of  $\kappa = 0$  and  $\kappa = 0.1$  ( $g = 0.5$ , and  $g = 1.0$ ).

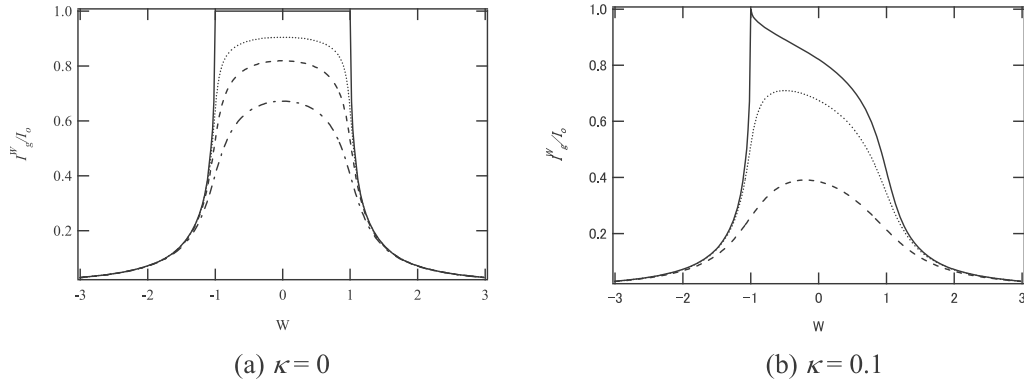


Fig. 6.2.6 Rocking curves for Bragg case

(Infinitely thick crystal with absorption considered)

As implied by Fig. 6.2.6, the rocking curve for  $\kappa \neq 0$  is asymmetric. This is because the ranges  $-1 > W > 0$  and  $0 < W < 1$  correspond to Bloch wave  $\alpha$  and Bloch wave  $\beta$ , respectively, and the former is less affected by absorption than the latter.

### 6.2.7 X-ray Standing Wave

Bloch wave  $\alpha$  and Bloch wave  $\beta$  in the crystal are each a superposition of the wave (O wave) propagating in the incident direction and the wave (G wave) propagating in the diffraction direction. Four waves exist within the crystal. Here, for the Bragg case, when the crystal is infinitely thick, of the two pairs of Bloch waves, only one each exists for Bloch wave  $\alpha$  or Bloch wave  $\beta$ . If the crystal is thin, all four waves exist, including both Bloch wave  $\alpha$  and Bloch wave  $\beta$ . Here, the O waves and G waves interfere separately, generating Pendellosung fringes. We will discuss in detail the behavior of these Bloch waves in the crystal.

A Bloch wave in the crystal can be given by the following formula:

$$\begin{aligned} \mathbf{E}_j &= \mathbf{E}_{oj} \exp(i\mathbf{k}_{oj} \cdot \mathbf{r}) + \mathbf{E}_{gj} \exp(i\mathbf{k}_{gj} \cdot \mathbf{r}) \\ &= \exp(i\mathbf{k}_{oj} \cdot \mathbf{r}) \{ \mathbf{E}_{oj} + \mathbf{E}_{gj} \exp(i\mathbf{g} \cdot \mathbf{r}) \} \quad (j = 1, 2) \end{aligned} \quad \text{Formula 6.2.66}$$

Here, to determine the behavior of the Bloch waves in the crystal, we calculate the intensity of each Bloch wave at depth  $z$  from the surface. If we assume that components  $k_{ojz}^j$  and  $k_{giz}^j$  of the imaginary components of  $\mathbf{k}_{oj}$  and  $\mathbf{k}_{gj}$  perpendicular to the crystal surface pointing to the crystal interior (the  $z$  components) are equal to each other and if we ignore absorption, the following formula gives the intensity of the Bloch wave at depth  $z$ :

$$E_j^2 = E_{oj}^2 \left\{ 1 + \left( \frac{E_{gj}}{E_{oj}} \right)^2 + 2P \frac{E_{gj}}{E_{oj}} \cos(\mathbf{g} \cdot \mathbf{r}) \right\} \quad \text{Formula 6.2.67}$$

This formula expresses a standing wave. The nodes or antinodes are on planes in which  $\mathbf{g} \cdot \mathbf{r}$  is constant. This means that the wave front of the standing wave is parallel to the lattice planes and has a period equal to the interplanar spacing.

For the Bragg case, Bloch wave  $\alpha$  is generated on the lower angle side ( $W \leq -1$ ) of the total reflection range. Here, since  $E_{g1}/E_{o1} < 0$ , the nodes of the standing wave are on the lattice planes. On the higher angle side ( $W \geq 1$ ), Bloch wave  $\beta$  is generated. Since  $E_{g2}/E_{o2} > 0$ , the antinodes of the standing wave are on the lattice planes. Fig. 6.2.7 illustrates this behavior.

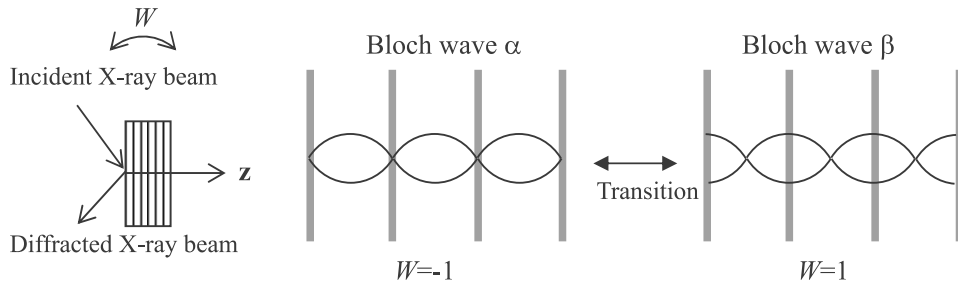


Fig. 6.2.7 Standing wave for Bragg case (for  $\sigma$  polarization)

X-ray absorption by the atoms constituting the lattice planes is greater when the antinodes of the standing wave are on the lattice planes than when the nodes are on the lattice planes. Bloch wave  $\alpha$  and Bloch wave  $\beta$  are differently affected by absorption. Bloch wave  $\beta$  is absorbed to a greater extent. This is the cause of the asymmetric shape of the rocking curve, as indicated in the example of the calculation in Fig. 6.2.6, in which diffraction intensity is weaker on the higher angle side than the lower angle side.

### 6.2.8 Extinction Distance

When X-rays enter a crystal and are diffracted, the intensity of the X-ray beam propagating in the incident direction decays as the X-ray beam propagates farther into the crystal. Here, the **extinction distance** is the quantity used as a guide to the degree of X-ray penetration depth into the crystal. The extinction distance  $l_B$  for the Bragg case is defined as the depth at which X-ray intensity declines to  $1/e$  for  $W = 0$ , as expressed below:

$$l_B = \frac{\Lambda \tan \theta_B}{2\pi} = \frac{\lambda \sin \theta_B}{2\pi |P| |\chi_g|} = \frac{v_c \sin \theta_B}{2 |P| |r_e \lambda| |F_g|} = \frac{v_c}{4 |P| |dr_e| |F_g|} \quad \text{Formula 6.2.68}$$

The value is generally several micrometers to several dozen micrometers.

### §6.3 Dynamical Theory of Diffraction in Multilayer Film Crystals

In general, for a multilayer film sample of a heteroepitaxial crystal, the lattice constants differ in the substrate and in the film. In such cases, X-rays behave as if the lattice is strained at the interface between the substrate and the film and between the layers in the film. To understand dynamical diffraction phenomena in multilayer films and interpret measurement results, we must apply the dynamical theory of diffraction in a strained crystal. Numerous theories have been proposed depending on the type of strain in question. This chapter uses one of the theories, called Darwin's approach, to calculate the rocking curve, and discusses the relationship between this theory and evaluations of epitaxial crystals.

#### 6.3.1 Dynamical Theory of Diffraction for Strained Crystal

Given below are examples of dynamical theories of diffraction for strained crystals.

1. Darwin's method

Darwin's method regards a multilayer film crystal as a combination of perfect crystals with different interplanar spacings, and the diffraction theory for a perfect crystal is repeated. It is applied to local defects and planar defects, including stacking faults, multilayer films, twin crystals, and grazing boundaries.

2. Eikonal theory

The eikonal theory is also called the beam theory. It describes the process whereby the X-rays propagate in the crystal while being bent. It is applied to gradual elastic strain over a wide region.

3. Takagi-Taupin theory

The Takagi-Taupin theory describes the propagation of the wave field in the strained crystal as a differential equation. It can be applied to both elastic strain and local strain.

Here, we describe 1 **Darwin's method**, which can be used to handle multilayer films and allows for relatively quick calculations. Note that all theories use approximation, although Theory 3 is considered more widely applicable, since it requires less rigorous conditions for valid approximations than Theory 1 or 2. Theory 2 cannot be applied to a crystal containing large local strains.

#### 6.3.2 Rocking Curve of Multilayer Film

A multilayer film can be regarded as two or more thin crystals overlaid. For example, consider the sample shown in Fig. 6.3.1, in which the substrate is numbered  $n = 0$  and each layer of the multilayer film over the substrate is numbered from  $n = 1$  to  $n = N$ . When we take an arbitrary layer  $n = m$ , it can be regarded as a thin perfect crystal, to which the dynamical theory of

diffraction for a thin crystal as discussed in 2. of Section 6.2.6 applies. If we obtain the ratio  $E_{gj}^m/E_{oj}^m$  of the amplitude of the electric field of the wave (O wave) propagating in the transmission direction and the amplitude of the wave (G wave) propagating in the diffraction direction, we can use it as a recurrence formula and calculate the amplitude ratio from the substrate,  $n = 0$ , to the topmost layer,  $n = N$ . In this manner, we can obtain the amplitude ratio of the electric fields of the incident X-rays entering the surface and the diffracted X-rays exiting from the surface. By squaring the amplitude ratio, we obtain the intensity ratio of the incident and diffracted X-rays, or the rocking curve.

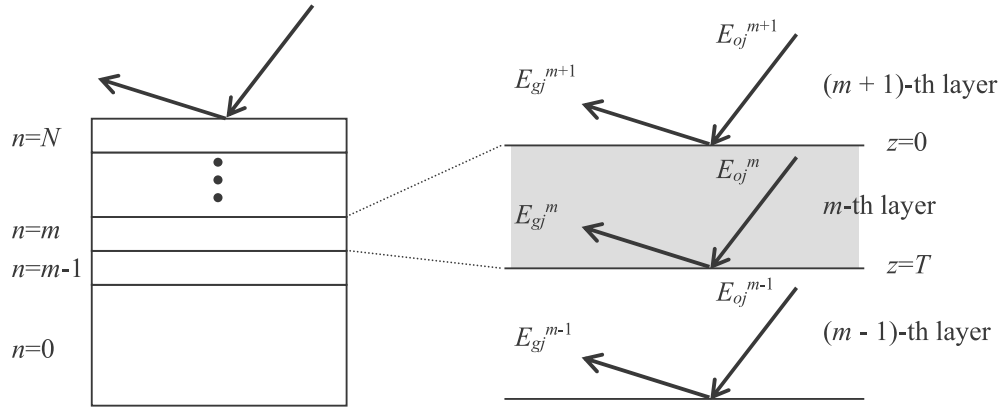


Fig. 6.3.1 X-rays in multilayer film

As indicated to the right of Fig. 6.3.1,  $E_{oj}^{m+1}$  is incident on the  $m$ -th layer in the incident direction from the  $(m+1)$ -th layer nearer to the surface, while  $E_{gj}^m$  exits into the  $(m+1)$ -th layer in a similar manner. Further,  $E_{gj}^{m-1}$  is incident on the  $m$ -th layer in the diffraction direction from the  $(m-1)$ -th layer nearer to the substrate, and  $E_{oj}^m$  exits into the  $(m-1)$ -th layer in a similar manner. Here, the waves  $E_{oj}^m$  and  $E_{gj}^m$  exist in the  $m$ -th layer and satisfy the boundary conditions at the interfaces on the surface and substrate sides. In the case of a multilayer film, boundary conditions must be satisfied at all interfaces between the layers as well as at the crystal surface.

The boundary conditions for a multilayer film are more complex than those for the substrate alone. However, we can simplify the boundary conditions by assuming that the wave vectors of the incident and diffracted X-rays are the same in all layers.

When we take  $z = 0$  for the interface on the surface side of the  $m$ -th layer and  $z = T_m$  for the interface on the substrate side of the  $m$ -th layer, the boundary conditions at each interface are given by the following formula:

$z = 0$ :

$$\begin{aligned} E_o^{m+1} &= E_{o1}^m + E_{o2}^m \\ E_g^{m+1} &= E_{g1}^m + E_{g2}^m \end{aligned} \quad \text{Formula 6.3.1}$$

$z = T_m$ :

$$\begin{aligned} E_{o1}^m \exp(ik_{o1z}T_m) + E_{o2}^m \exp(ik_{o1z}T_m) &= E_o^{m-1} \exp(ik_{oz}T_m) \\ E_{g1}^m \exp(ik_{g1z}T_m) + E_{g2}^m \exp(ik_{g1z}T_m) &= E_o^{m-1} \exp(ik_{gz}T_m) \end{aligned} \quad \text{Formula 6.3.2}$$

Here, using the expressions below,

$$r_j^n = \frac{E_{gj}^n}{E_{oj}^n} \quad \text{Formula 6.3.3}$$

$$\begin{aligned} e &= \exp(i(k_{o2z} - k_{o1z})T_m) \\ e_{o2} &= \exp(ik_{o2z}T_m), \quad e_{g2} = \exp(ik_{g2z}T_m) \end{aligned} \quad \text{Formula 6.3.4}$$

Formula 6.3.2 can be expressed in matrix form. We use a matrix to easily calculate the recurrence formula.

$$\begin{aligned} \begin{pmatrix} E_g^n \\ E_o^n \end{pmatrix} &= \frac{1}{r_1^n - r_2^n} \begin{pmatrix} r_1^n e - r_2^n & r_1^n r_2^n (1 - e) \\ e - 1 & r_1^n - r_2^n e \end{pmatrix} \begin{pmatrix} e_{g2} & 0 \\ 0 & e_{o2} \end{pmatrix} \begin{pmatrix} E_g^{n-1} \\ E_o^{n-1} \end{pmatrix} = \mathbf{M}_n \begin{pmatrix} E_g^{n-1} \\ E_o^{n-1} \end{pmatrix} \\ \mathbf{M}_n &\equiv \frac{1}{r_1^n - r_2^n} \begin{pmatrix} r_1^n e - r_2^n & r_1^n r_2^n (1 - e) \\ e - 1 & r_1^n - r_2^n e \end{pmatrix} \begin{pmatrix} e_{g2} & 0 \\ 0 & e_{o2} \end{pmatrix} \end{aligned}$$

Formula 6.3.5

If we assume no X-rays enter the substrate from the rear surface ( $E_g^{-1} = 0$  and  $E_o^{-1} = 1$ ), we can apply Formula 6.3.5 from the substrate toward the surface layer one by one to obtain the amplitude ratio of the electric fields of the incident and diffracted X-rays and the corresponding intensity ratio: in short, the rocking curve.

$$\begin{pmatrix} E_g^{N+1} \\ E_o^{N+1} \end{pmatrix} = \prod_{n=N}^0 (\mathbf{M}_n) \begin{pmatrix} 0 \\ 1 \end{pmatrix} \quad \text{Formula 6.3.6}$$

$$\frac{I_g}{I_o} = \left| \frac{E_g^{N+1}}{E_o^{N+1}} \right|^2 \quad \text{Formula 6.3.7}$$

The rocking curve expressed by Formula 6.3.7 changes in various ways depending on the layer structure. Fig. 6.3.2 shows the example of the rocking curve calculated for the (004) plane of the sample consisting of a GaAs (001) substrate and 200 nm of  $\text{In}_{0.01}\text{Ga}_{0.99}\text{As}$  film. Here, we assume that the crystal axes of the substrate crystal and the thin film crystal are not tilted with respect to each other and that the lattice of the film is not relaxed.

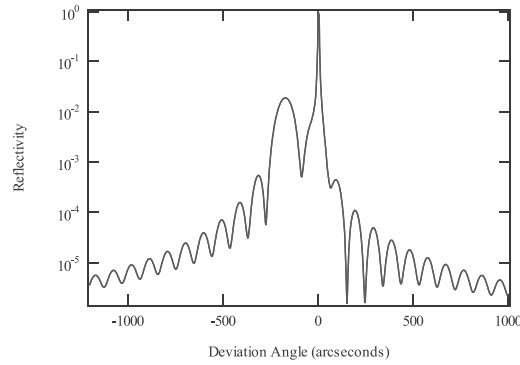


Fig. 6.3.2 Rocking curve of GaAs/GaAs (004)

As implied by Fig. 6.3.2, the diffraction peak of the thin film appears on the lower angle side of the sharp diffraction peak of the substrate and the diffraction intensity oscillates on both sides of the diffraction peak. This oscillation corresponds to the Pendellosung fringes related to the reflected wave moving from the interface between the film and the substrate.

### 6.3.3 Rocking Curve Analysis

In general, the thickness and composition of the multilayer film cannot be determined directly from the measured rocking curve. In actual analysis, we must simulate the rocking curve of a multilayer film model (of hypothetical film thickness and composition) as described in the previous section and change the thickness and the composition to reproduce the measured rocking curve in the analysis. This section presents several examples to help clarify the relationship between the rocking curve and the layer structure.

### 1. Single layer film

Fig. 6.3.3 (a) shows the assumed layer structure, while Fig. 6.3.3 (b) shows the rocking curve for the (004) plane calculated with this model.

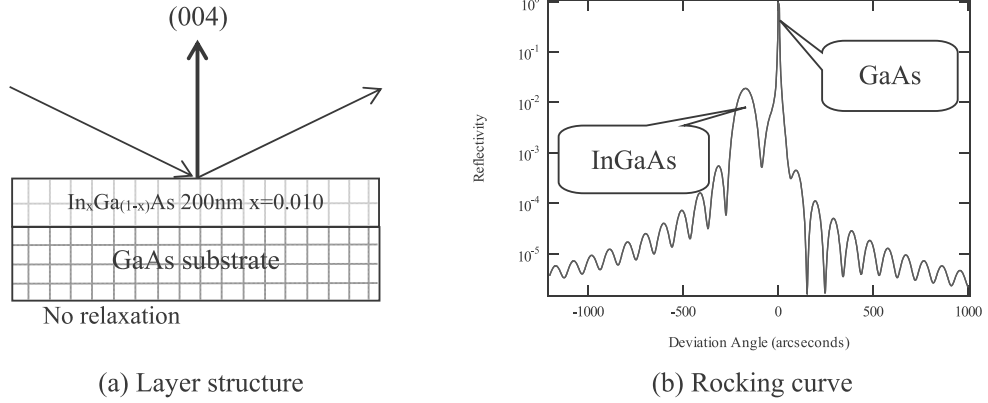
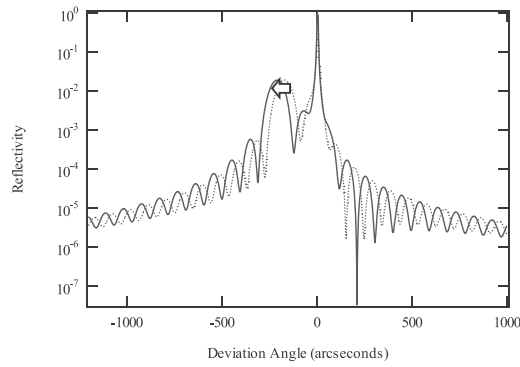


Fig. 6.3.3 Layer structure and rocking curve

As shown in Fig. 6.3.3, the diffraction peak of the film appears at a lower diffraction angle with wider width and lower intensity than the diffraction peak of the substrate. This is because the film has a wider interplanar spacing in the (004) direction and because the crystal has a lesser volume contributing to the diffraction than the substrate. From the shift of the diffraction peaks of the substrate and the film, we can calculate the lattice constants of the film if the lattice constants of the substrate are known. If the presence or absence of lattice relaxation and the elastic constant are known, we can use the lattice constants to determine the composition ratio of the mixed crystal (in this example, the ratio of InAs and GaAs) based on Vegard's law. Additionally, the diffraction intensity oscillates on both sides of the diffraction peak of the film. We can obtain the thickness of the film based on the period of this oscillation.

Fig. 6.3.4 shows the changes in the rocking curve when  $x$  (the ratio of InAs and GaAs) of  $\text{In}_x\text{Ga}_{(1-x)}\text{As}$  ( $x = 0.010$ ) is changed from 1.0% to 1.2% (when we increase the interplanar spacing).



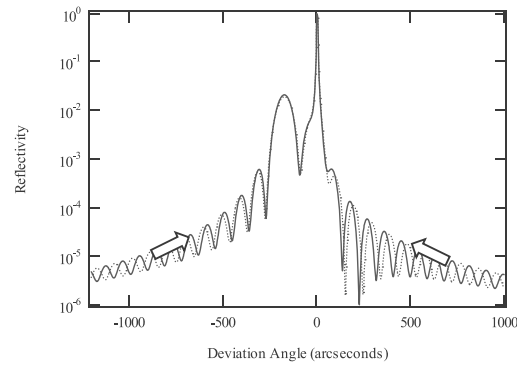


(Dashed curve: 1.0%, solid curve: 1.2%)

Fig. 6.3.4 Rocking curve

As shown by Fig. 6.3.4, when the interplanar spacing increases, the diffraction peak of the InGaAs film shifts to the lower angle side, and the position of the oscillation in the diffraction intensity shifts accordingly. If the position of the diffraction peak of the thin film does not agree for the measurement and simulation, adjust the model using the composition ratio and lattice relaxation rate so that the interplanar spacing of the film changes.

Fig. 6.3.5 shows the changes in the rocking curve when the thickness of the  $\text{In}_x\text{Ga}_{(1-x)}\text{As}$  ( $x = 0.010$ ) film increases from 200 nm to 210 nm.



(Dashed curve: 200 nm, solid curve: 210 nm)

Fig. 6.3.5 Rocking curve

Fig. 6.3.5 shows that when the film thickness increases, the period of the oscillation in the diffraction intensity decreases. If the period of the oscillation in the diffraction intensity of the thin film does not agree for the measurement and simulation, adjust the model by changing the film thickness.

## 2. Multilayer film

Fig. 6.3.6 (a) shows the layer structure assumed, and Fig. 6.3.6 (b) shows the rocking curve for the (004) plane calculated with this model.

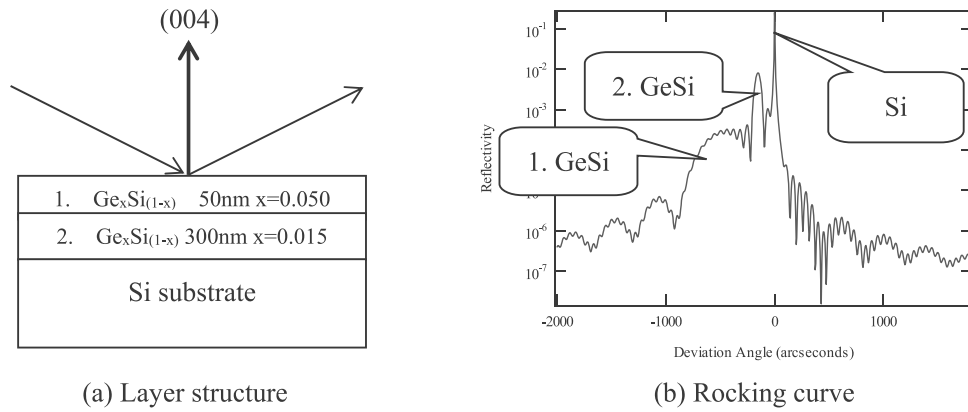


Fig. 6.3.6 Layer structure and rocking curve

As shown in Fig. 6.3.6, the diffraction peaks of Film 1 and Film 2 and the oscillation in the diffraction intensity appear superposed in the rocking curve. The wide diffraction peak appearing farther on the lower angle side of the diffraction peak of the substrate is considered attributable to Film 1 based on its characteristics of a larger Ge composition ratio (high difference in interplanar spacing compared to Si substrate) and lower film thickness. The oscillation in the diffraction intensity accompanying this diffraction peak appears at a larger period because the film is thinner. The diffraction peak relatively narrower and closer to the substrate peak is considered attributable to Film 2 based on its characteristics with a smaller Ge composition ratio (low difference in interplanar spacing compared to Si substrate) and greater film thickness. The oscillation in the diffraction intensity accompanying this diffraction peak appears at a smaller period because the film is thicker.

Since the X-rays in each layer are related by boundary conditions and are not independent, the rocking curve of a multilayer film is not a superposition of the rocking curves of the independent layers in the strictest sense. However, if we have a rough idea of the layer structure, the diffraction peaks and oscillating components of the diffraction intensity can be assigned to each layer as above.

### 3. Superlattice

Fig. 6.3.7 (a) shows the superlattice structure assumed, while Fig. 6.3.7 (b) shows the rocking curve for the (004) plane calculated with this model.

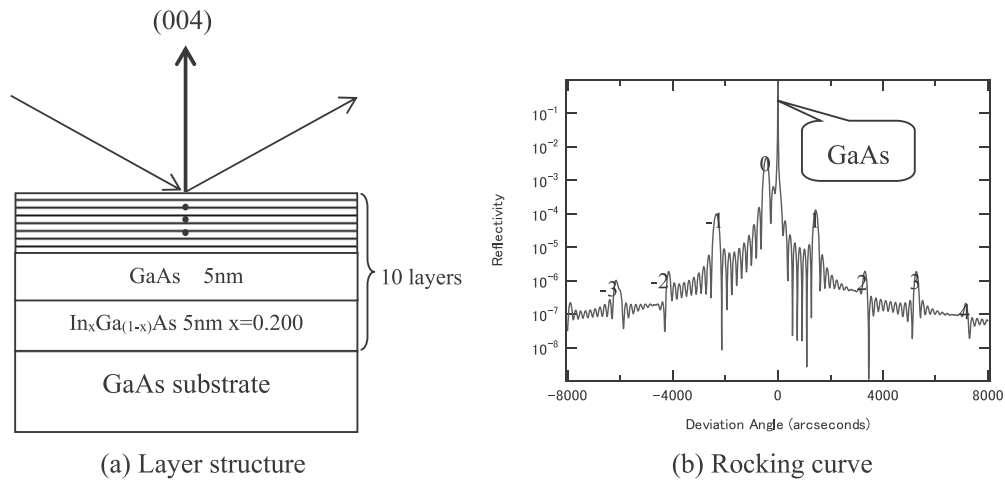


Fig. 6.3.7 Layer structure and rocking curve

As shown in Fig. 6.3.7, the rocking curve of a superlattice has many diffraction peaks called **satellite peaks**. Of these satellite peaks, the peak appearing at the position corresponding to the average lattice constant of the two layers constituting the superlattice, GaAs and  $\text{In}_{0.2}\text{Ga}_{0.8}\text{As}$ , is called the zeroth order satellite peak. From the position of the zeroth order satellite peak, we can obtain the average lattice constant of the superlattice. For this example, we can use the lattice constant to obtain the composition ratio  $x$ . On both sides of the zeroth order satellite peak, the  $n$ -th order satellite peaks appear at the interval corresponding to the thickness of the entire superlattice film. This interval can be used to determine the thickness of the entire superlattice film. Generally speaking, the number of repetitions in a superlattice film is known from film growth conditions. In this case, we can obtain the thickness of a unit of the superlattice structure—the period of the superlattice.

If the positions of the diffraction peaks do not agree for the measurement and simulation, adjust the model by changing the average lattice constant for the position of the zeroth order satellite peak and by changing the superlattice period for the interval of the satellite peaks. Since the ratio of the thickness of the two layers constituting a unit of the superlattice structure influences the relative intensity ratio of the satellite peaks, adjusting the model to reproduce the entire rocking curve measured can provide detailed information on the superlattice.

## §6.4 Summary

This chapter discussed the dynamical theory of diffraction, which is applied to perfect crystals (e.g., Si, Ge, and GaAs). Summarized below are the important formulas described in this chapter.

1. Fundamental equation of dynamical theory of diffraction

$$\frac{k_g^2 - K^2}{K^2} \mathbf{E}_g = \sum_h \chi_{g-h} \mathbf{E}_h$$

2. Boundary conditions

$$E_t = E_t^a, \quad D_z = D_z^a$$

$$\sum_{k_{gt}=K_{mt}} E_g \exp(ik_{gz} Z_s) = \sum_{k_{gt}=K_{mt}} E_m^a \exp(iK_{mz} Z_s)$$

3. Wave field in crystal under two-wave approximation

$$\mathbf{E} = \mathbf{E}_o \exp(i\mathbf{k}_o \cdot \mathbf{r}) + \mathbf{E}_g \exp(i\mathbf{k}_g \cdot \mathbf{r})$$

4. Rocking curve

Bragg case, infinitely thick crystal, absorption disregarded

$$\frac{I_g^W}{I_o} = \left| \frac{E_g^a}{E_o^a} \right|^2 = \begin{cases} \left( |W| - \sqrt{W^2 - 1} \right)^2 & : |W| \geq 1 \\ 1 & : |W| < 1 \end{cases}$$

Bragg case, thin crystal, absorption disregarded

$$\frac{I_g^W}{I_o} = \left| \frac{E_g^a}{E_o^a} \right|^2 = \begin{cases} \frac{\sin^2(\pi T \sqrt{W^2 - 1} / \Lambda)}{W^2 - 1 + \sin^2(\pi T \sqrt{W^2 - 1} / \Lambda)} & : |W| \geq 1 \\ \frac{\sinh^2(\pi T \sqrt{1 - W^2} / \Lambda)}{1 - W^2 + \sinh^2(\pi T \sqrt{1 - W^2} / \Lambda)} & : |W| < 1 \end{cases}$$

Bragg case, infinitely thick crystal, absorption considered

$$\frac{I_g}{I_o} = L - \sqrt{L^2 - 1}$$

$$L = \frac{W^2 + g^2 + \sqrt{(W^2 - g^2 - 1 + \kappa^2)^2 + 4(gW - \kappa)^2}}{1 + \kappa^2}, \quad g = \frac{\chi_o''}{|P||\chi_g'|}, \quad \kappa = \frac{\chi_g''}{\chi_g'}$$

5. Extinction distance

$$l_B = \frac{\Lambda \tan \theta_B}{2\pi} = \frac{\lambda \sin \theta_B}{2\pi |P| |\chi_g|} = \frac{v_c \sin \theta_B}{2|P| r_e \lambda |F_g|} = \frac{v_c}{4|P| |dr_e| |F_g|}$$

6. Rocking curve of multilayer film (Darwin's approach)

$$\frac{I_g}{I_o} = \left| \frac{E_g^{N+1}}{E_o^{N+1}} \right|^2$$

$$\begin{pmatrix} E_g^{N+1} \\ E_o^{N+1} \end{pmatrix} = \prod_{n=N}^0 (\mathbf{M}_n) \begin{pmatrix} 0 \\ 1 \end{pmatrix}$$

$$\begin{pmatrix} E_g^n \\ E_o^n \end{pmatrix} = \frac{1}{r_1^n - r_2^n} \begin{pmatrix} r_1^n e - r_2^n & r_1^n r_2^n (1-e) \\ e-1 & r_1^n - r_2^n e \end{pmatrix} \begin{pmatrix} e_{g2} & 0 \\ 0 & e_{o2} \end{pmatrix} \begin{pmatrix} E_g^{n-1} \\ E_o^{n-1} \end{pmatrix} = \mathbf{M}_n \begin{pmatrix} E_g^{n-1} \\ E_o^{n-1} \end{pmatrix}$$

$$\mathbf{M}_n \equiv \frac{1}{r_1^n - r_2^n} \begin{pmatrix} r_1^n e - r_2^n & r_1^n r_2^n (1-e) \\ e-1 & r_1^n - r_2^n e \end{pmatrix} \begin{pmatrix} e_{g2} & 0 \\ 0 & e_{o2} \end{pmatrix}$$

## Chapter 7 Kinematical Theory of Diffraction

The **kinematical theory of diffraction** describes the intensity or angle distribution of the X-ray diffraction generated by a mosaic crystal. A mosaic crystal refers to a crystal containing numerous lattice defects such as grain boundaries and dislocations and disordered three-dimensional periodicity. Due to these disorders, the incident X-ray beam can be assumed to scatter only once in the crystal. This is the concept of the kinematical theory of diffraction.

The size of a crystal grain determines whether we select the dynamical theory (discussed in Chapter 6) or kinematical theory of diffraction. If the size of the crystal grain is several micrometers or less, the kinematical theory of diffraction is generally regarded to hold. If the crystal grain is greater, the dynamical theory of diffraction is regarded to hold. The dynamical theory of diffraction holds only in a limited number of materials such as semiconductors (including Si and Ge) and compound semiconductors (including GaAs and AlGaP). The kinematical theory of diffraction discussed in this chapter applies to most inorganic and organic crystals.

### §7.1 General Description of X-Ray Scattering by Materials

This section discusses the amplitude of the **Thomson scattering** of X-rays by a material of arbitrary form—i.e., not necessarily a crystal.

We assume that X-rays are scattered only once in the material. We also assume that the incident beam in the material contributes only to diffraction and is not weakened by absorption.

#### 7.1.1 Description of Scattered X-Rays

We define  $\mathbf{k}_0$  and  $\mathbf{k}$  as the wave vectors of the incident and scattered waves when an X-ray beam enters a material and is scattered. (A wave vector is a vector whose length is  $1/\lambda$  (the inverse of the wavelength,  $\lambda$ ) and whose direction is the same as the direction of the X-ray propagation.) The vector,  $\mathbf{k}-\mathbf{k}_0$ , is called the scattering vector and expressed as  $\mathbf{K}$ .

$$\mathbf{K} = \mathbf{k} - \mathbf{k}_0 \quad \text{Formula 7.1.1}$$

The magnitude of  $\mathbf{K}$  is given by the following formula:

$$K = \frac{2}{\lambda} \sin \frac{\Theta}{2} \quad \text{Formula 7.1.2}$$

Here,  $\Theta$  is the angle between  $\mathbf{k}_0$  and  $\mathbf{k}$ , and is called the scattering angle. Fig. 7.1.1 shows the relationship between  $\mathbf{k}_0$ ,  $\mathbf{k}$ ,  $\mathbf{K}$ , and  $\Theta$ .

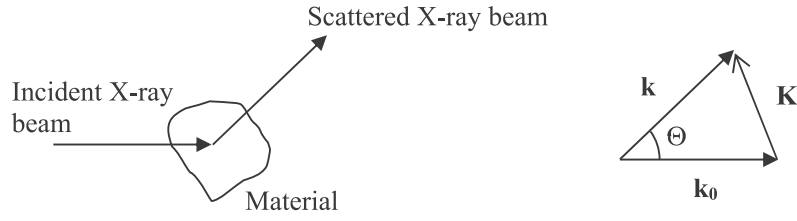


Fig. 7.1.1 Wave vectors of the incident and scattered waves and the scattering vector.

### 7.1.2 X-Ray Scattering from Entire Material

X-rays in a material are scattered by electrons. In general, the distribution of electrons is not uniform, with electron density varying depending on the position within the material. For this reason, the amplitude of the scattered wave moving from the entire body of the material is the sum of the amplitudes of the scattered waves from different positions in the material with the phase shift considered.

Assume an arbitrary position in the material to be the origin of the coordinates and denote the electron density at the point A separated from the origin by  $\mathbf{r}$  as  $\rho(\mathbf{r})$ . The scattered wave moving from point A has phase difference  $\mathbf{K} \cdot \mathbf{r}$  compared to the scattered wave moving from the origin (we calculate phase difference by multiplying  $2\pi/\lambda$  and the optical path difference). When  $\rho(\mathbf{r}) d\mathbf{r}$  denotes the probability of existence of an electron in the infinitesimal volume element  $d\mathbf{r}$  at point A, the amplitude of the wave scattered at point A is proportional to  $\rho(\mathbf{r})e^{-i\mathbf{K} \cdot \mathbf{r}}$ , taking into account the phase shift depending on the position. Thus, the amplitude of the scattered wave from a scattering element is obtained by solving the following formula below which integrates  $\rho(\mathbf{r})e^{-i\mathbf{K} \cdot \mathbf{r}}$  over the entire scattering element by the scattering amplitude, -re, for a single electron:

$$\int_{\text{scattering body}} \rho(\mathbf{r})e^{-i\mathbf{K} \cdot \mathbf{r}} d\mathbf{r} \equiv A(\mathbf{K}) \quad \text{Formula 7.1.3}$$

$A(\mathbf{K})$  is the Fourier transformation of the electron density of the scattering element and is called the **structure factor**. The structure factor is related to the structure of the scattering element and is a fundamental quantity in structure analysis.

The amplitude of the electric field of the X-rays undergoing such a scattering process is expressed as follows at position  $\mathbf{r}$  of the scattering element:

$$\mathbf{E}(\mathbf{r}) = \varepsilon_0 e^{i\mathbf{k}_0 \cdot \mathbf{r}} + \left\{ -r_e \varepsilon_0 \cdot \varepsilon_s A(\mathbf{K}) \right\} \frac{\varepsilon_s e^{i\mathbf{k} \cdot \mathbf{r}}}{\mathbf{r}} \quad \text{Formula 7.1.4}$$

Here,  $\varepsilon_0$  is the permittivity of vacuum and  $\varepsilon_s$  the permittivity of the material. The second term expresses the scattered wave, which propagates as a spherical wave moving from the scattering element. The intensity of the scattered wave is given by the square of this term, as follows:

$$I = I_0 \frac{Pr_e^2}{r^2} |A(\mathbf{K})|^2 \quad \text{Formula 7.1.5}$$

This is proportional to the square of the Fourier transform  $A(\mathbf{K})$  of the electron density of the scattering element.

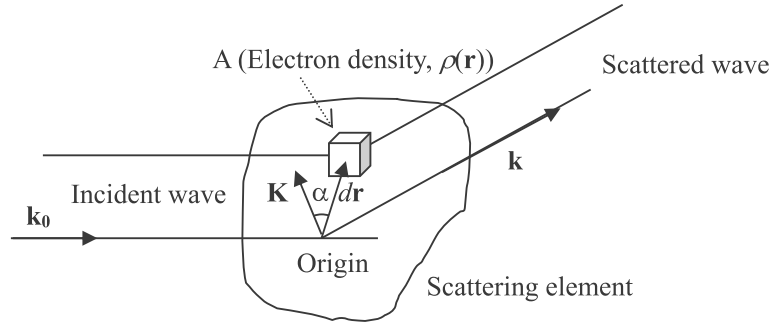


Fig. 7.1.2 X-ray scattering by scattering element

Here,  $I_0$  denotes the intensity of the incident wave. When  $I_e$  denotes the scattering intensity for a single electron, intensity can be rewritten, as follows:

$$I = I_e |A(\mathbf{K})|^2 = I_e \left| \int_{\text{scatterer}} \rho(\mathbf{r}) e^{-i\mathbf{K} \cdot \mathbf{r}} d\mathbf{r} \right|^2 \quad \text{Formula 7.1.6}$$

This formula is a generic formula that applies whether the scattering element is a solid, liquid, or gas. It constitutes the foundation of the kinematical theory of diffraction.

## §7.2 X-Ray Scattering from Crystalline Material

At the beginning of Section 7.1.2, we stated that the electron density in a material is not uniform. The concentration and regularity in the electron density depends on the type of element constituting the material, the crystallinity, and the symmetry of the crystal. Next, we discuss scattering based on the type of element and the crystal system.

### 7.2.1 Atomic Scattering Factor and Crystal Structure Factor

The **atomic scattering factor** expresses the scattering intensity of the X-rays based on the electron density distribution of a single atom. The atomic scattering factor is obtained by applying the formula for the entire scattering element to a single atom as follows:

$$\int_{\text{atom}} \rho(\mathbf{r}) e^{-i\mathbf{K} \cdot \mathbf{r}} d\mathbf{r} \equiv f(\mathbf{K}) \quad \text{Formula 7.2.1}$$



$A(\mathbf{K})$  in Formula 1.2.11 is specifically expressed as  $f(\mathbf{K})$  when referring to a single atom.  $f(\mathbf{K})$  is a non-dimensional quantity and is a real number when the absorption by an atom is not considered. The amplitude of the scattering by an atom is  $r_e f$ . The scattering intensity is given by the following formula:

$$I = I_e f^2 = I_0 \frac{r_e^2 f^2}{r^2} \quad \text{Formula 7.2.2}$$

We determine the expression for  $f$  by assuming a spherical symmetry in the electron density distribution of an atom. Electron density  $\rho(\mathbf{r})$  is a function of only  $r$ , which is the magnitude of  $\mathbf{r}$ . When we take the direction of  $\mathbf{K}$  as the polar axis of the spherical coordinates  $(\rho, \alpha, \beta)$ ,  $f$  is given by the following formula:

$$\begin{aligned} f(K) &= \int_0^\infty \int_0^\pi \int_0^{2\pi} \rho(r) \exp(-iKr \cos \alpha) r^2 \sin \alpha d\beta d\alpha dr \\ &= \int_0^\infty 4\pi r^2 \rho(r) \frac{\sin Kr}{Kr} dr \end{aligned} \quad \text{Formula 7.2.3}$$

The atomic scattering factor  $f$  has the same value for different wavelengths of the X-rays if the magnitudes of the scattering vectors are the same.

The electron density distribution is calculated as the square of the wave function  $\psi(r)$  of an electron in the atom.

$$\rho(\mathbf{r}) = |\psi(\mathbf{r})|^2 \quad \text{Formula 7.2.4}$$

The wave function  $\psi(r)$  is calculated by the Hartree-Fock method or the Thomas-Fermi method;  $f$  is calculated based on the results.

The atomic scattering factor  $f$  calculated as such depends on the atomic number and the scattering angle. Fig. 7.2.1 shows the dependence of the atomic scattering factor on the atomic number and the scattering angle for several elements. The horizontal axis,  $\sin \Theta / \lambda$ , corresponds to the direction of the scattered X-ray with respect to the incident X-ray. When  $\sin \Theta / \lambda = 0$ , the scattering direction is the same as the direction of the incident X-ray propagation. As  $\sin \Theta / \lambda$  increases, the X-ray is scattered more to the back.

An element with a larger atomic number scatters X-rays more strongly, increasing the magnitude of  $f$ . The intensity of the scattered X-ray is proportional to the atomic number along the direction of X-ray propagation.

The intensity of the scattered X-rays is highest in the direction of the incident X-ray propagation and gradually decreases to the side and backwards. Along the direction of X-ray propagation, X-rays scattered by any electrons in the atom have the same phase, and the scattered X-rays interfere constructively. In the direction opposite the direction of X-ray propagation, the phase of the X-ray scattered by each electron differs depending on the position of the electron. The scattered X-rays interfere destructively, resulting in a low intensity.

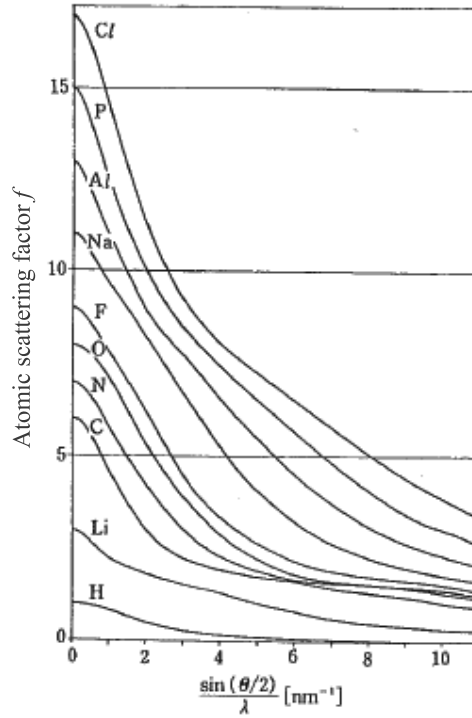


Fig. 7.2.1 Angle dependence of atomic scattering factor

Here, the curves differ depending on the elements because the orbitals of the electrons for each element and their spatial distribution differ. When the spread of the orbitals is small, X-rays scattered at any position have only small phase differences, since the distances between the scattering positions are small. When the spread of the orbitals is large, the phase difference may be large, depending on the positions at which the X-rays are scattered.

The atomic scattering factor basically does not depend on the wavelength of the X-rays. However, when X-rays have a wavelength extremely close to the absorption edge of the atom and demonstrate strong absorption, we observe the resonance effect and are compelled to consider **anomalous scattering**. The atomic scattering factor including anomalous scattering is given by the following formula:

$$f(\mathbf{K}) = f_0(\mathbf{K}) + \Delta f'(\mathbf{E}) + i\Delta f''(\mathbf{E}) \quad \text{Formula 7.2.5}$$

Here,  $f_0(\mathbf{E})$  is the atomic scattering factor,  $f'(\mathbf{E})$  the real component of anomalous scattering, and  $f''(\mathbf{E})$  the imaginary component of the anomalous scattering. The parameters  $f'(\mathbf{E})$  and  $f''(\mathbf{E})$  depend on the element and wavelength of the X-rays and have been calculated based on theory.

The anomalous scattering occurs mainly due to the electrons in the K shell. Since the spatial spread of the K shell is small, the anomalous scattering terms of the atomic scattering factor lack strong scattering angle dependence. If we use X-rays with wavelengths a slight distance from the absorption edge, the anomalous scattering is small compared to  $f_0$  and can generally be ignored. However, it cannot be ignored for precise discussions of electron distribution. To perform analysis for a particular atom in a crystal, select a wavelength close to the absorption edge to use the anomalous scattering terms.

### 7.2.2 Crystal Structure Factor

A crystalline material is a three-dimensional regular structure of atoms or molecules. The **crystal structure factor** indicates the scattering caused by the entire material (in other words, the entire crystal) when atoms having atomic scattering factors characteristic to each element form a three-dimensional periodic structure in the crystal.

In a crystal, electron density distribution  $\rho(\mathbf{r})$  has a three-dimensional periodicity. Assume the origin (0, 0, 0) to be an arbitrary lattice point in the crystal and denote the fundamental vectors of the three-dimensional structure as  $\mathbf{a}$ ,  $\mathbf{b}$ , and  $\mathbf{c}$ . If the coordinates of a lattice point are  $(p, q, r)$ , this lattice point is at position  $p\mathbf{a} + q\mathbf{b} + r\mathbf{c}$  from the origin. When the distance to a point in the unit cell to which this lattice point belongs is denoted as  $\mathbf{r} = (p\mathbf{a} + q\mathbf{b} + r\mathbf{c}) + \mathbf{r}'$ ,  $\rho(\mathbf{r}) = \rho(\mathbf{r}')$  holds, since the crystal has a repeating structure.

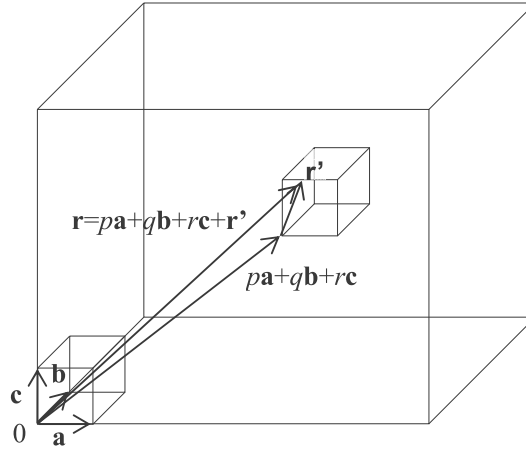


Fig. 7.2.2 Unit cell and scattering point in crystal

The amplitude of the scattered wave moving from the entire crystal is obtained by rewriting the formula expressing the amplitude of the scattered wave from an atom for the entire crystal. As the crystal has a regular structure, the formula can be transformed as follows:

$$A(\mathbf{K}) = \int_{\text{crystal}} \rho(\mathbf{r}) e^{-i\mathbf{K} \cdot \mathbf{r}} d\mathbf{r} \quad \text{Formula 7.2.6}$$

$$= \sum_p \sum_q \sum_r \exp\{-i\mathbf{K} \cdot (p\mathbf{a} + q\mathbf{b} + r\mathbf{c})\} \int_{\text{unit lattice}} \rho(\mathbf{r}') \exp(-i\mathbf{K} \cdot \mathbf{r}') d\mathbf{r}' \quad \text{Formula 7.2.7}$$

Formula 1.3.9 shows that the scattering amplitude from the entire crystal is equivalent to the scattering amplitude calculated by assuming a scattering element at each lattice point with a proportional scattering amplitude, as expressed below:

$$F(\mathbf{K}) = \int_{\text{unit lattice}} \rho(\mathbf{r}) e^{-i\mathbf{K} \cdot \mathbf{r}} d\mathbf{r} \quad \text{Formula 7.2.8}$$

This  $F(\mathbf{K})$  is called the crystal structure factor and depends on the electron density in the unit cell or on the atomic arrangement.

We can express the electron distribution in the crystal as a superposition of the electron distribution of free electrons. Assume that the  $j$ -th atom in the unit cell is at position  $\mathbf{r}_j$  with respect to the origin of the unit cell and express the electron density distribution associated with this atom as  $\rho_j(\mathbf{r} - \mathbf{r}_j)$ . Then, the electron density distribution in the unit cell is given by the following formula:

$$\rho(\mathbf{r}) = \sum_j \rho_j(\mathbf{r} - \mathbf{r}_j) \quad \text{Formula 7.2.9}$$

Thus, the crystal structure factor is expressed as follows:

$$\begin{aligned} F(\mathbf{K}) &= \sum_j \int \rho_j(\mathbf{r} - \mathbf{r}_j) \exp(-i\mathbf{K} \cdot \mathbf{r}) d\mathbf{r} \\ &= \sum_j \exp(-i\mathbf{K} \cdot \mathbf{r}_j) \int \rho_j(\mathbf{r}') \exp(-i\mathbf{K} \cdot \mathbf{r}') d\mathbf{r}' \\ &= \sum_j f_j(\mathbf{K}) \exp(-i\mathbf{K} \cdot \mathbf{r}_j) \end{aligned} \quad \text{Formula 7.2.10}$$

Here, we used  $\mathbf{r} - \mathbf{r}_j = \mathbf{r}'$  and expressed the atomic scattering factor of the  $j$ -th atom as  $f_j(\mathbf{K})$ . The crystal structure factor is the sum of the atomic scattering factors of the atoms in the unit cell with the phase shift  $\mathbf{K} \cdot \mathbf{r}_j$  regarded to be the contribution from the atom at position  $\mathbf{r}_j$ .

### 7.2.3 Laue Function

The **Laue function** is a function incorporated into the crystal structure factor and expresses the relationship between crystallinity and angular distribution of the scattered X-rays.

In the crystal structure factor of Formula 7.1.8, denote the sum over the lattice points in the first half as  $G(\mathbf{K})$ . If the crystal is a parallelepiped having three sides parallel to the  $a$ ,  $b$ , and  $c$  axes and the numbers of repeating unit cells along these directions are  $N_a$ ,  $N_b$ , and  $N_c$ , respectively,  $G(\mathbf{K})$  is given by the following formula:

$$\begin{aligned}
G(K) &= \sum_p \sum_q \sum_r \exp\{-i\mathbf{K} \cdot (p\mathbf{a} + q\mathbf{b} + r\mathbf{c})\} \\
&= \sum_{p=0}^{N_a-1} \exp(ip\mathbf{K} \cdot \mathbf{a}) \sum_{q=0}^{N_b-1} \exp(ip\mathbf{K} \cdot \mathbf{b}) \sum_{r=0}^{N_c-1} \exp(ip\mathbf{K} \cdot \mathbf{c})
\end{aligned}
\tag{Formula 7.2.11}$$

A discussion of scattering intensity requires  $|G|^2$ , given by the following formula:

$$|G|^2 = \frac{\sin^2\left(\frac{N_a}{2}\mathbf{K} \cdot \mathbf{a}\right)}{\sin^2\left(\frac{1}{2}\mathbf{K} \cdot \mathbf{a}\right)} \frac{\sin^2\left(\frac{N_b}{2}\mathbf{K} \cdot \mathbf{b}\right)}{\sin^2\left(\frac{1}{2}\mathbf{K} \cdot \mathbf{b}\right)} \frac{\sin^2\left(\frac{N_c}{2}\mathbf{K} \cdot \mathbf{c}\right)}{\sin^2\left(\frac{1}{2}\mathbf{K} \cdot \mathbf{c}\right)}
\tag{Formula 7.2.12}$$

This function is called the Laue function. Finally, the amplitude of the X-rays scattered by the crystal is derived from the expression of  $A(\mathbf{K})$  and given by the following formula:

$$A(\mathbf{K}) = G(\mathbf{K})F(\mathbf{K})
\tag{Formula 7.2.13}$$

The scattering intensity is given by the following formula:

$$I = I_e |G(\mathbf{K})|^2 |F(\mathbf{K})|^2
\tag{Formula 7.2.14}$$

Here, we discuss the characteristics of the Laue function.

Figure 7.2.3 below shows  $\sin^2\left(\frac{N_a}{2}\mathbf{K} \cdot \mathbf{a}\right) / \sin^2\left(\frac{1}{2}\mathbf{K} \cdot \mathbf{a}\right)$  with  $\mathbf{K} \cdot \mathbf{a}$  as the horizontal axis. It has major local maximum peaks when  $\mathbf{K} \cdot \mathbf{a} = 2\pi h$  ( $h$  is zero or a positive or negative integer) is satisfied and is zero at  $\pm 2\pi / N_a$ ,  $\pm 4\pi / N_a$ , and  $\pm 6\pi / N_a$  on both sides of the major peaks. Smaller minor local maximum peaks appear in between. The height of the major peaks is  $N_a^2$ , and the FWHM of the major peaks is approximately  $2\pi / N_a$ . As  $N_a$  increases, the height of the major peaks increases significantly and width decreases. The height of the minor peaks is—for example, when  $N_a = 10$ —4.5% of the major peaks for the first minor peaks and 1.6% of the major peaks for the second minor peaks. When  $N_a$  is large, they can generally be disregarded. In the case of an ordinary crystal with large values for  $N_a$ ,  $N_b$ , and  $N_c$ , the Laue function has sharp peaks only at

$$\mathbf{K} \cdot \mathbf{a} = 2\pi h, \quad \mathbf{K} \cdot \mathbf{b} = 2\pi k, \quad \mathbf{K} \cdot \mathbf{c} = 2\pi l
\tag{Formula 7.2.15}$$

where  $h$ ,  $k$ , and  $l$  are zero or positive or negative integers.

The local maximum peak value is given by the following formula:

$$|G(\mathbf{K})|^2 = (N_a N_b N_c)^2 = N^2
\tag{Formula 7.2.16}$$

The condition for the above local maximum peaks is called the Laue condition.

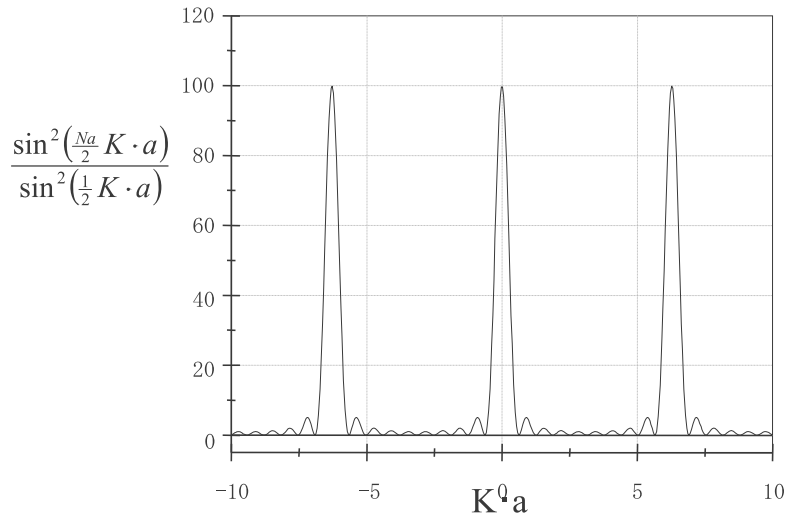


Fig. 7.2.3 Laue function:  $\frac{\sin^2(\frac{Na}{2} K \cdot a)}{\sin^2(\frac{1}{2} K \cdot a)}$  (For  $N_a = 10$ )

Now we will discuss the spatial relationship between the Laue functions for different axes. Consider the scattering that occurs when the X-ray beam is incident on a single crystal sample placed at a certain orientation. When the single crystal sample is positioned, we determine the direction ( $\mathbf{a}$ ) of the sample  $a$  axis. When the X-ray beam is incident on the sample, we also determine the incident wave vector  $\mathbf{k}_0$ . The Laue function for the  $a$  axis restricts only the scalar product of the scattering vector  $\mathbf{K}$  and the unit cell vector  $\mathbf{a}$ , so that  $\mathbf{K}$  is not determined uniquely. The scattering wave vector  $\mathbf{k}$  that defines  $\mathbf{K}$  together with  $\mathbf{k}_0$  forms a cone and is also not uniquely determined. Fig. 7.2.4 shows this relationship schematically. The thickness of the circle on which the tip of the vector  $\mathbf{K}$  rests corresponds to the width of the major local maximum peaks of the Laue function indicated in Figure 7.1.3.

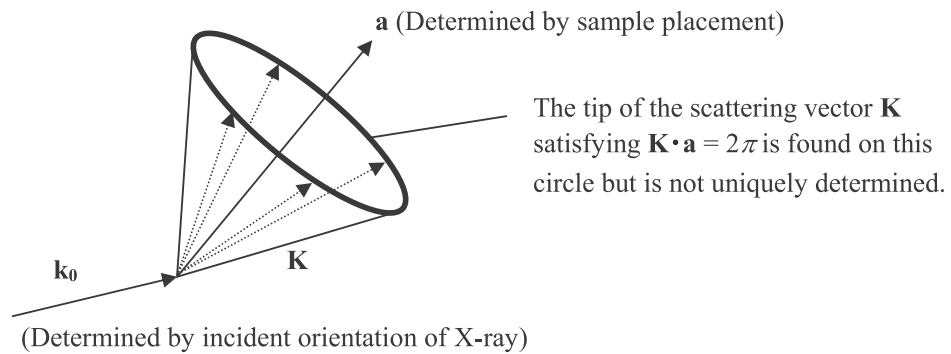


Fig. 7.2.4 Laue function for a axis

In addition to the  $a$  axis, the  $b$  and  $c$  axes are also present in the sample. The Laue function can be drawn for the  $b$  and  $c$  axes in a manner similar to the  $a$  axis. Fig. 7.2.5 shows the Laue function for the  $b$  axis added to Fig. 7.2.4. The scattering vectors satisfying both conditions are restricted to two vectors. When we consider the Laue function for the  $c$  axis, the scattering vector  $\mathbf{K}$  is restricted to a single vector. Clearly, we observe only one diffracted beam from the  $(hkl)$  plane of a single crystal sample.

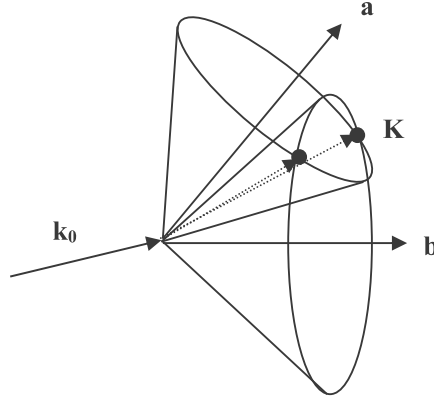


Fig. 7.2.5 Laue function for  $a$  and  $b$  axes

The distribution of the scattering vector  $\mathbf{K}$  is narrower when the widths of the circles specified by the Laue function for the  $a$ ,  $b$ , and  $c$  axes are thinner. In other words, when the number of unit cells constituting the crystal is greater, the scattered X-rays are generated across a narrower range of angles. If the single crystal has an anisotropic shape such as an acicular crystal, a plate crystal, or a single crystal thin film, and the number of the unit cells stacked in the direction of each axis differs, the spread in the scattered X-rays exhibits anisotropy.

#### 7.2.4 Extinction Rule

The magnitude of  $F(\mathbf{K})$  also depends on the value of  $(p\mathbf{a} + q\mathbf{b} + r\mathbf{c})$ ; that is, the coordinates of the atoms contained in the unit cell and the Miller indices. Here we discuss how the value of  $F(\mathbf{K})$  changes based on the type of Bravais lattice and Miller indices, using an example of a cubic crystal composed of a single type of atom.

##### A. Simple Cubic Lattice

A simple unit cell is expressed as a lattice formed by eight atoms, as shown in the figure below. Among these atoms, the coefficients  $(x_j, y_j, z_j)$  of the coordinates  $(ax_j, by_j, cz_j)$  of the atom at the origin are expressed as  $(0, 0, 0)$ . Other atoms are also found at the origin of the unit cells adjacent to this unit cell, and the coordinates for the atoms in a simple unit cell are all given as  $(0, 0, 0)$ .

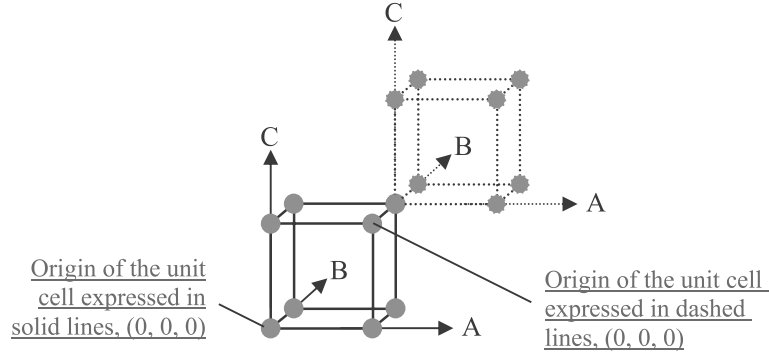


Fig. 7.2.6 Coordinates of the atoms in the simple unit cell

The factor  $e^{2\pi i(hx_j + ky_j + lz_j)}$  within Formula 1.3.9, which expresses the crystal structure factor for a simple unit cell, does not depend on the Miller indices, due to the relationship,  $e^{n\pi i} = e^{-n\pi i} = (-1)^n$ . Instead, it is given by the following formula:

$$e^{2\pi i(hx_j + ky_j + lz_j)} = e^{2\pi i \times 0} = 1 \quad \text{Formula 7.2.17}$$

Thus, for a simple unit cell, the following formula holds:

$$F(K) = f(K) \quad \text{Formula 7.2.18}$$

### B. Body-Centered Cubic Lattice

The coordinates of the atoms are expressed as (0, 0, 0) and (1/2, 1/2, 1/2) for a body-centered cubic lattice. The crystal structure factor is calculated as follows:

$$\begin{aligned} F(K) &= \sum_{j=1}^n f_j(K) e^{2\pi i(hx_j + ky_j + lz_j)} \\ &= \sum_{j=1}^n f_j(K) e^{2\pi i \times 0} + \sum_{j=1}^n f_j(K) e^{2\pi i\{(1/2)h + (1/2)k + (1/2)l\}} \end{aligned} \quad \text{Formula 7.2.19}$$

In short, the value of the crystal structure factor for a body-centered cubic lattice depends on the Miller indices and is expressed by the following formulas:

$$\begin{aligned} F(K) &= 2f(K) && : \text{when } h + k + l \text{ is an even number.} \\ F(K) &= 0 && : \text{when } h + k + l \text{ is an odd number.} \end{aligned}$$



A crystal with a body-centered cubic lattice does not cause diffraction by crystal planes such as (111) and (221). The formula describing the phenomenon whereby  $F(\mathbf{K}) = 0$  for a set of  $(hkl)$  with a specific relationship is called the **extinction rule**.

### C. Face-Centered Cubic Lattice

The coordinates of the atoms are expressed as (000), (1/2, 1/2, 0), (1/2, 0, 1/2), and (0, 1/2, 1/2) for a face-centered cubic lattice. The extinction rule is expressed as follows:

$$\begin{aligned} F(K) &= 4f(K) && : \text{when } h, k, \text{ and } l \text{ are all odd or all even numbers.} \\ F(K) &= 0 && : \text{when } h, k, \text{ and } l \text{ are a mixture of even and odd numbers.} \end{aligned}$$

### D. Cubic Lattice with Diamond Structure

A cubic lattice with a diamond structure has an atomic arrangement formed by overlaying two face-centered cubic lattices whose origin is at (0, 0, 0) and (1/4, 1/4, 1/4). The extinction rule is expressed as follows:

$$\begin{aligned} F(K) &= 8f && : \text{when } h + k + l = 4m \\ F(K) &= 4(1 \pm i)f && : \text{when } h + k + l = 4m \pm 1 \text{ (m is zero or a positive or negative integer)} \\ F(K) &= 0 && : \text{when } h + k + l = 4m \pm 2 \end{aligned}$$

### E. Cubic Lattice with Rock Salt Structure

The cubic lattice with a rock salt (sodium chloride) structure has an atomic arrangement formed by overlaying the face-centered cubic lattice of the  $\text{Na}^+$  ions with its origin at (0, 0, 0) and the face-centered cubic lattice of the  $\text{Cl}^-$  ions with an origin at (1/2, 1/2, 1/2).

$$\begin{aligned} F(K) &= 4(f_{\text{Na}^+} + f_{\text{Cl}^-}) && : \text{when } h, k, l \text{ are all even numbers} \\ F(K) &= 4(f_{\text{Na}^+} - f_{\text{Cl}^-}) && : \text{when } h, k, l \text{ are all odd numbers} \\ F(K) &= 0 && : \text{when } h, k, \text{ and } l \text{ are a mixture of even and odd numbers.} \end{aligned}$$

When several types of elements are present in the crystal (as in the case of sodium chloride), the degree of decline in the diffraction intensity due to the extinction rule also depends on the values of the atomic scattering factors. For example, in KCl and CsI, the atomic scattering factors of the cations and anions are virtually the same. Thus, the diffraction intensity is extremely small when  $h, k, l$  are all odd.

## 7.2.5 Effects on X-Ray Scattering Phenomena Other Than Crystal Structure

We describe X-ray scattering by the structures indicated above for an ideal case in which the atom positions are all completely fixed in a crystal free of lattice disorders. Actual materials, of course, are subject to thermal vibration and disorders in three-dimensional periodicity, which spread the angular distribution of the scattered X-rays and reduce intensity.

## References

### **Basics of X-ray diffraction**

*“Elements of X-Ray Diffraction (New Edition)”* : written by Cullity and translated by Gentaro Matsumura, Agne

*Ceramics basic course 3, “X-ray Diffraction Analysis”* : by Masanori Kato, Uchida Rokakuho Publishing

*Material Science series, “X-ray Structural Analysis”* : by Yoshio Waseda & Eiichiro Matsubara, Uchida Rokakuho Publishing

### **Basics of X-ray diffraction and dynamical theory of diffraction**

*Physical Engineering Experiments 15, “X-ray Diffraction and Scattering Techniques,” Volume 1*, by Seishi Kikuta, University of Tokyo Press

*Physics for contemporary readers 6, “X-ray diffraction and structure evaluation”* : by Norio Kato, Asakura Publishing

*“Dynamical Theory of X-Ray Diffraction”* : by Andre Authier, Oxford Univ Press

### **Applications of X-ray analysis**

*Frontier of X-ray analysis*: supervised by Yoichi Goshi & edited by Kimitaka Sato, Agne Gijutsu Center

### **Thin film analysis by X-rays**

*“X-Ray and Neutron Reflectivity: Principles and Applications”* : by Jean Daillant & Alain Gibaud, Springer-Verlag Telos

*“High Resolution X-ray Diffractometry and Topography”* : by D.K. Bowen & B.K. Tanner, Taylor & Francis

## Index

|  |          |   |     |
|--|----------|---|-----|
| $\alpha$ branch .....  | 143      | Four-Crystal Monochromator .....                  | 124 |
| analyzer .....   | 12       | Fourier transformation .....                      | 89  |
| anomalous scattering .....   | 166      | fundamental equation .....                        | 133 |
| asymmetric reflection .....  | 30       | Halving Adjustment .....                          | 98  |
| asymmetric reflections .....   | 117      | height limiting slit .....                        | 14  |
| asymmetry factor .....   | 117      | high-resolution X-ray diffraction method<br>..... | 112 |
| atomic scattering factor .....   | 164      | horizontal Soller slit .....                      | 14  |
| attenuator .....   | 5        | in-plane arm .....                                | 3   |
| blind regions .....  | 35       | in-plane measurement .....                        | 37  |
| Bloch wave .....   | 137      | In-plane measurement .....                        | 50  |
| Bloch wave $\alpha$ .....  | 143      | Kiessig fringe .....                              | 81  |
| Boundary conditions .....  | 84       | kinematical theory of diffraction .....           | 162 |
| CBO unit .....   | 7        | lattice relaxation .....                          | 59  |
| channel-cut crystal .....  | 8, 121   | Laue function .....                               | 168 |
| channel-cut monochromator optics .....                                 | 127      | Laue point .....                                  | 142 |
| crystal structure factor .....   | 167      | length limiting slit .....                        | 14  |
| Darwin's method .....  | 152      | monochromator .....                               | 9   |
| degree of preferred orientation .....                                  | 54       | monochromator and collimator .....                | 113 |
| diffraction plane indices of the<br>double-crystal monochromator ..... | 11       | mosaic crystals .....                             | 132 |
| dispersion point .....   | 143      | mosaicity .....                                   | 54  |
| dispersion spheres .....   | 142      | multiple crystal method .....                     | 113 |
| dispersion surfaces .....  | 142      | multiple scattering .....                         | 132 |
| double-crystal monochromator .....                                     | 9        | Multiple scattering .....                         | 112 |
| Double-Crystal Monochromator .....                                     | 122      | non-parallel arrangement .....                    | 119 |
| DuMond diagram .....   | 118      | origin of the reciprocal lattice .....            | 19  |
| dynamical theory of diffraction .....                                  | 112, 132 | Out-of-plane measurement .....                    | 49  |
| evanescent wave .....  | 85       | paraboloidal synthetic multilayer mirror ...      | 6   |
| Ewald sphere .....   | 27       | parallel arrangement .....                        | 119 |
| extinction distance .....  | 151      | Pendellosung fringes .....                        | 147 |
| extinction rule .....  | 173      | perfect crystal .....                             | 132 |
| Fine Halving Adjustment .....  | 100      | pole figure .....                                 | 53  |
| four-circle goniometer .....   | 34       | Pole figure measurement .....                     | 52  |
| four-crystal monochromator .....                                       | 9, 12    | q coordinates .....                               | 38  |

|  |          |                                       |     |
|--|----------|---------------------------------------|-----|
| real lattice .....                     | 21       | Soller slit.....                      | 14  |
| real space .....                       | 21       | swing.....                            | 72  |
| reciprocal lattice .....               | 19       | symmetric reflection .....            | 30  |
| reciprocal lattice point.....          | 19       | symmetric reflections.....            | 117 |
| reciprocal lattice vector .....        | 19       | Thin film measurement.....            | 50  |
| reciprocal space .....                 | 21       | Thomson scattering.....               | 162 |
| reciprocal space coordinates.....      | 38       | tilt axes.....                        | 72  |
| Reciprocal space Mapping (RSM) .....   | 56       | total reflection.....                 | 80  |
| refractive index.....                  | 82       | total reflection critical angle ..... | 80  |
| resolution function .....              | 42       | two-wave approximation .....          | 141 |
| rocking curve.....                     | 115, 143 | Vegard's law .....                    | 114 |
| Rocking curve measurement .....        | 55       | vertical Soller slit.....             | 14  |
| root mean square (rms) roughness ..... | 88       | wave vector.....                      | 20  |
| satellite peaks .....                  | 159      | width-limiting slit .....             | 13  |
| scattering vector .....                | 23       | $\theta_D$ axis .....                 | 3   |
| selection slit.....                    | 7        | $\theta_S$ axis .....                 | 3   |